UNIVERSIDAD DE MÁLAGA

Facultad de Ciencias

Departamento de Ingeniería Química

TESIS DOCTORAL

Para optar al Título de:

Doctor en Ingeniería Química con Mención Internacional

Catalizadores de base carbonosa para reacciones de oxidación y deshidratación de alcoholes

Autor: **María José Valero Romero**

Directores: **Dr. D. José Rodríguez Mirasol**

Dr. D. Tomás Cordero Alcántara

Málaga, 2015

Publicaciones y Divulgación Científica

AUTOR: María José Valero Romero
EDITA: Publicaciones y Divulgación Científica. Universidad de Málaga

D. TOMÁS CORDERO ALCÁNTARA, Catedrático de Ingeniería Química de la Universidad de Málaga,

D. JOSÉ RODRÍGUEZ MIRASOL, Catedrático de Ingeniería Química de la Universidad de Málaga,

CERTIFICAN: Que el trabajo de investigación recogido en la presente Memoria ha sido realizado bajo su dirección en el Departamento de Ingeniería Química de la Universidad de Málaga por la Ingeniera Dña. MARÍA JOSÉ VALERO ROMERO, y reúne, a su juicio, contenido científico suficiente y las condiciones necesarias para ser presentado y defendido ante el Tribunal correspondiente para optar al Grado de Doctor con Mención Internacional.

Málaga, Abril de 2015

Fdo.: Tomás Cordero Alcántara Fdo.: José Rodríguez Mirasol

A mi familia

"*No importa el tamaño del problema,*

importa la determinación al resolverlo"

(desconocido)

Índice de contenidos

Overview

Activated carbons materials have attracted considerable attention because their interesting applications in many fields, such as catalysis, gas and liquid phase adsorption and gas and energy storage. The carbon materials present an additional advantage since they can be prepared from different carbonaceous precursors, as agricultural wastes or by-products, that are abundant, environmentally friendly disposal and cost decrease associated with activated carbon production. Consequently, there is a great research effort in this direction. However, the use of carbon materials in catalysis is limited since they would gasify to CO_2 (or CO) in the presence of oxygen at relatively low temperatures. Nevertheless, it has been shown that it is possible to prepare carbon materials with a relatively large amount of phosphorus on the carbon surface by chemical activation of lignocellulosic materials with phosphoric acid. This activation procedure leads to phosphorus surface complexes, in form of $COPO_3$, CPO_3 and C_3P groups, which remain very stable on the carbon surface, at relatively high temperatures, and confer to the carbon a high oxidation resistance and high acidity, increasing the catalytic applications in which these catalysts can be used.

The main purpose of the present thesis is to provide some insights into the role of the different phosphorus species on the oxidation resistance of activated carbons, prepared by activation of biomass with phosphoric acid. In addition to this, it is shown some of their potential applications in catalytic processes, as catalytic supports or as catalysts by themselves, for reactions that take place at relatively high temperatures and under oxidizing conditions. Two types of reacctions have been studied in gas phase; i) the catalytic decomposition (dehydration/dehydrogenation) of bioalcohols and ii) the selective oxidation of light hydrocarbons.

This P. h. D. thesis is divided into 7 chapters. The first one, introduction, and a final summary are writing in Spanish, whereas the rest of the thesis is presented in English.

Chapters 2 and 3 present an extensive study of the oxidation state evolution of the activated carbons surface groups, after subjecting them to thermal treatments in oxidizing and inert conditions. In these chapters, we will discuss the role of the phosphorus surface groups on the high oxygen content and oxidation resistance of this

type of porous carbons. The catalytic conversion of methanol and ethanol over an acid carbon-based catalyst obtained by chemical activation of olive stone with H_3PO_4 has also been analyzed and the results are presented in Chapters 4 and 5, respectively. Specifically, we have examined the effect of oxygen concentration in the carrier gas, reaction temperature, alcohol inlet partial pressure and space time in the conversion and product selectivity of the alcohols decomposition reactions. A kinetic study of the methanol and ethanol decomposition on the acid carbon is also presented in which the presence and absence of water vapor in the reactor feed, in concentrations similar to that of the biomethanol and bioethanol, has been also analyzed. The corresponding kinetics and thermodynamics parameters were obtained.

The data provided in Chapters 6 and 7 are adapted from already published papers. These chapters are devoted to the use of phosphoric acid activated carbons as catalyst supports of vanadium oxide species, thus VPO (Vanadium and Phosphorus mixed oxides) catalysts are obtained. These VPO materials are commercially used as catalysts for the transformation of n-butane into maleic anhydride and we have investigated the corresponding carbon supported vanadium oxide catalysts in the propylene partial oxidation reaction. These activated carbons can be also prepared with controlled morphology, by this manner VPO supported catalysts with spherical morphology and high surface areas have been described in Chapter 7. The preparation and characterization of bulk oxide VPO materials, with high surface areas, are also analyzed in this chapter. These materials have been tested during the propane oxidative dehydrogenation (ODH) reaction.

Each chapter has their own abstract and conclusions. A final chapter will provide general conclusions and give a small insight in the remaining and future work coming as a result of this thesis.

Chapter 1

Introducción

Abstract Biorefineries use biomass as an abundant and renewable resource for the production of energy, biofuels and valuable chemicals though different processes that requires the use of a catalyst. Thus, the use of biomass waste for the preparation of the catalytic materials required by the biorefineries could be interesting. Nowadays, a general tendency in the design of catalytic materials is based on nanostructured catalysts, since they present valuable advantages from both industrial and academic points of view. In this sense, activated carbons are very attractive as catalytic supports and/or as catalysts by themselves since they satisfy the majority of the properties that requires a suitable support: high surface area, chemical stability in both highly acid and basic media; in addition, the chemistry of the carbon surface can be modulated. However, carbon materials would gasify to CO_2 (or CO) at relatively low temperatures under an oxidant atmosphere. Phosphorus has been noted in many studies to be effective at moderate temperatures, acting as a physical barrier and/or blocking the active carbon sites for the oxidation reaction. Thus, phosphorus-containing activated carbons exhibit high oxidation resistance and open new possibilities for the use of carbon-based materials as catalyst supports for reactions that take place under oxidizing conditions at high temperatures, such as the selective oxidation of light hydrocarbons.

Keywords: Activated carbons, phosphoric acid, alcohol decomposition reactions, VPO catalyst, selective oxidation reactions, nanocasting

1. El carbón activo

1.1. Métodos de preparación de carbón activo

Prácticamente cualquier material orgánico con proporciones relativamente altas de carbono es susceptible de ser transformado en carbón activado. Además, si los materiales se preparan a partir de residuos biomásicos o lignocelulósicos se obtiene un doble beneficio, económico y medioambiental ya que se realiza una gestión eficaz de un residuo incrementando su valor añadido. Por otro lado, como el carbón activo producido proviene de materias primas lignocelulósicas no contribuye al aumento de las emisiones de CO_2.

Los carbones activados obtenidos industrialmente pueden provenir de madera y residuos forestales u otros tipos de biomasa, turba, lignito y otros carbones minerales, así como de diferentes polímeros y fibras naturales o sintéticas. Existen, no obstante, algunas limitaciones a la hora de elegir el material precursor. Desde un punto de vista estructural los carbones activados son carbones muy desordenados e isótropos y, por tanto, no serán adecuados para su preparación aquellos materiales carbonosos que pasen por un estado fluido o pseudofluido durante su carbonización, dado que durante la resolidificación de esta fase suelen formarse estructuras ordenadas en los carbones resultantes; carbones coquizables, salvo que se eliminen sus propiedades coquizantes mediante una oxidación previa, por ejemplo; y residuos termoplásticos.

En la elección del precursor adecuado hay que tener en cuenta factores como una buena disponibilidad y bajo coste, bajo contenido en materia mineral, que el carbón resultante posea unas buenas propiedades mecánicas y capacidad de adsorción, constancia de sus características físico-químicas durante el almacenaje, proximidad a planta y /o facilidad de transporte y facilidad de activación.

Como la demanda mundial de carbón activado está creciendo sin parar debido al conocimiento de las buenas propiedades adsorbentes de éste, se están estudiando gran multitud de precursores renovables de bajo coste para la producción de carbones activados [1-16]. Entre los precursores renovables para carbón activo, podemos destacar el uso de varios subproductos agrícolas como cáscaras de nueces, huesos de frutas, desechos procedentes de la caña de azúcar, hueso de aceituna y serrín.

En la presente tesis doctoral el precursor utilizado para la preparación del carbón activo fue el hueso de aceituna.

La extracción de aceite de oliva y las aceitunas de mesa constituyen dos actividades industriales de gran importancia en los países mediterráneos. El proceso de extracción produce impacto medioambiental como consecuencia de la generación de aguas contaminadas y/o un residuo sólido dependiendo del método de extracción del aceite de oliva o del proceso de preparación de las aceitunas. En la industria de extracción del aceite de oliva el hueso triturado se puede recuperar mediante filtración del residuo sólido resultante, alpeorujo en el caso del procedimiento de extracción en dos fases y orujo para el de tres fases. En el caso de la industria de la aceituna de mesa, se obtiene el hueso entero por separación de la pulpa. Los principales productores son España, Italia y Grecia, que por sí solos representan el 75 % de la producción mundial. España es el primer productor de aceite de oliva, con una producción promedio aproximada de 670.000 toneladas, seguido por Italia, con una producción media estimada de 540.000 ton y, en tercer lugar, Grecia con 350.000 ton [17]. Estas cantidades dan idea de la importancia que tiene el aprovechamiento de los residuos generados y, en concreto, del hueso de aceituna.

Actualmente se utilizan dos métodos para la preparación de carbones activos: la activación física y la activación química. La Figura 1 presenta un esquema simplificado de estas dos vías de producción de carbón activo. La utilización de un método de activación u otro dependerá de la naturaleza de la materia prima, así como de las propiedades que se deseen para el carbón activo obtenido.

1.1.1. Activación física

La activación física consta de dos etapas: carbonización y activación propiamente dicha. La carbonización se realiza en una atmósfera inerte y con ella se eliminan los heteroátomos unidos al carbono, tales como hidrógeno, oxígeno y trazas de azufre y nitrógeno, en forma gaseosa por descomposición pirolítica. Con la carbonización se produce un reordenamiento de los átomos de carbono, pero no se produce un desarrollo muy significativo de la estructura porosa, para lo cual es necesaria una segunda etapa de gasificación parcial o activación.

La gasificación es una reacción heterogénea de tipo gas-sólido donde están presentes como agentes gasificantes, oxígeno, CO_2, vapor de agua o una mezcla de ellos en función de la finalidad del proceso. La gasificación parcial es un caso particular de gasificación en el que la conversión del carbón no es total y resulta un sólido poroso (carbón activo) como consecuencia de una gasificación controlada; esto es lo que se conoce como activación física del carbón.

1.1.2. Activación química

La segunda vía comercial para producir carbón activo es la activación química, en la que se produce la desvolatilización del precursor carbonoso con la intervención de algún agente activante que orienta la descomposición térmica. La activación química se realiza en una sola etapa, desarrollándose la porosidad durante el tratamiento térmico a temperaturas comprendidas, en general, entre 400 y 700 ºC. El material de partida se impregna con una disolución concentrada del agente activante (deshidratante), formando una pasta que luego se seca y carboniza/activa en un horno, produciendo una fuerte deshidratación que provoca el desarrollo de la estructura porosa. El producto se lava para eliminar el agente activante, que se recupera. La viabilidad de los procesos de activación química depende, en gran medida, de la eficacia en la recuperación del agente químico.

Los parámetros fundamentales que controlan el proceso de activación química son la relación de impregnación, la temperatura de activación y el tiempo de residencia. Los valores que tomen estos parámetros van a tener una influencia notable en la estructura final del carbón.

Los agentes activantes más usados industrialmente son el $ZnCl_2$ y el H_3PO_4. También se han usado otros ácidos de Lewis, como por ejemplo $AlCl_3$ o $FeCl_3$ y bases como KOH o NaOH.

Aunque el mecanismo de activación difiere para cada agente activante, la característica común de estas sustancias es su acción deshidratante que orienta la descomposición pirolítica hacia una menor formación de alquitranes y aumenta el rendimiento en sólido. En general, la acción de estos reactivos promueve el entrecruzamiento, lo que favorece la formación de una estructura tridimensional rígida.

Al ser menor la producción de volátiles y, particularmente, de compuestos de carbono, el rendimiento en sólido es mayor y la contracción de la matriz sólida resultante, menos significativa.

Los catalizadores utilizados en el presente trabajo fueron preparados mediante activación química con H_3PO_4.

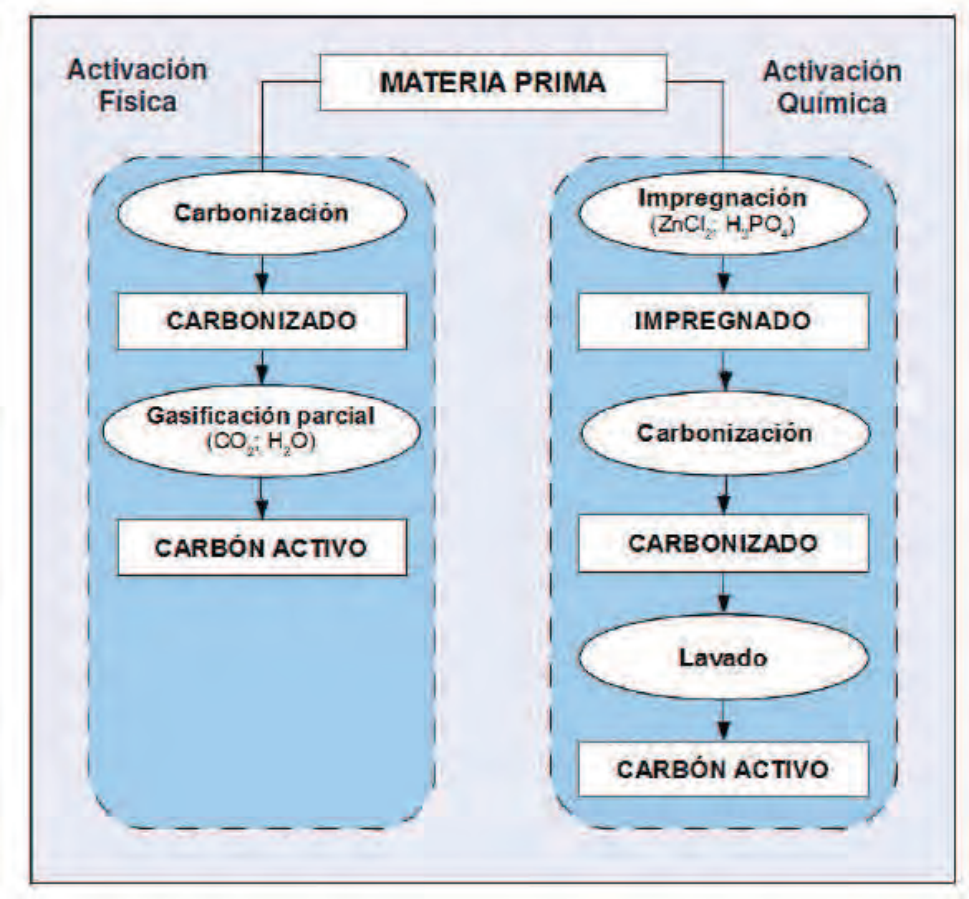

Figura 1: Etapas en la activación física y química para la producción de carbón activo

1.2. Activación química con H_3PO_4

El proceso de activación de materiales de origen biomásico, con ácido fosfórico, ha sido estudiado en detalle por Jagtoyen y Derbyshiren [18], los cuales analizaron la evolución de la reacción con la temperatura.

Los compuestos biomásicos están formados por tres componentes mayoritarios, celulosa, hemicelulosa y lignina. Las proporciones típicas de estos tres biopolímeros en la biomasa son: 40-60% de celulosa, 20-40% de hemicelulosa y 10-25% de lignina.

La reacción de la biomasa con el ácido fosfórico comienza en el proceso de impregnación, cuando se mezclan los componentes. Ya cuando se calienta la mezcla hasta 50 ºC existen evidencias de cambios físicos y químicos en la biomasa. Se cree que el ácido ataca, inicialmente, a la hemicelulosa y a la lignina, posiblemente, debido a que el acceso a estos polímeros amorfos es más sencillo que a la estructura cristalina de la celulosa. La celulosa parece ser más resistente a la hidrólisis ácida que otros polisacáridos, como demuestra el hecho de que la estructura celular permanece prácticamente inalterada después de la reacción con H_3PO_4, incluso a elevadas temperaturas. Uno de los efectos iniciales del ataque ácido es la hidrólisis de los enlaces glucosídicos de la celulosa y la hemicelulosa y la ruptura de los enlaces ariloéter de la lignina. Estas reacciones se acompañan, además, de deshidratación, degradación y condensación. Las reacciones primarias conllevan una reducción del peso molecular, principalmente de la hemicelulosa y la lignina.

Al aumentar la temperatura ($150 < T < 450$ ºC) predominan las reacciones de entrecruzamiento sobre las reacciones de despolimerización y de ruptura de enlaces. El elevado rendimiento en carbono obtenido por el tratamiento ácido a temperaturas superiores a 300 ºC se debe, precisamente, a este entrecruzamiento que retiene las especies de peso molecular relativamente bajo en el seno de la fase sólida. Evidentemente, existe una relación directa entre el desarrollo de porosidad y el proceso de dilatación de la estructura. La formación de ésteres fosfato por reacción de la celulosa con el ácido fosfórico se muestra en la Figura 2, que ilustra como el ácido fosfórico se puede insertar entre las cadenas de celulosa, sustituyendo los puentes de hidrógeno y, al mismo tiempo, separando las cadenas y produciendo la dilatación de la estructura por la adición o inserción de grupos fosfato.

A 280 ºC, las estructuras son pequeñas unidades poliaromáticas conectadas entre sí por enlaces de tipo fosfato o polifosfato, incluidas conexiones del tipo polimetileno [(CH2)n]. Al aumentar la temperatura se producen reacciones de ciclación y condensación, que aumentan la aromaticidad y el tamaño de las unidades poliaromáticas, como consecuencia de la escisión de los enlaces del tipo C-O-P. Entre 350 y 500 ºC, el carbonizado es estable, pero a partir de 430 ºC, la ruptura continua de entrecruzamientos produce un crecimiento del tamaño de las unidades aromáticas.

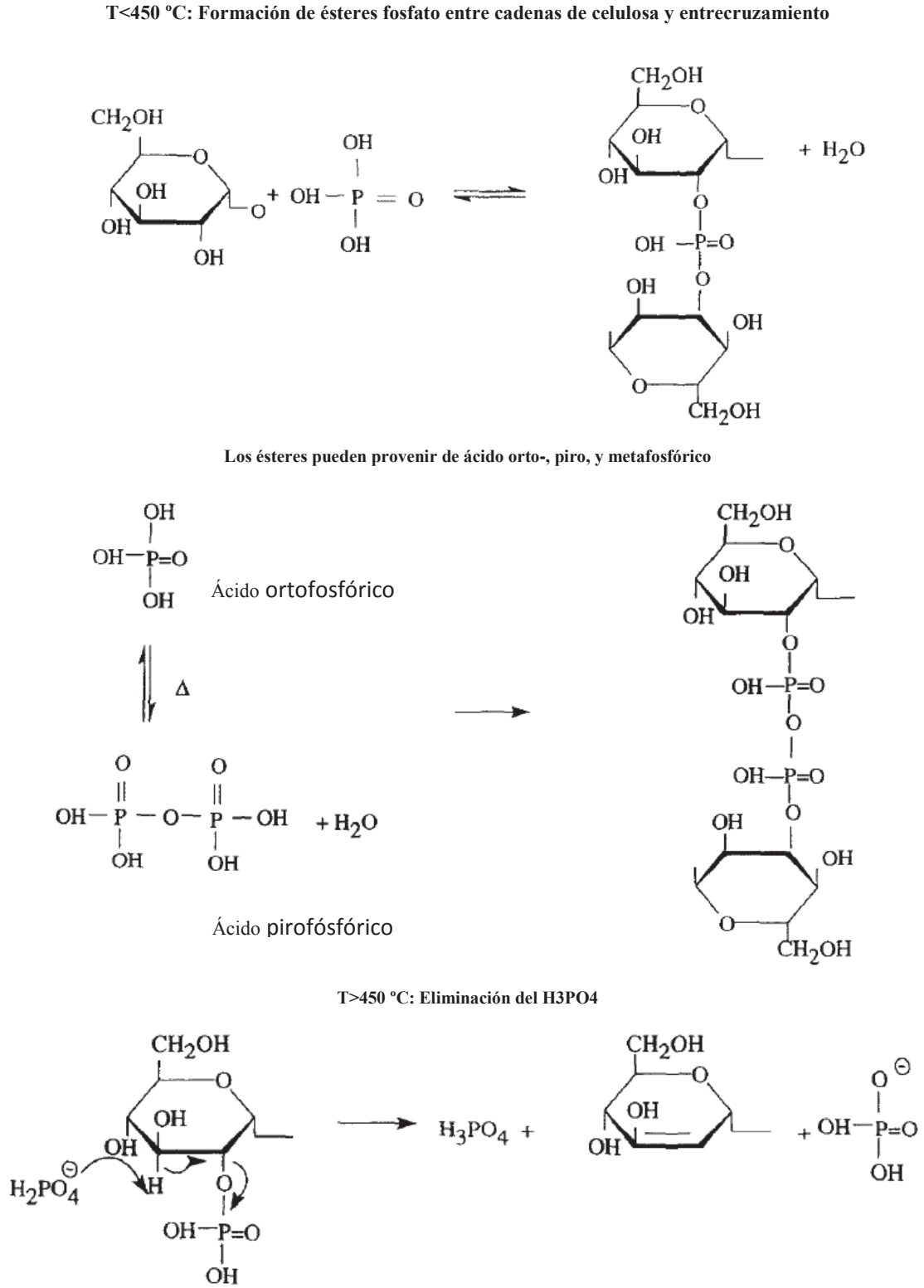

Figura 2. Mecanismo de formación de ésteres fosfato entre las cadenas de celulosa [18]

Así, el ácido fosfórico parece actuar de dos formas, (i) como catalizador ácido promoviendo las reacciones de ruptura de enlaces y la formación de entrecruzamientos vía procesos de ciclación y condensación y (ii) combinándose con las especies orgánicas

para formar enlaces de tipo fosfato, ésteres polifosfatos, que sirven para conectar y entrecruzar los fragmentos de biopolímeros.

A temperaturas superiores a 450 ºC, la estructura comienza a contraerse. El volumen de microporo decrece de forma progresiva a partir de temperaturas intermedias (aproximadamente 350 ºC), no observándose variación en el volumen de mesoporo hasta unos 550 ºC, temperatura a partir de la cual comienza a disminuir rápidamente. Entre 450 y 550 ºC, la contracción estructural es absorbida por el estrechamiento del diámetro de poro sin causar un cambio significativo del tamaño de poro. Esta contracción se asocia a la ruptura de los enlaces de tipo fosfato, térmicamente inestables a temperaturas superiores a unos 450 ºC. La reducción en la cantidad de los entrecruzamientos resulta en una estructura más densamente empaquetada con la consecuente reducción en el desarrollo de la porosidad.

1.3. Resistencia a la oxidación

La importancia de mejorar la resistencia a la oxidación de los materiales de carbono mediante la introducción de distintos grupos superficiales, silicio [19-21], boro [22-25] o compuestos de fósforo [25-28], se pone de manifiesto al comprobar la gran cantidad de publicaciones que se encuentran en la bibliografía sobre este tema. Esto se debe a la baja resistencia a la oxidación que presentan los materiales de carbono [29] y que limitan su uso en aplicaciones catalíticas en atmósfera oxidante.

La inhibición de la oxidación por formación de complejos químicos estables en los sitios activos, parece ser la alternativa más prometedora para evitar la gasificación del soporte de carbono. En la bibliografía se recoge un número limitado de compuestos inhibidores de la oxidación, además de los ya mencionados, destacar los compuestos órgano-halogenados, fosfatos, óxido de boro, compuestos órgano-boro y compuestos órgano-fosforado. En la actualidad la mayoría de las investigaciones en este tema se centran en el dopado con compuestos de fósforo.

Se ha observado un efecto de inhibición a la oxidación por impregnación de carbón con compuestos organo-fosforados [25,30], H_3PO_4 [26], $POCl_3$ [31], fosfatos ácidos [28] y fosfatos metálicos [32-37]. También, se ha observado un efecto inhibidor

de la reacción de oxidación mediante la incorporación de pentóxido de fósforo en carbones [38,39], o por lavado de materiales compuestos C/C con ácido fosfórico, seguido de un tratamiento térmico hasta su temperatura de descomposición [40].

En términos generales, se plantean dos explicaciones para el efecto inhibidor de los compuestos de fósforo. La primera se basa en un mecanismo de bloqueo físico y la segunda se basa en el envenenamiento de los centros activos del carbón. El recubrimiento con fosfatos de la superficie exterior es muy efectivo para la protección de los carbones frente a la oxidación [41]. Este tipo de recubrimiento reduce el contacto carbón/catalizador y carbón/oxígeno aumentando, de esta forma, la resistencia a la oxidación catalítica de compuestos carbonosos [35-36]. Un requisito fundamental para la eficacia de este tipo de recubrimientos es una distribución uniforme de los depósitos de fosfatos [36]. El mecanismo de envenenamiento de los sitios activos fue propuesta por McKee et al [22-23] y, posteriormente apoyado por otros autores [25,26,30]. McKee et al propuso que los compuestos de fósforo forman compuestos menos reactivos sobre los centros activos en la superficie del carbón, tales como grupos fosfato o fosfito. Se ha propuesto que los complejos formados son C-O-$POCl_2$, para el caso de impregnación con $POCl_3$ como precursor y grupos C-O-PO_3 y C-PO_3, en el caso de emplear compuestos organo-fosforados como precursores. En este sentido, Radovic et al [27] describe el efecto inhibidor a la oxidación de carbones activos dopados con $POCl_3$ y $CH_3OP(OH)_2$. Los autores describen la presencia de grupos C-O-PO_3 y C-PO_3 en la superficie de los carbones. Además, sugieren que el bloqueo de los centros activos del carbón es debido, principalmente, a la presencia de grupos de P enlazados al carbón, mientras que los grupos metafosfato funcionan como una barrera física entre el catalizador y la superficie del carbón. La presencia de los grupos C-O-PO_3, en los que el fósforo está enlazado al carbón mediante un átomo de oxígeno, son primordiales para mantener el efecto inhibidor de los depósitos de fósforo. Por lo tanto, la pérdida de ese oxígeno o la rotura del enlace C-O resultarían en la pérdida de la inhibición a la oxidación. En este trabajo, además, los autores calcularon las energías de los enlaces de los grupos C-O-P y C-P-O, y concluyeron que el enlace O-P en los grupos C-O-P es el más débil. Por tanto, a elevadas temperaturas los grupos C-O-PO_3 descomponen a CO, mientras que el fosforo se reduce a C-PO_3.

Rosas el at [42] describe la resistencia a la oxidación de carbones obtenidos mediante activación química de residuos lignocelulósicos con H_3PO_4. A diferencia de

los trabajos descritos anteriormente, la activación con H_3PO_4 genera carbones activos con distintos grupos superficiales de fósforo (C-O-PO_3 y C-P-O_3) durante la etapa de activación, no siendo necesario el dopado a posteriori de los carbones. Además, estos grupos superficiales permanecen estables en la superficie de los carbones ya que no se eliminan tras la etapa de lavado. Los autores observaron que la presencia de estos grupos superficiales de fósforo producen un cambio en el mecanismo de gasificación de los carbones activos cuando se comparan con carbonizados del mismo precursor. La oxidación de los carbonizados tiene lugar en toda la superficie disponible de las partículas de carbón, mientras que la gasificación de los carbones activados con ácido fosfórico se produce, principalmente, en el exterior de las partículas (shrinking unreacted core model). El los capítulos 2 y 3 de la presente tesis se estudia la evolución de la oxidación de este tipo de carbones activos a distintas temperaturas de oxidación y el papel de los distintos grupos superficiales de fósforo en la mejora de la resistencia a la oxidación de los mismos.

1.4. Carbón activo en la catálisis heterogénea

El carbón activo presenta numerosas aplicaciones que afectan a industrias tan diversas como la alimentaria, farmacéutica, química, nuclear, petrolífera, de tratamiento de aguas de consumo y depuración de efluentes industriales y domésticos, tratamiento de aire y de gases, etc. La multitud de aplicaciones del carbón activo resultan del hecho de que es el adsorbente muy versátil debido a que posee alta superficie específica, distribución polimodal de tamaños de poro, estructura porosa en forma de rendija y capacidad de presentar diferentes tipos de naturaleza química en su superficie. Las aplicaciones del carbón activo, pueden ser en fase líquida o gas.

En catálisis heterogénea el carbón activo se utiliza fundamentalmente como soporte de fases activas para múltiples reacciones, aunque también se emplea directamente como catalizador. Hoy en día, el carbón activo es un soporte de catalizadores plenamente consolidado en el mercado mundial utilizándose por ejemplo en la hidrogenación de benceno y de compuestos nitrados tanto alifáticos como aromáticos [41]. Sin embargo, a pesar de que existe un creciente interés, sigue siendo bajo el número de procesos catalíticos que utilizan el carbón activo como catalizador a

nivel industrial. De hecho, se estima que las aplicaciones catalíticas que emplean carbón activo representan menos del 5% del volumen total. Entre estas reacciones, la más importante es la producción de fosgeno o cloruro de carbonilo, $COCl_2$, que se usa en la síntesis de diferentes productos químicos y polímeros.

La presencia de grupos superficiales de oxígeno e hidrógeno tiene una gran influencia en las propiedades adsorbentes y, por tanto, en las propiedades catalíticas del carbón activo, por lo que su estudio ha atraído mucha atención en los últimos años.

Las principales ventajas de la utilización del carbón activo en reacciones de catálisis heterogénea son:

- La estructura del carbón es resistente a medios tanto ácidos como básicos.
- La estructura es estable a elevadas temperaturas (incluso por encima de 700 ºC), en ausencia de aire.
- La estructura porosa se puede controlar en el proceso de obtención, produciendo catalizadores con una distribución de tamaño de poro adecuada para una determinada reacción.
- Los carbones activos se pueden preparar con muy diferentes formas y tamaños (granular, polvo, pellets, fibras, telas, aereogeles…).
- Aunque la superficie de los carbones es esencialmente hidrofóbica, la química de la superficie se puede modificar para aumentar su carácter hidrofílico e, incluso, se pueden obtener carbones con propiedades de intercambio iónico.
- En los catalizadores soportados sobre carbón, la fase activa se puede recuperar fácilmente de los catalizadores agotados mediante combustión del soporte carbonoso, lo cual es una gran ventaja cuando la fase activa es un metal precioso.
- El coste de los carbones activos es generalmente menor que el de otros soportes tradicionales como la alúmina o la sílice.

Una desventaja tradicional de los carbones activos, ha sido la presencia de materia inorgánica procedente bien del precursor, o bien introducida durante el proceso de preparación. Aunque es cierto que muchos carbones activos tienen contenidos altos en cenizas (de hasta 10-15%), especialmente si se han obtenido a partir de carbones minerales, actualmente es posible preparar carbones porosos con contenidos muy bajos en materia mineral, mediante la elección de un precursor adecuado, tales como los precursores de origen biomásico. Superado este problema, el principal inconveniente para la utilización del carbón activo en algunas reacciones catalíticas puede considerarse que es su baja resistencia a la oxidación.

Como se ha mencionado en apartado 1.3, la activación de residuos lignocelulósicos con H_3PO_4 genera carbones activos con grupos superficiales de fósforo que presentan una elevada estabilidad térmica y química y les confiere a los carbones una elevada resistencia a la oxidación y acidez superficial. Además, la activación con H_3PO_4 genera carbones con un elevado desarrollo de su estructura mesoporosa a elevadas relaciones de impregnación (H_3PO_4/precursor) lo que los hace muy interesantes para ser utilizados como soportes catalíticos, o bien, como catalizadores ácidos por sí mismos en reacciones que se lleven a cabo en atmósfera oxidante a temperaturas relativamente elevadas. No obstante, en la bibliografía no existen muchos trabajos en los que se utilicen estos carbones con elevada resistencia a la oxidación como catalizadores o soportes catalíticos, por lo que su estudio resulta muy interesante.

2. Los alcoholes

La descomposición catalítica de diferentes tipos de alcoholes, por deshidrogenación o deshidratación, ha sido ampliamente analizada en la bibliografía [43-47]. La actividad y la selectividad de este tipo de reacciones está gobernada por las características texturales y las propiedades ácido-básicas y electrónicas del catalizador.

Estas reacciones se utiliza para obtener productos a escala industrial y como reacción tipo test para caracterizar las propiedades ácido-básicas de las superficies de catalizadores, ya que está ampliamente aceptado que los productos de deshidrogenación, es decir, aldehídos y cetonas, se producen preferentemente sobre catalizadores básicos, mientras que los productos de deshidratación, olefinas y éteres se generan

fundamentalmente sobre catalizadores ácidos [48-50]. Los alquenos u olefinas se producen por reacción de deshidratación catalizada por un único protón (deshidratación intramolecular), mientras que la formación de éteres supone una reacción de acoplamiento intermolecular (deshidratación intermolecular). La relación entre la cantidad de productos de deshidrogenación y de deshidratación no depende únicamente de la naturaleza del catalizador, sino que también es función de la temperatura de reacción. En general, la reacción de deshidrogenación se produce a mayores temperaturas de reacción que la de deshidratación como consecuencia de su mayor energía de activación [51].

Entre los catalizadores empleados para la descomposición de alcoholes se encuentran óxidos metálicos simples y compuestos [52-56], silicoaluminatos o alúminas [57-60] y zeolitas [61-63]. Sin embargo son pocos los trabajos en los que se ha empleado como catalizador para la descomposición de alcoholes el carbón activo, ya sea como soporte de fase activa o como catalizador.

A continuación se analizan la descomposición catalítica de los alcoholes utilizados en esta tesis, etanol y metanol, sobre materiales de carbono.

Etanol

Szymański et al. [64] llevó a cabo la descomposición de etanol sobre distintos carbones obtenidos a partir de polifulfuril alcohol por activación física con CO_2, sin oxidar y oxidados con ácido nítrico, y con Ni depositado. El carbón activo inicial mostraba una actividad muy baja en la descomposición de etanol. Se producía deshidrogenación y deshidratación, generándose como productos principales acetaldehído (mayoritario), etileno y dietil éter junto con pequeñas cantidades de dietilacetal. La oxidación con ácido nítrico produce un carbón con una superficie más ácida lo que se traduce en un aumento muy significativo en la actividad del carbón hacia la reacción de deshidratación. La introducción del Ni produce un aumento de la reacción de deshidrogenación, como consecuencia de la presencia de cationes Ni^{2+} sobre la superficie del carbón. La actividad catalítica aumenta con la temperatura del proceso, pero a temperaturas superiores a 120 ºC, se producía una caída de la actividad debida a la descomposición térmica de los grupos superficiales oxigenados. Grunewald y Drago [65], analizaron la conversión de diferentes alcoholes sobre un tamiz molecular

carbonoso. Cuando el etanol se diluía en $_{N2}$ y reaccionaba sobre el tamiz molecular carbonoso a 230 ºC, el catalizador mostraba una baja actividad con una alta selectividad hacia etileno. Sin embargo, si el gas se cambiaba de N_2 a aire la actividad del catalizador aumentaba, alcanzándose conversiones cercanas al 70%. En este caso, los productos dominantes eran acetato de etilo y acetaldehído. La descomposición de etanol también ha sido estudiada por el grupo de Carrasco-Marín [66]. Ellos analizaron el efecto de la oxidación del carbón activo con $(NH_4)_2S_2O_8$ en la reacción de descomposición de etanol. De acuerdo con sus resultados, el carbón activo si oxidar tan solo era capaz de catalizar la reacción de deshidrogenación, siendo el principal producto el acetaldehído. Por otro lado, los carbones oxidados mostraban una actividad moderada y se obtuvieron principalmente productos de deshidratación, siendo el dietil éter el mayoritario y una pequeña cantidad de productos de deshidrogenación cuando el gas de reacción es He. Los autores confirmaron que la actividad es consecuencia de la introducción de grupos carboxilos durante el tratamiento de oxidación.

Metanol

No existen muchos trabajos publicados sobre la descomposición de metanol sobre materiales de carbono. Zawadzki et al. mostraron que el carbón sin una etapa previa de oxidación no reaccionaba en la descomposición de metanol [67]. Los carbones eran activos sólo cuando se oxidaban en atmósfera de oxígeno. Estos resultados evidenciaron, además, la participación de intermediarios metóxido y formaldehido en la descomposición de metanol. Moreno-Castilla et al. [68] estudiaron la reacción de descomposición de metanol catalizada por carbones activos oxidados con diferentes agentes oxidantes, H_2O_2, $(NH_4)_2S_2O_8$ y HNO_3 para introducir grupos oxigenados superficiales y aumentar su acidez superficial. Los carbones oxidados con $(NH_4)_2S_2O_8$ desarrollaron los grupos ácidos más fuertes y demostraron ser los más activos en la deshidratación de metanol a dimetil éter. Un aumento en la temperatura de reacción producía una rápida disminución de su actividad en la deshidratación de metanol. La razón es una descomposición gradual de los grupos carboxilos presentes en la superficie del carbón a temperaturas superiores a 180ºC.

Por tanto, resulta de gran interés la preparación de carbones activos con grupos superficiales ácidos de elevada estabilidad térmica y química y sin la necesidad de una etapa adicional de oxidación. En este sentido, Jorge Bedia et al [69,70], ha estudiado la

descomposición de 2-butanol e isopropanol sobre carbones activos preparados mediante activación química de residuos lignocelulósicos con H_3PO_4. Los carbones activos mostraron ser activos para las reacciones de deshidratación de estos alcoholes y mostraron tener elevada estabilidad térmica y química. En la presente tesis, se analizarán las reacciones de descomposición de metanol y etanol sobre este tipo de carbones activos.

2.1. Descomposición de (bio)etanol y (bio)metanol

El término biocombustible engloba a los siguientes carburantes líquidos y gaseosos: bioetanol, biodiesel, biometanol, biobutanol, aceites vegetales, biogás, gas de síntesis (bio-syngas), biohidrógeno y biocombustibles líquidos obtenidos por el proceso Fischer-Tropsch. Los biocombustibles pueden generarse a partir de biomasa vegetal fácilmente disponible y abundante, son medioambientalmente sostenibles, poseen un impacto económico positivo debido a que reducen la dependencia en las importaciones del petróleo y aumento de inversiones, tienen un balance energético positivo, ya que la cantidad de energía contenida en el producto es superior a la requerida para su producción y distribución [71], y emiten menos dióxido de carbono porque están producidos por un ciclo de carbono a corto plazo, estimándose que en su combustión devuelven a la atmósfera el dióxido de carbono que la planta ha fijado para su crecimiento [72]. Debido a dichos beneficios, la producción global de biocombustibles ha experimentado un crecimiento sostenido en la pasada década, desde los 16 mil millones de litros en el año 2000 hasta más de 100 mil millones de litros en el año 2013. Así, la producción de biocombustibles a partir de biomasa vegetal proporciona una fuente de energía renovable y limpia, ya que no contribuyen a aumentar la cantidad de dióxido de carbono emitido a la atmósfera.

El (Bio)metanol es una de las sustancias químicas más versátiles producidas actualmente, utilizándose en su forma pura así como componente base para la producción de otros productos como es el dimetil éter (MTD) u otros procesos catalíticos, tales como metanol a hidrocarburos (MTH) [73-75] o metanol a olefinas (MTO) [76,77]. El DME es una sustancia que se emplea como compuesto base para la obtención de múltiples productos químicos como el acetato de metilo, dimetil sulfato y

olefinas ligeras/gasolinas. Además está aumentando su uso como proponente en la formulación de aerosoles reemplazando a los clorofluorocarbonos (CFC), que se ha demostrado que destruyen la capa de ozono [78-79]. El mayor incremento en su demanda se debe a su empleo como combustible alternativo limpio, ya que su eficiencia es muy similar a la de los combustibles diésel tradicionales, disminuye la formación de NO_x, casi no producen humos y reduce el ruido que generan los motores de combustión.

Por otro lado, resulta de interés industrial la transformación catalítica del (Bio) etanol a etileno, denominado BTE (bio-ethanol-to-ethylene) [80-81]. El etileno es uno de los productos principales en la industria petroquímica ya que se utiliza para la preparación de una gran variedad de compuestos, tales como polietileno, etilenglicol, óxido de etileno y policloruro de vinilo [82]. La producción de etileno mediante deshidratación de bioetanol, actualmente, solo se emplea a escala comercial en unos pocos países como India y Brasil, debido a su elevado coste de producción y al elevado consumo de energía. Sin embargo, la creciente escasez de recursos naturales y energía, y el encarecimiento del crudo de petróleo hace de la deshidratación catalítica de etanol (especialmente de bioetanol) una alternativa cada vez más competitiva.

3. El objetivo de la oxidación química selectiva

Una de las tecnologías más destacada en la Industria Química actual son los procesos de oxidación selectiva. La producción selectiva de un producto de reacción, de entre varios compuestos cuya formación es termodinámicamente posible, es uno de los conceptos clave en el desarrollo de procesos químicos más sostenibles. En este sentido, en 2008, un informe del Subcomité Científico para la Energía de los Estados Unidos destacaba la necesidad de incrementar la selectividad de las transformaciones químicas en los procesos de producción de combustibles como una de las claves en el acercamiento a un futuro energético sostenible [83]. Décadas de investigación y desarrollo han dado lugar a un gran número de catalizadores heterogéneos, principalmente sólidos, empleados a escala industrial pero cuyas características más determinantes requieren de estudios a un nivel de observación nanométrico [84]. Por lo tanto, la denominada nanociencia, definida como la aplicación de herramientas de física, química y ciencia de materiales en la preparación y caracterización de materiales a

escala nanométrica, se ha revelado como indispensable en el estudio de las propiedades de los catalizadores heterogéneos, así como en la síntesis de nuevos materiales catalíticos con propiedades controladas.

Durante las últimas décadas, una de las aplicaciones más importantes de la oxidación selectiva ha sido la funcionalización de olefinas e hidrocarburos aromáticos para transformarlos en monómeros de gran interés en la industria de polímeros. Estos procesos resultan imprescindibles en la actualidad, ya que a partir de ellos se produce alrededor del 25% de los compuestos orgánicos más usados en la producción industrial de bienes de consumo [85-95]. Entre estos compuestos se incluyen: óxido de etileno, óxido de propileno, acrilonitrilo, ácido acrílico, acroleína, ácido metacrílico, anhídrido maleico, anhídrido ftálico, 1,2.dicloroetano, ciclohexanol, ciclohexanona, fenol y MTBE (metiltert-butil éter). La mayoría de estos procesos se llevan a cabo en fase heterogénea, aunque todavía existe un número considerable de procesos de catálisis homogénea.

En los procesos de oxidación catalítica heterogénea, las olefinas han sido, hasta el momento, la materia prima más empleada. La obtención relativamente fácil a partir de petróleo, junto a su alta reactividad, han hecho de las olefinas una de las materias primas básicas en la industria petroquímica. Sin embargo, la gran demanda actual y la dificultad de aumentar la producción mundial con los medios existentes, junto a motivos medioambientales (alto consumo de energía y tasas de CO_2 relativamente altas), justifican el desarrollo de nuevos métodos de producción de olefinas y/o la sustitución de olefinas por otras materias primas más accesibles, baratas y menos contaminantes. En este sentido, los alcanos ligeros (etano, propano o n-butano, además de metano) parecen materias primas adecuadas. Es por estos motivos que, en los últimos veinte años, se ha estudiado intensamente tanto desde un punto de vista fundamental como aplicado, la síntesis de nuevos materiales para ser empleados como catalizadores en procesos de oxidación parcial de alcanos.

4. Catalizadores VPO

Los óxidos mixtos de vanadio-fósforo (VPO), son catalizadores para la oxidación y amoxidación de hidrocarburos en fase gas. Esto es de gran importancia ya que, hasta hace relativamente poco tiempo, la activación directa de alcanos era impensable debido a la gran estabilidad de los enlaces simples. Por tanto, con estos catalizadores se podrían reemplazar procesos que actualmente usan olefinas como materias primas por los correspondientes a partir de alcanos.

Los catalizadores VPO se usan a nivel industrial en la síntesis del anhídrido maleico a partir de n-butano, único proceso comercial en la actualidad que utiliza un hidrocarburo lineal de bajo peso molecular para producir un oxigenado. Por citar algunos datos de producción, la compañía química BASF opera en Feluy (Bélgica) una planta para la producción de anhídrido maleico utilizando butano, con una capacidad de 115.000 toneladas por año.

Existe una gran variedad de fases VPO que difieren unas de otras en el estado de oxidación del vanadio, grado de condensación de grupos fosfatos y contenido de moléculas de agua. Se sabe que la transformación de una fase VPO en otra se puede inducir por tratamientos térmicos y por la atmósfera a la que se realizan [96]. La Figura 3 resume los precursores y las distintas fases VPO obtenidas por calcinación, en unas condiciones determinadas [97].

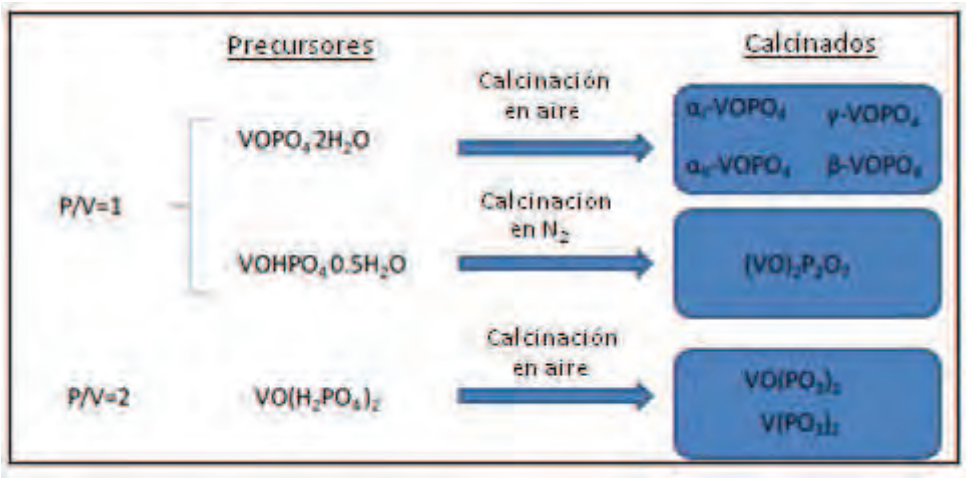

Figura 3. Diferentes fases VPO a partir de sus precursores más comunes [97]

La estructura cristalina y la morfología superficial va a depender del método de preparación, del precursor utilizado y de las condiciones de calcinación (tiempo, atmósfera, temperatura). Entre todos los precursores, las fases más comunes son aquellas con una relación molar P/V =1, fosfato de vanadilo dihidrato ($VOPO_4 \cdot 2H_2O$) y el hidrógenofosfato de vanadilo semihidrato ($VOHPO_4 \cdot 0.5H_2O$). Cuando el precursor $VOHPO_4 \cdot 0.5H_2O$ se calcina en unas condiciones adecuadas, da lugar a la formación del pirofosfato de vanadilo [$(VO)_2P_2O_7$], la cual se considera la fase activa para la producción de anhídrido maléico a partir de n-butano [98]. En esta fase el vanadio presenta un estado de oxidación V^{4+}. El tratamiento térmico de $VOPO_4 \cdot 2H_2O$ da lugar a diferentes fases anhídridas, tales como, α_I–$VOPO_4$, α_{II}–$VOPO_4$, β–$VOPO_4$, γ–$VOPO_4$ y δ–$VOPO_4$ entre otros [99-103]. En todas ellas el vanadio presenta un estado de oxidación V^{5+}.

Los VPO, como la mayoría de los óxidos, presentan bajas áreas superficiales y tienden a sinterizar, lo cual limita sus propiedades catalíticas (número de centros, resistencia mecánica, estabilidad química…). Una alternativa para paliar estos problemas es el uso de un soporte catalítico (sílice, alúmina, zeolitas, zirconio…) [104].

Recientemente, el grupo de investigación de *Tecnología de residuos y medio ambiente* de la Universidad de Málaga, ha propuesto la utilización de carbones activos como soportes de especies de óxidos de vanadio ya que satisfacen la mayoría de las propiedades que requiere un buen soporte, tales como, elevada área específica y estabilidad química en medio ácido y básico [105-108]. Además de que la química de los materiales de carbono puede ser modificada con relativa facilidad. Estos catalizadores de óxidos de vanadio y fósforo soportados han sido utilizados como catalizadores en la reacción de oxidación parcial de propano y propileno, demostrando poseer sitios redox/ácidos.

5. El carbón activo como molde (“nanocasting”)

En los últimos años se ha despertado un interés creciente en la síntesis de catalizadores nanoestructurados, es decir, con nano o micro morfología controlada. Estos materiales presentan buenas propiedades estructurales como catalizadores debido

a su elevada relación superficie/volumen y su bajo peso. Sin embargo, con los métodos habituales de preparación de óxidos mixtos es difícil controlar la morfología y la estructura porosa [109]. En la práctica, hay muchos trabajos que describen la síntesis de óxidos sencillos con estructura esférica, tal como ZnO_2, SnO_2, TiO_2, In_2O_3, WOx, CdO, CuO, NiO, TeO_2 o MoO_3, entre otros [110,115]. Sin embargo, apenas se encuentran descripciones de síntesis satisfactorias de óxidos mixtos con estructura esférica. Los óxidos metálicos porosos son, además, materiales utilizados en una gran variedad de aplicaciones, incluyendo: catalizadores propiamente dichos, soporte para catalizadores, tamices moleculares o como componentes de sistemas *host-guest* [116].

Otra alternativa para aumentar la porosidad de los óxidos es la síntesis de óxidos con porosidad mediante síntesis hidrotermales [117] o mediante métodos sol-gel [118]. Con estos métodos se pueden obtener óxidos con áreas superficiales BET en torno a 20-40 m^2/g, sin embargo, no se controla la morfología del óxido.

Por ello en la presente tesis doctoral, además de utilizar carbones activos como soporte de catalizadores basados en óxidos mixtos de vanadio y fósforo (Capitulo 6) se propondrá un método novedoso para la obtención de óxidos mixtos con una morfología y estructura porosa controlada (Capítulo 7) basado en la técnica de nanomoldeo, del inglés “nanocasting”.

En términos generales, la técnica de nanomoldeo consiste en obtener una réplica inversa del sistema de poros de un mole. El procedimiento consiste en impregnar los poros de los carbones activos con soluciones que contienen el precursor inorgánico elegido seguido de su solidificación. Durante el proceso de solidificación/estabilización se producen diferentes tipos de interacciones entre la superficie del carbón y el precursor inorgánico, desde débiles fuerzas dispersivas hasta interacciones electrostáticas, intercambio iónico o reacciones químicas. Tras este proceso de impregnación, se retira el carbón por medio de una calcinación, resultando en óxidos metálicos porosos [119-121]. Uno de los principales atractivos de utilizar carbones activos como molde de sacrificio es la posibilidad de controlar su porosidad y que se eliminan fácilmente tras una etapa de calcinación. Si además, los carbones presentan distintas morfologías será otro factor positivo a tener en cuenta a la hora de sintetizar los óxidos metálicos.

Titirici y colaboradores [14,115,122] han sido los pioneros en la utilización de esta técnica basándose en el uso de materiales carbonosos con morfología esférica, obtenidos por carbonización hidrotermal, como moldes para sintetizar esferas huecas de óxidos metálicos. Estos materiales resultan muy interesantes por su baja densidad y presentan numerosas aplicaciones [123]: suministro y retirada controlada de medicamentos y drogas, tintas y colorantes, catalizadores y soportes catalíticos, encapsulación y protección de macromoléculas biológicas como proteínas o encimas, encapsulación y retirada de residuos y relleno para compuestos ligeros o de baja densidad [124]. Sin embargo, ésta técnica no permiten un control adecuado de la porosidad (volumen de poros y área superficial) de los óxidos cristalinos resultantes.

Por lo tanto, investigar nuevas rutas de síntesis para la fabricación de esferas huecas de óxidos mixtos, que exhiban medias o altas áreas superficiales resulta muy interesante.

Referencias

[1] J de D López-González, F Martínez-Vilchez, F Rodríguez-Reinoso Preparation and characterization of active carbons from olive stones Carbon 1980, 18, 413-418

[2] F Rodríguez-Reinoso, M Molina-Sabio Activated carbons from lignocellulosic materials by chemical and/or physical activation: an overview Carbon 1992, 30, 1111-1118

[3] MT González, M Molina-Sabio, F Rodríguez-Reinoso Steam activation of olive stone chars, development of porosity Carbon 1994, 32, 1407-1413

[4] JC González, MT González, M Molina-Sabio, F Rodríguez-Reinoso, A Sepúlveda-Escribano Porosity of activated carbons prepared from different lignocellulosic materials Carbon 1995, 33, 1175-1177

[5] A Baçaoui, A Yaacoubi, A Dahbi, C Bennouna, R Phan Tan Luu, FJ Maldonado-Hodar, J Rivera-Utrilla, C Moreno-Castilla Optimization of conditions for the preparation of activated carbons from olive-waste cakes Carbon 2001, 39, 425-432

[6] C Moreno-Castilla, F Carrasco-Marín, MV López-Ramón, MA Alvarez-Merino Chemical and physical activation of olive-mill waste water to produce activated carbons Carbon 2001, 39, 1415-1420

[7] R Ubago-Pérez, F Carrasco-Marín, D Fairén-Jiménez, C Moreno-Castilla Granular and monolithic activated carbons from KOH-activation of olive stones Microp Mesop Mat 2006, 92, 64-70

[8] J Rodríguez-Mirasol, T Cordero, JJ Rodríguez High-temperature carbons from kraft lignin Carbon 1996, 34, 43-52

[9] E González Serrano, T Cordero, J Rodríguez-Mirasol, JJ Rodríguez Development of porosity upon chemical activation of kraft lignin with $ZnCl_2$ Ind Eng Chem Res 1997, 36, 4832-4838

[10] J Rodríguez-Mirasol, T Cordero, JJ Rodríguez Activated carbons from carbon dioxide partial gasification of eucalyptus kraft lignin Energy& Fuels 1993, 7, 133-139

[11] N Tancredi, T Cordero, J Rodríguez-Mirasol, JJ Rodríguez Activated carbons from Uruguayan eucalyptus wood Fuel 1996, 75, 1701-1706

[12] J Rodríguez-Mirasol, T Cordero, JJ Rodríguez Preparation and characterization of activated carbons from eucalyptus kraft lignin Carbon 1993, 31, 87-95

[13] O Ioannidou, A Zabaniotou Agricultural residues as precursors for activated carbon production—A review Renewable and Sustainable Energy Reviews 2007, 11, 1966-2005

[14] JM Dias, MCM Alvim-Ferraz, MF Almeida, J Rivera-Utrilla, M Sánchez-Polo Waste materials for activated carbon preparation and its use in aqueous-phase treatment: A review J Environ Manag 2007, 85, 833-846

[15] JS Macedo, L Otubo, OP Ferreira, IF Jiménez, IO Mazali, LS Barreto Biomorphic activated porous carbons with complex microstructures from lignocellulosic residues Microp Mesop Mat 2008, 107, 276-285

[16] P Álvarez, C Blanco, M Granda The adsorption of chromium (VI) from industrial wastewater by acid and base-activated lignocellulosic residues J Hazar Mat 2007, 144, 400-405

[17] Consejo Oleícola Internacional http://wwwinternationaloliveoilorg/

[18] M Jagtoyen, F Derbyshire Activated carbon from yellow poplar and white oak by H_3PO_4 activation Carbon 1998, 36, 1085-1097

[19] Zhu YC, Ohtani S, Sato Y, Iwamoto N The improvement in oxidation resistance of CVD-SiC coated C/C composites by silicon infiltration pretreatment Carbon 1998, 36(7–8), 929–35

[20] JE Atwater, JR Akse, TC Wang, S Kimura, DC Johnson Preparation of silicon-carbide-coated activated carbon using a high-temperature fluidized bed reactor Chem Eng Sci 2001, 56(8), 2685–93

[21] Dhami TL, Bahl OP, Awasthy BR Oxidation-resistant carbon– carbon composites up to 1700 ºC Carbon 1995, 33(4), 479–90

[22] DW McKee Borate treatment of carbon fibers and carbon/carbon composites for improved oxidation resistance Carbon 1986, 24(6), 737–41

[23] DW McKee, CL Spiro, EJ Lamby The inhibition of graphite oxidation by phosphorus additives Carbon 1984, 22, 285-290

[24] LE Jones, PA Thrower Influence of boron on carbon fiber microstructure, physical properties, and oxidation behavior Carbon 1991, 29(2), 251–69

[25] X Wu, CGM Pantano, LR Radovic Inhibition of catalytic oxidation by boron and phosphorus Extended abstracts, the international carbon conference Lexington, (Kentucky USA): American Carbon Society; 2001 p 2–33

[26] S Labruquère, R Pailler, R Naslain, B Desbat Oxidation Inhibition of Carbon Fibre Preforms and C/C Composites by H_3PO_4 J European Ceramic Society 1998, 18(13), 1953-1960

[27] X Wu, LR Radovic Inhibition of catalytic oxidation of carbon/carbon composites by phosphorus Carbon 2006, 44(1), 141-151

[28] W Lu, DDL Chung Oxidation protection of carbon materials by acid phosphate impregnation Carbon 2002, 40(8), 1249–54

[29] JX Zhao, RC Bradt, PL Walker Jr Effect of air oxidation at 873 K on the mechanical properties of a carboncarbon composite Carbon 1985, 23, 9-13

[30] SG Oh, NM Rodríguez In situ electron microscopy studies of the inhibition of graphite oxidation by phosphorus J Mater Res 1993, 8, 2879-2888

[31] TL Dhami, OP Bahl, BR Awasthy Oxidation-resistant carbon–carbon composites up to 1700 ºC Carbon 1995, 33, 479-490

[32] WF Wilson, E Tenn Oxidation retardant for graphite US patent 4439491, 1984

[33] LE McAllister, NE Jannasch Barrier coating and penetrant providing oxidation protection for carbon– carbon materials US patent 4837073, 1989

[34] J-C Cavalier, A Nale Process for obtaining an article made of a carbon-containing composite materials protected against oxidation US patent 5102689, 1992

[35] ER Stover, RP Dietz Inhibition of catalyzed oxidation of carbon–carbon composites US patent 5401440, 1995

[36] ER Stover Method of inhibiting catalyzed oxidation of carbon–carbon composites US patent 5759622, 1998

[37] TB Walker, LA Booker Inhibition of catalytic oxidation in carbon–carbon composite friction materials In: The international carbon conference Berlin, Alemania, 2000 pp 235–236

[38] JF Rakszawski, WE Parker The effect of group IIIA–VIA elements and their oxides on graphite oxidation Carbon 1964, 2, 53–63

[39] T Durkic, A Peric, M Lausevic, A Dekanski, O Neskovic, M Veljkovic, Z Lausevic Boron and phosphorus doped glassy carbon: I Surface properties Carbon 1997, 35, 1567–1572

[40] EJ Hippo, N Murdie, W Kowbel The effect of acid treatments on subsequent reactivity of carbon–carbon composites Carbon 1989, 27, 331–336

[41] SA Suvorov, EV Chaikun, SL Korobkin, GS Sokolova Protective mechanism of phosphorus-containing coatings Ceramics Abstracts 1988, 9, 24–27

[42] JM Rosas, R Ruiz-Rosas, J Rodríguez-Mirasol, T Cordero Kinetic study of the oxidation resistance of phosphorus containing activated carbons Carbon 2012, 50, 1523-1537

[43] OV Krylov Catalysis by nonmetals Academic Press, Nueva York, EEUU, 1970, p 115

[44] H Knözinger Specific poisoning and characterization of Ca-catalytically active oxide surfaces Adv Catal 1975, 25, 184-271

[45] F Pepe, C Angeletti, S de Rossi Catalytic behavior and surface chemistry of the ZnO/Al_2O_3 system for the decomposition of 2-propanol J Catal 1989, 118,1-9

[46] MM Wu, WW Kaeding Conversion of methanol to hydrocarbons : II Reaction paths for olefin formation over HZSM-5 zeolite catalyst J Catal 1984, 88, 478-489

[47] A Gervasini, A Auroux Acidity and basicity of metal oxide surfaces II Determination by catalytic decomposition of isopropanol J Catal 1991, 131, 190-198

[48] JM Campelo, A Garcia, JF Herencia, D Luna, JM Marinas, AA Romero Conversion of Alcohols ,α-Methylated Series, on $ALPO_4$ Catalysts J Catal 1995, 151, 307-314

[49] J March Advanced organic chemistry Reactions, mechanism and structure John Wiley and Sons, 4th ed, Nueva York, EEUU ,1992, pp 982-1010

[50] MA Aramendia, V Borau, C Jiménez, JM Marinas, A Parras, FJ Urbano Magnesium oxides as Basic catálisis for organic processes Study of the dehydrogenation-dehydration of 2-propanol J Catal 1996, 161, 829-838

[51] JB Nagy, JP Lange, A Gourgue, P Bodart, Z Gabelita Catalysis by acid and bases Elsevier, Amsterdam, Holanda , 1985, p 127

[52] MP Rosynek, RJ Koprowski, GN Dellisante The nature of catalytic sites on lanthanum and neodymium oxides for dehydration/dehydrogenation of ethanol J Catal 1990, 122, 80-94

[53] G Larsen, E Lotero, LM Petkovic DS Shobe Alcohol dehydration reactions over tungstated zirconia catalysts J Catal 1997, 169, 67-75

[54] ME Manríquez, T López, R Gómez, J Navarrete Preparation of TiO_2-ZrO_2 mixed oxides with controlled acid-basic properties J Mol Catal A 2004, 220, 229-237

[55] N Satoh, JI Hayashi, H Hattori Kinetic study of hydrogen adsorption on sulfated zirconia-supported platinum Appl Catal A 2000, 202 ,207-213

[56] JA Wang, X Bokhimi, O Novaro, T López, R Gómez Effects of the surface structure and experimental parameters on the isopropanol decomposition catalyzed with sol–gel MgO J Mol Catal A 1999, 145, 291-300

[57] H Knözinguer, H Büll, K Kochloefl The dehydration of alcohols on alumina : XIV Reactivity and mechanism J Catal 1972, 24, 57-68

[58] H Knözinguer, A Schengllia Influence of steric and inductive effects on product distributions in the dehydration of secondary alcohols on alumina J Catal 1974, 33, 142-144

[59] JL Swecker, AK Datye Alcohol dehydration over model nonporous alumina powder J Catal 1990, 121, 196-201

[60] R Takahashi, S Sato, T Sodesawa, K Arai, M Yabuki Effect of diffusion in catalytic dehydration of alcohol over silica–alumina with continuous macropores J Catal 2005, 229, 24-29

[61] DE Bryant, WL Kranich Dehydration of alcohols over zeolite catalysts J Catal 1967, 8, 8-13

[62] E Santacesaria, D Gelosa, E Giorgi, S Carrà Role of basic and acid sites in the bimolecular dehydration of alcohols catalyzed by HY zeolite J Catal 1984, 90, 1-9

[63] PA Jacobs, M Tielen, JB Uytterhoeven Active sites in zeolites: Part 6 Alcohol dehydration over alkali cation-exchanged X and Y zeolites J Catal 1977, 50, 98-108

[64] GS Szymanski, G Rychlicki, AP Terzyk Catalytic conversion of ethanol on carbon catalysts Carbon 1994, 32, 265-271

[65] GC Grunewald, RS Drago Carbon molecular sieves as catalysts and catalysts supports J Am Chem Soc 1991, 113, 1636-1639

[66] F Carrasco-Marín, A Mueden, C Moreno-Castilla Surface treated activated carbons as catalists for the dehydration and dehydrogenation reactions of ethanol J Phys Chem B 1998, 102, 9239-9244

[67] J Zawadzki, B Azambre, O Heintz, A Krztoń, J Weber IR study of the adsorption and decomposition of methanol on carbon surfaces and carbon-supported catalysts Carbon 2000, 38, 509-515

[68] C Moreno-Castilla, F Carrasco-Marín, C Parejo-Pérez, MV López Ramón Dehydration of methanol to dimethyl ether catalyzed by oxidized activated carbons with varying surface acidic character Carbon 2001, 39, 869-875

[69] J Bedia, JM Rosas, J Márquez, J Rodríguez-Mirasol, T Cordero Preparation and characterization of carbon based acid catalysts for the dehydration of 2-propanol Carbon 2009, 47, 286–294

[70] J Bedia, R Ruiz-Rosas, J Rodríguez-Mirasol, T Cordero Kinetic study of the decomposition of 2-butanol on carbon-based acid catalyst AIChE J 2010, 56, 1557-1568

[71] P Mckendry, Bioresour Energy production from biomass (part 1): overview of biomass Technol 2002, 83, 37–46

[72] D Puppan, Period Polytechnol Environmental evaluation of biofuels Ser Soc Man Sci 2002, 10, 95–116

[73] M Stocker Methanol-to-hydrocarbons: catalytic materials and their behavior Microporous Mesoporous Mater 1999, 29, 3–48

[74] FJ Keil Methanol-to-hydrocarbons: process technology Microporous Mesoporous Mater 1999, 29, 49–66

[75] AG Gayubo, PL Benito, AT Aguayo, M Olazar, J Bilbao Ralationship between surface acidity and activity of catalysts in the transformation of methanol into hydrocarbons J Chem Technol Biotechnol 65 (1996) 186–192

[76] AT Aguayo, AG Gayubo, R Vivanco, M Olazar, J Bilbao Role of acidity and microporous structure in alternative catalysts for transformation of methanol into olefins Appl Catal A 2005, 283, 197–207

[77] AG Gayubo, AT Aguayo, AE Sánchez del Campo, AM Tarrío, J Bilbao Kinetic modelling of methanol transformation into olefins on a SAPO-34 catalyst Ind Eng Chem Res 39 (2000) 292–300

[78] DM Brown, BL Bhatt, TH Hsiung, JJ Lewnard, FJ Waller Novel Technology for the Synthesis of Dimethyl Ether from Syngas A Catal Today 1991, 8, 279–304

[79] WW Kaeding, SA Butter Production of chemicals from methanol: I Low molecular weight olefins J Catal 1980, 61, 155–164

[80] R Le Van Mao, P Levesque, GP McLaughlin, LH Dao Ethylene from ethanol over zeolite catalysts Appl Catal 1987, 34, 163–179

[81] R Le Van Mao, TM Nguyen, GP McLaughlin The bioethanol-to-ethylene (BETE) process Appl Catal 1989, 48, 265–277

[82] PM Morse Taking a measure of sustainability Chem Eng News 1999, 77, 20–22

[83] J Hemminger (chairman) New Science for a Secure and Sustainable Energy Future Basic Energy Science Advisory Committee, (US Department of Energy) (2008)

[84] A T Bell The Impact of Nanoscience on Heterogeneous Catalysis Science 2003, 299, 1688-1691

[85] R K Grasselli Fundamental principles of selective heterogeneous oxidation catalysis Topics in Catalysis 2002, 21, 79-88

[86] J D Burrington, R K Grasselli Aspects of selective oxidation and ammoxidation mechanisms over bismuth molybdate catalysts Journal of Catalysis 1979, 59, 79-99

[87] R K Grasselli, J D Burrington Selective Oxidation and Ammoxidation of Propylene by Heterogeneous Catalysis Advances in Catalysis 1981, 30, 133-163

[88] P Arpentinier, F Cavani, F Trifirò The Technology of Catalytic Oxidations Chemical, Catalytic and Engineering Aspects, vol 1; Ed Technip: Paris, 2001

[89] P Arpentinier, F Cavani, F Trifirò The Technology of Catalytic Oxidations Safety Aspects, vol 2; Ed Technip: Paris, 2001

[90] G Centi, F, Cavani, F Trifiró Selective Oxidation by Heterogeneous Catalysis; Kluwer Academic/Plenum Publishers: New York, 2001

[91] S Albonetti, F Cavani, F Trifiro Key aspects of catalyst design for the selective oxidation of parafins Catalysis Reviews-Science and Engineering 1996, 38, 413-438

[92] J Haber Heterogeneous Hydrocarbon Oxidation BK Warren and S (EDs) ACS Symp Series 638, (1996) p 20

[93] E K Novakova, V C Vedrine Metal Oxides, Chemistry and Applications; Fierro, J L G, Ed; CRC Press: New York, 2006

[94] F Cavani, J H Teles Sustainability in Catalytic Oxidation: An Alternative Approach or a Structural Evolution? Chemsuschem 2009, 2(6), 508-534

[95] J M López Nieto The selective oxidative activation of light alkanes From supported vanadia to multicomponent bulk V-containing catalysts Topics in Catalysis 2006, 41(1), 3-9

[96] A Caldarelli et al The design of a new ZrO_2-supported V/P/O catalyst for n-butane oxidation to maleic anhydride: The build-up of the active phase during thermal treatment Catalysis Today 2010, 157, 204-210

[97] I Sádaba-Zubiri Catalizadores para biorrefinería: obtención de furfural y su transformación a productos de condensación aldólica Tesis doctoral (2012) Instituto de Catálisis y Petroleoquímica (CSIC)

[98] T Okuhara, M Misono Key Reaction Steps and Active Surface Phase of Vanadyl Pyrophosphate for Selective Oxidation of Butane Catalysis Today 1993, 16, 61-67

[99] C J Kiely, G J Hutchings Adventures with vanadium phosphate catalysts: Reflections on a long standing collaboration with J C Volta Applied Catalysis 2007, 325, 194-197

[100] E A Lombardo et al The Effect of Preparation Methods and Activation Strategies upon the Catalytic Behavior of the Vanadium-Phosphorus Oxides Catalysis Today 1992, 15, 407-418

[101] R M Contractor et al Butane Oxidation to Maleic Anhydride over Vanadium Phosphate Catalysts Catalysis Today 1987, 1, 49-58

[102] J S Buchanan et al Pretreatment and Activation of a Vanadium Phosphate Catalyst for Butane Oxidation to Maleic Anhydride Applied Catalysis 1985, 19, 65-75

[103] BK Hodnett Comparison of Models for n-Butane Oxidation to Maleic Anhydride over Vanadium Phosphorus Oxide Catalysts Catalysis Today 1993, 16, 131-138

[104] N Hiyoshi et al Selective oxidation of n-butane over novel V-P-O/silica-composites prepared through intercalation and exfoliation of layered precursor Studies in Surfaces and Catalysis 2000, 130, 175-1720

[105] MO Guerrero-Pérez, JM Rosas, R López-Medina, MA Bañares, J Rodríguez-Mirasol, T Cordero Lignocellulosic-derived catalysts for the selective oxidation of propane Catalysis Communications 2011, 12, 989-992

[106] MO Guerrero-Pérez, JM Rosas, R López-Medina, MA Bañares, J Rodríguez-Mirasol, T Cordero On the Nature of Surface Vanadium Oxide Species on Carbons Journal of Physical Chemistry 2012, 116, 20396-20403

[107] MO Guerrero-Pérez, MJ Valero-Romero, S Hernández, JM López Nieto, J Rodríguez-Mirasol, T Cordero Lignocellulosic-derived mesoporous materials: An answer to manufacturing non-expensive catalysts useful for the biorefinery processes Catalysis Today 2012, 195, 155-161

[108] MJ Valero-Romero, A Cabrera-Molina, MO Guerrero-Pérez, J Rodríguez-Mirasol, T Cordero. Carbon materials as template for the preparation of mixed oxides with controlled morphology and porous structure Catalysis Today 2014, 227, 233-241

[109] IE Wachs, K Routray Catalysis Science of Bulk Mixed Oxides ACS Catal 2012, 2, 1235-1246

[110] S Cheng, D Yan, JT Chen, RF Zhuo, JJ Feng, HJ Li, HT Feng, PX Yan, J Soft-Template Synthesis and Characterization of ZnO2 and ZnO Hollow Spheres PhysChem C 113 2009, 113, 13630-13635

[111] X-L Li, T-J- Lou, X-M Sun, Y-D Li Highly sensitive WO_3 hollow-sphere gas sensors, Inorg Chem 2004, 43, 5442

[112] D Zhang, L Qi, J Ma, H Cheng Adv Mater Synthesis of Submicrometer-Sized Hollow Silver Spheres in Mixed Polymer–Surfactant Solutions 2002, 14, 1499-1502

[113] Y Chang, JJ Teo, HC Zeng Formation of colloidal CuO nanocrystallites and their spherical aggregation and reductive transformation to hollow Cu_2O nanospheres Langmuir 2005, 21, 1074-1079

[114] NS Ramgir, DJ Late, AB Bhise, MA More, IS Mulla, DS Joag, K Vijayamohanan ZnO multipods, submicron wires, and spherical structures and their unique field emission behavio J Phys Chem 2006, 110, 18236-18242

[115] MM Titirici, M Antonietti, A Thomas A generalized synthesis of metal oxide hollow spheres using a hydrothermal approach Chemistry of Materials 2006, 18, 3808-3812

[116] M E Davis Ordered porous materials for emerging applications Nature 2002, 417, 813-821

[117] VV Guliants y JH Lin Colloidal synthesis and characterization of alumina-supported Cu/Ni core-shell nanoparticles in water gas-shift reaction Applied Catalysis A: General, 2012, 445–446, 187-194

[118] D Farrusseng, A Julbe, M Lopez, C Guizard Investigation of sol–gel methods for the synthesis of VPO membrane materials adapted to the partial oxidation of n-butane Catalysis Today, 2000, 56, 211-220

[119] A Dong, N Ren et al General synthesis of mesoporous spheres of metal oxides and phosphates Journal American Chemistry Society 2003, 125, 4976-4977

[120] M Kang, D Kim, SH Yi y JU Han Preparation of stable mesoporous inorganic oxides via nano-replication technique Catalysis Today 2004, 695, 93-95

[121] AH Lu, A Taguchi et al Hollow Mesoporous Silica Fibers: Tubules by Coils of Tubules Angew Chem Int Ed 2002, 41, 3489

[122] MM Titirici, M Antonietti Chemistry and materials options of sustainable carbon materials made by hydrothermal carbonization Chemical Society Reviews 2010, 39(1), 103-116

[123] M Ohmori y E Matijevic Preparation and properties of uniform coated colloidal particles VII Silica on hematite Journal of Colloid Interface Science 1992, 150, 594-598

[124] DL Wilcox et al Hollow and Solid Spheres and Microspheres: Science and Technology Associated with their Fabrication and Applications Materials Research Society, Pittsburgh 1995, 372

Chapter 2

Role of surface phosphorus complexes on the oxidation of porous carbons

Abstract Chemical activation of olive stone with phosphoric acid produces activated carbons with a relatively high content of phosphorus groups that remain very stable on the carbon surface at relatively high temperatures. Changes in the surface chemistry of phosphoric acid activated carbon after subjecting it to thermal treatments in oxidizing and inert conditions were studied by different techniques, including temperature-programmed desorption (TPD) and X-ray photoelectron spectroscopy (XPS). TPD and XPS results point out that P surface groups preferentially reacts with oxygen, prior to carbon gasification, through the oxidation of C-P bond to C-O-P ones, which are thermally stable at temperatures lower than 750 ºC. At higher temperatures, these C-O-PO_3 type surface groups decompose under thermal treatment to less oxygenated phosphorus groups on the carbon surface (probably C-PO_3 type) generating CO (and CO_2). These C-PO_3 type surface groups seem to be very reactive and are reoxidized upon contact with air, even at room temperature, forming again C-O-PO_3 type groups. Thus, the presence of these oxygen-containing phosphorus surface groups with an interesting redox functionality of high chemical and thermal stability seems to be responsible of the high oxygen content and oxidation resistance of this type of porous carbons.

Keywords: Activated carbons, temperature-programmed desorption, phosphorus-containing carbons, phosphorus surface groups, oxidation resistance, redox functionality, TPD, XPS.

1. Introduction

Porous carbon materials have attracted considerable attention because of their interesting applications in many fields, such as catalysis, gas and liquid phase adsorption and gas and energy storage. These carbon materials can be prepared from different low-cost and abundant carbonaceous precursors, such as agricultural wastes and by-products. Consequently, there is a great research effort in this direction [1-3]. The possibility of tailoring both the pore structure and the surface chemistry is an additional advantage that promotes them as suitable catalysts supports or as catalysts by themselves [4].

The nature and concentration of functional groups on the surface of the carbon material has a significant influence on the catalyst performance, since this groups act as anchoring sites for the active phase in the preparation of supported catalysts or they can even be the active sites for specific catalytic reactions. Oxygen functional groups are the most important in this context, as they can be formed spontaneously by exposure to the atmosphere or can be further generated or modified by oxidative and thermal treatments. In order to fix oxygen surface groups (OSG), the activated carbons are usually treated with oxidizing agents in liquid phase ($(NH_4)_2S_2O_8$, HNO_3, H_2O_2) [5-7] and also in the gas phase (O_2, O_3, N_2O, and HNO_3 vapor) [8-11]. These methods usually results in the fixation of a certain amount of oxygen surface complexes, such as carboxylic and lactonic acid groups, in a relatively high concentration. However, these surface acid groups show a low to moderate thermal stability and, in addition, such treatments may cause the destruction of the pore structure of the carbon material or produce high carbon burn-off under certain conditions. In fact, this is the main limitation of the use of activated carbon as catalysts or as catalytic supports, since they would gasify to CO_2 (and CO) when they are used in reactions involving oxidizing conditions above 250 ºC. Thus, the oxidation resistance enhancement of activated carbons is critical to avoid operation limitations on some of their applications in catalysis.

Activation of lignocellulosic materials with phosphoric acid is a well-established method for the preparation of activated carbons with a relatively large amount of phosphorus surface complexes of very high thermal stability that confer to the activated carbons high surface acidity and oxidation resistance, increasing the possibilities of these materials for applications in catalysis [2,12,13]. In previous works, we have

shown that these acid carbons are very active for 2-propanol, 2-butanol and ethanol decomposition reactions yielding mainly dehydration products [14-16]. The results reported show that the presence of oxygen in the reaction atmosphere not only leads to a significant enhancement of alcohol conversions, but also inhibits catalyst deactivation and allows steady state conditions to be reached. In addition to its use as solid acid catalyst, redox functionality has been incorporated by impregnation of these phosphorus containing activated carbons with vanadium species, obtaining a bifunctional catalyst that is active for hydrocarbon partial oxidation reactions [17-19]. The use of phosphoric acid activated carbons as catalysts or as catalysts supports for toluene oxidation [20], decomposition of H_2O_2 [21] and for the catalytic oxidative desulfuration of diesel [22] have also been reported. Oxygen plays a key role not only in all these catalytic processes, but also in the catalyst performance, since the carbon surface chemistry is modified during the reactions involving oxidizing conditions. Recent investigations have also showed that the use of air instead of argon during thermal treatment enhanced the cation exchange properties of these materials, which made them useful for the removal of heavy metals from aqueous solutions [23].

Much information is available concerning the pore structure [2,3,24-26] and surface chemistry [2, 27-30] of phosphoric acid activated carbons. The use of this activation agent produces activated carbons with well-developed porous structure that together with their high cation exchange capacity makes them useful materials for applications as adsorbents [23,31-33]. Regarding the surface chemistry, the studies of phosphoric acid activated carbons by FTIR, XPS and solid-state NMR methods pointed out that the remaining phosphorus over the surface of the carbon is most likely in form of C-O-PO_3, C-PO_3 groups. These phosphorus surface groups are directly generated during the preparation process under specific conditions and, as already mentioned, remain very stable on the carbon surface at relatively high temperatures, which represents an advantage over other complex surface coating/doping methods. However, their surface chemistry evolution under inert and oxidizing conditions is less well understood. Furthermore, some discrepancies are found in the literature associated to the chemical state and stability of the surface P in phosphorus-containing carbons. Some authors based on both experimental data and theoretical calculations proposed that C-O-P bond presents a relatively high thermal stability [34,35]. Other authors argued that this surface group would not be strong enough to survive at high temperature and proposed

C-P-O bonding as an alternative structure [30,36]. In addition to this, enrichment of surface oxygen groups of phosphoric acid activated carbons has been observed in most of the above mentioned works, when the carbons were prepared at relatively high temperatures or were treated to high temperatures under inert conditions. In this sense, it would be of interest to study whether surface re-oxidation may take place on this type of activated carbon during different storage conditions.

The main purpose of the present work is to study the role of the phosphorus surface groups of activated carbons prepared by activation of biomass (olive stone) with phosphoric acid on the carbon surface oxidation and reduction reactions. For that, an extensive study of the oxygen and phosphorus surface complexes evolution before and after thermal treatments in air and inert atmosphere of the activated carbons has been carried out using temperature-programmed desorption (TPD) and X-ray photoelectron spectroscopy (XPS). As a baseline, an activated carbon with similar textural characteristics, but without surface phosphorus group, was also prepared by physical activation of olive stone by CO_2 partial gasification at the same temperature.

2. Experimental Section

2.1. Activated carbons preparation

Two different activated carbons (with and without phosphorous) were prepared through different pathways: chemical activation with phosphoric acid and physical activation by partial gasification with CO_2, in a conventional laboratory tubular furnace. Olive stone waste (provided by Sca Coop. And. Olivarera y Frutera San Isidro, Periana (Málaga)) was used, in both cases, as carbonaceous precursor. The olive stone waste was cleaned with deionized water, dried at 100 ºC, and ground with a roller mill to obtain samples of 400–800 μm particle size. For the chemical activation process, the raw material was impregnated with concentrated commercial H_3PO_4 (85 wt.%, Sigma Aldrich) at room temperature, with a weight ratio of 2/1 (H_3PO_4 /olive stone) and dried for 24 h at 60 °C. The impregnated samples were activated at 800 ºC under continuous N_2 (purity 99.999%, Air Liquide) flow (150 cm^3 STP/min) in a conventional tubular furnace. The activation temperature was reached at a heating rate of 10 °C/min and maintained for 2 h. The activated sample was cooled inside the furnace under the same N_2 flow and then washed with distilled water at 60 °C until neutral pH and negative

phosphate analysis in the eluate [37]. The resulting activated carbon, denoted by ACP2800, was dried at 60 °C and, then, grinded and sieved (100-300 μm).

For the physical activation process, a procedure described previously by our research group was followed [1,38], in which the gasification conditions, i.e. gasification temperature and reaction time, as well as the particle sizes, were set in order to warrant chemical reaction control to achieve a carbon burn-off value of around 55%. An olive stone char was obtained by carbonization of the same carbon precursor under N_2 flow at 800 ºC. This char was heated under N_2 atmosphere to the gasification temperature (800 ºC). Then, the gas feed was switched to CO_2 (99.998%, Air Liquide) with a flow rate of 150 cm^3 STP/min for 7 h. The resulting activated carbon was denoted by ACG800.

2.2. Thermogravimetric analysis

Thermogravimetric analysis (TG) were performed in a CI Electronics MK2 balance under air flow (150 cm^3 STP/min) from room temperature to 900 ºC at a heating rate of 10 ºC/min, with a sample weight of about 10 mg.

2.3. Porous texture characterization

The porous structure of the samples was characterized by N_2 adsorption–desorption at -196 ºC and by CO_2 adsorption at 0 ºC, using an ASAP 2020 apparatus (Micromeritics). Samples were previously out-gassed at 50 torr for 8 h, at 150 ºC. From the N_2 adsorption/desorption isotherm, the apparent surface area (A_{BET}) was determined from the BET equation [39]. The micropore volume (V_{DR}) was obtained by the Dubinin–Radushkevich (DR) method applied to the CO_2 and N_2 adsorption isotherms [40]. The mesopore volume (V_{mes}) was determined as the difference between the adsorbed volume of N_2 at a relative pressure of 0.95 and the micropore volume (V_{DR}), covering only the pore sizes between 2 and 40 nm, according to the Kelvin equation [41].

2.4. Surface chemistry characterization and elemental composition

Ultimate analysis of the carbons was carried out in a Leco CHNS-932 system, being the oxygen content calculated by difference. The total amount of P was analyzed by inductively coupled plasma optical emission spectrometry (ICPOES).

The surface chemistry of the samples was analyzed by X-ray photoelectron spectroscopy (XPS) using a 5700C model Physical Electronics apparatus with MgKα radiation (1253.6 eV). For the analysis of the XPS peaks, the C_{1s} peak position was set at 284.5 eV and used as reference to locate the other peaks position. The deconvolution of the peaks was done using Gaussian-Lorentzian curves and a Shirley type background line. The difference between experimental and calculated curves was minimized by least-squares.

The surface chemistry of the samples were also analyzed by temperature-programmed desorption (TPD) experiments. TPD profiles were obtained in a customized quartz fixed-bed reactor placed inside an electrical furnace and coupled to a mass spectrometer (Pfeiffer Omnistar GSD-301) and to non-dispersive infrared (NDIR) gas analyzers (Siemens ULTRAMAT 22) in order to quantify CO, CO_2, H_2 and H_2O. In these experiments, 100 mg of the sample was heated from room temperature to 930 °C at a heating rate of 10 °C/min in nitrogen (purity 99.999%, Air Liquide) flow (200 cm^3 STP/min). The absence of any leak was carefully checked before each experiment and the samples submitted to this thermal treatment were denoted by -TT. Once the maximum temperature was reached during the first TPD analysis, the samples were cooled down to room temperature and in some experiments, without any exposure to air during all the experiment, it was heated again up to 930 ºC (-TT2). This experiment was repeated during a third TPD (-TT3) in an attempt to determine the amounts of oxygen surface complexes that remains on the surface of the thermal-treated samples and to elucidate their chemical nature and thermal stability.

XPS and TPD analysis were also carried out in order to characterize the OSG of the carbon catalyst generated after oxidations in air (purity 99.999%, Air Liquide) at different temperatures. The samples were heated from room temperature up to 120, 180, 240, 325 and 350 ºC at a heating rate of 10 ºC/min in nitrogen flow (200 cm^3 STP/min) that was changed to air when the chosen temperature was reached and maintain for 2 h. After these 2 hours of experiment, the gas inlet was again changed to nitrogen until all the oxygen was evacuated from the reactor and lines (followed by mass spectroscopy). Finally, the temperature was raised again up to 930 ºC in N_2 flow. The samples submitted to air oxidation were denoted by -OT, where T is the air oxidation temperature.

The total acidity and acid strength distribution of the catalysts were determined by adsorption and temperature-programmed desorption of ammonia. The NH_3-TPD was performed using 100 mg of catalysts saturated with NH_3 (20% vol in Helium) at 100ºC. After saturation, the NH_3 weakly adsorbed was desorbed in a He flow at the adsorption temperature, until no NH_3 was detected in the outlet gas. The TPD was performed by raising the temperature up to 500 ºC at a heating rate of 10 ºC/min. Outlet NH_3 concentrations were measured by mass spectroscopy (Pfeiffer Vacuum, OmniStar model).

3. Results and discussion

3.1. Characterization of the original activated carbons

Table 1 summarizes the yield and the porous structure parameters of the original activated carbons. The activated carbon obtained by gasification with CO_2, ACG800, shows very low yield (13.5 %, after carbonization and partial gasification). However, the activated carbon prepared by chemical activation with H_3PO_4 at the same temperature, ACP2800, presents a yield value of 38.7%, which is similar to those obtained under similar conditions with other biomass residues [2,29,42]. The activation agent restricts the formation of tars and volatiles during the carbonization process, thus increasing the yield of the remaining solid product [43].

Both activated carbons show higher DR micropore volume values when N_2 is used instead of CO_2 as the adsorbate gas, which indicates the presence of a wide microporous structure [44]. The phosphoric acid activated carbon, ACP2800, present higher values of BET surface area and mesopore volume, which confirm that phosphoric acid activation presents a significant contribution on mesoporosity. The activated carbon ACG800, obtained by physical activation, presents a similar surface area, but in this case, the volume of mesopores is lower.

The elemental composition and characterization of the surface chemistry of the activated carbons are shown in Table 2. The main elements found on the surface of the phosphoric acid activated carbons are carbon and oxygen, with lower amounts of phosphorus. Nitrogen was also detected, but at very low concentrations, probably being a remnant of nitrogen originally present in the carbon precursor. Phosphoric acid

appears to activate olive stone through the formation of phosphate and polyphosphate bridges that crosslink biopolymer fragments, avoiding the contraction of the structure by pyrolysis. Part of the activating agent is removed during the washing step, leading to a carbon matrix in an expanded state with an accessible and broader porous structure [2,12]. However, part of the P is retained in the structure during the activation procedure and seems to be stably bonded to carbon because they do not elute after the washing step. The maximum amount of phosphorus surface groups that are introduced into carbon structure during the activation process is attained at 700-800 ºC, according to previous works [2,3,16,29]. Suárez-García et al. [45] reported that higher activation temperatures results in a decrease of the phosphorus content due to volatilization of phosphorus compounds, most probably in the form of polyphosphoric acid or phosphorus pentoxide. The mass surface concentration of phosphorus determined by XPS (3.5 % wt) is similar to that obtained by ICP (3.7 % wt), indicating that phosphorus complexes are well distributed overall the carbon particles. No other inorganic elements were detected on the surface of ACP2800, as they are removed by the phosphoric acid activation treatment. On the other hand, the ACG800 surface is composed mostly by carbon and oxygen. Other mineral components like sodium, calcium and potasium, which are very effective catalysts of gasification reactions [13] and were originally present in the carbon precursor in very low amount, were removed to a large extent after a washing step, being present in quantity lower than 1%. In fact, the ash content reported in Table 2 and obtained from the weight of the ultimate solid residue, determined after exposure to air-TG at 900 ºC, is very low for ACG800 sample, 0.3%. In the case of phosphoric acid activated carbons, the main inorganic constituent of the activated carbon ashes is phosphorus, in form of P_2O_5, as revealed by XPS analysis (not shown).

Table 1. Yields and porous structural parameters values of the activated carbons.

	Yield	**N_2 isotherm**			**CO_2 isotherm**	
Sample	**(%)**	**A_{BET} (m^2/g)**	**V_{DR} (cm^3/g)**	**V_{mes} (cm^3/g)**	**A_{DR} (m^2/g)**	**V_{DR} (cm^3/g)**
ACG800	13.5	1355	0.570	0.064	870	0.349
ACP2800	38.7	1380	0.514	0.654	662	0.265

Table 2. Ash values, elemental composition and surface chemistry characterization (XPS) of the activated carbons.

	Ash	Elemental Analysis (% wt.)					XPS (% wt.)		
Sample	**(%)**	**C**	**O**	**H**	**N**	**S**	**C_{1s}**	**O_{1s}**	**P_{2p}**
ACG800	0.3	92.2	6.1	1.2	0.5	0.1	91.8	6.9	-
ACP2800	6.0	79.8	12.5	1.4	0.3	0.0	87.1	9.2	3.5

The elemental composition of activated carbons is also shown in Table 2. A very interesting feature observed here is that ACP2800 carbon contains a considerable amount of oxygen (12.5 %wt.), despite having been activated in an inert atmosphere (N_2). The oxygen content in phosphoric acid activated carbons has also shown to reach a maximum for samples activated at 700-800 ºC and decreases at higher temperatures, in parallelism with the phosphorus content [2,3,16,29], which might suggest that incorporation of oxygen to the carbon surface is related to the P surface content.

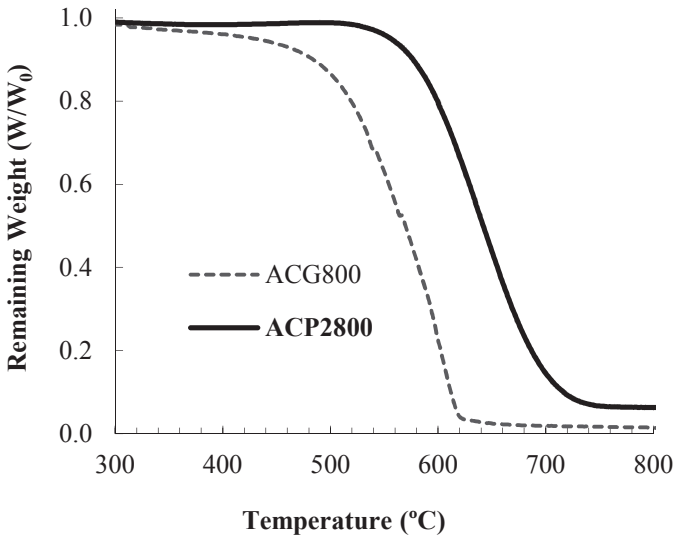

Figure 1. Non-isothermal oxidation resistance profiles (10ºC/min) of the ACG800 and ACP2800 activated carbons.

Figure 1 shows the thermogravimetric analysis profiles in air for the different activated carbons. ACP2800 carbon despite having similar BET surface area and higher

mesopore volume than ACG800 is resistant to air oxidation up to 550 ºC, whereas ACG800 carbon starts to lose weight at about 350 ºC. Therefore, chemical activation with phosphoric acid seems to affect the oxidation behaviour of the produced carbon (probably by modification of the carbon surface available for oxidation). Further discussion regarding the surface oxidation evolution with temperature of the phosphoric acid activated carbon ACP2800 and its chemical characterization are detailed in section 3.2.

Information about the chemical nature of oxygen surface groups (OSG) present in the activated carbons is obtained by analysing XPS and TPD profiles. The P_{2p} spectrum for ACP2800 (Figure 2a) shows a band with a main peak at a binding energy of about 133.7 eV, which is characteristic of pentavalent tetracoordinated phosphorus (PO_4) as in phosphates and/or polyphosphates [28,29]. This broad band can be deconvoluted in different doublets with an area ratio of 0.5 and a distance between peaks of 0.84 eV. Wu and Radovic assigned the peak at a binding energy about 134.0 eV to C-O-P type bonds [30], in where the P atom is bonded to four O atoms by one double bond and three single bonds, such as in C-O-PO_3 groups. These authors suggested that these groups could be in the form of numerous cross-linked structures attached to the carbon surface. Thus, $(C\text{-}O)_2PO_2$ and/or $(C\text{-}O)_3PO$ could also be formed on the surface of the carbon [46]. Wu and Radovic also attribute a binding energy of about 133.6 eV to C-P bonding as in C-PO_3 groups [30], where P is bonded to one C and three O atoms (two single and one double bonds). In this case, two of these O atoms (with single bond P-O) may also be bonding to C atoms, like in C-O-P. Lower values of binding energy (132.0 eV) can be associated to C_2PO_2 and/or C_3PO groups [30,46,47]. Finally, a low intensity doublet peak with the main peak centered at around 131.0 eV may be ascribed to C_3P groups [48]. The XPS P2p results for ACP2800 seem to indicate the presence of mainly C-PO_3 (46.9 %) and C-O-PO_3 (31.7 %) type groups on the activated carbon surface. The O1s spectrum of ACP2800 sample (Figure 2b) shows a high contribution for oxygen at a binding energy of 532.6 eV, which is characteristic of single bonded oxygen in C-OH, C-O-C and/or C-O-P linkages. Compared to ACG800, the O1s spectrum for ACP2800 shows a more pronounce shoulder at lower binding energies, characteristic of C=O and/or P=O groups (BE = 530.9 eV). A binding energy of 535.5 eV is related to chemisorbed oxygen and/or water [49].

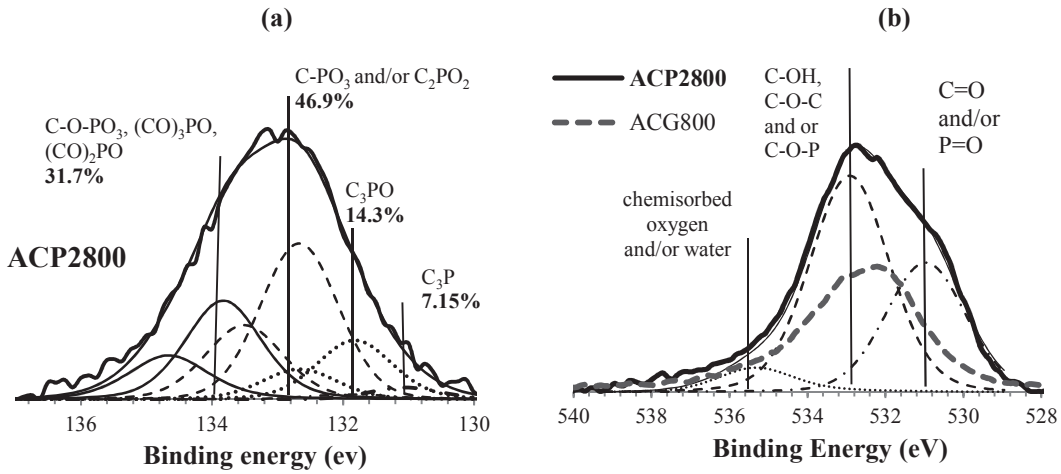

Figure 2. Representative XPS spectra (P2p region) of ACP2800 showing the deconvolution (a). O1s normalized XPS spectra of ACG800 and ACP2800 showing its deconvolution (b).

Carbon-oxygen groups of acidic character (carboxylic, lactonic) evolve as CO_2 upon thermal decomposition in a typical TPD analysis, whereas non acidic (carbonyl, ether, quinone and phenol) evolve as CO. Anydride surface groups evolve as both CO and CO_2 [8,50]. According to previous studies, phenols evolve as CO between 600-700 ºC [8,51,52], ether groups at around 700 ºC, carbonyls between 800-900 ºC and more stable chromenes or pyrone groups have also been reported to evolve as CO at around 1000 ºC [53,54].

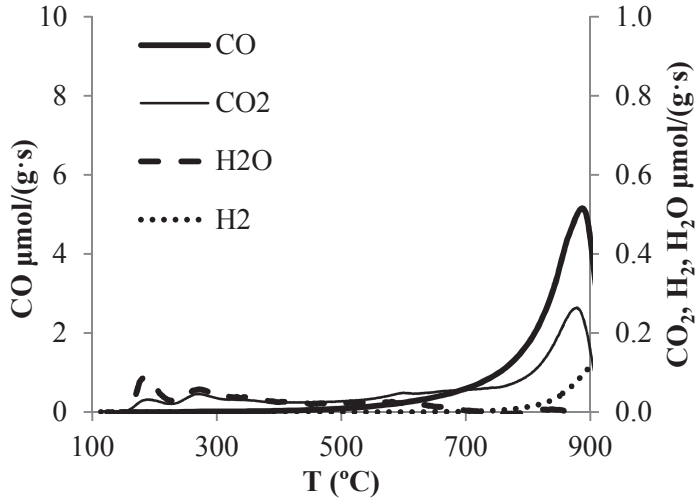

Figure 3. Amount of CO, CO_2, H_2O and H_2 evolved with temperature during the TPD performed to ACP2800.

Figure 3 shows the evolution with temperature of CO, CO_2, H_2O and H_2 during the TPD for ACP2800. Figures 4 a and b present the DTP profiles for ACG800. The TPD profile of ACP2800 (Figure 3) shows a significant CO evolution at temperatures higher than 750 ºC that presents a maximum at 860 ºC, which has been previously assigned to the decomposition of stable C–O–P bonds of C-O-PO_3 surface groups, producing C-PO_3 groups [2,30]. On the other hand, the CO_2 profile shows very low amount desorbed in comparison to that of CO, indicating a lower presence of carboxyl, lactonic and anhydride groups on this sample. The washing step performed after the chemical activation process could have introduced some of these OSG of low thermal stability. The relatively higher amount of CO_2 that evolves at temperatures higher to 750 ºC, associated to the peak of CO at those temperatures, is probably due to decomposition of stable O=C–O–P groups [39], although secondary reactions between the CO released at these temperatures and the OSG, cannot be disregarded [55].

The H_2O profile of the TPD for ACP2800 sample shows a peak at 150 ºC that corresponds mainly to physisorbed water, while a second desorption peak at 270 ºC can be associated to dehydration of two neighboring carboxylic groups. Besides, the absence of water desorbed at high temperatures indicates the lack of phenol groups on the surface of this sample, suggesting a high dehydration state reached by the phosphoric acid activation at a temperature of 800 ºC. There is also some H_2 release starting at 800 ºC, probably as a consequence of both aromatic condensation and the dehydrogenation of the acid phosphates C-O-PO_3 groups (or C-PO_3) that contains one or two OH) on the carbon surface. In the last case, generation of C-O-PO_2-O-C and/or C-O-$PO(OC)_2$ (or C-PO_2-O-C and/or C-$PO(OC)_2$) type surface groups might occur, if dehydrogenation of one or two OH of the phosphate group takes place, respectively, followed by the brakeage of the C-O-P bonds at higher temperatures (from 800 to 950 ºC), forming finally C_3PO type surface groups. Similar results have been observed for activated carbons obtained by chemical activation with phosphoric acid of different raw materials [46].

The main peak on the CO profile for ACG800 carbon (Figure 4a) is located at about 850 ºC and may be associated to carbonyl/quinone or esthers groups. Besides, the shoulder at 270 ºC and the large tail of the CO_2 profile between 350-650 ºC indicated the presence of anhydrides and lactonic groups (Figure 4b). The small amount of CO_2

that evolves at temperatures above 800 ºC is, probably, a result of secondary reactions between the CO and the OSG, as we commented before.

The amount of oxygen evolved during the TPDs for both carbons have been calculated from the total amounts of CO and CO_2 desorbed. The results are 6.0 and 7.2 wt. % of oxygen for ACG800 and ACP2800, respectively. Comparison of these results with those for the elemental composition, showed in Table 2, indicates that most of the oxygen on sample ACG has been desorbed as CO and CO_2 during the TPD up to 930 ºC, whereas ACP2800 still retains a relatively high amount of oxygen groups of higher thermal stability after the TPD experiment.

A second (-TT) and a third (-TT2) TPD experiments were performed immediately after the first one on ACG800 and ACP2800 activated carbons, without exposure to ambient air, in order to elucidate the thermal stability of the OSG (Figure 4). The results obtained showed a small but constant presence of CO at high temperatures (860 °C) and almost not evolution of CO_2 and H_2 (data not shown), which was associated to decomposition of C-O-PO_3 type groups. Different hypothesis must be examined in order to explain this behaviour.

The option that residual O_2 in the N_2 flow may re-oxidate the carbon surface could be disregarded given that subsequent TPD from ACG800 carbon showed that most of the oxygen complexes were desorbed as CO and CO_2 during the first TPD up to 930 ºC (Figure 4a-b). For the second TPD run, ACG800-TT, the amount of oxygen evolved became negligible (0.5 %wt. of O) and only residual CO-evolving groups were detected at high temperature. These results seem to indicate that there was not a significant re-oxidation of the carbon surface by nitrogen impurities (H_2O and O_2 contents below 3 ppm) or, even, by CO_2 evolved during the first TPD. Vivo-Vilche et al. [56] reported that re-oxidation of the carbon surface by CO_2 desorbed only takes place during thermal treatments below 700 ºC, based on experimental evidences. Theoretical studies on this question have also been made using different approaches (density functional theories or computational chemistry calculations) [57,58].

Other possibility is that remaining CO-evolving groups of very high thermal stability may show some degree of mobility on the carbon surface when the temperature is going down during the TPD experiment and move to previously generated free sites producing OSG of lower thermal stability that decompose as CO during the successive

TPDs. Experimental evidences of mobility of CO and CO_2-evolving groups has been previously reported [51,56].

The total oxygen content evolved from the sample was calculated from the total amounts of CO and CO_2 desorbed during the successive TPDs. The oxygen content for ACP2800 is 10.4% wt., which is slightly lower than the amount obtained by the elemental analysis (Table 2), supporting the fact that mobility of oxygen from CO-evolving oxygen groups of higher thermal stability may produce the oxidation of C-P to C-O-P type group, producing CO at ca. 860 ºC during successive TPDs.

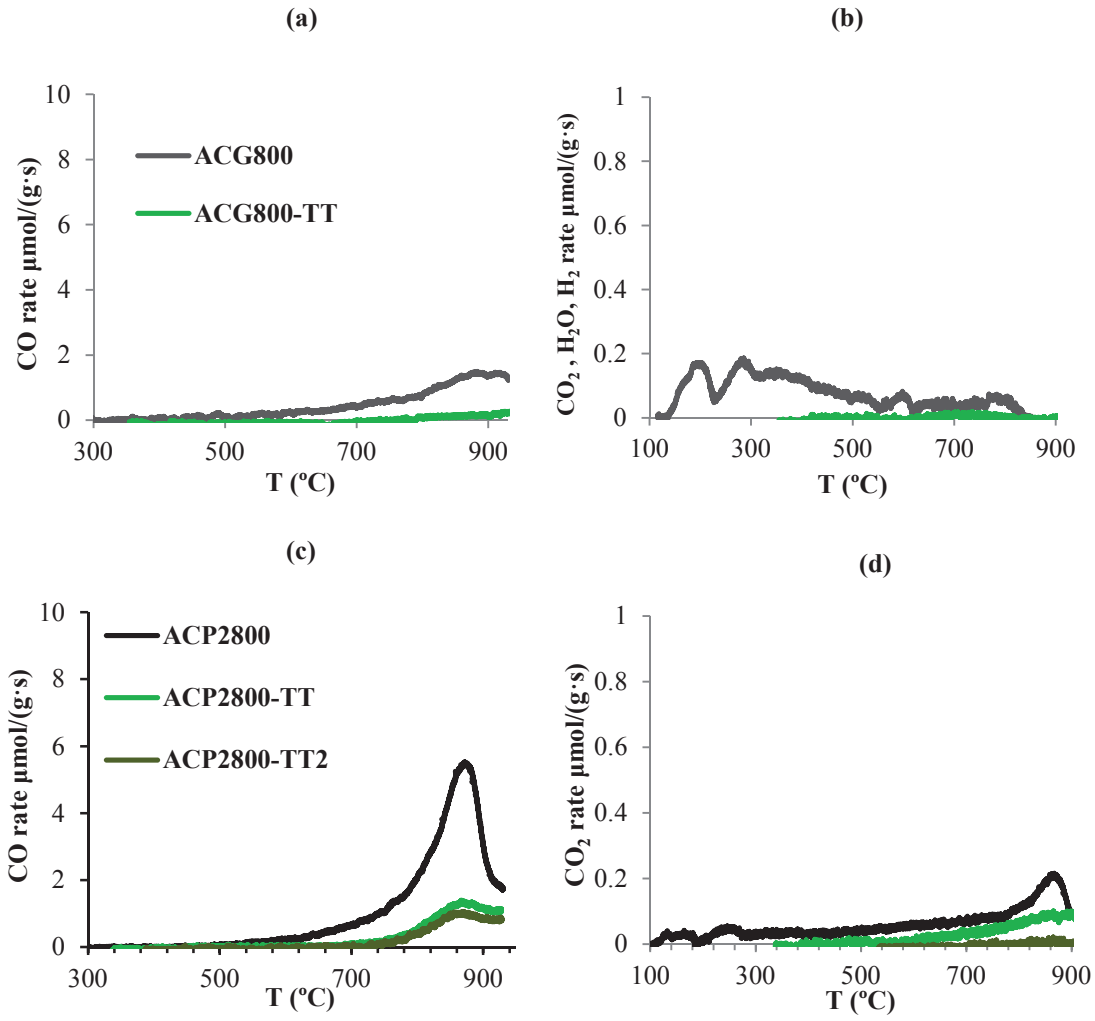

Figure 4. Amount of CO and CO_2 evolved with temperature during consecutive TPDs performed to ACG800 (a-b) and ACP2800 carbon (c-d), respectively.

3.2. Oxidation of activated carbons

The interest on improving the oxidation resistance of carbon materials by introduction of different kinds of surface groups is clear from the large number of research papers on this subject. Nevertheless, this is a matter under continuous discussion due to their inherent complexity. Phosphorus shows an important oxidation inhibition effect, observed in carbon impregnated with different compounds, such as organo-phophorus compounds [35], $POCl_3$ [59] or H_3PO_4 [59,60]. We should emphasize here that in our case the surface phosphorus groups are directly generated during the preparation process under specific conditions and seem to be strongly bonded to the carbon surface. The phosphorus complexes could be probably located at the edges of carbon crystallites, stabilizing the carbon active sites, which become less reactive for the oxidation reaction, as occurs when carbon materials are doped with phophorus [30,59,61,62]. Nevertheless, they could also act as a physical barrier, blocking the access of oxygen to the active sites.

To investigate the oxidation evolution of the carbon surface, the activated carbons were oxidized in air at different temperatures (between 120-350 ºC) for 2 h and then characterized in situ by TPD. It is interesting to mention that ACP2800 is resistant to gasification in air, with no significant weight loss observed during 2 h at 350 ºC. However, ACG800 produces a carbon burn-off of about 20 %wt. after air oxidation at 350 ºC for 2 h. Figure 5 shows the resulting CO and CO_2 evolution profiles during the TPD of the oxidized samples.

The TPD results after air oxidation at different temperatures evidence that oxidation of the phosphoric acid-activated carbon (ACP2800) at temperatures lower than 300 ºC increases significantly only the amount of CO evolved at about 860 ºC, accompanied by a small evolution of CO_2 at the same temperature, suggesting that oxidation of the carbon surface takes place through the oxidation of C-P surface bond, generating C-O-P bond that are thermally stable up to 800 ºC. At higher oxidation temperatures (325 and 350 ºC), the desorption of CO (CO_2) at high temperature (860 ºC) seems to keep constant, which suggests that the surface P groups are completely oxidized and other oxygen surface complexes, thermally less stable, are formed, decomposing as CO and CO_2 at lower temperatures (~700 ºC for CO and ~500 and 700 ºC for CO_2).

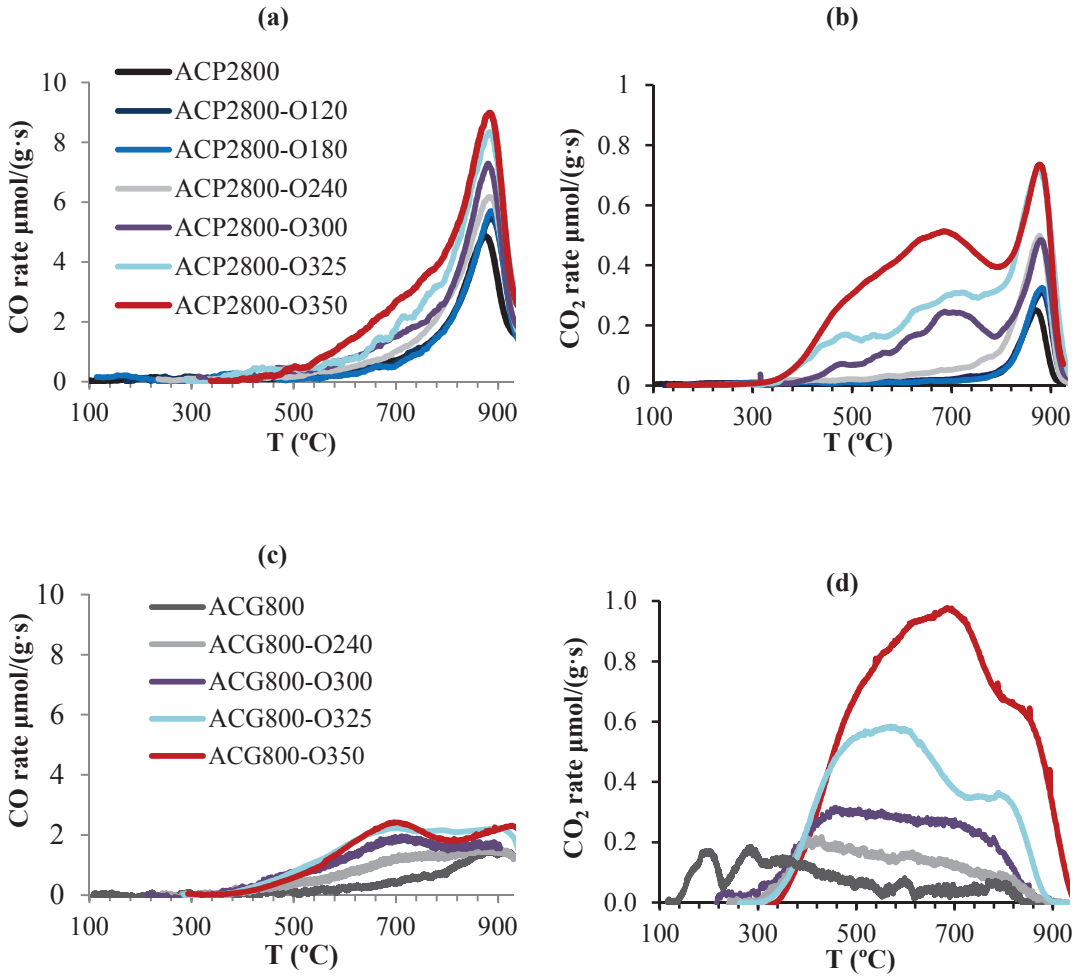

Figure 5. Amount of CO and CO_2 evolved with temperature during the TPD experiments of ACP2800 (a and b) and ACG800 (c and d) after air oxidation at different temperatures (120, 180, 240, 300, 325 and 350 ºC) for 2h.

Oxidation of ACG800 activated carbon that contains no surface P groups causes a more pronounce increase in the evolution of CO_2 (and CO) at low temperatures (400-500 ºC), compared to that of ACP2800, indicating that oxidation of this sample takes place preferentially on the carbon surface, generating OSG of lower thermal stability. Two broad peaks are found in the CO_2 profiles of ACP2800 and ACG800samples (Figures 5 b and d). The low temperature peak (c.a. 500 ºC for ACP2800 and 450 ºC for ACG800) could be attributed to decomposition of lactone groups and the higher temperature peak (c.a. 700 ºC) can be originated from the more stable anhydride groups, which decompose to CO_2 and CO. Oxidation at low temperature seems to preferentially form lactone type surface groups on the surface of ACG800 and anhydride ones on the

surface of ACP2800, increasing the amount of both surface oxygen groups with oxidation temperature, especially for ACG800, which is a typical behavior previously observed for other oxidized carbon materials. Otake and Jenkings [63] showed that oxidation temperature is a very important factor in determining the type of CO_2-evolving complex formed on a carbon surface. They found that chars air-oxidized above 325 ºC presented mainly carboxyl anhydrides groups, whereas lower air-oxidized temperatures generated mainly carboxylic acids. Gomez-Serrano et al. [64] reported that activation temperatures as low as 250 ºC favored the formation of lactonic structures to a large extent.

The results showed above suggest that in the case of phosphoric acid activated carbons oxygen reacts preferentially with the phosphorus surface groups through the oxidation of C-PO_3 groups to C-O-PO_3 ones, of high thermal stability. Only when the P surface groups seem to be completely oxidized, oxidation of the carbon surface starts to be significant, generating OSG of less thermal stability. On the other hand, oxidation of ACG800, with no P surfaces groups, generates OSG of lower thermal stability. This result may be of great interest to explain the effect of P surface groups on the enhancement of carbon oxidation resistance.

There is some controversy in the literature about the chemical nature and stability of phosphorus-containing carbons. In a classic paper, Mckee et al. [34] suggested that the C-P-O bonds are not very stable at high temperatures. Oh and Rodriguez proposed an alternative configuration of the bond, C-P-O, based on the formation of pπ–dπ bond by overlapping p orbitals between P and O. Simultaneously, $2p_z$ orbital of carbon interacts with a d_{xz} orbital of phosphorus to form a dπ–pπ orbital. They suggested that this type of bonding in which P=O groups is replacing two edge carbon atoms would be thermally stable to high temperatures [36]. Lee and Radovic analyzed the stability of C-O-P and C-P-O bonding in the context of oxidation inhibition of carbon materials [35]. Using quantum mechanical modelling, they showed that the structure with C-O-P bonding is more stable and able to survive longer than the structure with C-P-O bonding. This was later supported by Puziy et al. [27,28] based on IR, XPS and P-NMR methods, since high thermal treated carbons revealed a high contribution of condensed phosphates attached by C-O-P linkage to carbon matrix. Nevertheless, Wu and Radovic [30] observed the same release of CO at high temperatures for P-containing carbons during a TPD as that observed in the present

paper and associated this behavior to the presence of relatively weak C-O-PO_3 groups on the carbon surface at high temperatures. Based on Ab initio molecular orbital calculations they suggested that the O-P bond in the C-O-P system is the weakest one. Thus, when the activation temperature is increased to high temperatures, the formation of C-PO_3 groups, probably, from C-O-PO_3 ones seems to take place [2,30]. Besides, the ab initio results showed that the C-P bond may be more stable than the C-O-P bonds.

To elucidate the chemical nature and stability of phosphorus in phosphorus-containing activated carbons after successive thermal treatments in inert and oxidizing conditions, reduction and re-oxidation of the (phosphorus) surface groups have been studied after subjecting the ACP2800 carbon to successive thermal treatments in N_2 atmosphere up to 900 ºC (-TT) and oxidation at 180 and at 350 ºC for 2h (-O180 or –O350), successively.

TPD profiles of ACP2800 sample subjected to these successive reduction and oxidation treatments are shown in Figure 6. The TPD profile of the sample ACP2800 previously thermal treated in inert atmosphere up to 900 ºC, followed by oxidation in air at 180 ºC for 2 h (ACP2800-TT-O180) overlaps with that for ACP2800-O180, showing that the same OSG (decomposing as CO and CO_2) were formed (Figure 6 a and b). Moreover, at low oxidation temperatures (180 ºC in Figure 6) 2 h of exposition to air flow resulted enough to oxidize the P complexes, given that a similar experiment, but with oxidation at this temperature for 8 h resulted in a TPD profile that overlapped with those of ACP2800-O180 and ACP2800-TT-O180. In a second experiment, ACP2800 was previously subjected to air oxidation, then, it was thermal treated in inert atmosphere and, finally, it was air oxidized again. The TPD profile of this sample, ACP2800-O180-TT-O180, also coincides with the previous ones. These results evidenced that the P surface complexes of this carbon can be reduced and oxidized again and that this behavior is completely reversible, despite the fact that during the reduction/oxidation cycles slight gasification of the carbon surface takes place through the evolution of CO/CO_2 during the TPD experiments (with a total carbon burn-off of 5.3 % wt.). After the thermal treatment in inert atmosphere, the new surface sites generated by CO (and CO_2) release (probably of C-PO_3 type) seem to react with oxygen when exposed to air to regenerate the oxygen-phosphorus (C–O–PO_3) surface groups, indicating the reversibility of these sites on the surface of the activated carbon, which evidences a redox character.

This redox character seems to affect also to the other oxygen surface groups, less thermally stable, in the case that the oxidation temperature is higher than 300 ºC (see Figures 6 c and d for an oxidation temperature of 350 ºC). The carbon burn-off caused during the TPD treatment for ACP2800 oxidized at 350 ºC (ACP2800-O350) was of 10.5 % wt.

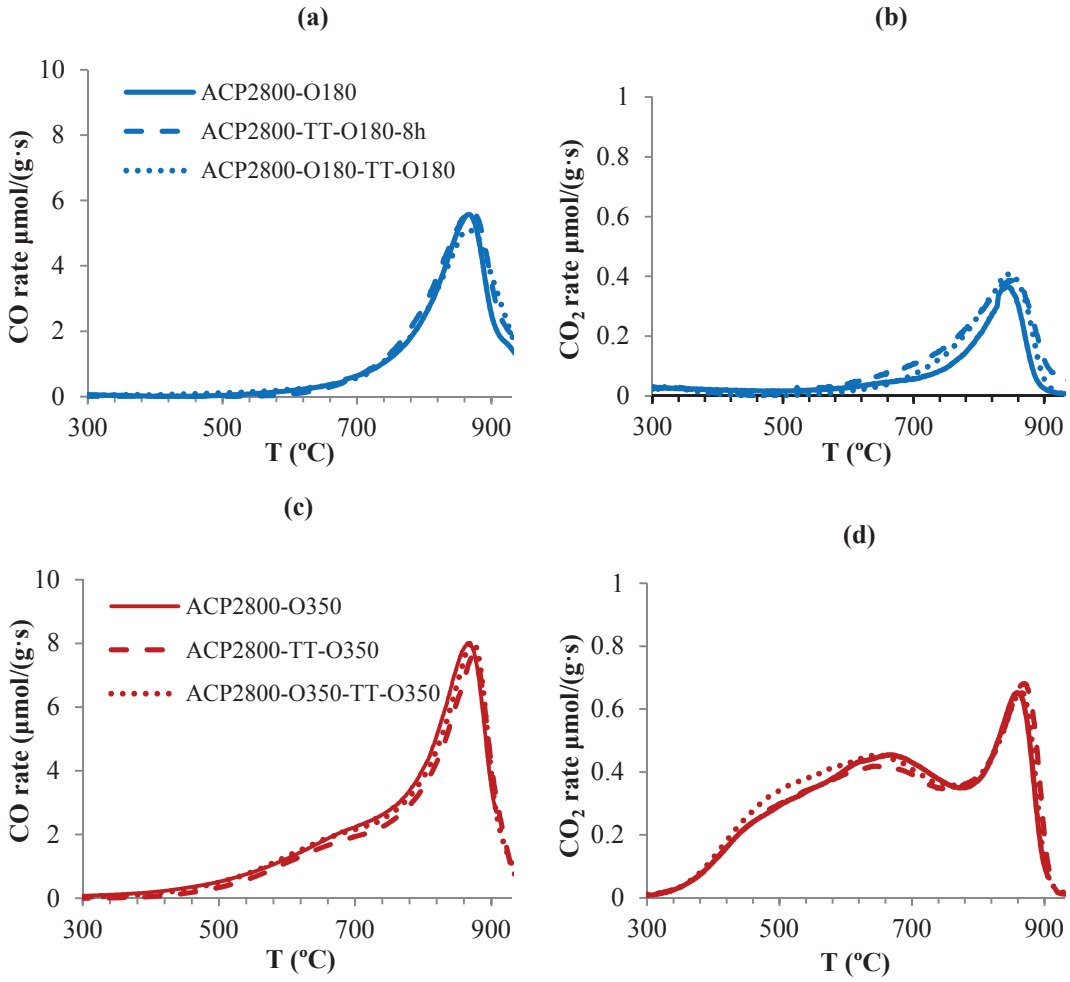

Figure 6. Amount of CO and CO_2 evolved with temperature during the TPD experiment for ACP2800 subjected to oxidations in air at180 ºC (-O180ºC) (a and b) and 350 ºC (-O350C) (c and d) and thermal treatments in inert atmosphere at 900 ºC (-TT).

It is well known that the carbon surface heat treated at high temperatures in N_2 is not stable and may re-adsorb oxygen even at room temperature [65]. Re-oxidation of the phosphoric acid activated carbons at room temperature may also take place during air storage taking into account the high concentration of free sites, highly reactive and

susceptible to be re-oxidized. It must be said, that after the TPD the ACP2800 carbon showed a self-heating effect upon contact with air after cooling down to room temperature, also observed by others authors [29]. Thus, it is suggested that new C-O-PO_3 groups could be generated on heat treated samples in inert atmosphere after exposure to air and storage at room temperature. For this reason, ACP2800 subjected to a thermal treatment in nitrogen at 900 ºC was exposed to air flow at 20 ºC for 2h. This sample was denoted as ACP2800-TT-O20. Figure 7 shows the CO and CO_2 TPD profiles for ACP2800-TT-O20. As a baseline, the TPD for ACP2800-TT without exposure to air flow is also presented. The TPD results for ACP2800-TT-O20 evidence desorption of CO at high temperatures in the same temperature range as that observed for the original activated carbon and for the oxidized sample to different temperatures, confirming the regeneration of the C-O-P type groups, even by oxidation at room temperature. These results would explain the large amount of oxygen left in all phosphoric acid activated carbons prepared or heated at high temperatures [2,27,29,30], and also that the surface chemistry of these thermally treated carbons could change during storage. In this sense, the original activated carbon, ACP2800, would correspond to that oxidize to 60 ºC (ACP2800-O60) since after the activation process it was exposed to ambient air, followed by a washing step and dried under static air overnight at 60 ºC in a conventional oven.

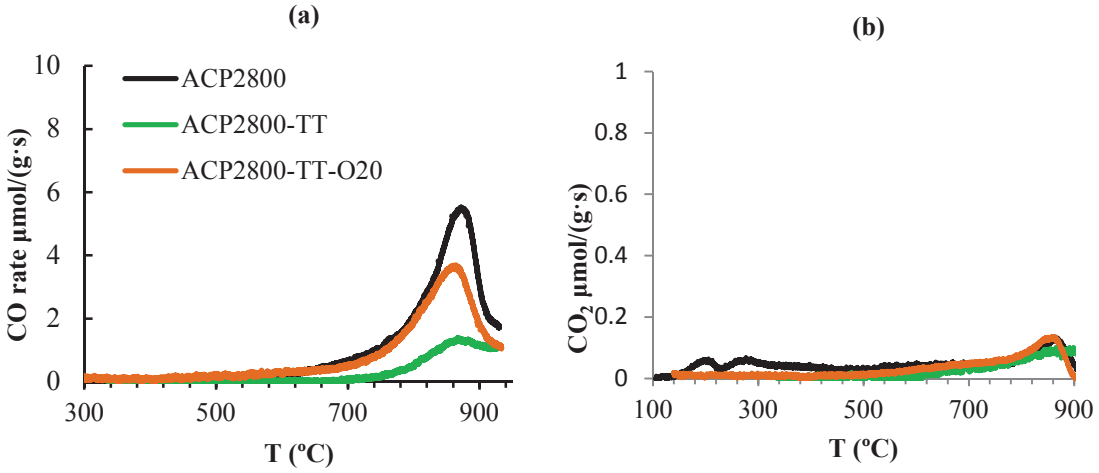

Figure 7. Amount of CO (a) and CO_2 (b) evolved with temperature during the TPD of ACP2800 and ACP2800-TT without exposure to air and that of ACP2800 submitted to a thermal treatment at 900º C, followed by oxidation in air at 20 ºC for 1 h (ACP2800-TT-O20).

In line with these observations, P2p spectra of ACP2800 and the corresponding treated samples are presented in Figure 8. As a general observation, it can be stated that there are not big differences among the P2p spectrum for the different samples, despite the fact that ACP2800 has been treated in very drastic different ways, air oxidation treatment at 350 ºC for 2 hours and thermal treatment in inert atmosphere at 900 ºC. After oxidation of ACP2800 at 350 ºC for 2 h (ACP2800-O350) the P2p peak shows a slightly displacement to higher binding energies, which can be associated to the presence of few more polyphosphates groups, of C-O-PO_3, $(CO)_2PO_2$ and $(CO)_3PO$ types, on the surface of the carbon. On the other hand, the thermally treated samples in inert atmosphere (-TT) should present a shift of the binding energy of the maximum of the P2p peak to lower binding energies compared to that for ACP2800, showing a reduction of the most oxygenated phosphorus groups (C-O-PO_3 type) to C-PO_3 ,C_2PO_2 and/or C_3PO type. However, the peaks are positioned at the same binding energies as that of the fresh activated carbon, suggesting that re-oxidation of the C-PO_3 type groups takes place once the samples are exposed to ambient air, before XPS analysis.

Table 3 presents the total amounts of CO and CO_2 released obtained by integration the areas under the TPD peaks and the C, O, and P surface concentrations measured by XPS for the treated samples (see Figure 8). The results obtained for ACP2800 and the derived carbons reveal high surface phosphorus content that is even slightly higher after the different treatments, confirming the high stability of these surface phosphorus complexes generated after the chemical activation of olive stone with H_3PO_4 at 800 ºC. This behaviour was also observed when other biomass were used as raw material for the preparation of activated carbons by chemical activation with phosphoric acid [2,12,32]. It has to be mentioned that the N_2 adsorption-desorption and the CO_2 adsorption results (data not shown) do not show relevant differences in the porous structure of the treated samples when they are compared to the fresh activated carbon, indicating the slightly partial gasification of the ACP2800 carbon during the different oxidation/reduction treatment did not modify the porous structure and specific surface area of this carbon.

From the amount of CO and CO_2 evolved during the TPD experiments, the total oxygen content, O(TPD), was calculated and compared to the surface oxygen content obtained from XPS analysis, O(XPS) (Table 3). Papier et al. [66] indicated that the 80-90% peak area of the O1s peak represents the contribution of surface atoms, or atoms of

the 3.5-4 nm thick outer shell. However, TPD results reveal also oxygen containing groups located on the surface of meso- or/and micropores, deeper in the carbon particle. The amount of oxygen bonded to phosphorus in the activated carbon prepared by chemical activation and the corresponding derived carbons has also been calculated taking into account both characterization techniques: i) from deconvolution of the TPD profile, quantifying the peak evolved at 860 ºC (O-P(TPD)) and ii) from the amount of the different surface phosphorus species obtained from deconvolution of the P2p spectra (O-P(XPS)). From the TPD results, only the amount of oxygen bonded to both a carbon site and a P group (C-O-P) is quantified, since these type of groups seem to decompose to CO (and CO_2) at 860 ºC, as it was previously indicated.

Table 3. Amount of CO and CO_2 evolved from the original and treated activated carbons and the surface chemistry characterization (XPS): total and surface oxygen concentrations.

	TPD				**XPS (%wt.)**			
Sample	**CO** (μmol/g)	**CO_2** (μmol/g)	**O(TPD)[a] % wt.**	**O-P(TPD)[b] % wt.**	**C_{1s}**	**P_{2p}**	**O_{1s}(XPS)[c]**	**O-P(XPS)[d] %**
ACG800	2891	427	6.0	n.a.	91.8	0.0	6.9	n.a.
ACG800-O350	4243	2114	14.2	n.a	89.7	0.0	9.9	n.a
ACG800-TT	270	22	0.5[e]	n.a.	95.6	0.3	3.5	n.a.
ACP2800	3915	305	7.2	5.2	87.2	3.5	9.2	5.0
ACP2800-O350	7357	1295	15.9	8.0	82.8	3.8	12.8	5.8
ACP2800-TT	1018	112	2.0[e]	1.9[e]	89.6	3.6	6.5	4.6
ACP2800-TT-O20	3304	111	5.6	4.0	89.4	3.7	6.6	4.7
ACP2800-TT-O350	6893	1182	14.8	7.7	85.3	4.0	10.4	6.0

[a] Total oxygen from the amounts of CO and CO_2 evolved

[b] Total oxygen bonded to P (as C-O-P) from the amounts of CO and CO_2 evolved at 860 ºC.

[c] Surface oxygen content from XPS measurements. The samples were exposed to ambient air.

[d] Surface oxygen bonded to P from XPS = $P\cdot(4\cdot COPO_3+3\cdot CPO_3+C_3PO)$

[e] not exposed to ambient air

n.a.: not applicable

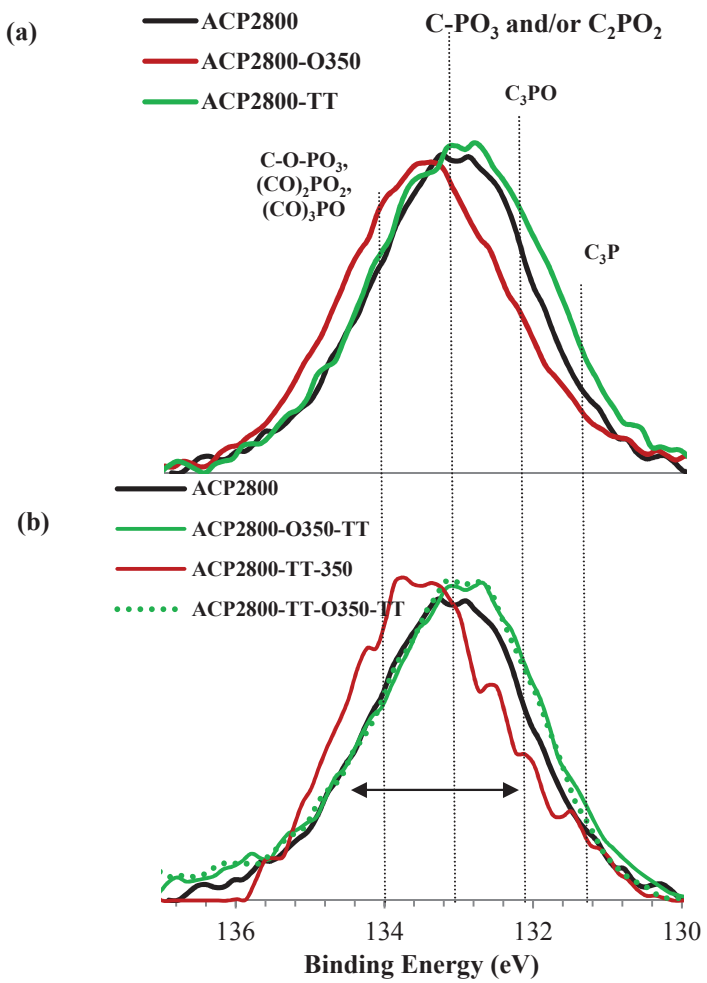

Figure 8. P_{2p} normalized XPS spectra for ACP2800 before and after being subjected to thermal treatments at 900 ºC in inert atmosphere or/and in air atmosphere at 350 ºC for 2 h.

The observed general trend for oxygen surface content on ACG800 and ACP2800 and their corresponding derived carbons was predictable, being lower after the thermal treatment and higher after the oxidation process. However, certain differences can be appreciated between these two carbons. Similar values of O(XPS) and O(TPD) for the fresh ACG800 activated carbon can be observed indicating an homogeneous distribution of oxygen surface groups on the whole particle surface. On the other hand, the high value of O(XPS) compared to that obtained from TPD, O(TPD), for ACP2800, could indicate that a higher proportion of oxygen groups could be concentrated on the external surface of the carbon particles. However, it has to be

pointed out that (and contrary to ACG800 sample) not all the oxygen surface content of this sample is being taking into account during the first TPD experiment, as was shown in Figures 4 c and d. In this sense, the O(TPD) value observed for ACP2800 after the thermal treatment (ACP2800-TT) of 2.0 %wt. represents about 28 % of that for the fresh carbon and this surface oxygen seems to be attached to surface P, given that the value of 1.9 %wt. of O-P(TPD) for this sample represent about 95 % of the O(TPD) value. Thus, successive TPDs become necessary to quantify the total oxygen content O(TPD) for this carbon that contains OSG of very high thermal stability (C-O-PO_3 type).

The relatively high values of O-P(XPS) and O-P(TPD) observed for ACP2800 and its derived carbons compared to their respective total XPS and TPD oxygen amount indicate that most of the oxygen present in the carbon particles seems to be bonded to surface phosphorus. It is also very interesting the fact that the values of O(XPS) and O-P(XPS) for ACP2800 and all the samples derived from it (after thermal treatment or oxidation process) are very similar, respectively (see Table 3). Surprisingly, the values of O(XPS) and O-P(XPS) for ACP2800-TT and ACP2800-TT-O20 are almost identical and very close to those for ACP2800 and ACP2800-TT-O350. It has to be noted that all the samples have been exposed to ambient air after the different treatments, before the XPS analysis was carried out. Thus, as the TPD results indicated, C-PO_3 type surface groups, formed after the thermal treatment in inert atmosphere at 900 ºC, can be oxidized to C-O-PO_3 type surface groups in ambient air, before the XPS analysis. In this sense, ACP2800-TT sample after stored to ambient air would be identical to ACP2800-TT-O20 and, as mentioned before, ACP2800 would be identical to that stored in a stove at 60 ºC.

These results also evidence the redox character of these P surface groups that can be oxidized with molecular oxygen and reduced by thermal treatments in inert atmosphere, restoring the original surface nature of the activated carbon. These results also explain the unexpectedly high oxygen content of different carbons prepared by chemical activation with phosphoric acid after being heat treated to high temperature in inert atmosphere reported in the literature [2,27,29,30]. In those cases, the oxygen content measurement was carried out by elemental analysis, FTIR, XPS, etc., in which the samples were exposed to ambient air before the analysis. In this sense, it is

important to point out that the characterization of these types of carbons should be carried out by an "*in situ"* analysis, without exposing the samples to ambient air.

These carbons were further characterized by adsorption/desorption of NH_3 in order to study the acid character of the carbon surface before and after the different treatment. The NH_3-TPD profiles for ACG800, ACP2800, ACP2800-TT, ACP2800-O350 and ACP2800-TT-O350 samples, after adsorption and desorption of NH_3 at 100 ºC, are compared in Figure 9. ACG800 sample presents an almost negligible desorption of NH_3.On the other hand, the NH_3 desorption profile of ACP2800 shows two maxima, at around 150 and 250 ºC. The first one is known to arise from desorption of weakly adsorbed NH_3 molecules (probably by hydrogen-bonded), identified on zeolite supports [67], although it can also be related to weak acidic groups of C-O-PO_3 type on these carbon materials, since ACP2800-TT-O20, which desorbs a slightly higher amount of NH_3 at this temperatures compared to that of ACP2800-TT, presented a higher amount of oxygen-containing P groups of C-O-PO_3 type, as was showed in Figure 7a. On the other hand, the shoulder at 250 ºC and the large tail at higher temperatures may originate from NH_3 adsorbed on strong Brönsted acid sites [46]. The acidity of this type is, mainly, related to the high amount of phosphorus retained on the carbon surface and probably associated to OH in the phosphates groups. The total surface acidity for ACP2800 increases after air oxidation at 350 ºC, given that a high amount of oxygen-containing P groups of C-O-PO_3 type are formed, as was showed in Figures 5 a and b and Table 3. The thermal treated sample, ACP2800-TT, was not exposed to ambient air before the adsorption of NH_3. This sample desorbed a small amount of CO (and CO_2) at high temperatures in the TPDs experiments (Figures 4 c and d), associated to decomposition of C-O-PO_3 groups, which suggest the presence of a relatively high amount of surface groups of C_2PO_2 and/or C_3PO type that may contribute to the low acidity of this sample, as can be observed in Figure 9. Finally, the similar NH_3-TPD profiles obtained for ACP2800-O350 and ACP2800-TT-O350 samples also confirm the re-generation (re-oxidation) of the carbon surface after thermal treatment in inert atmosphere and the acid character of these oxygen-containing P groups.

The results presented in this work support the conclusions derived from the work of Wu and Radovic [30], in the sense that C-O-PO_3 type surface groups and, specifically, the bridge O atoms play a key role in the carbon oxidation inhibition mechanism. Activated carbons prepared by chemical activation of lignocellulosic

materials with phosphoric acid present oxygen-containing P surface groups of type C-O-PO_3 (that include also CO_2PO_2 and CO_3PO groups). These P surface groups are thermally very stable and decompose only at temperatures higher than 750 ºC, producing CO (and CO_2) in the gas phase and C-PO_3 type surface groups (that may include C_2PO_2 and C_3PO, depending on the treatment temperature), very stable even at 950 ºC, given that P content on the surface of these carbons remains constant or even slightly increases after being treated at this temperature (see Table 3). Oxidation of the carbon surface with molecular oxygen at temperatures lower than 300 ºC takes place through the C-P bond of the later P surface groups type, producing C-O-P bonds; i.e., regenerating the C-O-PO_3 type groups (that may include C_2PO-O-C, C-$PO(OC)_2$ and $(CO)_3PO$ depending on the intensity of the oxidation treatment; although polyphosphate type groups cannot be disregarded) on the surface of the carbon. Only at temperatures higher than 300 ºC, these C-O-P bonds become saturated (all of them of $(CO)_3PO$ type groups) and oxidation of the rest of the carbon surface seems to be possible, with production of oxygen surface groups that are less stable, decomposing at lower temperatures (<700 ºC).

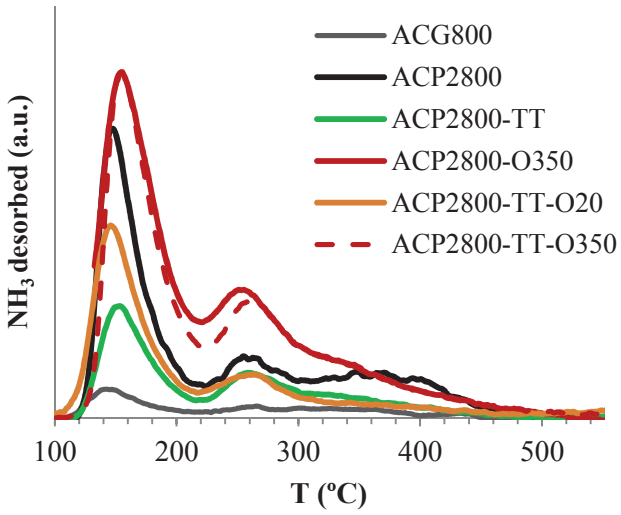

Figure 9. NH_3-TPD profiles of the activated carbons ACG800, ACP2800, ACP2800-O350 ACP2800-TT-O20 and ACP2800-TT-O350 after NH_3 adsorption/desorption at 100 ºC.

As Wu and Radovic [30] suggested, the presence of O bonded to both a carbon site and a P group (C-O-P) is a critical factor for maintaining the inhibition effect of P deposits, because these bonds can be generated at very low temperatures and are not broken at temperatures lower than 750 ºC. Thus, the inhibition effect seems to be, in this case, the result of site blockage. McKee et al [34] indicated that the C-O-PO_3 group's type may occupy a large proportion of the surface of the carbon. In this sense and assuming a cross sectional area of 40 $Å^2$ for these surface groups, a P surface content of 3.5 %wt. would occupy an area of approximately 87 m^2/g, which represents a larch part of the external surface area of ACP2800 (433 m^2/g). On the other hand, TPD and XPS results suggest that P surface groups present a uniform distribution on the carbon surface.

On the other hand, the surface of these activated carbons, with oxygen-containing P groups, should be a strong acceptor of spillover oxygen [68], which would explain the formation of other oxygen groups of low thermal stability on the carbon surface once P surface groups are saturated with oxygen at temperature higher than 300 ºC (see Figure 5). This effect would also explain the role of molecular oxygen in the reaction mechanism of ethanol decomposition on this type of acid carbon, oxidizing and removing the carbon deposited on the surface acid sites, avoiding catalyst deactivation [16].

4. Conclusions

Chemical activation of olive stone with phosphoric acid produces activated carbons with a relatively high content of phosphorus surface groups that remain very stable on the carbon surface at high temperatures. TPD and XPS results point out that P surface groups preferentially reacts with oxygen, prior to carbon gasification, through the oxidation of C-P bond, forming C-O-P ones, which are thermally stable at temperatures lower than 750 ºC. Thermal treatments at higher temperature (about 860 ºC) decompose the C-O-PO_3 type surface groups to less oxygenated phosphorus groups on the carbon surface (of C-PO_3 type) generating CO (and CO_2). These C-PO_3 groups seem to be very reactive and are re-oxidized upon contact with air, even at room temperature, forming again C-O-PO_3 type groups. Thus, the presence of these oxygen-

containing phosphorus surface groups with an interesting redox functionality of high chemical and thermal stability seems to be responsible of the high oxygen content and oxidation resistance of this type of porous carbons.

Acknowledgments

We gratefully thank Junta de Andalucia (P09-FQM-5156) and Spanish Ministry of Economy and Competitiveness (MINECO) and FEDER (Projects CTQ2012-36408) for financial support. M.J.V.R. gratefully thanks MINECO for a FPI fellowship (BES-2010-032213).

References

[1] Tancredi N, Cordero T, Rodríguez-Mirasol J, Rodríguez JJ. CO2 gasification of eucalyptus wood chars. Fuel 1996;75(13):1505–8.

[2] Rosas JM, Bedia J, Rodríguez-Mirasol J, Cordero T. Preparation of hemp-derived activated carbon monoliths.Adsorption of water vapor. Ind Eng Chem Res 2008;47(4):1288–96.

[3] Puzy AM, Poddubnaya OI, Martínez-Alonso A, Suárez-García F, Tascón JMD. Synthetic carbons activated with phosphoric acid III. Carbons prepared in air. Carbon 2003;41:1181-1191.

[4] Rodríguez-Reinoso F. The role of carbon materials in heterogeneous catalysis. Carbon 1998;36(3):159-75.

[5] Moreno-Castilla C, Ferro-García MA, Joly JP, Bautista Toledo I, Carrasco-Marín F, Rivera-Utrilla J. Activated carbon surface modifications by nitric acid, hydrogen peroside, and amonium peroxydisulfate treatments. Langmuir 1995;11(11):4386-92.

[6] Moreno-Castilla C, Lópes-Ramón MV, Carrasco-Marín F. Changes in surface chemistry of activated carbons by oxidation. Carbon 2000;38:1995-2001.

[7] Szymanski GS, Rychlicki G, Terzyk AP. Catalytic conversion of ethanol on carbon catalysts. Carbon 1994;32:265-271

[8] Figueiredo JL, Pereira MFR, Freitas MMA, Órfao JJM. Modification of the surface chemistry of activated carbons. Carbon 1999;37(9): 1379–1389.

[9] Byl O, Liu J, Yates JT. Etching of carbon nanotubes by ozones a surface area study. Langmuir 2005;21:4200–4.

[10] Xia W, Jin C, Kundu S, Muhler M. A highly efficient gas-phase route for the oxygen functionalization of carbon nanotubes based on nitric acid vapor. Carbon 2009;47:919–22.

[11] Gosselink RW, van den Berg R, Xia W, Muhler M, de Jong KP, BitterGas JH. phase oxidation as a tool to introduce oxygen containing groups on metal-loaded carbon nanofibers. Carbon 2012;50:4424-4431.

[12] Rosas JM, Bedia J, Rodríguez-Mirasol J, Cordero T. HEMP-derived activated carbon fibers by chemical activation with phosphoric acid. Fuel 2009;88:19-26.

[13] Rosas JM, Ruiz-Rosas R, Rodríguez-Mirasol J, Cordero T. Kinetic study of the oxidation resistance of phosphorus containing activated carbons. Carbon 2012;50:1523-1537

[14] Bedia J, Rosas JM, Márquez J, Rodríguez-Mirasol J, Cordero T. Preparation and characterization of carbon based acid catalysts for the dehydration of 2-propanol. Carbon 2009;47:286–294.

[15] Bedia J, Ruiz-Rosas R, Rodríguez-Mirasol J, Cordero T. Kinetic study of the decomposition of 2-butanol on carbon-based acid catalyst. AIChE J. 2010;56:1557-1568.

[16] Bedia J, Barrionuevo R, Rodríguez-Mirasol J, Cordero T. Ethanol dehydration to ethylene on acid carbon catalysts. Applied Catalysis B: Environmental 2011;103:302-310.

[17] Guerrero-Pérez MO, Rosas JM, López-Medina R, Bañares MA, Rodríguez-Mirasol J, Cordero T. Lignocellulosic-derived catalysts for the selective oxidation of propane. Catalysis Communications 2011;12(11):989-992.

[18] Guerrero-Pérez MO, Valero-Romero MJ, Hernández S, López Nieto JM, Rodríguez-Mirasol J, Cordero T. Lignocellulosic-derived mesoporous materials: An answer to manufacturing non-expensive catalysts useful for the biorefinery processes. Catalysis Today 2012;195:155-161.

[19] Valero-Romero MJ, Cabrera-Molina A, Guerrero-Pérez MO, Rodríguez-Mirasol J, Cordero T. Carbon materials as template for the preparation of mixed oxides with controlled morphology and porous structure. Catalysis Today 2014;227(15):233-241.

[20] Bedia J, Rosas JM, Rodríguez-Mirasol J, Cordero T. Pd supported on mesoporous activated carbons with high oxidation resistance as catalysts for toluene oxidation. Applied Catalysis B: Environmental 2010;94(1-2):8-18.

[21] Khalil LB, Girgis BS, Tawfik TAM. Decomposition of H2O2 on activated carbon obtained from olive stones. Journal of Chemical Technology and Biotechnology 2001;76(11):1132-1140.

[22] Haw KG, Bakar WA, Ali R, Chong JF, Kadir AAA. Catalytic oxidative desulfurization of diesel utilizing hydrogen peroxide and functionalized-activated carbon in a biphasic diesel-acetonitrile system. Fuel Processing Technology 2010;91(9):1105-1112.

[23] Puziy AM, Poddubnaya OI, Martínez-Alonso A, Castro-Muñiz Alberto, Suárez-García F, Tascón JMD. Oxygen and phosphorus enriched carbons from lignocellulosic material. Carbon 2007;45(10):1941-1950.

[24] Puziy AM, Poddubnaya OI, Martínez-Alonso A, Suárez-García F, Tascón J.M.D. Synthetic carbons activated with phosphoric acid II. Porous structure. Carbon 2002;40:1507–1519.

[25] Girgis BS, El-Hendawy A-NA. Porosity development in activated carbons obtained from date pits under chemical activation with phosphoric acid. Microporous and Mesoporous Materials 2002;52(2):105-117.

[26] Jagtoyen M, Derbyshire F. Some considerations of the origins of porosity in carbons from chemically activated wood. Carbon 1993;31(7):1185-1192.

[27] Puziy AM, Poddubnaya OI, Socha RP, Gurgul J, Wisniewski M. XPS and NMR studies of phosphoric acid activated carbons. Carbon 2008;46: 2113-2123.

[28] Puziy AM, Poddubnaya OI, Ziatdinov AM. On the chemical structure of phosphorus compounds in phosphoric acid-activated carbon. Applied Surface Science 2006;252:8036–8038

[29] Puziy AM, Poddubnaya OI, Martínez-Alonso A, Suárez-García F, Tascón JMD. Surface chemistry of phosphorus-containing carbons of lignocellulosic origin. Carbon 2005;43:2857–2868.

[30] Wu X, Radovic LR. Inhibition of catalytic oxidation of carbon/carbon composites by phosphorus. Carbon 2006;44(1):141-151.

[31] González-Serrano E, Cordero T, Rodríguez-Mirasol J, Cotoruelo L, Rodríguez JJ. Removal of water pollutants with activated carbons prepared from H3PO4 activation of lignin from kraft black liquors. Water Res. 2004;38(13):3043-3050.

[32] Puziy AM, Poddubnaya OI, Martínez-Alonso A, F Suárez-García, Tascón JMD. Synthetic carbons activated with phosphoric acid: I. Surface chemistry and ion binding properties. Carbon 2002:40(9);1493–1505.

[33] Altenor S, Carene B, Emmanuel E, Lambert J, Ehrhardt J-J, Gaspard S. Adsorption studies of methylene blue and phenol onto vetiver rootsactivated carbon prepared by chemical activation. Journal of Hazardous Materials 2009:165(1-3) 1029-1039.

[34] McKee DW, Spiro CL, Lamby EJ. The inhibition of graphite oxidation by phosphorous additives. Carbon 1984;22(3):285–90.

[35] Lee Y-J, Radovic LR. Oxidation inhibition effects of phosphorus and boron in different carbon fabrics. Carbon 2003;41(10):1987–97.

[36] Oh SG, Rodriguez NM. In situ electron microscopy studies of the inhibition of graphite oxidation by phosphorus. J Mater Res 1993;8(11):2879–88.

[37] González-Serrano E, Cordero T, Rodríguez-Mirasol J, Cotoruelo L, Rodríguez JJ. Water Res. 2004;38:3043-3050.

[38] Rodríguez-Mirasol J, Cordero T and Rodríguez JJ. CO2-Reactivity of eucaliptus kraft lignin chars. Carbon 1993;31:53-61.

[39] Brunauer S, Emmett PH, Teller E. Adsorption of gases in multimolecular layers. J Am Chem Soc 1938;60:309-319.

[40] Dubinin MM, Zaverina ED, Radushkevich LV. J Phys Chem 1947;21:1351-1362.

[41] Kaneko K, Ishii C. Superhigh Area Determination of Microporous Solids. Colloids Surf 1992;67(9):203-212.

[42] Vernersson T, Bonelli PR, Cerrella EG, Cukierman AL. Arundodonax cane as a precursor for activated carbons preparation by phosphoric acid activation. Bioresour Technol 2002;83(2):95–104.

[43] Jagtoyen M, Derbyshire F. Activated carbons from Yellow Poplar and White Oak by H3PO4 activation. Carbon 1998;36(7):1085–97.

[44-] Rodríguez-Reinoso F, Molina-Sabio M, González MT. The use of steam and CO2 as activating agents in the preparation of activated carbons. Carbon 1995;33(1):15–23.

[45] F. Suárez-García, S. Villar-Rodil, C. G. Blanco, A. Martíez-Alonso, and J. M. D. Tascón. Effect of Phosphoric Acid on Chemical Transformations during Nomex Pyrolysis. Chem. Mater. 2004;16:2639-2647.

[46] Bedia J, Ruiz-Rosas R, Rodríguez-Mirasol J, Cordero T. A kinetic study of 2-propanol dehydration on carbon acid catalysts. Journal of catalysis 2010;271:33-42.

[47] Moulder JF, Stickle WF, Sobol PE, Bomben KD, in:J. Chastain, R.C. King Jr. (Eds.), Handbook of X-ray Photoelectron Spectroscopy, Physical Electronics Inc. Eden Prairie, MN, 1995, pp. 4872-4875.

[48] Bedia J, Rosas JM, Vera D, Rodríguez-Mirasol J, Cordero T. Isopropanol decomposition on carbon based acid and basic catalysts. Catalysis Today 2010:158;89-96.

[49] D. Briggs, M.P. Seah (Eds.), Practical Surface Analysis, Auger and X-ray Photoelectron Spectroscopy, vol. 1, Wiley, Chichester, UK, 1990.

[50] Zielke U, Huttinger KJ, Hoffman WP. Surface-Oxidized Carbon Fibers: I. Surface Structure and Chemistry. Carbon 1996;34:983-998.

[51] Moreno-CastillaC, Carrasco-Marín F, Maldonado-Hódar FJ, Rivera-UtrillaJ. Effects of non-oxidant and oxidant acid treatments on the surface properties of an activated carbon with very low ash content. Carbon 1998; 36(1-2):145-51.

[52] Marchon B, Carrazza J, Heinemann H, Somorjai GA. TPD and XPS studies of O2, CO2 and H2O adsorption on clean polycristallite graphite. Carbon 1988;26(4):507-14.

[53] Bandosz TJ. in Carbon Materials for Catalysis (eds P. Serp and J. L. Figueiredo), John Wiley & Sons, Inc., Hoboken, NJ, USA. (2008) pp. 45-92, doi: 10.1002/9780470403709.ch2

[54] Montes-Morán MA, Suárez D, Menéndez JA, Fuente E. On the nature of basic sites on carbon surfaces: an overview. Carbon 2004;42(7):1219–25.

[55] Peter J. Hall and Joseph M. Calo. Secondary Interactions upon Thermal Desorption of Surface Oxides from Coal Chars. Energy and Fuels 1989;3:370-376.

[56] Vivo-Vilches JF, Bailón-García E,. Pérez-Cadenas AF, Carrasco-Marín F, Maldonado-Hódar FJ. Tailoring the Surface chemistry and porosity of activated carbons: Evidence of reorganization and mobility of oxygenated Surface groups. Carbon 2014;68:520-530.

[57] Montoya A, Mondragón F, Truong TN. Formation of CO precursors during char gasification with O2, CO2 and H2O. Fuel Process Technol 2002;7778:125–30.

[58] Radovic LR. The mechanism of CO2 chemisorption on zigzag carbon active sites: a computational chemistry study. Carbon 2005;43(5):907–15.

[59] Labruquère S, Pailler R, Naslain R, Desbat B. Oxidation Inhibition of Carbon Fibre Preforms and C/C Composites by H3PO4. J. European Ceramic Society 1998;18(13):1953-1960.

[60] Lu W, Chung DDL. Oxidation protection of carbon materials by acid phosphate impregnation. Carbon 2002;40(8):1249–54.

[61] Wu X, Pantano CGM, Radovic LR. Inhibition of catalytic oxidation by boron and phosphorus. Extended abstracts, the international carbon conference. Lexington, (Kentucky USA): American Carbon Society; 2001. p. 2–33.

[62] Lu W, Chung DDL. Oxidation protection of carbon materials by acid phosphate impregnation. Carbon 2002;40(8):1249–54.

[63] Otake Y, Jenkins RG. Characterization of oxygen-containing surface complexes created on a microporous carbon by air and nitric acid treatment. Carbon 1993;31(1):109–21.

[64] Gómez-Serrano V, Piriz-Almeida F, Durán-Valle CJ, Pastor- Villegas J. Formation of oxygen structures by air activation. A study by FT–IR spectroscopy. Carbon 1999;37:1517–28.

[65] F. Carrasco-Marín, J. Rivera-Utrilla, J.P. Joly and C. Moreno-Castilla. Effects of ageing on the oxygen surface complexes on fa oxidized activated carbon. J. Chem. Soc., Faraday TRasn. 1996;92(15):2779-2782.

[66] Papier E, Lacroix R, Donnet JB, Nanse G, Fioux P. XPS study of the halogenation of carbon black-Part 1. Bromination. Carbon 1994;32(7):1341-58.

[67] N. Katada, H. Igi, J. H. Kim, M. Niwa. Determination of the Acidic Properties of Zeolite by Theoretical Analysis of Temperature-Programmed Desorption of Ammonia Based on Adsorption Equilibrium. J. Phys. Chem. B 1997;101:5969 – 5977.

[68] G. Mul, J.P.A. Neeft, F. Kapteijn, J.A. Moulijn. The formation of carbon surface oxygen complexes by oxygen and ozone. The effect of transition metal oxides Carbon 1998;36:1269–1276.

Chapter 3

On the chemical nature and thermal stability of surface phosphorus groups on carbons by TPD experiments

Abstract Chemical structure and thermal stability of phosphorus groups in two activated carbons prepared by phosphoric acid activation at 500 and 800 ºC were investigated by X-ray photoelectron spectroscopy (XPS) and temperature-programmed desorption experiments (TPD). It has been shown that the activation temperature results in the thermal stabilization of P surface groups (C-O-P type bonds) on the carbon surface. C-O-PO_3 groups (that may include polyphosphates structures) in which the phosphorus is attached to the carbon surface through one oxygen atom and contains one or two OH are most probable on the surface of the carbon prepared at 500 ºC, as revealed the high amount of H_2 desorbed above 500 ºC from this sample, which are thermally stable up to 700 ºC. Treatments at higher temperature increases the less oxygenated phosphorus groups on the carbon surface (probably C_3-PO) generating CO (and CO_2), which upon contact with air re-oxidized forming C-O-P type groups, such as C_2-PO(OC), C-$PO(OC)_2$ and C-O-$PO(OC)_2$, depending on the intensity of the oxidation treatment. These groups have been shown to be thermally more stable and more abundant over the carbons prepared at 800 ºC and those thermal treated up to 900 ºC in N_2 atmosphere. The presence of C-P bonds-surface complexes with redox functionality seems to enhance the oxidation resistance of these types of porous carbons. To the best of our knowledge, the possible phosphate structures and their thermal stability on the surface of different carbons materials prepared by chemical activation with H_3PO_4 of a lignocellulosic precursor are described for the first time.

Keywords: Activated carbons, temperature-programmed desorption, phosphorus, oxidation, thermal stability.

1. Introduction

Phosphoric acid activation is a widely used route for activated carbon production due, mainly, to the possibility of tailoring both, their pore structure and their surface chemistry [1-4]. The use of high impregnation ratios (i.e. phosphoric acid/precursor mass ratio) results in carbons with a wide porous structure and a significant contribution of the mesoporosity [5,6]. Furthermore, this method yields carbons with a relatively high concentration of phosphorus on the carbon surface which confers to the activated carbons high surface acidity and oxidation resistance [7-12].

The studies of phosphoric acid activated carbons by chemical analysis, FTIR spectroscopy, XPS and solid-state NMR methods have shown that the remaining phosphorus over the surface of the carbon is most likely in form of C-O-P and C-P-O type bonds [3,7,13,14,15]. However, their surface chemistry evolution under inert and oxidizing conditions and their thermal stability is less well understood. As far as we know, there is little information available on the thermal stability of surface phosphorus groups on carbons. In a classical paper, Wu and Radovic suggested that the O-P bond in the C-O-P system is the weakest one and may be broken at high temperature leading to the decomposition of CO followed by the formation of C-P-O bonds [7]. On this question, Rosas et al. [3,5] also found the same release of CO at high temperature during TPD experiments performed to phosphoric acid activated carbons prepared from hemp canes and fibers prepared at different chemical activation temperatures (from 350 to 500 ºC).

In an earlier work [10], we evidenced experimentally that the more stable groups seem to be C-PO_3 ones which are very reactive and re-oxidized to C-O-PO_3 type groups, even at room temperature, upon contact with air. The presence of these oxygen-containing phosphorus surface groups with an interesting redox functionality of high chemical and thermal stability seems to be responsible of the high oxygen content and oxidation resistance of this type of porous carbons. Thus, the main objective of the present work is to provide additional insights into the possible phosphate structures (and their thermal stability) on the surface of carbons materials prepared by chemical activation of a lignocellulosic precursor with H_3PO_4 and at different activation temperatures. A comparative study of the carbon surface oxidation and reduction reactions of two activated carbons prepared at 500 and 800 ºC have been also carried

out by using temperature-programmed desorption (TPD) and non-isothermal oxidation (thermogravimetric analysis in Air, TGA) experiments. The carbon surface oxidation results will contribute to clarify the role of the different P surface complexes on the carbon surface oxidation mechanism of this type of porous carbons.

2. Experimental Section

Different activated carbons were prepared by chemical activation with phosphoric acid at different temperatures. Olive stone waste (provided by Sca. Coop. Olivarera and Frutera San Isidro, Periana (Málaga)) was the raw material used for the preparation of the activated carbon. This carbon precursor was impregnated with concentrated commercial H_3PO_4 (85 wt.%, Sigma Aldrich) at room temperature, with a weight ratio of 2/1 (H_3PO_4 /olive stone), and dried for 24 h at 60 °C. The impregnated samples were thermally treated under continuous N_2 (purity 99.999%, Air Liquide) flow (150 cm^3 STP/min) at 350, 500, 650 and 800 ºC. The activation temperature was reached at a heating rate of 10 °C/min and maintained for 2 h. The activated sample was cooled inside the furnace under the same N_2 flow and then washed with distilled water at 60 °C until neutral pH and negative phosphate analysis in the eluate [16]. The resulting activated carbons, denoted by ACP2350, ACP2500, ACP2650 and ACP2800, were dried at 60 °C and grinded and sieved (100-300 μm).

The ultimate analysis of the samples was performed in a Leco CHNS-932 system, being the oxygen content calculated by difference. The ash content of the sample was calculated following the ASTM procedure [17].

Thermogravimetric analyses under air flow (150 cm^3 STP/min) (TGA) were performed in a CI Electronics MK2 balance from room temperature to 900 ºC at a heating rate of 10 ºC/min with a sample weight of about 10 mg.

The porous structure of the samples was characterized by N_2 adsorption–desorption at -196 ºC and by CO_2 adsorption at 0 ºC, using an ASAP 2020 apparatus (Micromeritics). Samples were previously out-gassed at 50 torr for 8 h, at 150 ºC. From the N_2 adsorption/desorption isotherm, the apparent surface area (A_{BET}) was determined from the BET equation [18]. The micropore volume (V_{DR}) was obtained by the Dubinin–Radushkevich (DR) method applied to the CO_2 and N_2 adsorption isotherms

[19]. The mesopore volume (V_{mes}) was determined as the difference between the adsorbed volume of N_2 at a relative pressure of 0.95 and the micropore volume (V_{DR}), covering only the pore sizes between 2 and 40 nm, according to the Kelvin equation [20].

The surface chemistry of the samples was analyzed by X-ray photoelectron spectroscopy (XPS) and temperature programmed desorption (TPD). The XPS analyses of the samples were obtained using a 5700C model Physical Electronics apparatus with MgKα radiation (1253.6 eV). For the analysis of the XPS peaks, the C_{1s} peak position was set at 284.5 eV and used as reference to locate the other peaks. Mass surface concentrations of the samples have been obtained by numerical integration of the peaks. The deconvolution of the peaks was done using Gaussian-Lorentzian curves and a Shirley type background line. The difference between experimental and calculated curves was minimized by least-squares. TPD profiles were obtained in a customized quartz fixed-bed reactor placed inside an electrical furnace and coupled to a mass spectrometer (Pfeiffer Omnistar GSD-301) and to non-dispersive infrared (NDIR) gas analyzers (Siemens ULTRAMAT 22). In these experiments, 100 mg of the sample was heated from room temperature to 900 °C at a heating rate of 10 °C/min in nitrogen (purity 99.999%, Air Liquide) flow (200 cm^3 STP/min). The leak absence was carefully checked before any experiment and the samples submitted to this thermal treatment were denoted by adding -TT.

XPS and TPD analysis were also carried out in order to characterize the oxygen surface groups (OSG) of the carbon catalyst generated after oxidations in air (purity 99.999%, Air Liquide) at different temperatures. The samples were heated from room temperature up to 180, 300 and 350 ºC at a heating rate of 10 ºC/min in nitrogen flow (200 cm^3 STP/min), which was changed to air when the chosen temperature was reached and maintain for 2 h. The gas inlet was again changed to nitrogen until the nitrogen flow was identical at the entry and the exit of the reactor tube (followed by mass spectroscopy). Finally, the temperature was raised again up to 930 ºC. The samples submitted to air oxidation were denoted by -OT, where T is the air oxidation temperature.

3. Results

3.1. Characterization of activated carbons

The evolution of the surface chemistry and the porous structure with the impregnation ratio (R, H_3PO_4/olive stone) and the activation temperature was studied for olive stone in a previous work [21]. In the present paper, the physicochemical properties of two selected activated carbons prepared at activation temperatures of 500 and 800 ºC and an impregnation ratio of R = 2 are presented. In addition, a detailed characterization study of their surface chemistry evolution by XPS and temperature-programmed desorption experiments is carried out. Table 2 shows the physicochemical properties of the activated carbons. Yield values of 48 and 38 % for ACP2500 and ACP2800, respectively, were obtained, similar to those obtained from other biomass natural waste pyrolyzed at comparable temperatures [3,5,22-25] and slightly higher than those reported for olive stone with different activation agents [26-28]. The phosphoric acid limits the formation of tars during the carbonization treatment, increasing the yield of the remaining solid product [29]. Moreover, the yield values decrease slightly with the activation temperature studied, as a consequence of a deeper dehydration of the carbonaceous structure of the precursor. The elemental composition of the activated carbon is also shown in Table 2. Oxygen content was determined by difference. An interesting feature observed is the relatively high oxygen values (ca. 9 % for ACP2500 and 12 % for ACP2800), characteristic in this type of activated carbons, as a result of the incorporation into the carbon matrix formed of the oxygen bound to the phosphorus 15,[30].

The values of the structural parameters, as derived from N_2 adsorption-desorption and CO_2 adsorption isotherms are also shown in Table 1. The values of micropore volume obtained from the N_2 adsorption isotherm, V_{DR}^{N2}, are higher than those obtained from the CO_2 adsorption isotherm, V_{DR}^{CO2}, which is indicative of a wide porous structure [31]. Moreover, the carbons present high values of BET surface area and mesopore volume, which confirms the effect of phosphoric acid activation on the porosity development of lignocellulosic residues. The increase of the activation temperature produces a slightly higher BET surface area and micropore volumes measured by N_2 and CO_2 adsorption isotherms.

Table 1. Porous structure and chemical properties of activated carbons

Ultimate analysis (% d.a.f.)	**ACP2500**	**ACP2800**
C	83.7	79.8
H	3.4	1.4
N	0.1	0.3
O*	9.1	12.5
Surface area and porosity		
N2 adsorption (-196 ºC)		
A_{BET} (m^2/g)	1326	1380
At (m^2/g)	476	433
V_{DR} (cm^3/g)	0.443	0.514
V_{mes} (cm^3/g)	0.724	0.654
CO_2 adsorption (0 ºC)		
A_{DR} (m^2/g)	537	662
V_{DR} (cm^3/g)	0.215	0.265

* *: obtained by difference (100% – C –N –H –S –ash)*

The surface chemistry of the activated carbons has been evaluated by XPS and DTP measurements. Table 2 shows the mass surface concentrations of the most abundant elements as obtained from XPS analyses. The well-known presence of stably bonded phosphorus complexes on the surface of phosphoric acid activated carbons has been previously reported [3,5,30]. This activation method produces the reaction between the acid and some organic species, forming phosphate bridges, which are responsible for connecting and crosslinking the biopolymer fragments [29] and have been proven to remain over the carbon surface after the washing step. The retained phosphorus amount on these samples ranges between 2.3 and 3.6 % wt., which is in line with results obtained for phosphoric acid activated carbons of olive stones and similar lignocellulosic biomass wastes. The amount is slightly higher when the chemical activation proceeds at 800 ºC (ACP2800) what suggests that the increase in the activation temperature results in phosphorus combined in more stable forms with the carbon surface, decreasing the efficiency of the washing step. Furthermore, these surface phosphorus groups are thermally stable, as can be seen from the similar or even higher P amounts detected after the thermal treatment at 900 ºC (ACP2500-TT and ACP2800-TT), confirming the phosphorus groups are strongly bonded to the carbon surface. In addition to phosphorus, the pristine activated carbons have an oxygen rich surface which is mostly due to the presence of phosphorus-containing groups, as we mentioned before. However, the presence of phenolic groups cannot be disregarded,

especially for ACP2500, as we will be shown later on. The thermal treatment cleansed partly the surface oxygen groups, producing a decrease in the surface oxygen amount measured by XPS from 8.2 to 4.3 % wt. and from 9.2 to 6.5 % wt. for ACP2500 and ACP2800, respectively. The relatively high oxygen amount of the thermal treated samples is related to the presence of oxygen bonded to phosphorus groups like in phosphine and phosphonate groups that either are stable even at 900 ºC or to newly formed polyphosphate groups caused by the surface re-oxidation [10].

Table 2. XPS mass surface concentration (%) and P_{2p} deconvolution of the activated carbons before and after the thermal treatment at 900 ºC under N_2.

	XPS (% wt.)			P 2p deconvolution			
Sample	**C_{1s}**	**O_{1s}**	**P_{2p}**	**$(C\text{-}O)_nPO$**	**$C\text{-}PO_3$ and C_2PO_2**	**C_3PO**	**C_3P**
ACP2800	87.1	9.2	3.5	31.7	46.9	14.3	7.1
ACP2800-TT	89.6	6.5	3.6	24.9	43.6	22.8	8.6
ACP2500	89.0	8.2	2.3	54.8	35.2	10.0	0
ACP2500-TT	93.0	4.3	2.5	19.0	38.6	31.1	11.2

P_{2p} region for the pristine and thermal treated activated carbons is represented in Figure 1a, whereas Figure 1b shows the deconvolution of the P_{2p} region for ACP2800 carbon. The phosphorus spectrum was deconvoluted in four doublets with an area ratio of 0.5 and a distance between peaks of 0.84 eV. Wu and Radovic assigned the peak at a binding energy about 134.0 eV to C-O-P type bonds [7], in where the P atom is bonded to four O atoms by one double bond and three single bonds, such as in $C\text{-}O\text{-}PO_3$ groups. These authors suggested that these groups could be in the form of numerous cross-linked structures attached to the carbon surface. Thus, $C\text{-}O\text{-}PO_2(OC)$ and/or $C\text{-}O\text{-}PO(OC)_2$ could also be formed on the surface of the carbon [12]. Scheme 1 summarizes the possible C-O-P and C-P-O bonds formed during the chemical activation and thermal treatment. A binding energy of about 133.2 is characteristic of C-P bonding as in $C\text{-}PO_3$ and/or C_2PO_2 groups [7]. Lower intensity peaks at 132.0 and 131.0 eV is associated to C_3PO [12,7] and C_3P groups [32], respectively. The main peak position was fitted using

a margin of ± 0.2 eV, whilst the full width at medium height (FWMH) was set to 1.4± 0.1 eV. The percentages of each group with respect to total P2p spectrum area are compiled at the last columns of Table 2. It can be seen that the increase of the activation temperature to 800 ºC (ACP2800) results in a shift of the maximum of the P_{2p} peak to lower binding energies, indicating the presence mainly of C-PO_3/C_2PO_2 (47 %) and C-O-PO_3 (31.7 %) type groups on the activated carbon surface, whereas ACP2500 carbon surface is mostly composed of C-O-PO_3 type groups (54.8 %). This behavior has been previously observed for other carbons obtained by chemical activation of biomass waste with phosphoric acid [5,21]. The thermal treatment carried out over ACP2500 leaded to a reduction of C-OPO_3 groups, whilst the same treatment produced a lesser amount of reduced groups when conducted over the ACP2800 sample. In fact, ACP2500-TT and ACP2800-TT present similar binding energies of the maximum of the P_{2p} peak to that obtained for ACP2800 sample. In our earlier work [10], it was evidenced that C-P bonds are very easily reoxidized to C-O-P bonds upon contact with air, even at low temperatures. Thus, the surface re-oxidation after the samples were exposed to ambient air, before XPS analysis, would explain this result and the relatively high oxygen surface concentration of the thermal treated samples, as aforementioned.

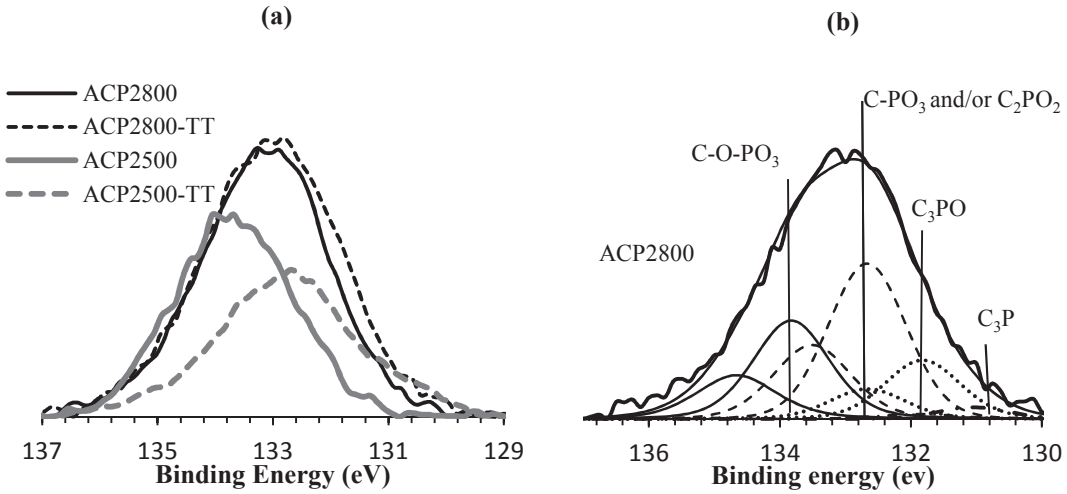

Figure 1. Representative XPS spectra (P2p region) of ACP2800 showing the deconvolution (a) and P_{2p} normalized XPS spectra of the activated carbons and thermal treated samples (b).

Scheme 1. Possible phosphorus surface groups formed during H_3PO_4 activation, as C-O-P and C-P-O bonds.

Possible C-O-P bonds

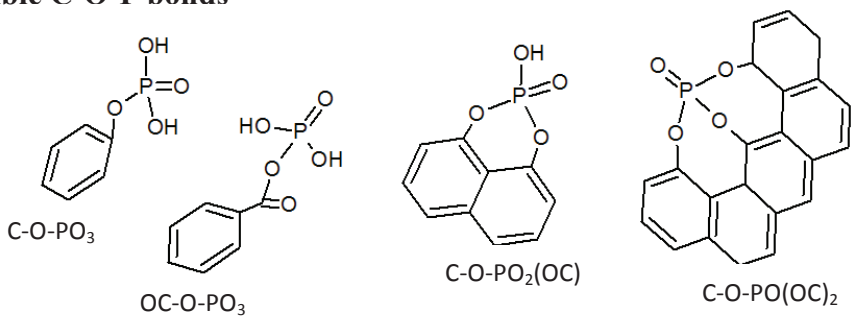

Possible C-P-O bonds

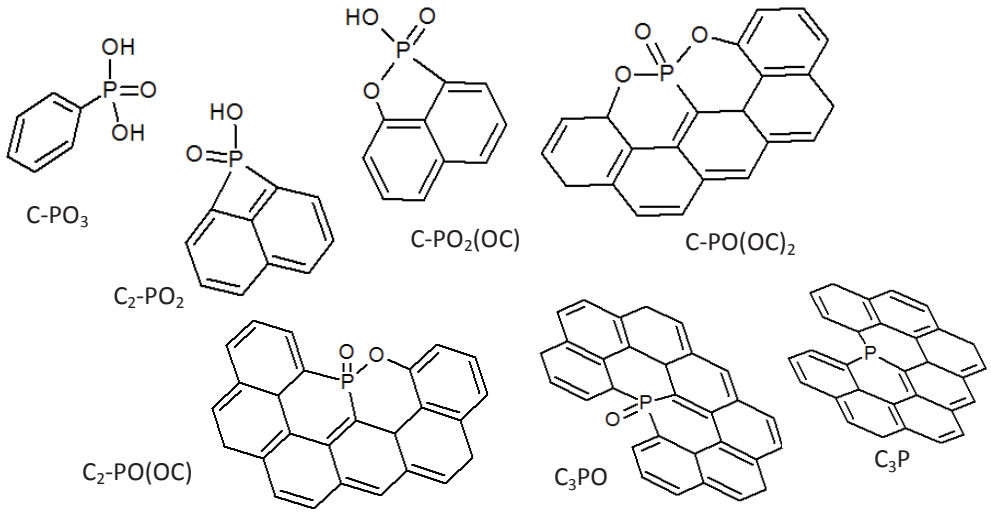

The O1s spectrum for the pristine activated carbons is represented in Figure 2, showing the deconvolution of the O1s region for ACP2800 sample. The O1s spectra of ACP2500 shows a higher contribution for oxygen at a binding energy of 532.6 eV which is characteristic of single bonded oxygen in C-OH, C-O-C and/or C-O-P linkages, whereas ACP2800 O1s spectrum shifts slightly to lower binding energies characteristic of C=O and/or P=O groups (BE = 530.9 eV). A binding energy of 535.5 eV is characteristic of chemisorbed oxygen and/or water [33].

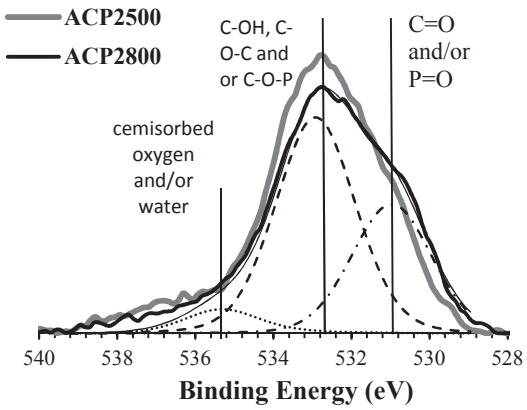

Figure 2. O1s normalized XPS spectra of ACP2500 and ACP2800 showing the deconvolution.

The joint use of XPS and TPD allow a more precise assessment of the surface composition of the activated carbons. TPD technique is recognized as one of the most adequate for identify chemical nature of oxygenated surface groups (OSG), especially those surface oxygen groups that decompose upon thermal treatment producing the evolution of CO and CO_2. According to literature, carbon-oxygen groups of acidic character, such as carboxylic and lactonic, evolve as CO_2 upon thermal decomposition, whereas non acidic, such as carbonyl, ether, quinone and phenol, evolve as CO. Anydride surface groups evolve as both CO and CO_2 [34,35].

Figure 3a and b compares the results of the CO and CO_2 TPD profiles, respectively, for ACP2500 and ACP2800 activated carbons, while the total CO and CO_2 released obtained by integrating the areas under the TPD peaks are reported in Table 3. For comparison, the TPD profiles of two activated carbons prepared at 350 and 650 ºC, which contain 1.9 and 3.2 % wt. of surface P content, respectively, are also included. As can be observed, the activation process results in the thermal stabilization of the oxygen surface groups that evolve as CO. For instance, the main band for the evolution of CO for carbon ACP2500 appears at ~790 ºC. However, the most significant CO evolution for the activated carbon ACP2800 takes place at higher temperatures (~870 ºC), and this change in the thermal stability of the oxygen surface groups that evolve as CO seems to be significant for activation temperatures above 350 °C. Based on the work of Wu and Radovic [7] and on our previous results with olive stone-derived activated carbons [10],

the CO evolution at high temperatures can be related to the formation P-surface groups during the phosphoric acid activation, as relatively weak C–O–PO_3 surface groups on the carbon surface at high temperatures. Therefore, for activated carbons from olive stone, most of the CO evolved at high temperatures, and a lower amount desorbed at temperatures below 700 ºC probably in the form of anhydride, phenol and ether groups. According to previous studies, phenols evolve as CO between 600-700 ºC [34,36,37], ether groups at around 700 ºC, carbonyls and quinone between 800-950 ºC and more stable chromenes or pyrone groups have also been reported to evolve as CO at around 1000 ºC [38,39].

Furthermore, an interesting feature observed in Figure 3 is the increasing evolution in the amount of CO (and CO_2) desorbed at high temperatures (T > 700 ºC), as the activation temperature used for the preparation of the activated carbons increases. This tendency can be due to the higher amount of surface P complexes that decomposes as CO (and CO_2), as indicated by XPS, but also these results may suggest that C-O-PO_2(OC), C-O-$PO(OC)_2$ and C-$PO(OC)_2$) groups, in which the P is bonded to the carbon surface through more than one oxygen, are favourably formed on the surface of phosphoric acid activated carbons prepared at higher activation temperatures.

On the other hand, the CO_2 profiles (Figure 3b) show lower desorbed amounts compared to those for CO, indicating a lower presence of carboxyl, lactonic and anhydride groups. Moreover, the relatively high amount of CO_2 that evolves at the same temperatures that those observed for the maxima release of CO (~790 ºC for ACP2500 and ~860 ºC for ACP2800) is probably as a consequence of decomposition of stable O=C–O–P groups [27] (see Scheme 1). However, secondary reactions between the CO released at these temperatures and the OSG cannot be disregarded [40].

Figure 4 and 5 shows the evolution with temperature of CO, CO_2, H_2O and H_2 during the TPD for ACP2500 and ACP2800, respectively. In addition, a second TPD experiment was performed immediately after the first one on ACP2500 and ACP2800 activated carbons, without exposure to ambient air, in order to elucidate the thermal stability of the OSG. The CO-TPD profiles during the second TPD run (CO-2nd TPD) are also presented (green line).

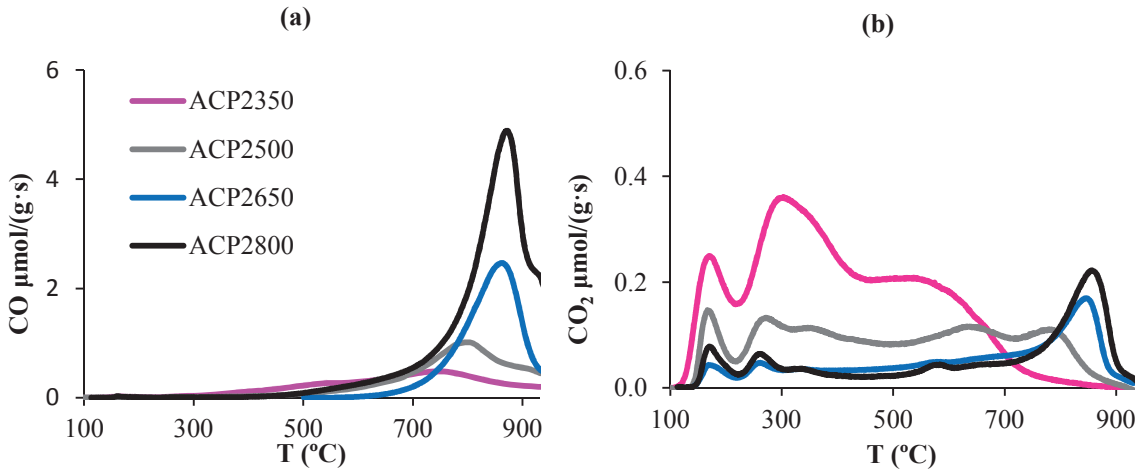

Figure 3. Amount of CO (a) and CO_2 (b) evolved with temperature during the TPD performed to ACP2350, ACP2500, ACP2650 and ACP2800.

As can be observed, the H_2O profile of the TPD for ACP2500 (Figure 4) sample is significantly higher to that observed for ACP2800 carbon (Figure 5), indicating an incomplete dehydration of the phosphoric-impregnated carbon precursor at low activation temperature. The first peak of water desorption at 150 ºC corresponds mainly to the physisorbed water while the second desorption peak at 260 ºC can be associated to the dehydration of two neighboring carboxylic groups. Besides, the coincidence of CO-desorption with the highest peak in the H_2O profile at about 700 ºC indicates a large proportion of phenol groups in this sample. Therefore, it is probably that aqueous solution of phosphoric acid protonates surface C-OH groups through hydrogen bonding during the impregnation step which decomposes to CO at about 700 ºC. Puziy et al. [15] and Fu et al. [41] found that an increase of the activation temperature between 400 and 600 ºC resulted in greater amounts of phenol and ether groups. On the other hand, the absence of water desorbed at high temperatures for ACP2800 sample indicates both, the lack of phenol groups on the surface of this sample and thus the high dehydration state reached by the phosphoric acid activation at a temperature of 800 ºC.

There is also an important H_2 release for ACP2500 which is significantly lower for ACP2800 and both releases coincide with the maximum peak of CO desorption. The desorbed H_2 may be a consequence of both aromatic condensation and the dehydrogenation of the acid phosphates C-O-PO_3 groups (or C-PO_3) that contains one or two OH on the carbon surface. In the last case, generation of C-O-PO_2(OC) and/or C-

O-PO(OC)$_2$ (or C-PO$_2$(OC) and/or C-PO(OC)$_2$) type surface groups might occur, if dehydrogenation of one or two OH of the phosphate group takes place, respectively, followed by the brakeage of the C-O-P bonds at higher temperatures (from 750 to 950 ºC), forming finally C_3PO type surface groups (see Scheme 1). These results are similar to those observed for activated carbons obtained by chemical activation with phosphoric acid of different raw materials [10,27].

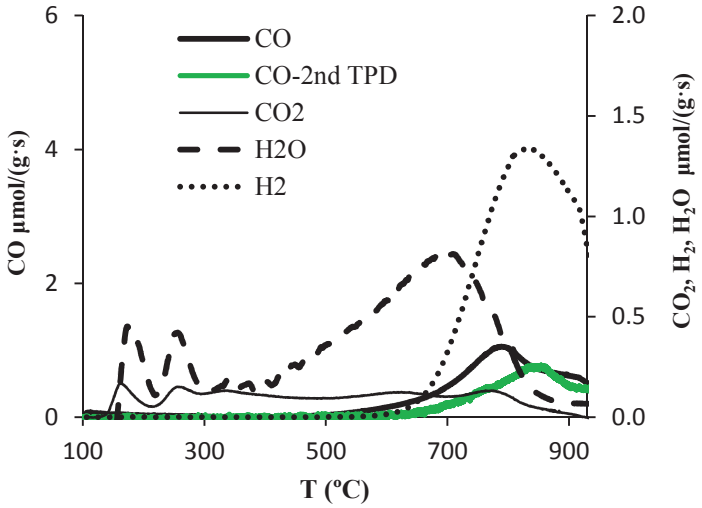

Figure 4. Amount of CO, CO_2, H_2O and H_2 evolved with temperature during the TPD performed to ACP2500 and amount of CO evolved with temperature during a consecutive TPD.

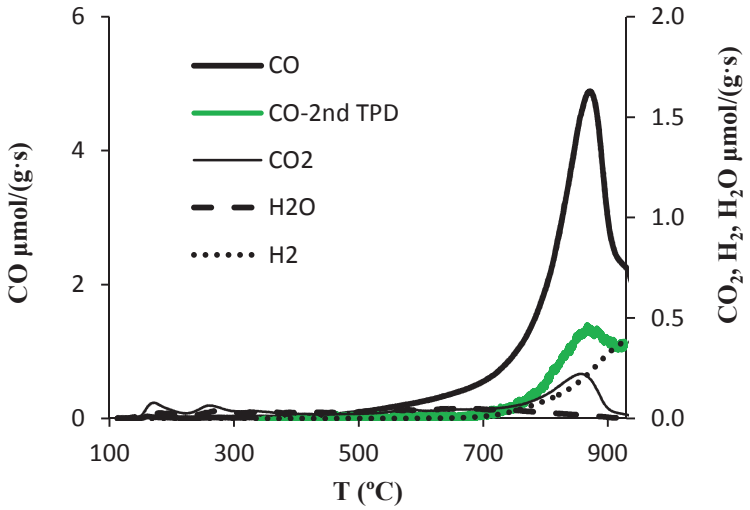

Figure 5. Amount of CO, CO_2, H_2O and H_2 evolved with temperature during the TPD performed to ACP2800 and amount of CO evolved with temperature during a consecutive TPD.

The results obtained during the second TPD for both activated carbons showed a small but constant presence of CO at high temperatures (>800 °C), which was associated to decomposition of C-O-P type bonds, and almost not evolution of CO_2 (>800 °C), H_2 and H_2O (not shown for brevity). According to the literature, remaining CO-evolving groups of very high thermal stability may show some degree of mobility on the carbon surface [10,36,42,]. Thus, when the temperature is going down during the TPD experiment these CO-evolving groups may migrate to previously generated free sites producing OSG of lower thermal stability that decompose as CO during the successive TPDs [10].

A very interesting feature observed during the second TPD run is that the maximum of the CO (and CO_2) TPD profile for ACP2500 sample shifts from 790 to ~860 ºC (see CO-2nd TPD in Figure 4). In contrast, ACP2800 sample during the second TPD run presents the maximum of the CO (and CO_2) peak at 860 ºC (Figure 5), similar to that observed for pristine ACP2800 that had been previously activated at an elevated temperatures (800 ºC). Thus, it is suggested that decomposition of remaining and/or newly formed C_2-PO(OC) and C-PO$(OC)_2$ groups present on the carbon surface after the first TPD run might result again in desorption of CO (and CO_2) at relatively higher temperatures (~860ºC) during the second TPD run for ACP2500 and ACP2800. The presence of these phosphate and polyphosphate linkages of higher thermal stabilities on the selected activated carbon surfaces is quite interesting in order to further explain their surface chemistry evolution under oxidizing conditions.

3.2. Oxidation of activated carbons

Non-isothermal oxidation experiments before and after a thermal treatment up to 900 ºC in inert atmosphere (designed as –TT) were carried out and the results are shown in Figure 6. These figures depict the thermogravimetric analysis profiles in air for ACP2500 (a) and ACP2800 (b). In general, both activated carbons in spite of having high BET surface areas and mesopore volumes are resistant to air oxidation at about 500 ºC for ACP2500 and about 550 ºC for ACP2800. Thus, this result seems to point out that, at least at lower conversions, the higher the phosphorus content, the lower the oxidation rate. Nevertheless, an increase in the carbonization temperature may also produce a certain ordering of the carbon structure, thus increasing the oxidation onset

temperature for ACP2800. According to previous works, activated carbons without phosphorus-containing groups usually start to oxidize significantly below 400 ºC, although it may vary depending on the carbon precursor [43,9,10]. The high oxidation resistant of phosphoric acid activated carbons has been previously reported for activated carbon derived from hemp fibers, lignin and olive stone and was related to the presence of phosphorus groups on the carbon surface [9,10]. It was reported that the phosphorus complexes could act as a physical barrier and/or block the active carbon sites for the oxidation reaction, as occurs when carbon materials are doped with phosphorus [7,8,44-46]. But most recently, based on TGA, XPS and DTP results [9,10] our research group suggested that oxidation of the most reduced phosphorus groups as those where phosphorus is bonded to carbon, C-P, to most oxygenated phosphorus groups, mainly C-O-PO_3, avoids the carbon oxidation and thus retards the gasification of the carbon support. This would explain also the enhanced oxidation resistance observed for ACP2800 with respect to ACP2500, given that higher activation temperatures leads to activated carbons with a higher amount of surface C-P bonds as revealed the XPS results (Table 2). On this question, Figures 6a and 6b also shows the in situ TGA profiles of thermal treated activated carbons ACP2500-TT and ACP2800-TT, respectively. The reduction of the phosphorus groups with the thermal treatment has derived a higher oxidation resistance of the ACP2500 activated carbon, whereas the TGA profile for ACP2800-TT is similar to that obtained for ACP2800. The thermal treatment temperature up to 900 ºC may have produced a certain ordering of the carbon structure, as we mentioned before, thus increasing partly the oxidation onset temperature for ACP2500. However, the slightly mass increase observed in the air-TG profile (Figure 1) for ACP2500-TT from 350 to about 520 ºC, which was not observed for ACP2500, also confirms that the inhibition effect could be caused by the complete oxidation of the C-P phosphorus surface bonds to C-O-P ones.

In order to obtain a more precise assessment of the oxidation state evolution of the carbons surface groups under oxidizing conditions, the activated carbons were oxidized in air at different temperatures (180, 300 and 350 ºC) for 2 h and later characterized by TPD. Figure 7(a-b) and (c-d) shows the resulting CO and CO_2 evolution profiles during the TPDs of the oxidized ACP2500 and ACP2800 samples, respectively, while the total CO and CO_2 releases are also summarized on Table 3.

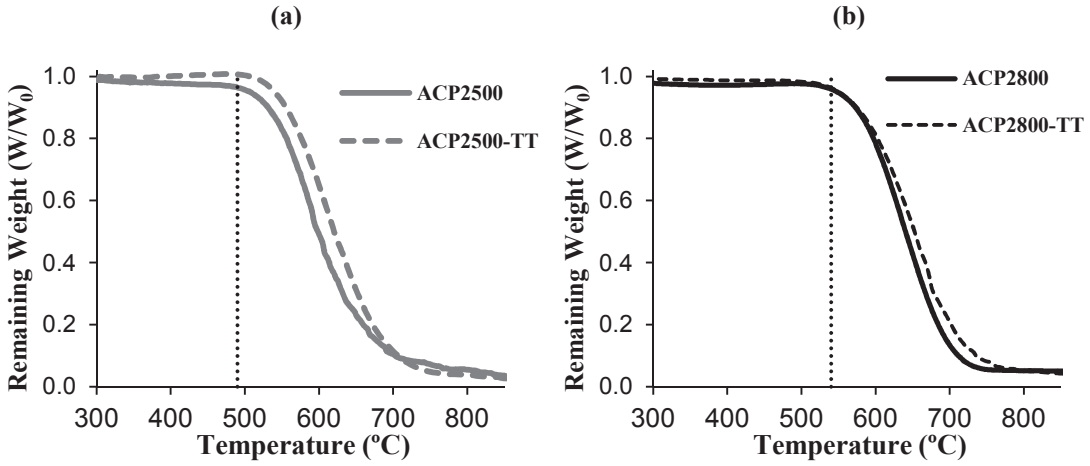

Figure 6. Non-isothermal oxidation resistance profiles (10 ºC/min) of the activated carbons ACP2500 (a) and ACP2800 (b) and their corresponding thermal treated samples.

The TPD results after air oxidation at different temperatures performed to ACP2500 (Figure 7a-b) evidence that oxidation of this carbon at 180 ºC increases slightly the amount of CO evolved at about 790 ºC, which seems to keep constant upon oxidation at 300 ºC. However, a progressive increasing evolution of CO and CO_2 at lower temperatures (~670 ºC for CO and ~500 and 630 ºC for CO_2) is observed with an increase of the oxidation temperature above 180 ºC. At 350 ºC the amount of CO and CO_2 evolved increases significantly due to ACP2500 produced a carbon burn-off of 16 % after air oxidation at this temperature for 2 h.

On the other hand, oxidation of ACP2800 activated carbon at temperatures lower than 300 ºC increases significantly the amount of CO evolved at about 860 ºC, accompanied by a small evolution of CO_2 at the same temperature (Figure 7c and d). At higher oxidation temperatures (350 ºC) desorption of CO (CO_2) at high temperatures (860 ºC) seems to keep constant and OSG of lower thermal stability are generated (~700 ºC for CO and ~500 and 700 ºC for CO_2). According to literature, the low temperature peak (c.a. 500 ºC) could be attributed to decomposition of lactone groups and the higher temperature peak (ca. 630 ºC for ACP2500 and 700 ºC for ACP2800) can be originated from anhydride groups. The contribution of both groups increases with oxidation temperature for ACP2500 and ACP2800 carbons, in line with other oxidized carbon materials [47,48]. Moreover, contrary to ACP2500 sample, ACP2800 is resistant to

gasification in air, with no significant weight loss observed, during 2 h at 350 ºC. In fact, according to the TPD results the carbon oxidation onset temperature appears to be at about 300 ºC for ACP2500 and about 350 ºC for ACP2800 (Figure 7), which are in line with the TGA conclusions given that ACP2500 started to lose weight about 50 ºC lower than ACP2800 (Figure 6).

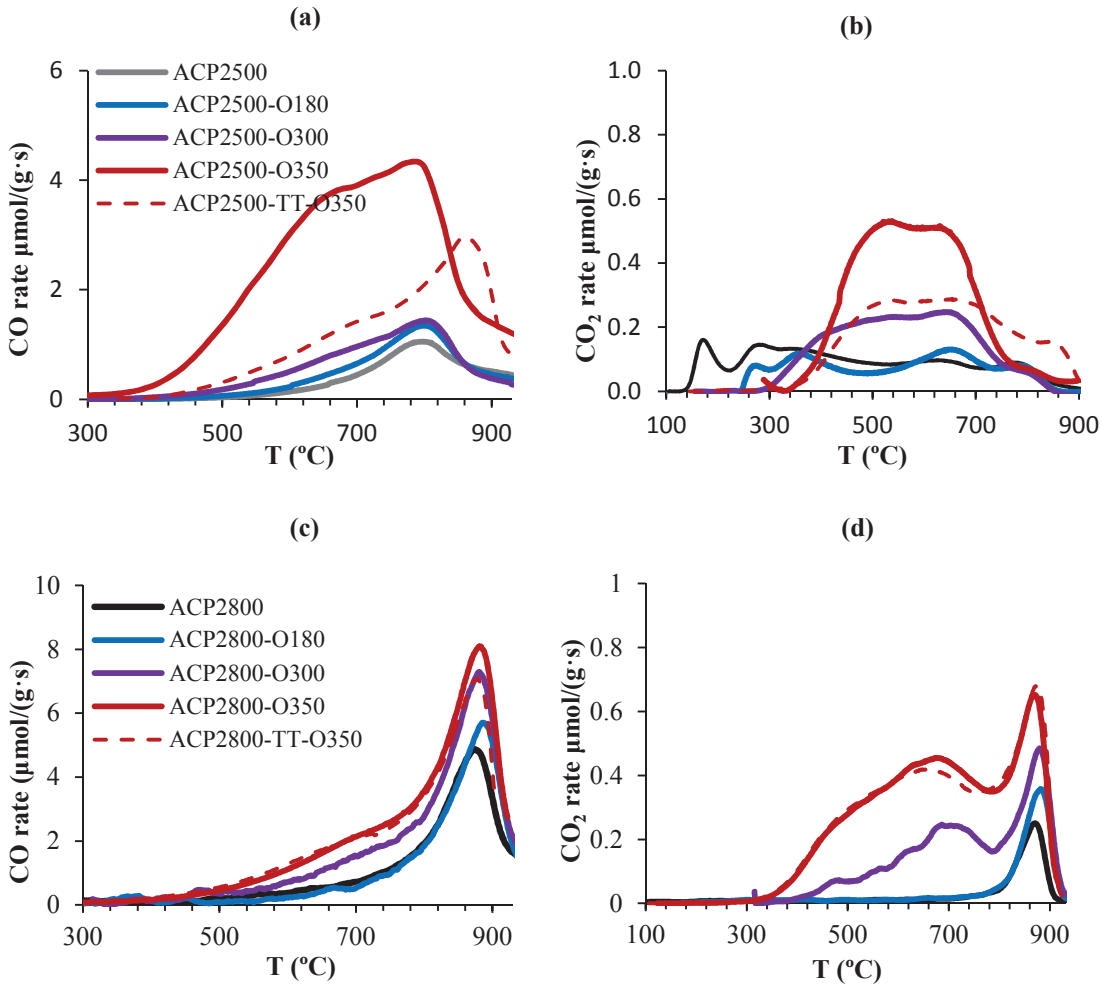

Figure 7. Amount of CO and CO_2 evolved with temperature during the TPD experiments of ACP2500 (a-b) and ACP2800 (c-d) after air oxidation at different temperatures (180, 300 and 350 ºC) for 2h.

These TPD results indicate that oxidation of the activated carbon surfaces takes place through the oxidation of C-P surface bonds, generating C-O-P bonds, especially for ACP2800, that are thermally stable to high temperatures (up to 700 ºC for ACP2500

and up to 800 ºC for ACP2800). When the P complexes are completely oxidized other oxygen surface complexes, thermally less stable, are formed, decomposing as CO and CO_2 at lower temperatures. It could be defined as an oxygen spill-over from oxidized P groups to the carbon surface (demonstrated by the CO desorption peak that appears at intermediate temperature in the TPD of oxidized carbons (Figure 7)), which provide reactive oxygen atoms that oxidize the carbon surface, forming CO and CO_2.

On the other hand, the low activation temperature used for the preparation of ACP2500 carbon did not result in the generation of a high contribution of C-P bonds as reveals the XPS results with respect to ACP2800 (Table 2). This would explain the lower amount of CO during the TPD at high temperatures (~790 ºC) of oxidized ACP2500 samples and the lower oxidation resistance of this sample (Figure 6a). The inhibition effect seems to be, in this case, the result of site blockage, which support the conclusions derived from the work of Wu and Radovic [7]. They suggested that site blockage is mainly a result of the presence of P groups bonded to carbon sites (C-O-P and C-P-O), whereas metaphophates (including metal-based) may function as a physical barrier between the catalyst and carbon surfaces.

Furthermore, when ACP2500 activated carbon was heated in nitrogen up to 900 ºC for in situ reduction of the phosphorus groups to C-P bonds, then cooled down to 200 ºC and finally heated again to 900 ºC in air atmosphere (see ACP2500-TT Figure 6a), the weight lost was delayed 25 ºC compared to that of the original profile, supporting that re-oxidation of newly produced C-P surface groups prior to carbon gasification takes place. Regarding to this experiment, ACP2500 was thermal treated in inert atmosphere up to 900 ºC and then oxidized in air at 350 ºC for 2h, without a significant carbon burn-off observed. The CO and CO_2 TPD profiles of this sample, ACP2500-TT-O350, is represented in Figure 7a and b, respectively. As can be observed, the CO TPD profile of this sample is different to that obtained for ACP2500-O350 but similar to that for ACP2800-O350 (Figure 7c), suggesting that the same OSG releasing CO at elevated temperatures (~860 ºC) were formed. The same experiment performed to ACP2800 carbon (Figure 7c and d) evidences that the TPD profile of ACP2800-TT-O350 overlaps with that for ACP2800-O350, indicating that the P surface complexes of this carbon can be reduced and oxidized again and that this behavior is completely reversible, despite the fact that during the reduction/oxidation cycles slight gasification of the carbon surface takes place through the evolution of CO/CO_2 during the TPD experiments (with

a total carbon burn-off of 5.3 % wt.). These results suggest that after the thermal treatment performed to ACP2500 and ACP2800 above 700 ºC, the new surface sites generated by the CO (and CO_2) release (probably C_3PO groups) seem to react with oxygen when exposed to air to regenerate the oxygen-phosphorus surface groups [10]. Thus, C_2-PO(OC), C-PO$(OC)_2$ and C-O-PO$(OC)_2$ (depending on the intensity of the oxidation) might be formed, which decompose to CO (and CO_2) at temperatures above 800 ºC during a second TPD experiment. Therefore, the presence of C-PO_3 groups on the carbon surface with redox functionality seems to enhance the oxidation resistance of these thermal treated porous carbons or those prepared at high activation temperatures, such as ACP2800.

From the amount of CO, CO_2 and H_2O evolved during the TPD experiments (Table 3), the total oxygen content, O (TPD), was calculated and compared to the amount of oxygen bonded to phosphorus, O-P (Table 3). The O-P values were calculated from deconvolution of the CO (and CO_2) TPD profile, quantifying the peaks that evolved above 700 ºC and which are associated to decomposition of C-OPO_3 (and O=C–O–P) groups of different thermal stabilities. As an example, Figures 8a and 8b show the deconvolution of the CO-TPD profiles for ACP2500 and ACP2800 samples, respectively, which summarize the different CO evolving groups. The deconvolution was done using a multiple Gaussian function, according to the literature data and to the discussions made before [10,34]. As observed, the deconvolution fits the data quite well for both, ACP2500 and ACP2800 carbons. Interestingly, although most of the CO is desorbed at about 790 ºC from ACP2500, a slightly amount of CO is desorbed at about 860 ºC indicating a slightly contribution of more stable C-O-PO_3 surface groups present on this sample. The same is observed for ACP2800, which presents the maximum of the CO peak at 860 ºC.

Regarding to the results reported in Table 3, it can be observed that the relatively high values of O-P observed for ACP2800 compared to the total oxygen amount (O) indicates that most of the oxygen present in this carbon seems to be bonded to surface phosphorus. However, in the case of ACP2500 sample ca. 40 % of the total oxygen is oxygen evolved as water due to the low dehydration degree reached at this activation temperature. When this sample is thermal treated up to 900 ºC followed by oxidation at 350 ºC (ACP2500-TT-O350), most of the oxygen is oxygen bonded to phosphorus given that the samples is completely dehydrated.

Table 3. Amount of CO and CO_2 evolved from the fresh activated carbons and treated samples: total oxygen concentrations.

Sample	CO (μmol/g)	CO_2 (μmol/g)	O[a] % wt.	O-P[b] % wt.	(O-P)/P
ACP2350	1018	723	3.9	n.d.	n.d.
ACP2650	2375	255	4.6	3.5	2.1
ACP2500	1119	364	5.6	1.7	1.3
ACP2500-O180	1562	278	6.1	1.9	1.6
ACP2500-O300	2110	492	7.6	2.1	1.7
ACP2500-O350	6502	835	10.6	3.5	2.9
ACP2500-TT	664	9	1.1[c]	1.0[c]	*0.8*
ACP2500-TT-O350	4031	641	8.5	4.7	3.5
ACP2800	3915	305	7.2	5.2	2.9
ACP2800-O180	4398	180	7.6	5.4	2.9
ACP2800-O300	5918	552	11.2	6.5	3.3
ACP2800-O350	7357	1295	15.9	8.0	3.7
ACP2800-TT	1018	112	2.0[d]	1.9[c]	1
ACP2800-TT-O350	6893	1182	14.8	7.5	3.3

[a] Total oxygen from the amounts of H_2O, CO and CO_2 evolved.
[b] Total oxygen bonded to P (as C-O-P) from the amounts of CO and CO_2 evolved at >700 ºC.
[c] not exposed to ambient air
n.d. Not determined

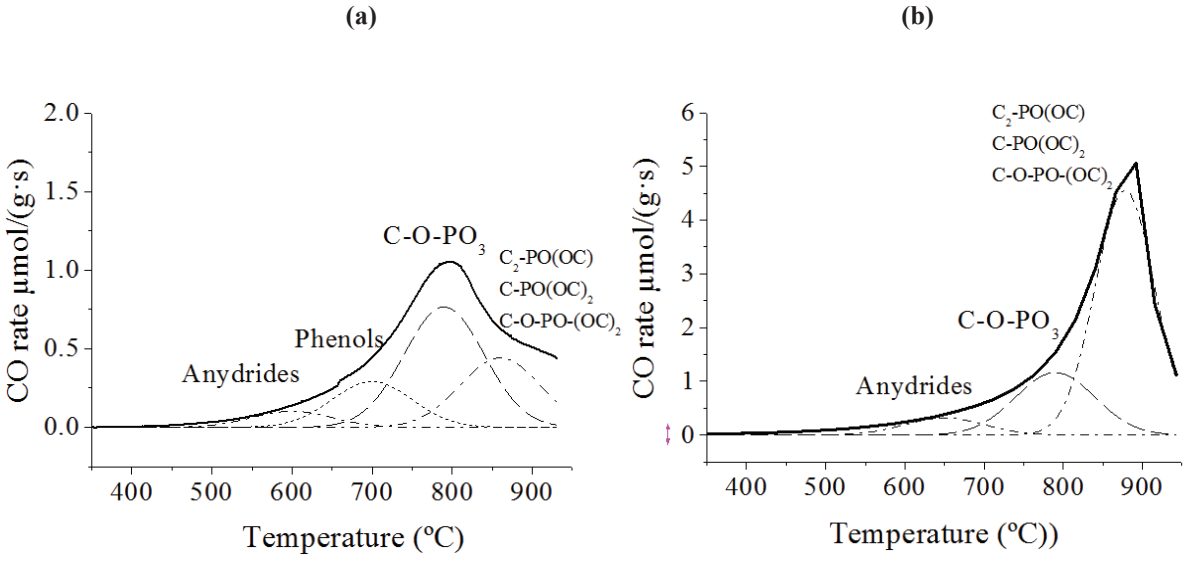

Figure 8. Deconvolution of CO TPD profiles of ACP2500 (a) and ACP2800 (b) using a multiple Gaussian function.

As expected, the oxygen content decreases after the thermal treatment and increases after the oxidation process. Furthermore, it has to be pointed out that the O-P values obtained after oxidation at 180 ºC for ACP2500 and at 300 ºC for ACP2800 would correspond, approximately, to the total oxygen that may react with the P complexes since the carbon oxidation start to be significant above these oxidation temperatures and other oxygen surface complexes, thermally less stable, are starting to be formed (Figure 7). Therefore, from the XPS and TPD results the ratio mol of O-P (from TPD) per mol of surface P (from XPS), O-P/P, has been calculated for ACP2500-O180 and ACP2800-O300 resulting about 1.5 and 3.3, respectively. These values may indicate that phosphorus groups in which the phosphorus atom is bonded to the carbon surface through one or two atoms of oxygen, such as C-OPO_3 and C-O-PO_2(OC) groups are mostly present on the surface of ACP2500-O180. On the other hand, C-O-$PO(OC)_2$ groups are most probably on ACP2800-O300 carbon surface. The ratio O-P/P could be slightly overestimated given that, the total oxygen content bonded to phosphorus was compared to the surface phosphorus content obtained from XPS analysis (O-P(TPD)/P(XPS)).

In addition, the O-P/P ratios for ACP2500-TT-O350 and ACP2800-TT-O350 are the same, indicating that the same phosphorus complexes are formed after thermal treatment up to 900 ºC and re-oxidation to 350 ºC.

4. Discussion

Phosphoric acid activation of lignocellulosic materials appears to generate phosphate and polyphosphate bridges that crosslink biopolymer fragments, avoiding the contraction of the structure by pyrolysis and thus resulting in activated carbons with an expanded porous structure (At = 476 m^2/g for ACP2500 and At = 433 m^2/g for ACP2800) [29]. Moreover, the resultant activated carbons present a relatively high amount of surface phosphorus (2.3 %wt for ACP2500 and 3.5 %wt for ACP2800) from the activation agent which seems to be very stable bonded to carbon, even after a thermal treatment up to 900 ºC (Table 2). The formation of oxygen-containing P surface groups during the phosphoric acid activation of type C-O-PO_3 (that include also C-O-PO_2(OC) and C-O-$PO(OC)_2$ groups) has been reported previously in the literature

[7,10]. In this sense and assuming a cross sectional area of 40 $Å^2$ for these surface groups, the P surface content on ACP2500 and ACP2800 would occupy an area of approximately 59 and 87 m^2/g, respectively, which represent about 13 and 21% of the external surface area of their respective activated carbons.

The activation temperature process results in the thermal stabilization of these P surface groups (C-O-PO_3) which are thermally very stable and decompose only at temperatures higher than 750 ºC, producing CO (and CO_2) in the gas phase and C-PO_3 type surface groups (that may include C_2PO_2 and C_3PO, depending on the treatment temperature). Moreover, the TPD profiles of ACP2500 and ACP2800 (Figure 4 and 5, respectively) revealed an important release of H_2 (lower for ACP2800) which suggests that dehydrogenation of the acid phosphates C-O-PO_3 groups (or C-PO_3) and the generation of C-O-PO_2-O-C and/or C-O-$PO(OC)_2$ (or C-PO_2-O-C and/or C-$PO(OC)_2$) type surface groups might occur, which are further decomposed to CO (and CO_2) at higher temperatures, forming finally the C_3PO type surface groups.

According to this, it is suggested that the degree of dehydrogenation reactions leading to the formation of different C-O-PO_3 groups with further decomposes to C-PO_3 ones, on the surface of the activated carbons, strongly depends on the activation temperature. In this sense, C-O-PO_3 groups (that may include polyphosphates structures) in which the phosphorus is attached to the carbon surface through one oxygen atom and contains two OH are most probable on the surface of ACP2500, as revealed the high amount of H_2 desorbed above 500 ºC from this sample, which are thermally stable up to 700 ºC. Although, the presence of phosphate groups thermally more stable is not disregarded due to this sample slightly decomposes to CO (and CO_2) at higher temperatures (~860 ºC) (Figure 8a). On the other hand, ACP2800 (or ACP2500-TT) carbon might generate higher amount of C_3PO surface groups after activation at 800 ºC (or after a thermal treatment up to 900 ºC) which are re-oxidized, upon contact with air, producing C-O-P bonds; i.e., regenerating the C-O-PO_3 type groups (that may include C_2-PO(OC), C-$PO(OC)_2$ and C-O-$PO(OC)_2$ depending on the intensity of the oxidation treatment) on the surface of the carbon. These C-O-P bonds are thermally more stable and decompose only at about 860 ºC, producing CO (and CO_2). Moreover, these results further explain the higher value of O-P/P for ACP2800 (2.9) compared to that for ACP2500 (1.3). Scheme 2 presents the possible phosphate structures on the surface of phosphorus-containing activated carbons prepared by

chemical activation of lignocellulosic precursors with H_3PO_4 and at different activation temperatures (500 and 800 ºC).

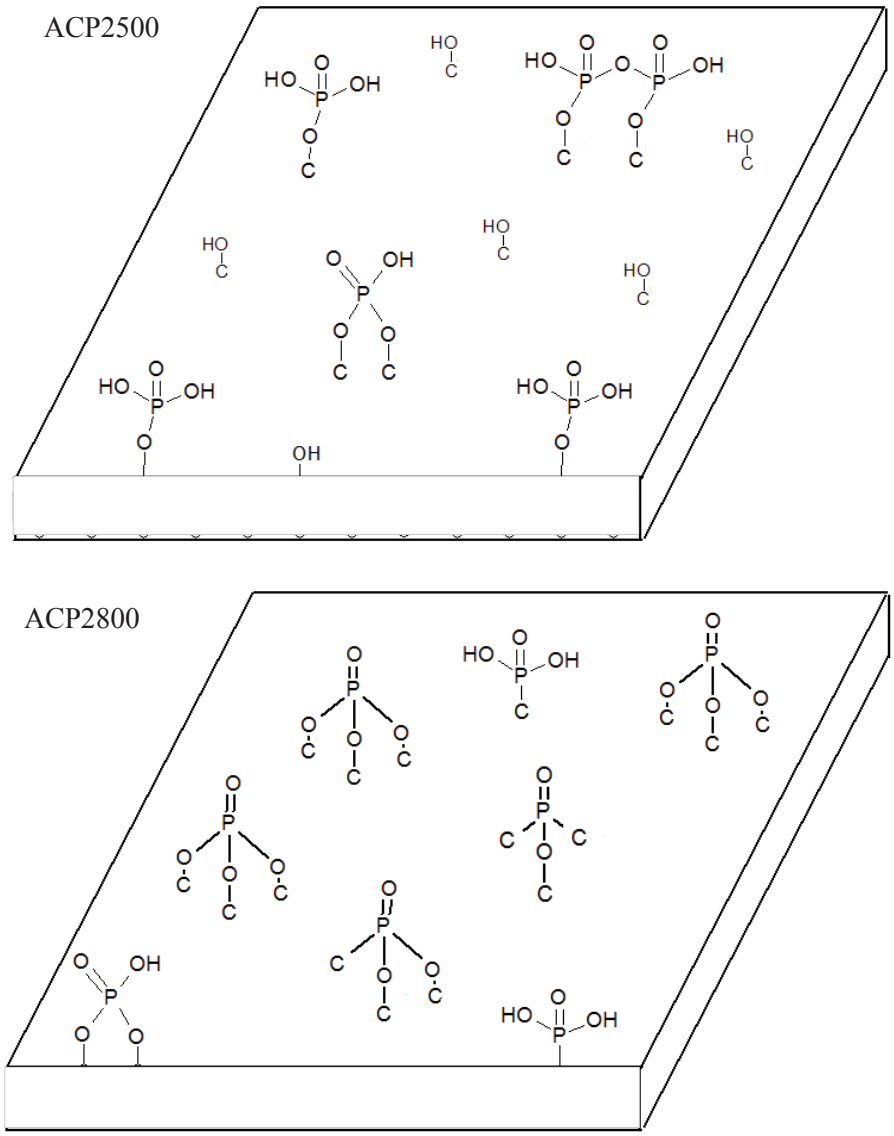

Scheme 2. Possible phosphate structures on the surface of phosphorus-containing activated carbons prepared by chemical activation of lignocellulosic precursors with H_3PO_4 and different activation temperatures.

Finally, oxidation of the activated carbons surface seems to proceed through two mechanisms. The presence of mainly C-O-PO_3 structures on the surface of ACP2500 correlates quite well with the work reported by Radovic, in which postulated that the bridge O atoms play a key role in the carbon oxidation inhibition mechanism. The

inhibition effect seems to be, in this case, the result of site blockage. On the other hand, the presence of P surface complexes with a redox functionality, as that observed by C_3PO groups on the surface of ACP2800 and ACP2500-TT carbons (Figure 7, see ACP2800-TT-O350 and ACP2500-TT-O350), seem to enhance the oxidation resistance of these type of porous carbons through the oxidation of C-P bonds to C-O-P ones.

5. Conclusions

Chemical structure and thermal stability of phosphorus groups in two activated carbons prepared by phosphoric acid activation at 500 and 800 ºC and an impregnation ratio (H_3PO_4/olive stone) of 2 were investigated by X-ray photoelectron spectroscopy (XPS) and temperature-programmed desorption experiments (TPD). It has been shown that the activation process results in the thermal stabilization of P surface groups (C-O-P type bonds), which are thermally stable at temperatures up to 700 ºC for ACP2500 and up to 800 ºC for ACP2800. Thermal treatments at higher temperature increases the less oxygenated phosphorus groups on the carbon surface (probably C_3-PO) generating CO (and CO_2), which upon contact with air re-oxidized forming C-O-P type groups, such as C_2-PO(OC), C-PO$(OC)_2$ and C-O-PO$(OC)_2$ depending on the intensity of the oxidation treatment. These groups have been shown to be thermally more stable and more abundant over the carbons prepared at 800 ºC and those thermal treated up to 900 ºC in N_2 atmosphere. Thus, the presence of these oxygen-containing phosphorus surface groups with an interesting redox functionality of high chemical and thermal stability seems to be responsible of the high oxygen content and oxidation resistance of this type of porous carbons. On the other hand, the lower oxidation resistance observed for ACP2500 carbon seems to be the result of site blockage by the presence of P groups bonded to carbon sites through an oxygen atom (C-O-PO_3 groups).

Acknowledgments

We gratefully thank Junta de Andalucia (P09-FQM-5156) and Spanish Ministry of Economy and Competitiveness (MINECO) and FEDER (Project CTQ2012-364086) for financial support. M.J.V.R. gratefully thanks MINECO for a FPI fellowship (BES-2010-032213).

References

[1] Bansal RC, Donnet JB, Stoeckli HF, Active Carbon, Marcel Dekker, New York, 1988.

[2] Rodríguez-Reinoso F, in: J.W. de Patrick (Ed.), Porosity in Carbons: Characterization and Applications, Edward Arnold, London, 1995.

[3] Rosas JM, Bedia J, Rodríguez-Mirasol J, Cordero T. Preparation of hemp-derived activated carbon monoliths. Adsorption of water vapor. Ind Eng Chem Res 2008;47(4):1288–96.

[4] Puzy AM, Poddubnaya OI, Martínez-Alonso A, Suárez-García F, Tascón JMD. Synthetic carbons activated with phosphoric acid III. Carbons prepared in air. Carbon 2003;41:1181-1191.

[5] Rosas JM, Bedia J, Rodríguez-Mirasol J, Cordero T. HEMP-derived activated carbon fibers by chemical activation with phosphoric acid. Fuel 2009;88:19-26.

[6] Puziy AM, Poddubnaya OI, Martínez-Alonso A, Suárez-García F, Tascón J.M.D. Synthetic carbons activated with phosphoric acid II. Porous structure. Carbon 2002;40:1507–1519.

[7] Wu X,. Radovic LR Inhibition of catalytic oxidation of carbon/carbon composites by phosphorus. Carbon 2006;44(1):141-151.

[8] McKee DW, Spiro CL, Lamby EJ. The inhibition of graphite oxidation by phosphorous additives. Carbon 1984;22(3):285–90.

[9] Rosas JM, Ruiz-Rosas R, Rodríguez-Mirasol J, Cordero T. Kinetic study of the oxidation resistance of phosphorus containing activated carbons. Carbon 2012;50:1523-1537.

[10] Valero-Romero MJ, Rodríguez-Mirasol J, Cordero T. Role of surface phosphorus complexes on the oxidation of porous carbons. Chapter 1.

[11] Guerrero-Pérez MO, Valero-Romero MJ, Hernández S, López Nieto JM, Rodríguez-Mirasol J, Cordero T. Lignocellulosic-derived mesoporous materials: An answer to manufacturing non-expensive catalysts useful for the biorefinery processes. Catalysis Today 2012;195:155-161.

[12] Bedia J, Ruiz-Rosas R, Rodríguez-Mirasol J, Cordero T. A kinetic study of 2-propanol dehydration on carbon acid catalysts. Journal of catalysis 2010;271:33-42.

[13] Puziy AM, Poddubnaya OI, Socha RP, Gurgul J, Wisniewski M. XPS and NMR studies of phosphoric acid activated carbons. Carbon 2008;46: 2113-2123.

[14] Puziy AM, Poddubnaya OI, Ziatdinov AM. On the chemical structure of phosphorus compounds in phosphoric acid-activated carbon. Applied Surface Science 2006;252:8036–8038

[15] Puziy AM, Poddubnaya OI, Martínez-Alonso A, Suárez-García F, Tascón JMD. Surface chemistry of phosphorus-containing carbons of lignocellulosic origin. Carbon 2005;43:2857–2868.

[16] González-Serrano E, Cordero T, Rodríguez-Mirasol J, Cotoruelo L, Rodríguez JJ. Water Res. 2004;38:3043-3050.

[17] ASTM. Standard test method for total ash content of activated carbon. D2866- 94; 2004.

[18] Brunauer S, Emmett PH, Teller E. Adsorption of gases in multimolecular layers. J Am Chem Soc 1938;60:309-319.

[19] Dubinin MM, Zaverina ED, Radushkevich LV. J Phys Chem 1947;21:1351-1362.

[20] Kaneko K, Ishii C. Superhigh Area Determination of Microporous Solids. Colloids Surf 1992;67(9):203-212.

[21] Bedia J, Barrionuevo R, Rodríguez-Mirasol J, Cordero T. Ethanol dehydration to ethylene on acid carbon catalysts. Applied Catalysis B: Environmental 2011;103:302-310.

[22] Puziy AM, Poddubnaya OI, Martínez-Alonso A, Sua´ rez-Garcı´a F, Tascón JMD. Surface chemistry of phosphorouscontaining carbons of lignocellulosic origin. Carbon 2005;43(14):2857–68.

[23] Vernersson T, Bonelli PR, Cerrella EG, Cukierman AL. Arundodonax cane as a precursor for activated carbons preparation by phosphoric acid activation. Bioresour Technol 2002;83(2):95–104.

[24] Guo Y, Rockstraw DA. Physicochemical properties of carbons prepared from pecan shell by phosphoric acid activation. Bioresour Technol 2007;98:1513–21.

[25] Blanco Castro J, Bonelli PR, Cerella EG, Cukierman AL. Phosphoric acidactivation of agricultural residues and bagasse from sugar cane: influence of the experimental conditions on adsorption characteristics of activated

carbons. Ind Eng Chem Res 2000;39:4166–72.

[26] Rodríguez-Reinoso, F.,Molina-Sabio, M. Activated carbons from lignocellulosic materials by chemical and/or physical activation: an overview. Catal. Today 2010;158:89-96.

[27] Bedia J, Rosas JM, Vera D, Rodríguez-Mirasol J, Cordero T. Isopropanol decomposition on carbon based acid and basic catalysts. Catalysis Today 2010;158(1-2):89-96.

[28] Moreno-Castilla C, Carrasco-Marín F, Mueden A. The creation of acid carbon surfaces by treatment with (NH4)2S2O8. Carbon 1997;35(10-11):1619-1626.

[29] Jagtoyen M, Derbyshire F. Activated carbons from yellow poplar and white oak by H3PO4 activation. Carbon. 1998;36(7–8):1085–97.

[30] Puziy AM, Poddubnaya OI, Martínez-Alonso A, F Suárez-García, Tascón JMD. Synthetic carbons activated with phosphoric acid: I. Surface chemistry and ion binding properties. Carbon 2002:40(9);1493–1505.

[31] Rodríguez-Reinoso F, Molina-Sabio M, González MT. The use of steam and CO_2 as activating agents in the preparation of activated carbons. Carbon 1995;33(1):15–23.

[32] Moulder JF, Stickle WF, Sobol PE, Bomben KD, in:J. Chastain, R.C. King Jr. (Eds.), Handbook of X-ray Photoelectron Spectroscopy, Physical Electronics Inc. Eden Prairie, MN, 1995, pp. 4872-4875.

[33] D. Briggs, M.P. Seah (Eds.), Practical Surface Analysis, Auger and X-ray Photoelectron Spectroscopy, vol. 1, Wiley, Chichester, UK, 1990.

[34] Figueiredo JL, Pereira MFR, Freitas MMA, Órfao JJM. Modification of the surface chemistry of activated carbons. Carbon 1999;37(9): 1379–1389.

[35] Zielke U, Huttinger KJ, Hoffman WP. Surface-Oxidized Carbon Fibers: I. Surface Structure and Chemistry. Carbon 1996;34:983-998.

[36] Moreno-CastillaC, Carrasco-Marín F, Maldonado-Hódar FJ, Rivera-UtrillaJ. Effects of non-oxidant and oxidant acid treatments on the surface properties of an activated carbon with very low ash content. Carbon 1998; 36(1-2):145-51.

[37] Marchon B, Carrazza J, Heinemann H, Somorjai GA. TPD and XPS studies of O2, CO2 and H2O adsorption on clean polycristallite graphite. Carbon 1988;26(4):507-14.

[38] Bandosz TJ. in Carbon Materials for Catalysis (eds P. Serp and J. L. Figueiredo), John Wiley & Sons, Inc., Hoboken, NJ, USA. (2008) pp. 45-92, doi: 10.1002/9780470403709.ch2

[39] Montes-Morán MA, Suárez D, Menéndez JA, Fuente E. On the nature of basic sites on carbon surfaces: an overview. Carbon 2004;42(7):1219–25.

[40] Peter J. Hall and Joseph M. Calo. Secondary Interactions upon Thermal Desorption of Surface Oxides from Coal Chars. Energy and Fuels 1989;3:370-376.

[41] Ruowen Fu, Ling Liu, Wenqiang Huang and Pingchun Sun Studies on the structure of activated carbon fibers activated by phosphoric acid. Volume 87, Issue 14, pages 2253–2261, 1 April 2003

[42] Vivo-Vilches JF, Bailón-García E,. Pérez-Cadenas AF, Carrasco-Marín F, Maldonado-Hódar FJ. Tailoring the Surface chemistry and porosity of activated carbons: Evidence of reorganization and mobility of oxygenated Surface groups. Carbon 2014;68:520-530.

[43] Rodríguez-Reinoso F. The role of carbon materials in heterogeneous catalysis. Carbon 1998;36(3):159-75

[44] Lu W, Chung DDL. Oxidation protection of carbon materials by acid phosphate impregnation. Carbon 2002;40(8):1249–54.

[45] Wu X, Pantano CGM, Radovic LR. Inhibition of catalytic oxidation by boron and phosphorus. Extended abstracts, the international carbon conference. Lexington, (Kentucky USA): American Carbon Society; 2001.

[46] Otake Y, Jenkins RG. Characterization of oxygen-containing surface complexes created on a microporous carbon by air and nitric acid treatment. Carbon 1993;31(1):109–21.

[47] Gómez-Serrano V, Piriz-Almeida F, Durán-Valle CJ, Pastor- Villegas J. Formation of oxygen structures by air activation. A study by FT–IR spectroscopy. Carbon 1999;37:1517–28.

Chapter 4

Insights into the catalytic performance of a carbon-based acid catalyst in methanol dehydration: Reaction scheme and kinetic modeling

Abstract The catalytic conversion of methanol over an acid carbon-based catalyst obtained by chemical activation of olive stone with H_3PO_4 has been studied. A significant amount of phosphorus remains over the catalyst surface after the activation process, mostly in form of C-O-PO_3 and C-PO_3 groups, which provide the carbon a relatively high oxidation resistance and surface acid and redox sites, as confirmed by temperature programmed surface reaction with methanol. Methanol decomposition on this catalyst yields selectivity to dimethyl ether higher than 82 % at 350 ºC and methanol conversion of 60 %, under the studied operating conditions. Catalytic activity tests performed under different atmospheres evidence that the catalyst performance strongly depends on the composition of the gas in which the reaction proceeds. In the absence of oxygen, the catalyst suffers a progressive deactivation due to both coke deposition on the strong Brönsted acid sites and to the reduction of the phosphorus groups (from C-O-P to C-P ones). However, in the presence of air, the P groups can be continuously reoxidized and they also ease the oxygen spillover on the catalyst surface, where the availability of labile oxygen inhibit catalyst deactivation and allow methanol steady state conversion to be reached. In consequence, the presence of oxygen leads to significant enhancement of methanol conversion without any significant change in the selectivity or reaction and even partially regenerates the catalyst after being used in inert atmosphere. Methanol conversion and selectivity to dimethyl-ether are slightly reduced when water vapor is added to the reactor. A kinetic study has been carried out where the methanol decomposition was proposed to proceed through an Eley-Rideal mechanism, which assumes the adsorption of water and oxygen spillover on the acid active sites. The rate expressions derived from the model described properly the experimental results, being the activation energy obtained for the formation of dimethyl ether around 85 kJ/mol.

Keywords: methanol decomposition, spill over oxygen, dimethyl ether, activated carbons, redox sites, temperature-programmed surface reaction.

1. Introduction

In the last decades the development of efficient routes to transform biomass into useful chemicals and (bio) fuels is of primary importance due to depletion of petroleum and environmental concerns. Among possible options for the valorization of biomass, the production of (bio) methanol has attracted considerable attention due to its versatility to be used as a source of a high amount of very valuable products through different catalytic processes, such as methanol to hydrocarbons (MTG process) [1,2] or methanol to olefins (MTO process) [3,4]. Moreover, methanol is today the primary candidate, as hydrogen carrier, for onsite or onboard production of hydrogen, due to its high hydrogen to carbon ratio, low boiling point and availability [5].

Methanol dehydration reaction has also attracted worldwide attention to produce dimethyl ether (DME), which is the previous stage in the transformation of methanol into hydrocarbons or olefins. DME is an important environmentally benign, non-toxic, biodegradable product whose global demand has significantly grown during the last decades, parallel to the increasingly stringent environmental regulations [6]. Besides its application in aerosol propellant formulations replacing banned chlorofluorocarbons (CFC) and as a building block for different chemicals, olefins and gasoline, it has been recognized as having one of the greatest potentials as alternative clean fuel [1,3,7,8]. Remarkable advantages of using DME as fuel are its high cetane rating, similar efficiency to that of the diesel traditional fuels and the strong reduction of NOx, sulfur dioxide, hydrocarbons and carbon monoxide evolution [9-11]. DME can be produced by methanol dehydration over solid acid catalysts or directly from syngas over bifunctional catalysts. The catalytic dehydration of methanol to DME has been widely studied in the literature over pure or modified γ-aluminas (γ-Al2O3) and, in a lower extent, over zeolites [12-14]. Most of these solid acid catalysts yield non desirable hydrocarbons or are negatively affected by the presence of water [15]. Besides, methanol dehydration produces catalysts fast deactivation due to the deposition of coke formed on the strong acid sites [16,17]. Hence, development of alternative catalysts that effectively succeed in overcoming the above-mentioned drawbacks would bring a great benefit. To avoid coke deposition and to increase the selectivity to DME, it has been claimed that the strength of the acid sites must be reduced [3,14,18]. Other authors have also shown that an oxidative atmosphere for dehydration reaction might enhance both the catalytic

activity and stability of the catalysts by inhibiting or reducing carbon deposition and thus increasing longevity of the catalyst [19-21].

Nevertheless, less effort has been focused in the study of methanol dehydration over activated carbons, despite their great potential and wide range of applications as catalysts and catalyst supports [22]. This kind of materials are receiving great attention in the last decades due to some advantages, such as their very high specific surface area, high thermal and chemical stability and the possibility of having stable basic and acid surface sites as oxygen surface groups [23,24]. They can also be obtained from many different raw materials including different types of lignocellulosic waste, which derives not only an environmental but also an economical profit. On this issue, Zawadzki et al. revealed that the non-oxidized carbon surface itself is not reactive in the decomposition of methanol [25] and therefore catalytic activity appeared only after carbon oxidation by gas oxygen. On this question, Moreno-Castilla et al. [26] studied methanol decomposition catalyzed by activated carbons oxidized by different oxidizing agents. They reported that activated carbons oxidized with (NH4)2S2O8 have the strongest acid groups and are the most active in the dehydration reaction of methanol to dimethyl ether. However, an increase in the catalyst heating temperature resulted in a rapid decrease in its activity in methanol dehydration due to a gradual decomposition of carboxyl groups present on the catalyst surface.

Our research group has previously reported the preparation and characterization of activated carbons by chemical activation of different lignocellulosic waste and by-products with phosphoric acid [27-29]. Carbons obtained by this method show a particular surface chemistry as a consequence of the phosphorus surface complexes, mainly in form of C-PO3 and C-O-PO3 groups, of very high chemical thermal stability that remain over the carbon surface despite the washing step [30,31]. These phosphorus complexes provide the carbons a high surface acidity and oxidation resistance, increasing the possibilities of these materials for applications in catalysis [30,32-34]. Furthermore, this type of carbons has proved their catalytic activity in the decomposition of 2-butanol, 2-propanol and ethanol, yielding essentially dehydration products [21,35,36]. Thus, activated carbons with high stable acid surface groups could be obtained from lignocellulosic waste in a single step, without needing additional oxidation treatments.

The present paper analyzes the catalytic decomposition of methanol, in the presence of molecular oxygen, over an acid carbon-based catalyst obtained by chemical activation of olive stone waste with H3PO4. The role and effect of the presence of oxygen and water on the catalytic activity of the catalyst was studied. A kinetic study of the catalytic decomposition of methanol on the carbon catalyst was also analyzed.

2. Experimental procedure

2.1. Catalyst preparation

The carbon catalyst used in this work, denoted as ACP2800, was prepared through chemical activation with phosphoric acid of olive stone waste (provided by Sca Coop. And. Olivarera y Frutera San Isidro, Periana (Málaga)). The raw material was cleaned with deionized water, dried at 100 ºC, and ground with a roller mill to obtain samples of 400–800 μm particle size. Then, the carbonaceous precursor was impregnated with concentrated commercial H3PO4 (85 wt.%, Sigma Aldrich) at room temperature, using a weight ratio of 2/1 (H3PO4/olive stone), and dried for 24 h at 60 °C. The impregnated sample was activated at 800 ºC, under continuous N2 (purity 99.999%, Air Liquide) flow (150 cm3 STP/min) in a conventional tubular furnace. The activation temperature was reached at a heating rate of 10 °C/min and maintained for 2 h. The activated sample was cooled inside the furnace under the same N2 flow and then washed with distilled water at 60 °C until neutral pH and negative phosphate analysis in the eluate. Finally, the activated carbon was dried at 100 °C, grinded and sieved (100-300 μm). The carbon obtained shows a relatively high yield (38.7 wt. %), similar to that obtained for the activation of other biomass natural waste at lower temperatures [37,38]. However, the higher concentration of the impregnation ratio used in this work results in a more accentuate restriction in the formation of tars and volatiles, leading to a higher carbon yield [39].

2.2. Catalyst characterization

Ultimate analysis (C, H, N, S amount) of the activated carbon was done in a Leco CHNS-932 system, being the oxygen content calculated by difference.

N_2 adsorption/desorption isotherm at -196 ºC and CO_2 adsorption isotherm at 0 ºC were carried out in an ASAP 2020 model equipment of Michromeritics Instruments Corporation. Samples were previously outgassed during at least 8 hours at 150 ºC. From the N_2 adsorption/desorption isotherm, the apparent surface area (A_{BET}) was determined applying the BET equation [40]; the micropore volume (V_t) and the external surface area (A_t) were calculated using the t-method [41]; and the mesopore volume (V_{mes}) was obtained as the difference between the adsorbed volume at a relative pressure of 0.95 and the micropore volume (V_t) [42]. Application of the Dubinin-Radushkevich method [43] to the CO_2 adsorption isotherm provided the narrow micropore surface area (A_{DR}) and micropore volume (V_{DR}). The surface chemistry of the fresh and used carbons was analyzed by X-ray photoelectron spectroscopy (XPS), temperature-programmed desorption (TPD), adsorption and temperature-programmed desorption of ammonia (NH_3-TPD), whereas the fresh carbon was also analyzed by methanol temperature-programmed surface reaction (CH_3OH-TPSR). The XPS analyses were obtained using a 5700C model Physical Electronics apparatus, with MgKα radiation (1253.6 eV). For the analysis of the XPS peaks, the C1s peak position was set at 284.5 eV and used as reference to position the other peaks. Mass surface concentrations of the samples have been obtained by numerical integration of the peaks. The deconvolution of the peaks was done using Gaussian-Lorentzian curves and a Shirley type background line and non-linear least-squares optimization.

TPD and TPSR experiments were performed in a custom quartz tubular reactor (i.d. 4 mm) placed inside an electrical furnace and coupled to a mass spectrometer (Pfeiffer Omnistar GSD-301) and to non-dispersive infrared (NDIR) gas analyzers (Siemens ULTRAMAT 22). For the TPD experiments, the samples were heated in helium (purity 99.999%, Air Liquide) flow (200 cm^3 STP/min) from room temperature up to 900 ºC at a heating rate of 10 ºC/min. The CO and CO_2 desorption rates were measured with the non-dispersive infrared gas analyzers. The NH_3-TPD and CH_3OH-TPSR were performed using 100 mg of catalyst that was saturated at 100 ºC with either NH_3 (20 % vol in Helium, 15 min) or methanol (4% in He, 90 min) flow (100 cm^3 STP/min), respectively. After saturation, the physisorbed probe NH_3 or CH_3OH molecules were removed from the surface of the sample by feeding pure He flow to the reactor for one hour at the same adsorption temperature. The TPD or TPSR run were completed by heating the sample up to 500 ºC, using a heating rate of 10 ºC/min for

NH_3-TPD and 5 ºC/min for CH_3OH-TPSR. Outlet concentrations were monitored by mass spectroscopy (Siemens ULTRAMAT 22). The registered m/z relations along with their assignations were: 2 (H_2), 4 (He), 17 (NH_3), 18 (H_2O), 26 (C_2H_4), 28 (CO), 30 (CH_2O), 31 (MeOH), 41 (C_3H_6), 44 (CO_2) and 45 (DME). The possible contribution of fragmented species on certain m/z lines was corrected by spectral subtraction considering the relative fragmentation coefficient of single compounds.

The surface acidity of the fresh catalyst was also studied by adsorption-desorption of pyridine carried out in a thermogravimetric system (CI Electronics) at 100 ºC. The inlet partial pressure of the organic base was 0.02 atm and was established by bubbling a helium stream through a saturator filled with pyridine at controlled temperature. The procedure begins with a pretreatment at 150 ºC in He of the carbon in order to remove any physisorbed specie on the carbon surface. Afterwards, pyridine is adsorbed at 100 ºC until saturation. Once the measured weight is steady (i.e. saturation is reached), a desorption process in pure He flow at the same adsorption temperature takes place until the weight remains constant. The amount of pyridine irreversible adsorbed after the desorption stage is used to quantify the surface acidity.

2.3. Methanol catalytic conversion

The catalytic activity of the activated carbon was studied by decomposition of methanol in the gas phase at atmospheric pressure in a fixed bed microreactor (i.d. 4 mm) placed inside a vertical furnace with temperature control, under different operating conditions. In a typical experiment 150 mg of catalyst (100-300 μm mesh) was used. Methanol was fed to the system in a controlled way by using a syringe pump (Cole-Parmer® 74900-00-05 model). The reaction was carried out in air atmosphere in the temperature range 250–350 ºC and in helium atmosphere at 350 ºC. This temperature range is considered to be the best suited for producing methanol from the synthesis gas [44]. To avoid condensation of any compound, all the lines were heated up to 120 ºC. The standard conditions were a methanol partial pressure of 0.02 atm and a space time of 0.100 g·s/μmol (GHSV = 43 m^3gas $kg^{-3}_{catalyst}$ h^{-1}). For the kinetic study under air atmosphere the methanol partial pressures were varied between 0.01 and 0.04 atm, the space time between 0.050 and 0.180 g·s/μmol (GHSV between 86 and 24 m^3gas $kg^{-3}_{catalyst}$ h^{-1}) and the water partial pressures between 0.01 and 0.06 atm.

The concentration of methanol and products in the outlet gas stream were analyzed by gas chromatography (490 micro-GC equipped with PPQ, 5A molsieve and Wax columns, Agilent). The conversion was defined as the molar ratio of methanol converted to methanol fed to the reactor. The selectivity was defined as the molar ratio of a given product to that of the total products formed. The carbon balance was reached with an error lower than 5 %.

3. Results and discussion

3.1. Characterization of the carbon acid catalyst

The physicochemical properties of the fresh carbon catalyst are presented in Table 1. The data presented are referred to structural parameters obtained from the N_2 adsorption-desorption and CO_2 adsorption isotherms, surface mass concentration obtained by XPS and surface acidity of the carbon obtained by pyridine irreversible adsorption. The carbon catalyst presents a high surface area of 1380 m^2/g. The higher value of A_{BET}^{N2} with respect to that of A_{DR}^{CO2} suggests the existence of a wide microporous structure [45]. The high values of the mesopore volume and the external surface area confirm that the carbon catalyst presents a significant contribution of mesoporosity. The presence of both a large surface area that provides a high amount of potential active sites and a well-developed pore structure that enhances the mass transfer rate are desirable features for catalytic applications. In relation with the surface chemistry of the sample, the main elements found on the activated carbon surface was carbon (87.1 wt. %) and oxygen (9.2 wt. %), with lower amount of phosphorus (3.5 wt. %) which remained over the carbon surface despite the washing process. The high surface oxygen amount on the activated carbon, despite having been activated in an inert atmosphere (N_2) to high temperatures, is associated, in a greatest extent, to the presence of phosphorus-containing groups. These surface phosphorus compounds formed during activation step seem to be homogeneously located in the carbon structure and stably bonded to carbon [28,29]. The presence of the phosphorus is supported by the binding energy of the maxima of the XPS P_{2P} peaks, around 132.5-133.5 eV, which have been reported elsewhere as characteristic of the existence of phosphorus groups on the surface of carbon materials [23,46]. From the deconvoluted XPS P2p spectra of the carbon catalyst [30], the main peaks appear at 134.0 and 133.4 eV, suggesting the

presence of mainly C-O-P type groups, 31.7 %, (C-O-PO_3, $(CO)_2$-PO_2 and $(CO)_3$-PO) and C-PO_3/C_2-PO_2 groups, 46.9 %, on the activated carbon surface. The contribution of reduced phosphorus compound as C_3-PO (14.3 %, 132.3 eV) and, in a lesser extent, C_3-P (7.1 %, 131.0 eV) groups cannot be discarded.

These C-PO_3 type surface groups have showed to be very reactive and are re-oxidized upon contact with air, even at room temperature, forming C-O-PO_3 type groups (mainly $(CO)_2$-PO_2 and $(CO)_3$-PO)) on the surface of ACP2800 carbon [30]. This explains that relatively high carbon surface oxygen content observed for ACP2800 higher to that obtained for activated carbons prepared at lower activation temperatures [31]. The P-OH groups of these surface phosphates ($(CO)_2$-PO_2, C-PO_2-O-C and/or C_2-PO_2) act as Brönsted acid sites and as we have reported in previous works they play an important role on the acid character of the carbon catalyst for 2-butanol [35] and iso-propanol [23] dehydration reactions. The total acidity surface of 1.09 mmol Pyridine adsorbed per gram of activated carbon was determined by pyridine adsorption-desorption-TPD. This value is high if compared with other phosphoric acid activated carbons prepared at lower activation temperatures [33].

Table 1. Porous structure and chemical properties of fresh catalyst

Porous structural parameters					XPS - Mass surface concentration (%)			Surface acidity (mmol/g)
$A_{BET}^{N_2}$ (m^2/g)	$V_{DR}^{N_2}$ (cm^3/g)	V_{meso} (cm^3/g)	$A_{DR}^{CO_2}$ (m^2/g)	$V_{DR}^{CO_2}$ (cm^3/g)	C_{1s}	O_{1s}	P_{2p}	Py-adsorbed
1380	0.514	0.654	660	0.265	87.1	9.2	3.5	1.09

The chemical nature of the surface sites of the catalyst has been also investigated by methanol temperature-programmed surface reaction (CH_3OH-TPSR). This is a well-establish technique to determine the chemical nature of the surface sites based on the gaseous desorption products; forlmaldehyde (CH_2O) indicates the presence of redox sites, dimethyl ether (CH_3OCH_3, DME) acidic sites, and carbon oxides basic sites [47-50]. But also, it is capable of giving information on surface intermediates [49,51,52] , as well as, monitoring the various steps of a heterogeneous catalytic process [53].

Several publications exist on MeOH adsorption and its surface reaction on metal oxides surfaces [49,50,52] and acidic zeolites [51,53]. However, less is known about MeOH adsorption on phosphoric acid activated carbon surfaces. Figure 1 displays the intensity on m/z lines corresponding to the main detected compounds in the outlet gas during the TPD of ACP2800 after adsorption-desorption of methanol at 100 ºC. The main products were H_2O, CO_2, CO and H_2 (Figure 1a). A blank TPD, where the activated carbon was heated in absence of methanol, showed evolution of some of these compounds but in negligible amounts, so their presence in CH_3OH-TPSR can be ascribed to methanol decomposition. The formation of formaldehyde (Figure 1a) was also observed, indicating the presence of redox sites over the carbon surface. Finally, methanol condensation products, i.e., DME and light olefins, were also detected, Figure 1b, confirming the presence of acid sites.

As can be observed in Figure 1a, methanol seems to be mainly adsorbed in form of molecular methanol at temperatures lower than 250 ºC. A very interesting feature is that the methanol desorption profile shows two peaks, one at 125 ºC and a broad asymmetric peak at about 163 ºC which have been previously observed for methanol adsorbed over ZSM-5 catalyst [53], TiO_2 [49] and Molybdenum-Heteropolyanions [48]. Previous results on the MTG process using different techniques (TPRS [53], IR[54,55], NMR [56]) attributed the higher methanol desorption energy peak to the methanol adsorbed directly on Brönsted sites, whereas the low temperature desorption peak was associated to methanol molecules adsorbed/interacting with the methanol adsorbed directly on the Brönsted sites, thus forming a protonate cluster. However, the presence of different adsorption acid sites for methanol decomposition cannot be discarded. The products of the dehydration of methanol, DME, m/z 45, and H_2O, m/z 18 were first observed at temperatures as low as 125 ºC and they were followed by ethylene (m/e 26) and propylene (41 m/e) desorption, which formation would require interaction between methanol and adsorbed DME molecules. Furthermore, DME shows a broad desorption peak between 200 and 400 ºC. This temperature region coincides with appearance of a second water peak and the onset desorption temperature of the hydrocarbons. Concentration of these compounds decayed during the ongoing TPSR, as methanol adsorbed molecules turned more isolated. The formation of these compounds at low temperature reveals the strong acidic character of the selected activated carbon. Another interesting feature is that DME peak in the CH_3OH-TPSR experiment appeared at a

temperature higher than that for the water peak, indicative that DME initially remains adsorbed on the acid active site.

On the other hand, remaining adsorbed methanol started to decompose in form of CO_2 at temperatures around 250 ºC and as carbon monoxide at higher temperatures. A similar TPRS profile for methanol adsorbed on H-ZSM-5 catalyst was reported by M. Jayamurzthy et al [53]. However, they also detected propane, butane and pentane along with trace amount of methane and ethane at temperatures higher to 350 ºC, indicative of the stronger acid character of H-ZSM-5 zeolite catalyst with respect to ACP2800. In fact, one of the main disadvantages for the selective formation of DME from methanol over zeolites is the large amounts of olefins formed [15]. Since the goal for this work is the selective formation of DME, the intermediate acidity of the proposed catalyst detected by MeOH-TPRS can be seen as a positive feature.

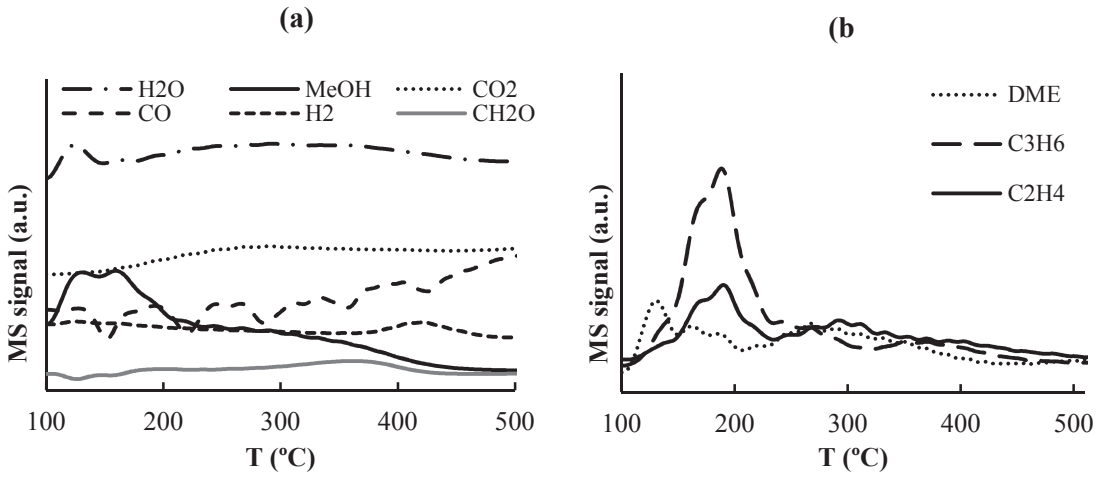

Figure 1. MS results from the CH_3OH-TPSR experiment over the ACP2800 activated carbon

3.2. Methanol catalytic dehydration

Figure 2 represents the methanol conversion, X_{MeOH}, as a function of time on stream (TOS) at reaction temperatures of 275, 300, 325 and 350 ºC in the presence of oxygen and at 350 ºC in the absence of oxygen (P_{MeOH} = 0.02, W/F_{MeOH} = 0.01 g·s/µmol). The presence of phosphorus on the surface of the carbon obtained by chemical activation with phosphoric acid increases the oxidation resistance of the resulting carbon as reported previously by our research group [30,32]. Thus, this allows

working at a reaction temperature as high as 350 ºC, under air atmosphere, without a noticeable gasification of the carbon catalyst. In the absence of oxygen, methanol conversion decreased more than 80 % within the first 15 minutes of reaction, indicating that the catalyst undergoes fast deactivation. When air is used as reaction gas, however, a steady state in which methanol conversion remained constant was reached straightaway at temperatures up to 325 ºC. At 350 ºC, steady state conditions are also achieved, although a decrease of about 20 % from the initial methanol conversion is observed after 60 min of reaction, indicating a partial deactivation of the catalyst.

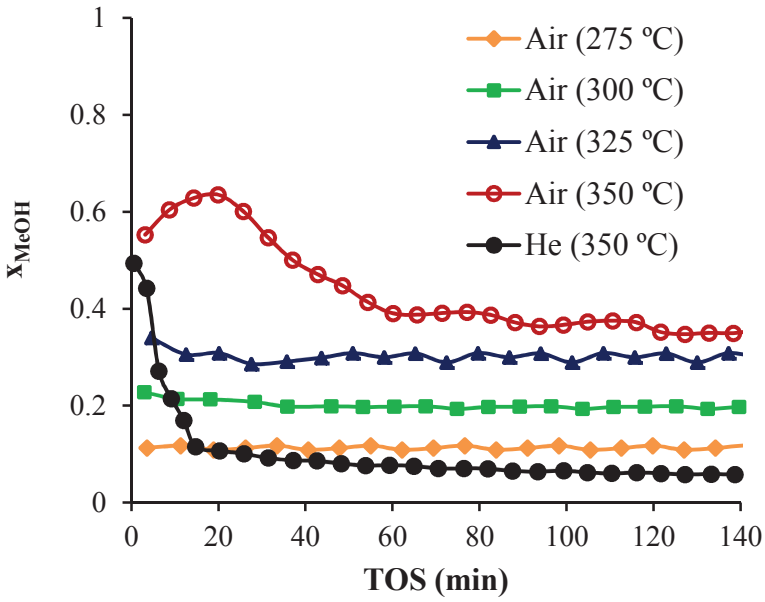

Figure 2. Methanol conversion as a function of TOS at different reaction temperatures in the presence (275, 30, 325 and 350 ºC) and absence (350 ºC) of air (PMeOH=0.02 atm, W/FMeOH = 0.1 g·s/µmol).

Table 2 summarizes the steady state conversion and selectivity values of detected carbon-based products obtained at different reaction temperatures at an inlet methanol vapor pressure of 0.02 atm and space time of 0.10 g·s/µmol. When helium (He) was used as reaction gas at 350 ºC, selectivity was mainly to dimethyl ether (DME) and traces of CH_4, C_3H_6, C_2H_4 and even of dimetoxymethane (DMM) and methyl formate (MF) were measured in the product stream. Given that no molecular oxygen is present in the reaction gas, the presence of DMM and MF suggest that the catalyst itself is the oxygen source for partially oxidizing methanol. Similarly, the use of

air atmosphere yields DME as the main dehydration product within all the temperature range studied. As shown in Table 2, selectivity higher to 90 % to DME was obtained at temperatures below 350 ºC, whereas selectivities to typical products of the partial oxidation of methanol (CO_2, CO, DMM and MF) are more significant than those obtained in He atmosphere and slightly increases with the reaction temperature. It must also be highlighted that in the absence of methanol and under air atmosphere no significant amounts of CO_2 and CO were detected, within the range of reaction temperatures, supporting adscription of these compounds to methanol partial oxidation nor direct methanol decomposition and not to carbon gasification. Formaldehyde, which is a commonly observed product with the methanol oxidation reaction, was not detected. Formaldehyde is considered an intermediate in the formation of DMM, MF and carbon oxides [57]. Therefore, the increasing selectivity to CO_x with reaction temperature can be due to the oxidation of these intermediate products, and also to the strong acid sites of the activated carbon, which are able to retain the reaction intermediates products for longer time, allowing further oxidation of the intermediates.

Table 2. Methanol steady state conversion and selectivities to detected carbon-based products at different reaction temperatures for reaction in air and He (P_{MeOH}=0.02 atm, W/F_{MeOH}=0.1 g·s/μmol).

T (ºC) - Atmosphere	MeOH conver. (%)	Selectivity (%)							
		CH_3OCH_3	CO_2	CO	$(CH_3O)_2CH_2$	$HCOOCH_3$	C_3H_6	C_2H_4	CH_4
250-Air	7.3	94.6	1.7	1.6	1.1	0.6	0.4	-	-
300-Air	19.5	93.3	2.9	2.7	0.3	0.5	0.3	-	-
325-Air	29.6	91.1	3.8	3.2	1.2	0.5	0.2	-	-
350-Air	43.0	87.4	5.3	3.9	2.8	0.5	0.1	-	-
350-He	5.7	95.9	0.3	0.4	0.02	0.1	1.1	0.2	1.9

The evolution of methanol conversion and selectivities to different products with time on stream (TOS) at 300 ºC is shown in Figure 3. A very small change in conversion (from 22 to 19 %), and DME selectivity (from 94 to 92 %) is observed for the catalysts after 23 h on stream. This suggests that the catalyst does not suffer significant deactivation at longer reaction times, at temperatures up to 300 ºC and under the experimental conditions used in this work, indicating a high stability of the surface

acidity available and not deactivated at shorter reaction times. For higher reaction temperatures (350 ºC), however, a decrease in conversions of 10 % is observed for the catalyst after 17 h on stream (data not shown).

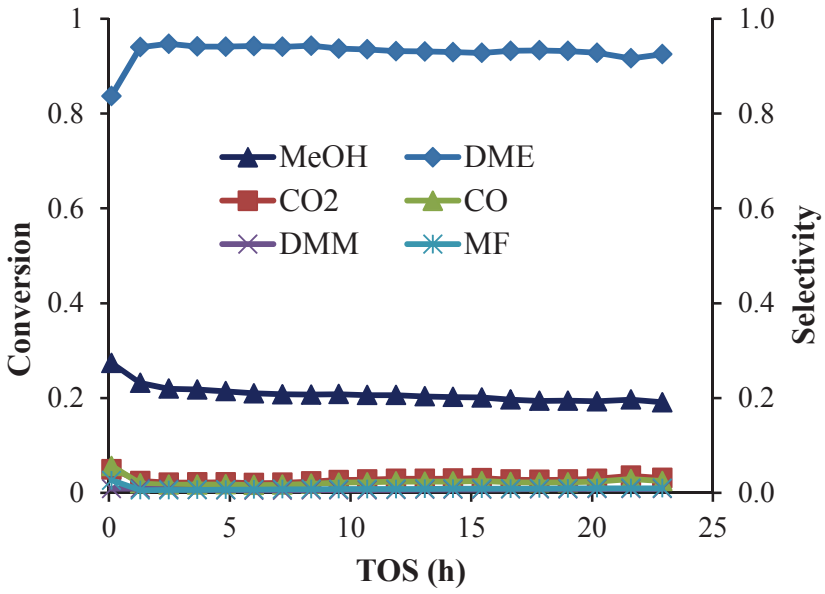

Figure 3. Conversion of methanol and selectivity to detected carbon-based products as a function of time on stream (TOS) at 300 ºC in air atmosphere (P_{MeOH} = 0.02 atm, W/F_{MeOH} = 0.1 g·s/μmol).

The methanol dehydration reaction rate obtained in this work at 300 ºC in air (Figure 2) is $2.9 \cdot 10^{-6}$ mol·g^{-1}·s^{-1}, which is in the range of that obtained by using modified alumina as catalysts at the same reaction temperature, as reported by Yaripour et al. [58,59]. A much higher value for the reaction rate, $140.0 \cdot 10^{-6}$ mol·g^{-1}·s^{-1}, was reported by Mollavali et al. [60] at 300 ºC, but at a much higher pressure, 16 atm. This points out that the carbon catalyst presented in this work shows a relevantly high activity if compared to other catalysts reported in the literature, with the noticeable advantage of being obtained from an inexpensive waste.

The effect of the presence of water vapor on methanol conversion and on selectivity is a key factor to analyze the potential of these carbon materials for catalyzing the dehydration of methanol to DME, especially given that water is usually found in company of methanol in the reactor feed during the industrial scale production

of DME. Figure 4 shows the methanol steady state conversion and selectivities to different products for different inlet partial pressures of water vapor ($P_{H2O,}$ 0.01-0.06 atm), at constant inlet methanol partial pressure of 0.02 atm and at 300 ºC in air. Both conversion and DME selectivity decrease progressively when water content in the feed is raised. The decrease of the methanol dehydration activity in the presence of water vapor has been previously reported in the literature [60,61]. Water is believed to block the active sites responsible of the methanol dehydration through competitive adsorption with methanol on the catalyst surface [2]. However, the ability of methanol to form hydrogen bonds with water molecules might also inhibit the rate of the ether formation. Taqvi et al. [62] reported the ability of methanol to form hydrogen bonds with water molecules, which results in enhanced water and methanol adsorption on activated carbons. J. Rodríguez-Mirasol et al. [63] also found that methanol adsorption is enhanced in the presence of water and ascribed the increased methanol uptake to the formation of water clusters, which were suggested to appear around the chemisorption sites that act as additional adsorption sites. More recently, J. F. DeWilde et al. [64] suggested that the formation of ethanol-water dimer species on the surface of Al_2O_3 is the cause of the lower dehydration activity of the catalyst in the presence of water vapor. The formation of these dimers might avoid the reaction between a methanol molecule adsorbed on the active sites and a molecule of methanol in the gas phase, which was proposed as the most probable reaction pathway for DME formation in the sight of CH_3OH-TPRS results, thus reducing the dehydration activity (Figure 4).

The influence of the oxygen concentration in the gas inlet on the catalytic dehydration of methanol was also studied. Figure 5 shows the conversion of methanol after 15 min of TOS as a function of temperature for different inlet oxygen concentrations. As can be observed, the methanol conversion significantly increases with oxygen concentration from a methanol conversion of 5 % in He atmosphere to 23 % in air atmosphere at 300 ºC. Moreover, in the presence of 10 % oxygen the catalyst was no longer deactivated, similarly to that observed in Figure 3. Therefore, timely supply and an excess of oxygen is necessary to keep the catalyst active.

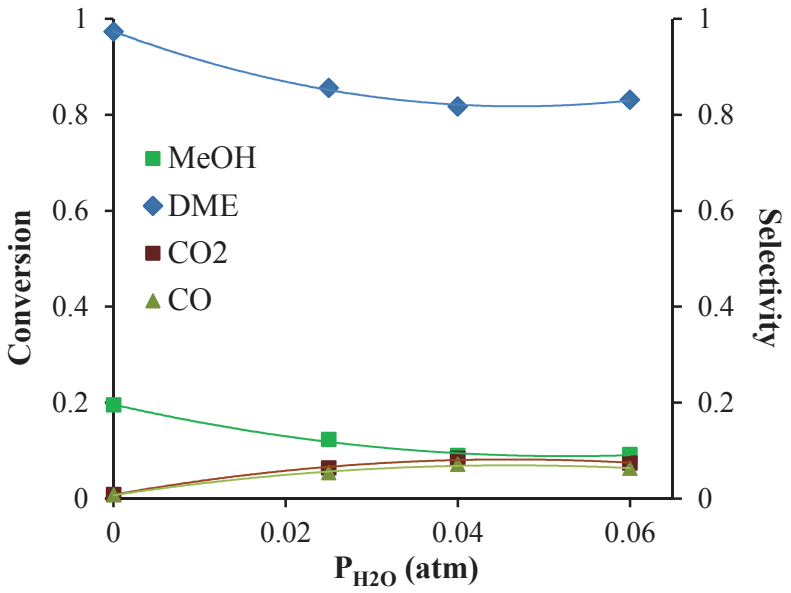

Figure 4. Evolution of the methanol conversion and selectivity to main products with the inlet water vapor partial pressure at 300 ºC (P_{MeOH} = 0.020 atm, W/F_{MeOH} = 0.10 g·s/µmol).

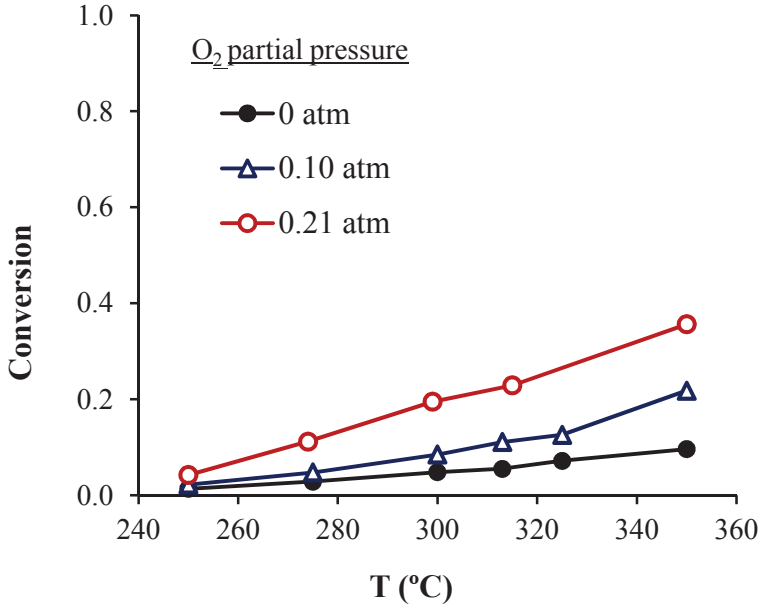

Figure 5. Evolution of the methanol conversion with temperature and different oxygen partial pressures (P_{MeOH} = 0.020 atm, W/F_{MeOH} = 0.10 g·s/µmol).

All these results evidence that ACP2800 catalytic performance on the gas phase methanol conversion strongly depends on the type of atmosphere in which the reaction proceeds, and suggest that oxygen is most likely to actively intervene on the mechanism of this catalytic process inhibiting the deactivation of the catalyst, either by reacting with certain intermediates species or by interacting with the catalyst surface. In this sense, the wasted catalysts resulting from MeOH decomposition in air and He atmospheres are analyzed in detail in the following section, in order to elucidate the role of oxygen in the decomposition reaction of methanol over phosphoric acid activated carbons.

3.3. The role of oxygen on the catalyst activity

3.3.1. Characterization of used catalysts

The surface chemistry of the carbon catalyst were analyzed after methanol decomposition using both He (ACP2800-RH) and air (ACP2800-RA) as reaction gases at a reaction temperature of 350 ºC after 2 h. Table 3 summarizes the mass surface concentration of the used catalysts (XPS (%wt.)). It is observed that the amount of surface phosphorus decreases from 3.5 wt. % for the fresh carbon catalyst to 2.1 and 1.7 wt. % for the catalyst after reaction in both air and He atmospheres, respectively. Moreover, when using He as the carrier, the amount of carbon increases significantly due to carbon species deposition, whereas in air the amount of surface carbon remains constant and the amount of surface oxygen increases, probably as the outcome of the oxidation of the carbon surface.

Table 3. XPS mass surface concentration (%) and phosphorous surface groups distribution (%) on ACP2800 before and after reaction in air and in He (350 ºC, 2h, P_{MeOH} = 0.02 atm; W/F_{MeOH} = 0.1 g·s/μmol)

	XPS (% wt.)			P 2p deconvolution			
Sample	**C_{1s}**	**O_{1s}**	**P_{2p}**	**C-OPO_3**	**C-PO_3 and C_2PO_2**	**C_3PO**	**C_3P**
ACP2800	87.1	9.2	3.5	31.7	46.9	14.3	7.1
ACP2800-RA	85.6	11.8	2.1	33.2	47.7	17.1	2.1
ACP2800-RH	91.3	6.6	1.7	14.6	26.3	52.6	6.5

Figure 6 represents the P 2p zone of the XPS for the fresh carbon and for the used carbons after methanol decomposition using air and He as reaction gases, whereas the amounts of the different surface phosphorus functional groups are compiled at the last columns of Table 3. As can be seen, in the presence of He, the signal intensity clearly decreases with respect to that for the fresh catalyst and the maximum of the P 2p band shifts to lower binding energies, probably due to the deposition of coke over the surface phosphorus acid species (H-phosphate groups:C-O-PO_3 and C-PO_3). However when the reaction takes place in the presence of air, in addition to a lower decrease of the signal intensity, the maximum of the P2p peak shifts to higher binding energies, characteristic of more oxygenated phosphorus compounds. The values reported in Table 3 confirm the higher amount of C-O-PO_3 type surface groups for ACP2800-RA. These experimental results suggest that deposition of carbon species on Brönsted acid sites seems to be a cause of catalysts deactivation, being more intense under He atmosphere than under air atmosphere when the reaction takes place at 350 ºC. They also point out that the presence of oxygen during methanol dehydration avoids partly the catalyst deactivation by oxidizing part of the surface phosphorus (from C-P to C-O-P bonds) and probably the carbon surface.

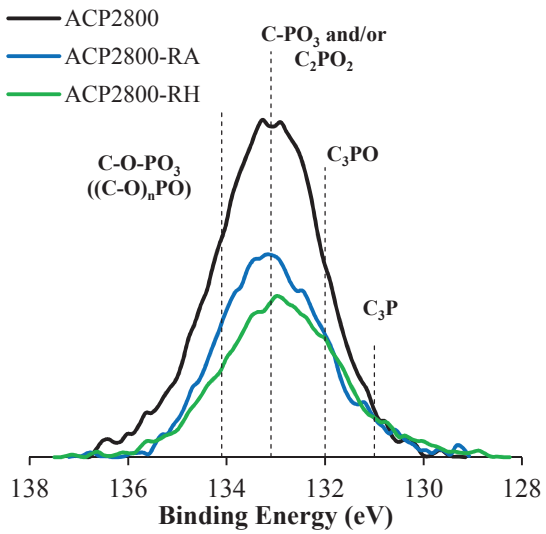

Figure 6. Normalized XPS spectra of ACP2800 before (black line) and after reaction (350 ºC, 2h) in air (blue line) and in He (green line) atmospheres.

In order to understand the distribution of surface acidity and strength of acid sites, the samples were further characterized by NH_3-TPD. Figure 7 shows the NH_3-TPD profiles for pristine ACP2800 and the wasted catalysts used in oxidative and inert

atmospheres. Previous NH_3-TPD measurements on phosphoric acid activated carbons demonstrated the occurrence of three desorption peaks, indicating the existence of different kinds of acid sites [30]. The most intense desorption peaks are obtained c.a. 150 ºC (I) and 250 ºC (II). The first is suggested to arise from the weakly adsorbed NH_3 molecules on phosphorus groups linked to the surface of the carbon through C-O-P bonds, whereas the shoulder at 250 ºC and the large tail at higher temperatures (III) may be originated to H-phosphate groups formed in the carbon surface during the activation process, which confers to the carbon strong Brönsted acid sites. As can be observed, the population of surface acid sites differs considerably when the catalyst is used under different reaction atmospheres at 350 ºC. Reaction under inert atmosphere (see ACP2800-RH) significantly reduces the total surface acidity. Only a small amount of less acidic surface sites seems to be present on the surface of the carbon catalyst after deactivation. This is an expected result, since strong acid-sites are known to promote the polymerization of olefins and thereby increase the rate of coke formation, thus being the main cause of catalysts deactivation in methanol decomposition reactions [14]. On the other hand, the catalyst recovered after being used in air atmosphere (see ACP2800-RA) is able to retain most of the surface acidity of moderate and intermediate strength, and only strong Brönsted acid sites are deactivated in such conditions. This result reveals that the most important role played by the oxygen is avoiding the blockage of both weak and moderate acid sites, which contribute to maintaining the dehydration activity of the catalyst during long reaction times (see Figure 1).

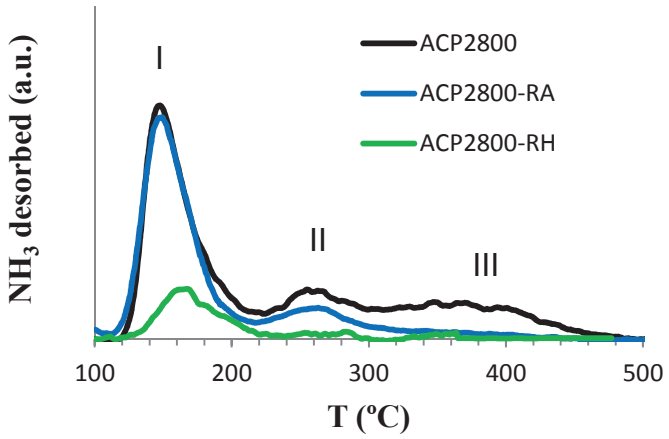

Figure 7. NH_3-TPD profiles of the catalyst before and after reaction in air and in He (350 ºC, 2h, P_{MeOH} = 0.02 atm; W/F_{MeOH} = 100000 g·s/mol).

TPD experiments on the fresh and used activated carbon catalyst were carried out in order to obtain a more precise assessment of possible changes in their surface composition during the reaction. TPD is recognized as one of the most adequate techniques to identify the chemical nature of oxygenated surface groups (OSG), specifically those that decomposes upon thermal treatment producing the evolution of CO and CO_2. According to literature, carbon-oxygen groups of acidic character, such as carboxylic and lactones, evolve as CO_2 upon thermal decomposition, whereas non acidic, such as carbonyl, ether, quinone and phenol, evolve as CO. Finally, anhydride surface groups evolve as both CO and CO_2 [65]. Figure 6 depicts the CO and CO_2 profiles obtained in TPD experiments for the carbon catalysts used for methanol dehydration in the presence of air and He at a reaction temperature of 350 ºC, whereas the amounts of CO and CO_2 evolved and the total oxygen concentration are summarized in Table 4. As can be observed, the samples show a significant CO (and CO_2) evolution at temperatures higher to 750 ºC which has been assigned to the decomposition of stable C–O–PO_3 (and O=CO–PO_3) groups, producing C–PO_3 groups [27,30]. Moreover, the fresh carbon, ACP2800, desorbs a small amount of CO_2 in the low temperature region, indicating the presence of carboxylic moieties, though in insignificant amounts.

The amount of oxygen surface groups decreases drastically when the methanol dehydration is carried out in He, in agreement with the results obtained from the XPS analyses. However, in the case of the carbon used in air the total amount of CO and CO_2 increases with respect to the fresh carbon (Table 4). This behavior is in agreement with previously results reported by our group [30]. In that work, we investigated the oxidation evolution of ACP2800 carbon surface in air at different temperatures (between 120-350 ºC) for 2h. For comparison purpose, TPD of ACP2800 after air oxidation at 350 ºC for 2 h (ACP2800-O350) is also represented in Figure 8. We found that oxygen reacts preferentially with the phosphorus surface groups through the oxidation of C–PO_3 groups to C–O–PO_3 ones, which are thermally stable up to 800 ºC, as denoted by the CO desorption rate profile of ACP2800-O350 (Figure 8). Only when the P surface groups seemed to be completely oxidized, oxidation of the carbon surface started to be significant, generating OSG of less thermal stability. In this sense, as we observed in Figure 8, the TPD profiles of ACP2800-RA revealed the formation of OSG with less thermal stability, whilst the CO desorption peak at 800 ºC did not reached the value of that obtained in the case of ACP2800-O350. That together with the huge

decrease in the amount of CO desorbed for ACP2800-RH suggests that the active sites are indeed the oxidized phosphorus surface groups, which are reduced by the methanol molecule (that probably form in consequence oxygenated products as DMM and MF, as seen in Table 2), and regenerated by oxygen, through the oxidation of C-P bonds to C-O-P ones. Similar results were observed by Grunewald and Drago [30] studying the ethanol conversion over carbon molecular sieves. They observed that under N_2 atmosphere the catalyst activity decreased to zero after a few hours, however, when N_2 was changed by air the catalyst recovered the activity. The authors pointed out that the active sites over the carbon surface were reduced by ethanol and regenerated by air.

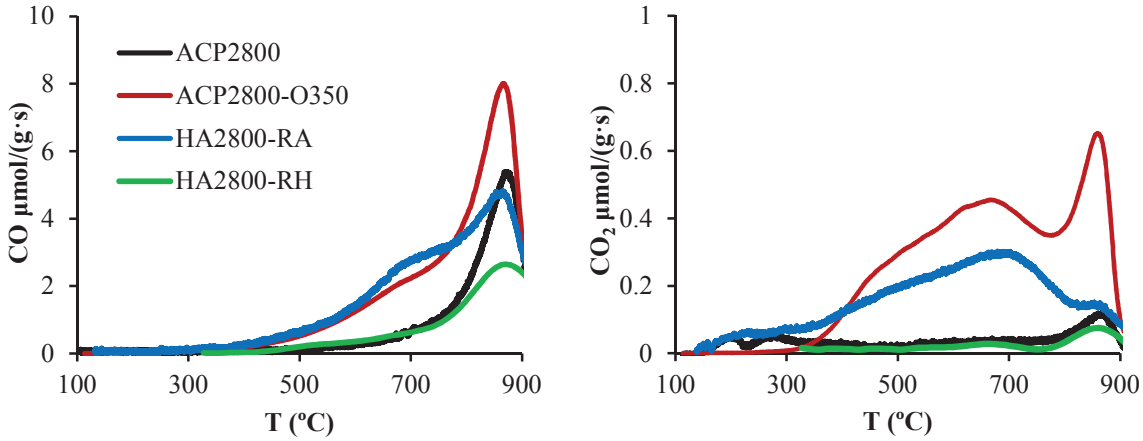

Figure 8. Amount of CO and CO_2 evolved with temperature during the TPD performed to ACP2800 before and after reaction in air and in He (350ºC, 2h, P_{MeOH} = 0.02 atm; W/F_{MeOH} = 0.1 g·s/µmol); and after air oxidation (350 ºC, 2h), ACP2800-O350.

Table 4. Amount of CO and CO_2 evolved from the fresh, oxidized and used activated carbons and total oxygen concentrations.

Sample	CO (µmol/g)	CO_2 (µmol/g)	O(TPD)[a] % wt.
ACP2800	3915	305	7.2
ACP2800-O350	7355	1295	15.9
ACP2800-RA	7025	745	13.6
ACP2800-RH	3470	115	5.9

[a] Total oxygen estimated from the evolved amounts of CO and CO_2

3.3.2. Catalyst regeneration

In order to analyze the stability of the carbon species/coke deposited on the catalyst active sites and the possible regeneration of its activity, a series of reaction-regeneration cycles have been carried out. Figure 9 displays the evolution of methanol conversion and the selectivity to DME at 350 ºC, in three successive reaction stages using first methanol in air, later methanol in He and finally, methanol in air again (with regeneration between the second and third reaction stages). In the first part of the experiment, using air in the reaction gas, a comparison is also drawn between the activity of the fresh catalyst and that of the carbon oxidized previously in air at 350 ºC for 2h, ACP2800-O350. Given that oxidation of ACP2800 carbon surface completely oxidized the surface P groups through the oxidation of C-P surface bonds to C-O-P ones, as revealed by the TPD results for ACP2800-O350 (Figure 8), it is expected that this catalyst has a higher surface acidity that would be translated into a higher activity. Indeed, the first stage shown in Figure 9 evidences that the initial catalytic activity is higher for ACP2800-O350. Even though, the catalyst is partially deactivated after 60 min of reaction, showing a conversion profile similar to that observed for the fresh catalyst. According to the discussions made above, only the moderate and weak acid sites seem to be stable enough to longer reaction times, while the strongest ones are deactivated by stable carbon deposits (probably carbon coke), which seems not to be combusted at the tested temperatures. The selectivity is around 90 % to dimethyl ether, and the presence of DMM, MF, CO_2 (and CO) were detected in the outlet stream.

In the second stage of the experiment, in He flow, the methanol conversion decreases to a low value, due to a partly deactivation of the catalyst by coke and/or less stable carbon species (C_xH_y) deposition on Brönsted acid sites and to the reduction of the C-O-PO_3 groups to C-PO_3 groups, or even ones with a lower oxidation state, as revealed the XPS and TPD results (Figure 6 and 8, respectively). The remaining weak acidic surface sites after the deactivation of the rest of active sites produce a selectivity of almost 100 % to DME under these experimental conditions. After deactivation in He flow for 150 min, air is immediately introduced again in the last step of the experiment. As can be observed, the activity is almost restored and the steady state methanol conversion increases from 7 to 27 %, supporting the suggestion made about the key role of the redox cycle of P-groups where methanol acts as the reductant and oxygen as the

oxidant. The selectivity to DME slightly decreases at the cost of higher CO and CO_2 selectivities, probably related to the combustion of accumulated C_xH_y deposits over the moderate acid sites thanks to the favoured spill-over of oxygen by P-groups. These results could be comparable with other previously reported in the literature by Zhout et al. [66] and Weng et al. [67]. They proposed the regeneration of coke deposited Brönsted reaction sites by spillover oxygen is more efficient than regeneration with gaseous oxygen. It has been also reported that addition of oxygen was efficient in avoiding the formation of carbon and reducing adsorption of carbon species on the active sites of vanadium pyrophosphate oxides catalyst in the glycerol dehydration reaction [20].

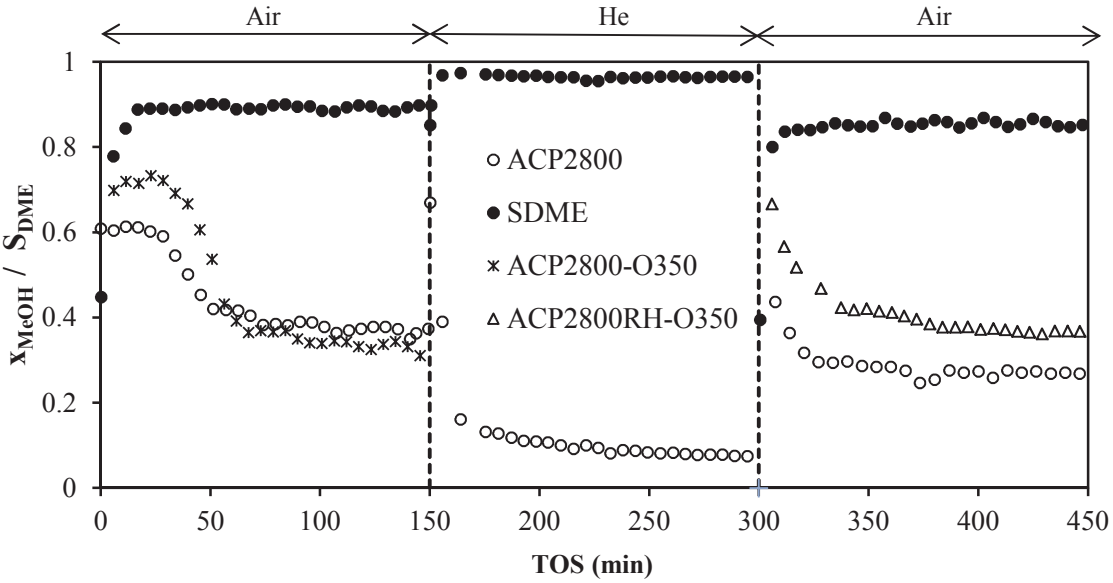

Figure 9. Methanol conversion and selectivity to DME as a function of TOS using first air (ACP2800, ACP2800-O350), then N_2 (ACP2800), and finally air as reaction gas (ACP2800RH, ACP2800RH-O350). (T=350ºC, P_{MeOH} = 0.020 atm, W/F_{MeOH} = 0.10 g·s/µmol).

On this sense, to restore completely the activity of the used catalyst in He, it was afterwards oxidized in air for 2 h at 350 ºC, ACP2800RH-O350, and then the methanol dehydration on the carbon catalyst in air atmosphere was studied again (Figure 9, third stage). As can be observed, the catalyst recovers its activity, showing similar methanol steady state conversions (37 %) than the fresh ACP2800 sample. Nevertheless, it is not observed the initial methanol conversion of about 60 % within the first 60 min of

reaction, when it is compared to ACP2800-O350 (stage 1). This loss of activity at short reaction times can be attributed to the deterioration of a fraction of the strongly acid Brönsted sites by stable coke deposits. These stable coke deposits are not oxidized at 350 ºC and it would be necessary higher temperatures for its complete combustion. Moreover, during the regeneration of the deactivated catalysts, traces of CO_2 were detected in the outlet gas, supporting the deposition of a light coke on the moderate acid active sites which is slowly removed in air atmosphere under the reaction conditions used. On this question, Pedro L. Benito et al. [68] proved that deposited coke in the catalyst in the range between 300 and 400 ºC by methanol decomposition is very unstable (constituted by alkylated aromatics and oligomers) and it is possible to be partially eliminated by a degasification step (under vacuum of 10^{-4} mmHg at 300 ºC). They also pointed out that H-ZSM-5 catalyst under the conditions of the MTG process completely recuperates its activity after a coke combustion step with air at 550 ºC [69].

From the characterization results of the wasted catalysts and from the catalyst regeneration experiments it can be concluded that the methanol decomposition over ACP2800 activated carbon may be seen as an equilibrium between the phosphorus groups being reduced by methanol and being regenerated by oxygen, through the oxidation of C-P bonds to C-O-P ones (explaining the higher CO desorption rate of ACP2800-RA when compared to ACP2800-RH, Figure 8). On the other hand, the oxygen spill-over from oxidized P groups to the carbon surface (demonstrated by the CO desorption peak that appears at intermediate temperature in the TPD of ACP2800-RA) provide reactive oxygen atoms that are able to oxidize the C_xH_y intermediates over the acid sites of moderate strength, forming CO, CO_2 and water in the process, but they cannot oxidize the coke deposits over the strong acid sites at the temperatures employed in the reaction.

3.4. Mechanism for methanol consumption

The ultimate goal of this paper, therefore, is to develop a mechanism for methanol decomposition on phosphoric acid activated carbons. Moreover, the kinetic expression obtained from the proposed kinetic model in the presence of molecular oxygen was used to obtain the kinetic and thermodynamics parameters by numerical optimization of the experimental data.

Two types of active sites have been proposed, one acid site (L) in which the alcohol dehydration takes place, this acid site involves both, C-O-PO_3 groups and P-OH acid sites. The second active site (L') is assumed for the dissociation of molecular oxygen, which is that associated to C-PO_3 groups, given that at oxidation temperatures lower than 350 ºC oxygen reacts preferentially with the phosphorus surface groups through the oxidation of C-PO_3 groups to C-O-PO_3 ones [30].

The reaction steps for the formation of DME, DMM, MF, CO_2 and CO are given in the following reaction scheme which accounts steps of adsorption on the active sites, surface reaction and desorption of the reaction products from the active sites.

Adsorption

$$CH_3OH(g) + L \xleftrightarrow{K_{MeOH-L}} CH_3OH - L \quad (1)$$

$$O_2(g) + 2L' \xleftrightarrow{K_{O-L'}} 2\,(O - L') \quad (2)$$

Surface reactions

Methanol dehydration

$$CH_3OH - L + CH_3OH(g) \xrightarrow{k_{DME}} CH_3OCH_3 - L + H_2O(g) \quad (3)$$

$$H_2O(g) + CH_3OH - L \xleftrightarrow{K_w} [H_2O]CH_3OH - L \quad (4)$$

Secondary reactions

$$CH_3OH - L + O - L' \xrightarrow{k_{CH_xO_y}} [CH_xO_y - L] + H_2O(g) + L' \quad (5)$$

$$[CH_xO_y - L] + 2CH_3OH(g) \xrightarrow{k_{DMM}} (CH_3O)_2CH_2 - L + H_2O(g) \quad (6)$$

$$[CH_xO_y - L] + CH_3OH(g) \xrightarrow{k_{MF}} HCOOCH_3 - L + H_2O(g) \quad (7)$$

$$[CH_xO_y - L] \xrightarrow{k_{CO}} CO - L + H_2O(g) \quad (8)$$

$$[CH_xO_y - L] + O - L' \xrightarrow{k_{CO_2}} CO_2 - L + H_2O(g) + L' \quad (9)$$

Desorption

$$CH_3OCH_3 - L \xleftrightarrow{1/K_{DME}} CH_3OCH_3(g) + L \quad (10)$$

$$(CH_3O)_2CH_2 - L \xleftrightarrow{1/K_{DMM}} (CH_3O)_2CH_2(g) + L \quad (11)$$

$$HCOOCH_3 - L \xleftrightarrow{1/K_{MF}} HCOOCH_3(g) + \quad L \tag{12}$$

$$CO_2 - L \xleftrightarrow{1/K_{CO2}} CO_2(g) + L \tag{13}$$

$$CO - L \xleftrightarrow{1/K_{CO}} CO(g) + L \tag{14}$$

Scheme 1 outlines the surface methanol dehydration mechanism proposed. Based on our previous results about alcohol dehydration on phosphoric acid activated carbons [23,40], it is proposed that methanol is first molecularly reversibly adsorbed through hydrogen bonds to the bridging hydroxyl on the Brönsted sites or through hydrogen bonds between the oxygen in C-O-P bonds and the alcohol hydroxyl group (1). DME is formed over the active sites, through a substitution reaction, S_{N2}, between the adsorbed methanol and gas methanol by Eley-Rideal mechanism ((3) and (10)). Based on the slight reduction of the methanol conversion and selectivity to DME with increasing water vapor pressures (see Figure 4), it has been assumed that the water formed in this dehydration reaction may be adsorbed on top of the chemisorbed methanol molecules via formation of hydrogen bonds, resulting in the growth of water clusters around the chemisorption active sites, forming H_2O-MeOH-L dimers (4) [63].On the other hand, adsorbed MeOH can also react with O-L' to produce formaldehyde (CH_2O) and formic acid (HCOOH) intermediates. These intermediates, CH_2O and HCOOH, may react with methanol or O-L' sites to produce DMM and MF and CO, respectively, or CO_2. For simplicity the intermediate species have been denoted as CH_xO_y in the general reaction scheme (5-9). Since all the experiments have been conducted using the same oxygen pressure, and the oxygen chemisorption and spillover are considered to be faster than the CO and CO_2 formation, the amount of spillover L'_O oxygen can be considered to remain invariable, and will be englobed in the $k_{CH_xO_y}$ and k_{CO_2} kinetic constants.

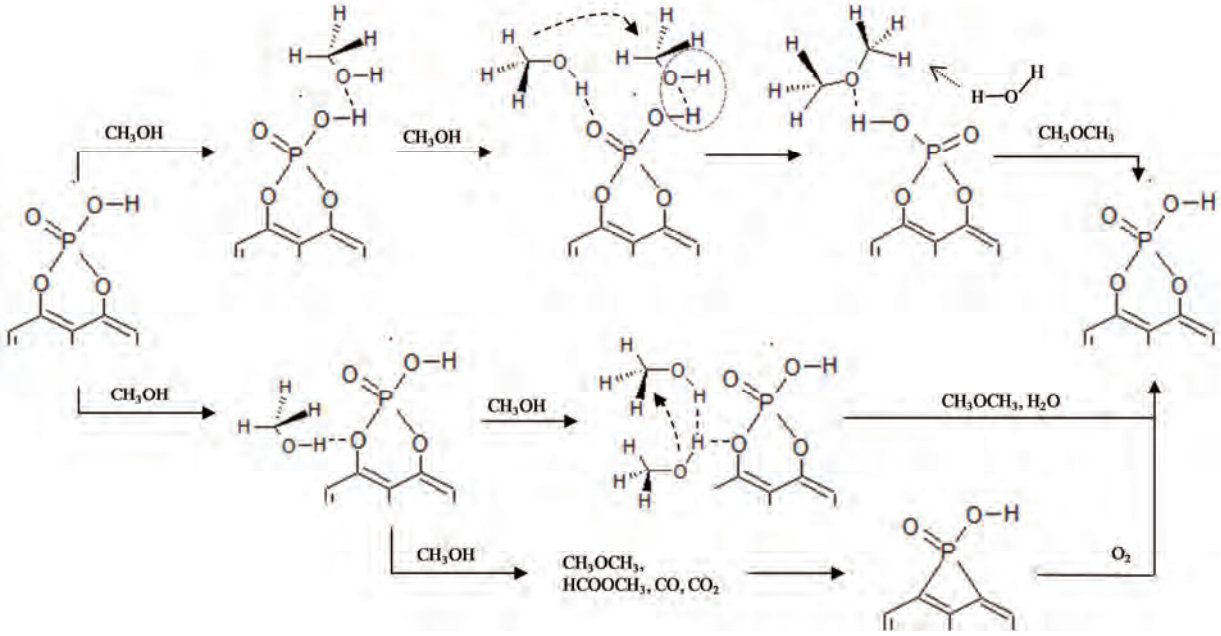

Scheme1. Scheme of the proposed surface dehydration mechanism from methanol molecule adsorbed on a phosphate group.

For the proposed kinetic model, it is assumed that all the adsorption reaches an equilibrium state. Moreover, desorption of the formed products is assumed to be fast, with the adsorbed amounts being negligible, thus they are not accounted in the kinetic expression. Besides, as the total conversion to DMM and MF are always lower than 1.5 %, until temperatures below 325 ºC (which is the scope of the kinetic model) the equations (6) and (7) are not considered. On the other hand, a quasi-equilibrium state is proposed for the formation and consumption rates of the CH_xO_y intermediate species. Taking these considerations into account, the kinetic rate expression for the formation of each product can be drawn from the above reaction scheme.

$$r_{DME} = k_{DME} \cdot P_{MeOH} \cdot \theta_{MeOH} = k_{DME} \cdot K_{MeOH-L} \cdot P_{MeOH}^2 \cdot \theta_f \quad (15)$$

$$r_{CO} = k_{CO} \cdot \theta_{CH_xO_y} = \frac{k_{CO} \cdot k_{CH_xO_y} \cdot K_{MeOH-L} \cdot P_{MeOH} \cdot \theta_f}{k_{CO} + k_{CO_2}} \quad (16)$$

$$r_{CO_2} = k_{CO_2} \cdot \theta_{CH_xO_y} \cdot \theta'_O = \frac{k_{CO_2} \cdot k_{CH_xO_y} \cdot K_{MeOH-L} \cdot P_{MeOH} \cdot \theta_f}{k_{CO} + k_{CO_2}} \quad (17)$$

$$-r_{MeOH} = 2 \cdot r_{DME} + r_{CO} + r_{CO_2} \quad (18)$$

where the free superficial fraction coverage of L sites is:

$$\theta_f = \frac{1}{1+K_{MeOH-L}\cdot P_{MeOH}\left[1+k_w\cdot P_w+\frac{k_{CH_xO_y}}{k_{CO}+k_{CO_2}}\right]} \quad (19)$$

Finally, the following suppositions were assumed: the reactor is considered as a plug flow integral reactor, homogeneous distribution of active sites on the catalyst surface, catalyst is assumed to operate at steady-state conditions, diffusional constraints and transport limitations are negligible (theoretically proven from Damköhler and Thiele modulus) and changes in temperature and pressure within the reactor are neglected. All these suppositions have been checked in previous work on alcohol dehydration where the same experimental procedure was utilized [23,40].

The dependence of the kinetic and thermodynamic parameters with the temperature was considered to follow an Arrhenius law for the kinetic constant (Eq. 21) or the Van´t Hoff law for the adsorption constants (Eq. 22)

$$k_i = k_{i0}\exp\left(\frac{-E_{ai}}{RT}\right) \quad (21)$$

$$K_i = K_{i0}\exp\left(\frac{-\Delta H_i}{RT}\right) \quad (22)$$

Finally, the molar balance to the plug reactor is employed for obtaining the methanol conversion and the product formation at a given space time

$$\frac{dX_i}{d(\frac{W}{F})} = r_i \quad (23)$$

Combining the molar balances, the kinetic rates equations and stoichiometric relationships, and using Runge-Kutta for the numerical solution of each differential equation, the set of differential equations can be solved, and the conversion and

selectivity can be estimated for every given operational condition employed in the kinetic study. Thus, the kinetic parameters that rule out the proposed model were calculated by minimizing the objective function (O.F.) using the Levenberg-Marquart optimization method as implemented in Matlab 2010a software:

$$O.F. = \frac{\sum_i (Xcal_i - Xexp_i)^2}{i} \quad (24)$$

where $Xexp_i$ represents the value of the conversion obtained experimentally, and $Xcal_i$ the calculated value. This optimization problem was solved given an O.F. value of 8.38 x 10^{-4}.

3.5. Kinetic study

Table 5 summarizes the values of the activation energy or enthalpy of adsorption and the preexponential factors (k_{i0}, K_{i0}) for all the implied reactions and equilibriums. The activation energy for the formation of DME is 85.4 kJ/mol, within the range of apparent activation energies obtained by Moreno-Castilla et al. [26] (65-110 kJ/mol) with different activated carbons oxidized with H_2O_2, $(NH_4)_2S_2O_8$ and HNO_3. Xu et al. [15] reported an apparent activation energy of around 105 KJ/mol for the dehydration of methanol to DME over a γ-Al_2O_3. The obtained thermodynamic parameters fulfill the requirements of negative enthalpies of adsorption, negative standard entropies of adsorption (-42.0 and -24.7 J/mol·K for methanol and water, respectively) and standard entropies of adsorption with absolute values smaller than the respective standard entropies in gas phase (239.9 and 188.0 J/mol·K for methanol and water, respectively). The rate constants have been obtained for a reaction temperature of 325 ºC and the results are reported in the last column of Table 5. It can be observed that the kinetic constants for the formation of CO_2 and CO are three orders of magnitude lower than the formation constant of the oxygenated intermediates, k_{CHxOy}, which causes the relative amount of the intermediates being the highest in the surface of the active site. As for the water interaction with methanol, it was observed that at the highest methanol

conversion, around 6% of adsorbed methanol was unavailable due to the interaction with the formed water.

Table 5. Kinetic and thermodynamic parameters obtained for methanol conversion.

	$k_{i,0}$, $K_{i,0-L,L'}$ (mol/g·s·atm, atm^{-1})	$Ea_i/\Delta H_{i-L,L'}$ (kJ/mol)	$k_i(325^oC)$, $K_i(325^oC)$ (mol/g·s·atm, atm^{-1})
K_{MeOH-L}	$6.3\cdot10^{-03}$	-28.6	2.0
$K_{w-MeOH-L}$	$5.1\cdot10^{-02}$	-30.4	$2.3\cdot10^{1}$
k_{DME}	$1.0\cdot10^{+07}$	85.4	3.6
k_{CHxOy}	$2.6\cdot10^{+09}$	132.6	$6.8\cdot10^{-02}$
k_{CO2}	$1.3\cdot10^{+03}$	107.9	$4.9\cdot10^{-07}$
k_{CO}	$2.2\cdot10^{+03}$	110.6	$4.8\cdot10^{-07}$

Figure 10a represents the steady-state methanol conversion as a function of the space time, from 0.050-0.180 g·s/µmol, at an inlet methanol partial pressure of 0.02 atm and at different reaction temperatures. On the other hand, Figure 10b displays the methanol steady state conversion as a function of methanol (0.01-0.004 atm) inlet partial pressures at different temperatures and at space time of 0.10 g·s/µmol. All shown data refers to experiments performed in air. The results predicted by the model are shown in solid lines for comparison sake. It is noteworthy the good agreement between experimental and calculated values provided by the kinetic model. A significant increment in methanol conversion with increasing temperature, space time and methanol partial pressure in the inlet stream can be noticed. Selectivity to DME remains very high and practically constant, although when temperature is raised there is a slight increase in the selectivities to CO_2 and CO, which are the most thermodynamically favored products (data not shown). Figure 11 represents the simulated conversion, X_{cal}, versus the conversion obtained experimentally, X_{exp} for dehydration of methanol on ACP2800 catalyst, as well as the calculated and experimental DME, CO and CO_2 yields (expressed as the selectivity multiplied by the methanol conversion). A proper fitting of the model to the experimental Methanol conversion and DME yield is observed in Figure 11a. However, calculated CO_2 and CO (Figure 11b) yields show a slight deviation from the experimental data due to difficulties in their determination because the low produced amount, affecting the accuracy of the experimental values.

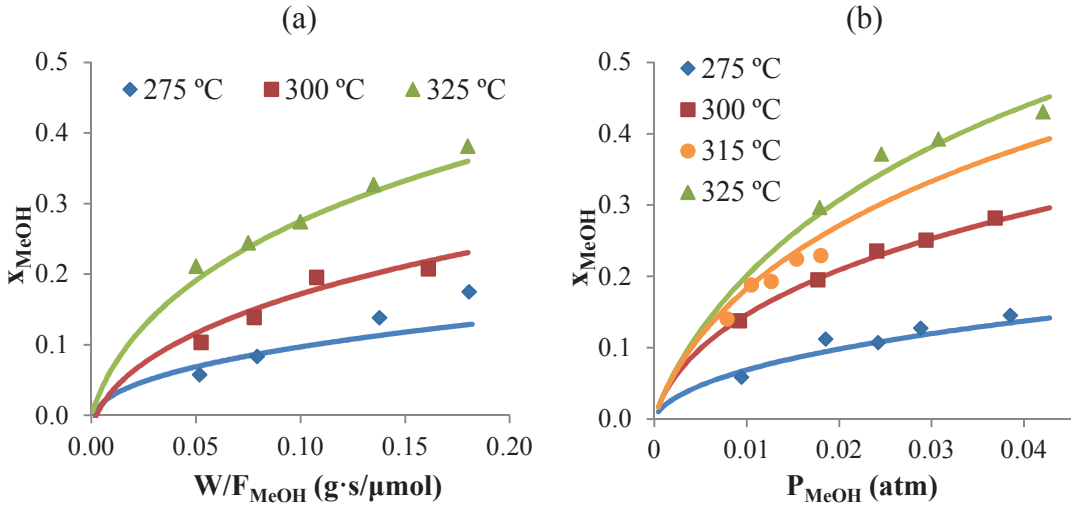

Figure 10. Steady state methanol conversion at different temperatures as a function of the space time (P_{MeOH} = 0.020 atm) (a) and as a function of the methanol partial pressure (W/F_{MeOH} = 0.10 g·s/µmol) (b) in air. (Symbols: experimental values, lines: calculated values).

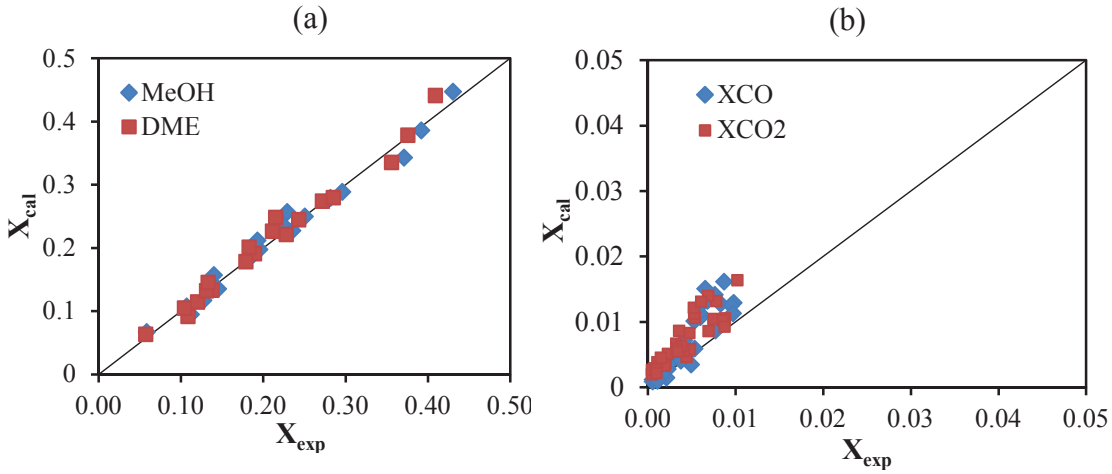

Figure 11. Calculated versus experimental conversions for (a) methanol and dimethyl ether and (b) carbon monoxide and carbon dioxide.

4. Conclusions

A carbon catalyst obtained by chemical activation of olive stone with phosphoric acid at an impregnation ratio of 2 and an activation temperature of 800 ºC has shown to be effective for the selective methanol dehydration to dimethyl ether. XPS analyses demonstrates the presence of phosphorus in form of C-O-PO_3 and C-PO_3 groups over the carbon surface, which confers to the carbon surface acid and redox sites as confirmed by MeOH-TPRS.

The catalytic results evidence that the catalyst performance strongly depends on the type of atmosphere in which the reaction proceeds, and suggest that oxygen plays a key role on this catalytic process. In the absence of oxygen, the catalyst suffers a progressive deactivation due to both coke deposition on the strong Brönsted acid sites and to the reduction of the phosphorus groups (from C-O-P to C-P ones). However, in the presence of air, the carbon surface chemistry is modified through oxygen spillover (favoured by the presence of surface phosphorus groups) on the catalyst surface, where the availability of labile oxygen inhibit catalyst deactivation and allow methanol steady state conversion to be reached. Furthermore, the presence of oxygen leads to significant enhancement of methanol conversion without any significant change in the selectivity or reaction and even partially regenerates the wasted catalysts obtained from inert experiences. Methanol conversion and DME selectivity are slightly reduced when water vapor is added to the reactor. A kinetic study has been carried out where the methanol decomposition was supposed to proceed through an Eley-Rideal mechanism, in which the surface reaction proceeds through a substitution mechanism, S_{N2}, between an adsorbed methanol molecule and a methanol molecule in gas phase. The rate expressions derived from the optimization of the kinetic parameters of the model properly described the experimental results, being the activation energy obtained for the formation of dimethyl ether around 85 kJ/mol.

Acknowledgments

We gratefully thank Junta de Andalucia (P09-FQM-5156) and Spanish Ministry of Economy and Competitiveness (MINECO) and FEDER (Project CTQ2012-364086) for financial support. M.J.V.R. gratefully thanks MINECO for a FPI fellowship (BES-2010-032213). E.M.C.M.

gratefully thanks MECD for a FPU fellowship (AP-2012-01359). R.R.R also thanks MINECO for economic support through a "Juan de la Cierva" contract (JCI-2012-12664).

Notation

$A_{BET}^{N_2}$= apparent surface area obtained by the BET method, $m^2 \cdot g^{-1}$

$A_{DR}^{CO_2}$ = apparent area of narrow micropores, $m^2 \cdot g^{-1}$

BET = Brunauer, Emmett, and Teller

DME = dimethyl ether

DMM = dimethoxymethane

DR = Dubinin-Raduskevich

Ea_i = activation energy of the formation of i, $kJ \cdot mol^{-1}$

ER = Eley-Rideal

F_{MeOH} = initial molar flow of methanol, $mol \cdot s^{-1}$

ΔH^0_{ad} = standard enthalpy of adsorption, J mol^{-1}

$\Delta H_{i\text{-}L}$ = enthalpy of adsorption of i on an acid site, $KJ \cdot mol^{-1}$)

$\Delta H_{i\text{-}L'}$ = enthalpy of adsorption of i on C-P site, $KJ \cdot mol^{-1}$

i – L = component i bonded to L site, MeOH-L; DME-L; DMM-L; MF-L; CO-L; CO_2-L

i – L = component i bonded to L' site, O-L'

k_i = i formation rate constant (mol g^{-1} s^{-1})

$K_{i\text{-}L}$ = Adsorption equilibrium constant for i on acid site, atm^{-1}

$K_{i\text{-}L'}$ = Adsorption equilibrium constant for i on C-P site, atm^{-1}

$K_{io\text{-}L}$ = preexponential factor of the i adsorption on acid site, atm^{-1}

$K_{io\text{-}L'}$ = preexponential factor of the i adsorption on C-P site, atm^{-1}

L = acid site

L'= C-P site

M, MeOH = methanol

MF = methyl formate

NDIR = nondispersive infrared

O.F. = objective function (Residual error)

P_{i0} = component i initial pressure, atm

P_i = component i final pressure, atm

r_i = rate of i formation (mol s^{-1} g^{-1})

R = universal gas constant, $J \cdot mol^{-1} \cdot K^{-1}$

Ri = rate equation for component i

Si = selectivity to i product

STP = standard temperature-pressure conditions

T = temperature (ºC)

TOS= time on stream

TPD = temperature-programmed desorption

$V_{DR}^{N_2}$ (cm^3/g) = micropore volume obtained by the DR method applied to the N_2 isotherm, $cm^3 \cdot g^{-1}$

$V_{DR}^{CO_2}$ = micropore volume obtained by the DR method applied to the CO_2 isotherm, $cm^3 \cdot g^{-1}$

V_{meso} = mesopore volumen, $cm^3 \cdot g^{-1}$

w = water

W= weight of catalyst, g (g)

W/F^o_{EtOH} = ethanol space time (g s mol^{-1})

$X_{MeOH} = \frac{P_{MeOHo} - P_{MeOH}}{P_{MeOHo}}$ = methanol conversion

X_{exp} = experimental conversion

X_{cal} = calculated conversion

XPS = X-ray photoelectron spectroscopy

Greek letters

θ_i = fractional coverage of specie i on acid sites

θ'_i = fractional coverage of specie i on C-P sites

References

[1] M. Stöcker, Micropor. Mesopor. Mater. 29 (1999) 3.

[2] A.G. Gayubo, P.L. Benito, A.T. Aguayo, M. Olazar, J. Bilbao, J. Chem. Technol. Biotechnol. 65 (1996) 186.

[3] A.T. Aguayo, A.G. Gayubo, R. Vivanco, M. Olazar, J. Bilbao, Appl. Catal. A: Gen. 283 (2005) 197.

[4] A.G. Gayubo, A.T. Aguayo, A.E. Sánchez Del Campo, A.M. Tarrío, J. Bilbao, Ind. Eng. Chem. Res. 39 (2000) 292.

[5] J. Agrell, K. Hasselbo, K. Jansson, S.G. Järås, M. Boutonnet, Appl. Catal. A: Gen. 211 (2001) 239.

[6] T.H. Fleisch, A. Basu, R.A. Sills, J. Nat. Gas Sci. Eng. 9 (2012) 94.

[7] P. Cheung, A. Bhan, G.J. Sunley, E. Iglesia, Angew. Chem. Int. Ed. 45 (2006) 1617.

[8] B.H. Minor, T.E. Chisolm, G.S. Shealy, US Patent 5 (1996) 572.

[9] A.M. Rouhi, Chem. Eng. News 73 (1995) 37.

[10] N. Inoue, Y. Ohno, Petrotech 24 (2001) 319.

[11] T.A. Semelsberger, R.L. Borup, H.L. Greene, J. Power Sources 156 (2006) 497.

[12] S.D. Kim, S.C. Baek, Y.-. Lee, K.-. Jun, M.J. Kim, I.S. Yoo, Appl. Catal. A: Gen. 309 (2006) 139.

[13] T.A. Semelsberger, K.C. Ott, R.L. Borup, H.L. Greene, Appl. Catal. B: Environ. 61 (2005) 281.

[14] V. Vishwanathan, K.-. Jun, J.-. Kim, H.-. Roh, Appl. Catal. A: Gen. 276 (2004) 251.

[15] M. Xu, J.H. Lunsford, D.W. Goodman, A. Bhattacharyya, Appl. Catal. A: Gen. 149 (1997) 289.

[16] A.G. Gayubo, A.T. Aguayo, M. Olazar, R. Vivanco, J. Bilbao, Chem. Eng. Sci. 58 (2003) 5239.

[17] A.G. Gayubo, A.T. Aguayo, A. Alonso, A. Atutxa, J. Bilbao, Catal. Today 106 (2005) 112.

[18] D.M. Brown, B.L. Bhatt, T.H. Hsiung, J.J. Lewnard, F.J. Waller, Catal. Today 8 (1991) 279.

[19] G.C. Grunewald, R.S. Drago, J. Am. Chem. Soc. 113 (1991) 1636.

[20] F. Wang, J.-. Dubois, W. Ueda, J. Catal. 268 (2009) 260.

[21] J. Bedia, R. Barrionuevo, J. Rodríguez-Mirasol, T. Cordero, Appl. Catal. B: Environ. 103 (2011) 302.

[22] F. Rodríguez-Reinoso, Carbon 36 (1998) 159.

[23] J. Bedia, R. Ruiz-Rosas, J. Rodríguez-Mirasol, T. Cordero, J. Catal. 271 (2010) 33.

[24] M. Calzado, M.J. Valero-Romero, P. Garriga, A. Chica, M.O. Guerrero-Pérez, J. Rodríguez-Mirasol, T. Cordero, Catal. Today (2014). doi:10.1016/j.cattod.2014.06.038

[25] J. Zawadzki, B. Azambre, O. Heintz, A. Krzton, J. Weber, Carbon 38 (2000) 509.

[26] C. Moreno-Castilla, F. Carrasco-Marín, C. Parejo-Pérez, M.V. López Ramón, Carbon 39 (2001) 869.

[27] E. Gonzalez-Serrano, T. Cordero, J. Rodriguez-Mirasol, L. Cotoruelo, J.J. Rodriguez, Water Res. 38 (2004) 3043.

[28] J.M. Rosas, J. Bedia, J. Rodríguez-Mirasol, T. Cordero, Fuel 88 (2009) 19.

[29] J.M. Rosas, J. Bedia, J. Rodríguez-Mirasol, T. Cordero, Ind. Eng. Chem. Res. 47 (2008) 1288.

[30] M.J. Valero-Romero, J. Rodriguez-Mirasol, T. Cordero. Role of surface phosphorus complexes on the oxidation of porous carbons. Chapter 2.

[31] M.J. Valero-Romero, J. Rodriguez-Mirasol, T. Cordero. On the chemical nature and thermal stability of surface phosphorus groups on carbons by TPD experiments. Chapter 3.

[32] J.M. Rosas, R. Ruiz-Rosas, J. Rodríguez-Mirasol, T. Cordero, Carbon 50 (2012) 1523.

[33] M.O. Guerrero-Pérez, M.J. Valero-Romero, S. Hernández, J.M.L. Nieto, J. Rodríguez-Mirasol, T. Cordero, Catal. Today 195 (2012) 155.

[34] M.J. Valero-Romero, A. Cabrera-Molina, M.O. Guerrero-Pérez, J. Rodríguez-Mirasol, T. Cordero, Catal. Today 227 (2014) 233.

[35] J. Bedia, R. Ruiz-Rosas, J. Rodríguez-Mirasol, T. Cordero, AIChE J. 56 (2010) 1557.

[36] J. Bedia, J.M. Rosas, J. Márquez, J. Rodríguez-Mirasol, T. Cordero, Carbon 47 (2009) 286.

[37] A.M. Puziy, O.I. Poddubnaya, A. Martínez-Alonso, F. Suárez-García, J.M.D. Tascón, Carbon 43 (2005) 2857.

[38] T. Vernersson, P.R. Bonelli, E.G. Cerrella, A.L. Cukierman, Bioresour. Technol. 83 (2002) 95.

[39] M. Jagtoyen, F. Derbyshire, Carbon 36 (1998) 1085.

[40] S. Brunauer, P.H. Emmett, E. Teller, J. Am. Chem. Soc. 60 (1938) 309.

[41] B.C. Lippens, J.H. de Boer, J. Catal. 4 (1965) 319.

[42] F. Rodríguez-Reinoso, M. Molina-Sabio, M.T. González, Carbon 33 (1995) 15.

[43] M.M. Dubinin, E.D. Zaverina, L.V. Radushkevich, J. Phys. Chem. (URSS) 21 (1947) 1351.

[44] C.N. Satterfield, Heterogeneous Catalysis in Industrial Practice, McGraw-Hill, New York, 1991.

[45] J. Rodriguez-Mirasol, T. Cordero, J.J. Rodriguez, Energy Fuels 7 (1993) 133.

[46] A.M. Puziy, O.I. Poddubnaya, A.M. Ziatdinov, Appl. Surf. Sci. 252 (2006) 8036.

[47] E.I. Kauppi, E.H. Rönkkönen, S.M.K. Airaksinen, S.B. Rasmussen, M.A. Bañares, A.O.I. Krause, Appl. Catal. B: Environ. 111-112 (2012) 605.

[48] L.A. Gambaro, L.E. Briand, Appl. Catal. A: Gen. 264 (2004) 151.

[49] K.S. Kim, M.A. Barteau, W.E. Farneth, Langmuir 4 (1988) 533.

[50] S.T. Korhonen, M.A. Bañares, J.L.G. Fierro, A.O.I. Krause, Catal. Today 126 (2007) 235.

[51] F. Chang, Y. Wei, X. Liu, Y. Zhao, L. Xu, Y. Sun, D. Zhang, Y. He, Z. Liu, Appl. Catal. A: Gen. 328 (2007) 163.

[52] W.E. Farneth, R.H. Staley, P.J. Domaille, R.D. Farlee, J. Am. Chem. Soc. 109 (1987) 4018.

[53] M. Jayamurthy, S. Vasudevan, Catal. Lett. 36 (1996) 111.

[54] A. Ison, R.J. Gorte, J. Catal. 89 (1984) 150.

[55] M.T. Aronson, R.J. Gorte, W.E. Farneth, J. Catal. 105 (1987) 455.

[56] C. Tsiao, D.R. Corbin, C. Dybowski, J. Am. Chem. Soc. 112 (1990) 7140.

[57] J.M. Tatibouët, Appl. Catal. A: Gen. 148 (1997) 213.

[58] F. Yaripour, F. Baghaei, I. Schmidt, J. Perregaard, Catal. Commun. 6 (2005) 147.

[59] F. Yaripour, F. Baghaei, I. Schmidt, J. Perregaarad, Catal. Commun. 6 (2005) 542.

[60] M. Mollavali, F. Yaripour, H. Atashi, S. Sahebdelfar, Ind. Eng. Chem. Res. 47 (2008) 3265.

[61] R. Ruiz-Rosas, J. Bedia, J.M. Rosas, M. Lallave, I.G. Loscertales, J. Rodríguez-Mirasol, T. Cordero, Catal. Today 187 (2012) 77.

[62] S.M. Taqvi, W.S. Appel, M.D. LeVan, Ind. Eng. Chem. Res. 38 (1999) 240.

[63] J. Rodríguez-Mirasol, J. Bedia, T. Cordero, J. Rodríguez, Sep. Sci. Technol. 40 (2005) 3113.

[64] J.F. DeWilde, H. Chiang, D.A. Hickman, C.R. Ho, A. Bhan, ACS Catal. 3 (2013) 798.

[65] J.L. Figueiredo, M.F.R. Pereira, M.M.A. Freitas, J.J.M. Órfão, Carbon 37 (1999) 1379.

[66] B. Zhou, T. Machej, P. Ruiz, B. Delmon, J. Catal. 132 (1991) 183.

[67] L.T. Weng, P. Ruiz, B. Delmon, D. Duprez, J. Mol. Catal. 52 (1989) 349.

[68] P.L. Benito, A.G. Gayubo, A.T. Aguayo, M. Olazar, J. Bilbao, Ind. Eng. Chem. Res. 35 (1996) 3991.

[69] P.L. Benito, A.T. Aguayo, A.G. Gayubo, J. Bilbao, Ind. Eng. Chem. Res. 35 (1996) 2177.

Chapter 5

Kinetic Study of the Decomposition of ethanol on carbon-based acid catalysts

Abstract Ethylene is essential material for the petrochemical industry. Ethylene production via catalytic dehydration of ethanol over an activated carbon prepared by chemical activation of olive stone with H3PO4 is reported in this paper. The XPS results suggest the existence mainly of C-OPO3 and C-PO3 surface groups, which are responsible of the wide distribution of acid sites on the carbon surface, as confirmed by NH3-TPD. The catalytic decomposition of ethanol over the activated carbon yields mainly dehydration products, mostly ethylene (selectivity > 90 % at 325 ºC) with lower amounts of diethyl ether. Only at low-temperatures, below 300 ºC, the selectivity to both diethyl ether and acetaldehyde, as dehydrogenation product, are significant. The effects of operation parameters, such as ethanol partial pressure, reaction temperature, space time, water vapor and concentration of oxygen in the carrier gas have been investigated experimentally. In absence of oxygen the catalysts suffer a progressive deactivation due to both coke deposition on Brönsted acid sites and to the reduction of the phosphorus groups (from C-O-P to C-P ones). In the presence of oxygen an increase in the activity of the catalysts is observed and no deactivation is produced up to 325 ºC. The presence of oxygen enables maintenance of the catalytic redox cycle of the P groups from C-P to C-O-P ones, and catalytic active sites are recovered. Ethanol conversion is reduced slightly when water vapor is added to the reactor. A kinetic study of the catalytic dehydration of ethanol was carried out, where a Langmuir-Hinshelwood mechanism, via a surface elimination reaction, E2, was analyzed for ethylene formation. The rate expressions derived from the model fitted properly the experimental results, being the activation energy obtained for the formation of the main product, ethylene, around 165 kJ/mol.

Keywords: Catalysis, Kinetics, Selectivity, Ethanol decomposition, Ethylene, Activated carbons.

1. Introduction

Diethyl-ether is a valuable chemical and an attractive motor vehicle fuel alternative [1] and ethylene is one of the major feedstock of the petrochemical industry. Production of petrochemicals from a non-petroleum, environment friendly feedstock and development of new efficient ethylene production processes are considered as challenging research areas [2,3]. Bioethanol is an attractive alternative feedstock to be used for the production of these chemicals, among others petrochemical raw materials [4]. Furthermore, bioethanol is a key product as automotive fuel mixed with gasoline or diesel [5] and for obtaining H_2 by catalytic reforming [6,7]. Consequently, bioethanol should be considered a key biomass-derived product to complement oil and reduce CO_2 emissions, along with other oxygenates derived from other lignocellulosic biomass treatments, such as methanol and dimethyl ether (obtained via gasification) and biooil (obtained via flash pyrolysis).

The catalytic transformation of bioethanol to ethylene, which is the objective of the BETE (bio-ethanol to ethylene) process [8,9], avoids the costly operations for the total water elimination to obtain anhydrous ethanol, making the catalytic dehydration of bio-ethanol a very attractive way to obtain ethylene from a non petroleum source. For the BETE process, the HZSM-5 zeolite is more active and stable than the traditionally used γ-Al_2O_3, with slow deactivation by coke, which is attenuated by treatments to moderate its acid strength [10,11]. However, irreversible deactivation of the catalyst by dealuminization of the HZSM-5 zeolite occurs when temperature and water content in the feed of bioethanol are increased [12]. This problem is common to other oxygenated transformation processes, as in the case of methanol [13].

However, less effort has been related to study the ethanol dehydration on carbon based catalysts. In this sense, Szymański et al. [14] and Carrasco–Marín [15] studied the effect of active carbon oxidation with HNO_3 and $(NH_4)_2S_2O_8$, respectively, on their activity and selectivity in ethanol decomposition reaction. These oxidized carbons showed to be active for ethanol decomposition, yielding mainly ethylene and diethyl ether, however these authors also proved that the catalytic activity decreases at temperatures higher than 300 ºC caused by thermal decomposition of surface oxygen groups. On the other hand, Grunewald and Drago [16] studied the ethanol decomposition reaction over carbon molecular sieves. They found that when this

process is carried out in inert atmosphere the catalytic activity decreases and the main reaction product is ethylene. However, they reported that when N_2 was change by air, the catalysts recovered the activity and the main products were acetaldehyde and ethyl acetate. In particular, our research group has been studying the oxidation resistance and the catalytic properties of activated carbons prepared by chemical activation with phosphoric acid of various bio-renewable carbon precursors [17-19]. This activation method results in the formation of oxygen-phosphorus surface groups of high thermal stability and high surface acidity, which confers to the carbon a high oxidation resistance. These carbons have been used as catalytic supports [20-22] or as catalysts by themselves for 2-2-butanol and 2-propanol decomposition reactions, yielding mainly dehydration products [23,24]. More recently, we have studied the gas phase methanol [25] and ethanol [26] decomposition reaction over different acid carbon catalysts prepared by chemical activation of olive stone with phosphoric acid. We found that in absence of oxygen the catalyst suffer a progressive deactivation, however, the presence of oxygen produces a significant increase of the methanol and ethanol conversion and avoids deactivation of the catalysts under the operation conditions studied. In this work we study the decomposition (dehydration and dehydrogenation) of ethanol by using the acid activated carbon catalyst with the highest activity. Specifically, we examine the effect of oxygen concentration in the carrier gas, reaction temperature, ethanol inlet partial pressure and space time in the conversion and product selectivity of the ethanol decomposition reaction. A kinetic study of the ethanol decomposition on the acid carbon is also presented in which the presence and absence of water vapor in the reactor feed, in concentrations similar to that of the bio-ethanol, has been also analyzed. The corresponding kinetics and thermodynamics parameters were obtained.

2. Experimental procedure

2.1. Catalyst preparation

The carbon catalyst used in this work, denoted as ACP2800, was from olive stones, an agricultural waste predominantly produces in the Mediterranean countries. Olive stones were obtained from local olive manufacturers, cleaned with deionized water, dried at 100 ºC, and ground with a roller mill to obtain samples of 1-2 mm

particle size. This olive stone waste was impregnated with concentrated commercial H_3PO_4 (85 wt.%, Sigma Aldrich) at room temperature, using a weight ratio of 2/1 (H_3PO_4/olive stone), and dried for 24 h at 60 °C. The impregnated sample was activated at 800 ºC, under continuous N_2 (purity 99.999%, Air Liquide) flow (150 cm^3 STP/min) in a conventional tubular furnace. The activation temperature was reached at a heating rate of 10 °C/min and maintained for 2 h. The activated sample was cooled inside the furnace under the same N_2 flow and then washed. In the washing process the carbonized sample was immersed in hot distilled water at 60 ºC for 2 h and afterward rinsed with room temperature distilled water at 60 °C until constant pH and negative phosphate analysis in the eluate [26]. Finally, the resulting activated carbon was dried at 100 °C, grinded and sieved (100-300 μm).

2.2. Catalyst characterization

The porous structure of the carbon was characterized by N_2 adsorption/desorption at -196 ºC and CO_2 adsorption at 0 ºC, carried out in an ASAP 2020 model equipment of Michromeritics Instruments Corporation. Samples were previously outgassed during at least 8 hours at 150 ºC. From the N_2 adsorption/desorption isotherm, the apparent surface area (A_{BET}) was determined applying the BET equation [27], the micropore volume (V_t) and the external surface area (A_t) were calculated using the t-method [28] and the mesopore volume (V_{mes}) was obtained as the difference between the adsorbed volume at a relative pressure of 0.95 and the micropore volume (V_t) [29]. The narrow micropore surface area (A_{DR}) and volume (V_{DR}) were obtained by the Dubinin-Radushkevich method [30] applied to the CO_2 adsorption isotherm.

The surface chemistry of the carbon was analyzed by X-ray photoelectron spectroscopy (XPS), temperature-programmed desorption (TPD), adsorption and temperature-programmed desorption of ammonia (NH_3-TPD). The XPS analyses were obtained using a 5700C model Physical Electronics apparatus, with MgKα radiation (1253.6 eV). For the analysis of the XPS peaks, the C1s peak position was set at 284.5 eV and used as reference to position the other peaks. The fitting of the XPS peaks was done by least squares using Gaussian-Lorentzian peak shapes. TPD profiles were obtained in a custom quartz tubular reactor (i.d. 4 mm) placed inside an electrical furnace. The sample was heated from room temperature up to 900 ºC at a heating rate of

10 ºC/min in helium (purity 99.999%, Air Liquide) flow (200 cm^3 STP/min).The amounts of CO and CO_2 desorbed from the samples were monitored with nondispersive infrared (NDIR) gas analyzers (Siemens ULTRAMAT 22).

The total acidity and acid strength distribution of the catalyst were determined by temperature programmed desorption of ammonia. The NH_3-TPD was performed using 80 mg of catalyst saturated with NH_3 (20% vol. in Helium) for 15 min at 100ºC. After saturation, the NH3 weakly adsorbed was desorbed in a H_2 flow, at the adsorption temperature, until no NH_3 was detected in the outlet gas. The NH_3-TPD was performed by raising the temperature up to 500ºC at a heating rate of 10ºC/min. The NH_3 was measured by mass spectrometer (Pfeiffer Omnistar GSD-301).

2.3. Ethanol decomposition

The catalytic activity of the obtained activated carbon was measured by the decomposition of ethanol performed at atmospheric pressure, in a quartz fixed bed microreactor (4 mm i.d.), placed inside a vertical furnace with temperature control. In a typical experiment 150 mg of catalysts (100-300 μm mesh) was used. Ethanol was fed to the system in a controlled way by using a syringe pump (Cole-Parmer® 74900-00-05 model). The reaction was carried out in different atmospheres (He, 2, 4 and 10 % vol. of O_2 in He and Air) in the temperature range 250–375 ºC. To prevent condensation of ethanol and its reaction products, all the connections, from the syringe pump to the chromatograph, were heated by a wired resistance up to 120 ºC. The conditions were ethanol partial pressures from 0.01 to 0.08 atm and space times between 0.052 and 0.35 g·s/μmol (GHSV between 72 and 12 $m^3_{gas}\ kg^{-3}_{catalyst}\ h^{-1}$). Water was also fed to the system and the water partial pressures were varied between 0.01 and 0.1 atm.

The concentration of ethanol and products in the outlet gas stream were analyzed by gas chromatography (490 micro-GC equipped with PPQ, 5A molsieve and Wax columns, Agilent). In all the cases carbon mass balances were closed with errors lower than 5%. The ethanol conversion is defined as the molar ratio of ethanol converted to ethanol fed to the reactor. The selectivity is defined as:

$$S_i = \frac{C_i}{\sum_i C_i}$$

where C_i is the molar flow of i product in the outlet stream. The carbon-containing products detected in the decomposition of ethanol (CH_3CH_2OH, EtOH) catalyzed by phosphoric acid activated carbons were ethylene (CH_2CH_2, E), diethyl ether ($CH_3CH_2OCH_2CH_3$, DEE) and acetaldehyde (CH_3CHO, ACC).

3. Results and discussion

3.1. Catalyst characterization

Catalyst selection was done based on the results of a previous work, in which different activated carbons were obtained by chemical activation of olive stone with phosphoric acid at different activation temperatures, in the interval 400-800 ºC, and impregnation ratios, between 0.5 and 2 (R, g H_3PO_4/g olive stone), and characterized and tested for ethanol decomposition [26]. Among the prepared catalysts, ACP2800 (R = 2 and carbonized at 800 ºC) showed the greatest conversions and lowest deactivation kinetics due to the wider porous structure and larger amount of stable surface phosphorous, both characteristics generated by the high impregnation ratio and activation temperature used for its synthesis.

The physicochemical properties of the carbon catalyst are presented in Table 1. The data presented are referred to structural parameters obtained from the N_2 adsorption-desorption and CO_2 adsorption isotherms, surface mass concentration obtained by XPS and surface acidity of the carbon obtained by adsorption, desorption and TPD of ammonia. The carbon catalyst presents a high apparent surface area (1400 m^2/g) and a wide microporous structure indicated by the higher value of A_{BET}^{N2} with respect to that of A_{DR}^{CO2} [31]. The carbon catalyst presents also a relatively high value of the external area (470 m^2/g) and a significant contribution of mesoporosity.

The mass surface concentrations measured by XPS reveal a significant amount of surface phosphorus, 3.4 % wt., as a consequence of the activation procedure, which increases with the activation temperature up to 800 ºC and decreases with the impregnation ratio [26,32-34]. It is well known that biomass activation with H_3PO_4 the acid is combined with organic species to form phosphate and polyphosphate bridges that connect and crosslink polymer fragments [35]. Combining XPS analyses of the P2p

reaction, E2, was analyzed for ethylene formation. The rate expressions derived from the model fitted properly the experimental results, being the activation energy obtained for the formation of the main product, ethylene, around 165 kJ/mol.

Acknowledgements

We gratefully thank Junta de Andalucia (P09-FQM-5156) and Spanish Ministry of Economy and Competitiveness (MINECO) and FEDER (Project CTQ2012-364086) for financial support. M.J.V.R. gratefully thanks MINECO for a FPI fellowship (BES-2010-032213).

Notation

ACC = acetaldehyde

A_{BET} = apparent surface area ($m^2\ g^{-1}$)

A_{DR} = narrow micropore surface area ($m^2\ g^{-1}$)

A_t = external surface area ($m^2\ g^{-1}$)

BET = Brunauer, Emmett, and Teller

Da = Damköhler number

DEE = diethyl ether

d_p = particle diameter (cm)

E = ethylene

Ea_i = activation energy of the formation of i ($KJ\ mol^{-1}$)

EtOH = ethanol

ER = Eley-Rideal

F_{EtOH} = initial molar flow of ethanol ($mol \cdot s^{-1}$)

ΔH^0_{ad} = standard enthalpy of adsorption ($J\ mol^{-1}$)

$\Delta H_{i\text{-}L}$ = enthalpy of adsorption of i on an acid site ($KJ\ mol^{-1}$)

$\Delta H_{i\text{-}L"}$ = enthalpy of adsorption of i on a basic site ($KJ\ mol^{-1}$)

k_i = i formation rate constant ($mol\ g^{-1}\ s^{-1}$)

$K_{i\text{-}L}$ = Adsorption equilibrium constant for i on acid site (atm^{-1})

$K_{i\text{-}L"}$ = Adsorption equilibrium constant for i on basic site (atm^{-1})

$K_{io\text{-}L}$ = preexponential factor of the i adsorption on acid site (atm^{-1})

$K_{io\text{-}L''}$ = preexponential factor of the i adsorption on basic site (atm^{-1})

L = acid site

L'' = basic site

L_b = bed length (cm)

n = reaction order

Pe_p = particle Peclet number

P^o_{EtOH} = ethanol partial pressure at the reactor inlet (atm^{-1})

P_i = i partial pressure (atm^{-1})

P/Po = relative pressure

R = universal gas constant (R = 8.31 J mol^{-1} K^{-1})

Re_p = particle Reynolds number

r_i = rate of i formation (mol s^{-1} g^{-1})

ΔS^0_{ad} = standard entropy of adsorption (J mol^{-1} K^{-1})

S^0_g = standard entropy in gas phase (J mol^{-1} K^{-1})

S_i = selectivity to i product

STP = standard temperature pressure conditions

T = temperature (ºC)

TOS = time on stream (min)

V_{ads} = N_2 adsorbed volume (cm^3 STP·g^{-1})

V_{DR} = narrow micropore volume (cm^3 g^{-1})

V_{mes} = mesopore volume (cm^3 g^{-1})

V_t = micropore volume (cm^3 g^{-1})

w = water

W = catalyst weight (g)

W/F^o_{EtOH} = ethanol space time (g s mol^{-1})

X_{exp} = experimental conversion

Xi = conversion of/to i

X_{cal} = calculated conversion

XPS = X-ray photoelectron spectroscopy

Greek letters

η = interphase internal effectiveness factor

η_{ext} = interphase external effectiveness factor

O.F. = objective function (Residual error)

θ_i = fractional coverage of specie i on acid sites

θ''_i = fractional coverage of specie i on basic sites

References

[1] Kito-Borsa T, Pacas DA, Selim S, Cowley SW. 1998. Properties of an ethanol diethyl ether water fuel mixture for cold start assistance of an ethanol-fueled vehicle. Industrial and Engineering Chemistry Research 1998; 37:3366-3374.

[2] Pereira CJ. New avenues in ethylene synthesis. Science 1999;285:670-671.

[3] Gucbilmez Y, Dogu T, Balci S. Ethylene and acetalehyde production by selective oxidation of ethanol using mesoporous V-MCM-41 catalysts. Industrial and Engineering Chemistry Research 2006;45:3496-3502.

[4] Gayubo AG, Alonso A, Valle B, Aguayo AT and Bilbao J. Kinetic Model for the Transformation of Bioethanol into Olefins over a HZSM-5 Zeolite Treated with Alkali. Ind. Eng. Chem. Res. 2010; 49:10836-10844.

[5] Balat M, Balat H, Oz C. Progress in bioethanol processing. Prog. Energy Combust. Sci. 2008;34:551-573.

[6] Navarro RM, Peña MA, Fierro JLG. Hydrogen production reactions from carbon feedstocks: Fossils fuels and biomass. Chem. ReV. 2007;107:3952-3991.

[7] Ni M, Leung DYC, Leung MKH. A review on reforming bio-ethanol for hydrogen production. Int. J. Hydrogen Energy 2007;32:3238-3247.

[8] Le Van Mao R, Levesque P, McLaughlin GP, Dao LH. Ethylene from ethanol over zeolite catalysts. Applied Catalysis 1987;34:163–179.

[9] Le Van Mao R, Nguyen TM, McLaughlin GP. The bioethanol-to-ethylene (BETE) process. Applied Catalysis 1989;48:265–277.

[10] Moser WR, Thompson W, Chiang Ch, Tong H. Silicon-rich H-ZSM-5 catalyzed conversion of aqueous ethanol to ethylene. J. Catal. 1989;117:19–32.

[11] Le Van Mao R, Nguyen TM, Yao J. Conversion of ethanol in aqueous solution over ZSM-5 zeolites. Influence of reaction parameters and catalyst acidic properties as studied by ammonia TPD technique. Appl Catal. 1990;61:161–173.

[12] Oudejans JC, Van Den Oosterkamp PF, Van Bekkum H, Appl. Catal. 1982;3:109–115.

[13] Gayubo AG, Aguayo AT, Olazar M, Vivanco R, Bilbao J. Kinetics of the irreversible deactivation of the HZSM-5 catalyst in the MTO process. Chem. Eng. Sci. 2003;58:5239–5249.

[14] Szymański GS, Rychlicki G, Terzyk AP. Catalytic conversion of ethanol on carbon catalysts. Carbon 1994;32:265-271.

[15] Carrasco-Marín F, Mueden A, Moreno-Castilla C. Surface-treated activated carbons as catalysts for the dehydration and dehydrogenation reactions of ethanol. Journal of Physical Chemistry B 1998;102:9239-9244.

[16] Grunewald GC, Drago RS. Carbon molecular sieves as catalysts and catalyst supports. Journal of American Chemical Society 1991;113:1636-1639.

[17] Rosas JM, Bedia J, Rodríguez-Mirasol J, Cordero T. HEMP-derived activated carbon fibers by chemical activation with phosphoric acid. Fuel 2009;88:19-26.

[18] Rosas JM, Ruiz-Rosas R, Rodríguez-Mirasol J, Cordero T. Kinetic study of the oxidation resistance of phosphorus containing activated carbons. Carbon 2012;50:1523-1537

[19] Valero-Romero MJ, Rodríguez-Mirasol J, Cordero T. Role of surface phosphorus complexes on the oxidation of porous carbons. Chapter 2.

[20] Bedia J, Rosas JM, Rodríguez-Mirasol J, Cordero T. Pd supported on mesoporous activated carbons with high oxidation resistance as catalysts for toluene oxidation. Applied Catalysis B: Environmental 2010;94(1-2):8-18.

[21] Guerrero-Pérez MO, Valero-Romero MJ, Hernández S, López Nieto JM, Rodríguez-Mirasol J, Cordero T. Lignocellulosic-derived mesoporous materials: An answer to manufacturing non-expensive catalysts useful for the biorefinery processes. Catalysis Today 2012;195:155-161.

[22] Valero-Romero MJ, Cabrera-Molina A, Guerrero-Pérez MO, Rodríguez-Mirasol J, Cordero T. Carbon materials as template for the preparation of mixed oxides with controlled morphology and porous structure. Catalysis Today 2014;227(15):233-241.

[23] Bedia J, Ruiz-Rosas R, Rodríguez-Mirasol J, Cordero T. Kinetic study of the decomposition of 2-butanol on carbon-based acid catalyst. AIChE J. 2010;56:1557-1568.

[24] Bedia J, Rosas JM, Márquez J, Rodríguez-Mirasol J, Cordero T. Preparation and characterization of carbon based acid catalysts for the dehydration of 2-propanol. Carbon 2009;47:286–294.

[25] M. J. Valero-Romero, E.M. Calvo-Muñoz, R. Ruiz-Rosas, J. Rodríguez-Mirasol, T. Cordero. Insights into the catalytic performance of a carbon-based acid catalyst in methanol dehydration: Reaction scheme and kinetic modelling. Chapter 4..

[26] Bedia J, Barrionuevo R, Rodríguez-Mirasol J, Cordero T. Ethanol dehydration to ethylene on acid carbon catalysts. Applied Catalysis B: Environmental 2011;103:302-310.

[27] S Brunauer, PH Emmett, E Teller. Adsorption of gases in multimolecular layers. J Am Chem Soc 1938, 60, 309–19.

[28] BC Lippens, JH de Boer. Studies on pore systems in catalysts V. The t method. J Catal 1965, 4, 319–23.

[29] F Rodríguez-Reinoso, M Molina-Sabio, MT González. The use of steam and CO2 as activating agents in the preparation of activated carbons. Carbon 1995, 33, 15–23.

[30] MM Dubinin, ED Zaverina, LV Radushkevich. Sorption and structure of active carbons. I. Adsorption of organic vapors. J Phys Chem [URSS] 1947, 21, 1351–62.

[31] Rodríguez-Mirasol J, Cordero T, Rodríguez JJ. Activated carbons from CO2 partial gasification of eucalyptus kraft lignin. Energy&Fuels. 1993, 7, 133-8.

[32] Rosas JM, Bedia J, Rodríguez-Mirasol J, Cordero T. Preparation of hemp-derived activated carbon monoliths.Adsorption of water vapor. Ind Eng Chem Res 2008;47(4):1288–96.

[33] Puzy AM, Poddubnaya OI, Martínez-Alonso A, Suárez-García F, Tascón JMD. Synthetic carbons activated with phosphoric acid III. Carbons prepared in air. Carbon 2003;41:1181-1191.

[34] Puziy AM, Poddubnaya OI, Martínez-Alonso A, Suárez-García F, Tascón JMD. Surface chemistry of phosphorus-containing carbons of lignocellulosic origin. Carbon 2005;43:2857–2868.

[35] Jagtoyen M, Derbyshire F. Activated carbons from Yellow Poplar and White Oak by H3PO4 activation. Carbon 1998;36(7):1085-97.

[36] Valero-Romero MJ, Rodríguez-Mirasol J, Cordero T. On the chemical nature and thermal stability of surface phosphorus groups on carbons by TPD experiments. Submitted to Carbon.

[37] Wu X, Radovic LR. Inhibition of catalytic oxidation of carbon/carbon composites by phosphorus. Carbon 2006;44(1):141-151.

[38] Varislia D, Dogua T, Dogub G. Ethylene and diethyl-ether production by dehydration reaction of ethanol over different heteropolyacid catalysts. Chemical entineering Science. 2007;62(18-20):5349-5352.

[39] Chen G, Li S, Jiao F, Yuan Q. Catalytic dehydration of bioethanol to ethylene over TiO2/g-Al2O3 catalysts in microchannel reactors. Catalysis Today 1007;125:111-119.

[40] Varisli D, Dogu T, Dogu G. Silicotungstic acid impregnated MCM-41-like mesoporous solid

acid catalysts for dehydration of ethanol. Ind. Eng. Chem. Res. 2008:47;4071–4076.

[41] Zaki T. Catalytic dehydration of ethanol using transition metal oxide catalysts. J. Colloid Interface Sci. 2005;284:606-613.

[42] Knözinger H, Köhne R. J. Catal. 1964;3(6):559-560.

[43] Knözinger H, Köhne R. The Dehydration of Alcohols over Alumina: I. The reaction scheme. Journal of Catalysis. 1966;5(2):264-270.

[44] Matthew A. Christiansen, Giannis Mpourmpakis, and Dionisios G. Vlachos. Density Functional Theory-Computed Mechanisms of Ethylene and Diethyl Ether Formation from Ethanol on γ-Al2O3(100). ACS Catal. 2013(3)1965-1975.

[45] Winter O, Ming-Teck E. Make ethylene from ethanol. Hydrocarbon Processing 1976;125-133

[46] Phillips CB, Datta R. Production of ethylene from hydrous ethanol on H-ZSM-5 under mild conditions. Ind. Eng. Chem. Res. 1997;36:4466-4475.

[47] Nguyen TM, Mao RLV. Conversion of ethanol in aqueous solution over ZSM-5 zeolites. Appl. Catal. 1990;58:119-129.

[48] Zhang X, Wang R, Yang X, Zhang Fo. Comparison of four catalysts in the catalytic dehydration of ethanol to ethylene. Microporous and Mesoporous Materials 2008;(116):1-3)210-215.

[49] Zhou B, Machej T, Ruiz P, Delmon B. Catalytic cooperation between MoO3 and Sb2O4 in N-ethyl-formamide dehydration. II. Nature of active sites and role of spill-over oxygen. J. Catal. 1991;132:183-199.

[50] Weng LT, Ruiz P, Delmon B and Duprez D. Evidence of the migration of oxygen species from Sb2O4 to MoO3 in MoO3-Sb2O4. J. Mol. Catal. 1989;52:349-360.

[51] Mul G, Neeft JPA, Kapteijn F, Moulijn JA. The formation of carbon surface oxygen complexes by oxygen and ozone. The effect of transition metal oxides Carbon 1998;36:1269-1276.

[52] Knozinger H, Khone R. The dehydration of alcohols over alumina: I. The reaction scheme. Journal of Catalysis 1996;5:264-270.

[53] Knozinger H, Buhl H, Kochloefl K. The dehydration of alcohols on alumina: XIV. Reactivity and mechanism. Journal of Catalysis 1972;24:57-68.

[54] Macht J, Janik MJ, Neurock M, Iglesia E. Catalytic Consequences of Composition in Polyoxometalate Clusters with Keggin Structure. Angewandte Chemie – International Edition 46 (2007) 7864-7868.

[55] Macht J, Janik MJ, Neurock M, Iglesia E. Mechanistic consequences of composition in acid catalysis by polyoxometalate Keggin clusters. Journal of the American Chemical Society 2008;130:10369-10379.

[56] Janik MJ, Macht J, Iglesia E, Neurock M. Correlating Acid Properties and Catalytic Function: A First-Principles Analysis of Alcohol Dehydration Pathways on Polyoxometalates. Journal of Physical Chemistry C 2009;113(5):1872-1885.

[57] Lee KY, Arai T, Nakata S, Asaoka S, Okuhara T, Misono M. Catalysis by Heteropoly Compounds. 20. An NMR Study of Ethanol Dehydration in the Pseudoliquid Phase of 12-Tungstophosphoric Acid. Journal of the American Chemical Society 1992;114:2836–2842.

[58] Chiang H, Bhan A. Catalytic consequences of hydroxyl group location on the rate and mechanism of parallel dehydration reactions of ethanol over acidic zeolites. Journal of Catalysis 2010;271:251–261.

[59] Saito Y, Niiyama H. Reaction mechanism of ethanol dehydration on/in heteropoly compounds: Analysis of transient behavior based on pseudo-liquid catalysis model. Journal of Catalysis 1987;106(2):329-336.

[60] Moulijn JA, Tarfaoui A, Kapteijn F. General aspects of catalyst testing. Catal Today. 1991;11:1-12.

[61] Satterfield CN. Heterogeneous Catalysis in Practice. New York: McGraw-Hill; 1991.

[62] Gierman H. Design of laboratory hydrotreating reactors. Scaling down of trickle-flow reactors. Applied Catalysis 1988;43:277-286.

[63] Vannice MA. Kinetics of Catalytic Reactions. Springer 2005:51–61.

[64] Saito Y, Niiyama H. Reaction mechanism of ethanol dehydration on/in heteropoly compounds: Analysis of transient behavior based on pseudo-liquid catalysis model. Journal of Catalysis 1987;106(2):329-336.

[65] Levenberg K. A method for the solution of certain non-linear problems in least squares. Quarterly of Applied Mathematics. 1944;2:164-168.

[66] Marquardt D. An algorithm for least-squares estimation of nonlinear parameters. SIAM Journal on Applied Mathemathics 1963;11:431-441.

[67] Rioux RM, Vannice MA. Hydrogenation/dehydrogenation reactions: isopropanol dehydrogenation over copper catalysts. Journal of Catalysis 2003;216:362-376.

[68] Boudart M, Meras DE, Vannice MA. Kinetics of heterogeneous catalytic reactions. Industrie chimique belge 1967;32:281-284.

[69] Vannice MA, Hyun SH, Kalpalci B, Liauh WC. Entropies of adsorption in heterogeneous catalytic reactions. Journal of Catalysis 1979;56:358-362.

[70] Deon JA. Lange's Handbook of Chemistry. 15th ed., McGraw-Hill 1999 p. 6.42.

Chapter 6

Lignocellulosic-derived mesoporous materials: An answer to manufacturing non-expensive catalysts useful for the biorefinery processes

This chapter is based on the following publication:

Guerrero-Pérez, M.O., Valero-Romero, M.J., Hernández, S., Nieto, J.M.L., Rodríguez-Mirasol, J., Cordero, T. Catalysis Today, (2011) 195, 155-161.

Abstract It is described the synthesis procedure and characterization of a mesoporous carbon obtained from biomass waste by a simple method, generating a low-cost material, with the corresponding waste revaluation. The use of phosphoric acid during the activation of the waste material induces the presence of stable phosphate groups, with acid characteristics, on the surface of the mesoporous carbon, which could find many applications as an acid solid catalyst. In addition, such phosphate groups increase the stability of the carbon material under oxidizing conditions at relatively high temperatures, increasing the range of catalytic applications in which this material could be used. This paper also shows how the redox functionality can be incorporated on the surface of this carbon material by impregnation with vanadium oxide species. The corresponding carbon supported vanadium oxide catalyst is active and relatively selective in the propylene partial oxidation to oxygenates. It is also discussed how the catalytic behavior of such vanadium-containing catalysts can be improved by the use of Zr as dopant.

Keywords: lignocelluloses, nanostructured catalysts, biomass, activated carbon; carbon-supported catalysts, vanadium oxide

1. Introduction and Objectives

Biorefineries use biomass as an abundant and renewable resource for the production of energy, biofuels and valuable chemicals though different processes that requires the use of a catalyst [1, 2]. Thus, the use of biomass waste for the preparation of the catalytic materials required by the biorefineries could be interesting. Nowadays, a general tendency in the design of catalytic materials is based on nanostructured catalysts, since they present valuable advantages from both industrial and academic points of view [3]. By this way, the active phases should be supported on a non-expensive material that acts as support, in order to avoid syntherization of the active phase, reducing the amount of active phase required for a satisfactory catalytic performance and improving the mechanical properties of the catalyst.

Moreover, the nature of the specific support has a significant influence on the performance of the catalysts. In this sense, carbon materials are attractive as catalyst support since they can satisfy most of the desirable properties required for a suitable support [4]: high surface area, chemical stability, and, in addition, once he catalysts are deactivated, the supported oxide active phases can be easily recovered by gasification/oxidation of this carbon material, without net contribution to CO2 emission. In the context of biorefinery, the carbon materials present an additional advantage since they can be obtained from biomass waste, which is an abundant and economical starting material.

However, carbon supports only could be used under certain conditions, for example, under an oxidant atmosphere they would gasify to CO_2 (or CO) at relatively low temperatures. Nevertheless, it has been shown [5,6,7] that it is possible to prepare carbon materials with a relatively large amount of phosphorus on the carbon surface by chemical activation of lignocellulosic materials with phosphoric acid. This activation procedure lead to phosphorus surface complexes in form of $COPO_3$, CPO_3, C_3PO and C3P groups, which remain very stable on the carbon surface at relatively high temperatures and confer to the carbons a high oxidation resistance, acting as a physical barrier and blocking the active carbon sites for the oxidation reaction [8]. Thus, these phosphoric-activated carbon materials, with high oxidation resistance, open new

possibilities for the use of carbon materials as catalytic supports for reactions that take place at relatively high temperatures under oxidizing conditions.

The synthesis and characterization of such carbon material is described in the present study, and also its catalytic applications. Since vanadium can be considered one of the key elements in the formulation of oxidation catalysts [9,10], vanadium species have been incorporated on the surface of a carbon material in order to evaluate their catalytic behavior for the partial oxidation of propylene. In addition, the effect of zirconium as promoter of these carbon-supported vanadium oxide catalysts has been also evaluated.

2. Experimental

2.1. Preparation of samples

In order to evaluate the effect of phosphorous in the catalytic behavior of the carbon support, two different activated carbons (with and without phosphorous) were prepared thought different pathways: chemical activation with phosphoric acid and physical activation by CO_2 gasification (Scheme 1). Olive stone waste (provided by Sociedad Cooperativa Andaluza Olivarera y Frutera, Periana) was used, in both cases, as starting material. The olive stone waste was cleaned with deionized water, dried at 100 ºC, and ground with a roller mill to obtain samples of 400–800 μm particle size. For the chemical activation process, the raw material was impregnated with concentrated commercial H_3PO_4 (85 wt.%, Sigma Aldrich) at room temperature, with a weight ratio of 3/1 (H_3PO_4/olive stone), and dried for 24 h at 60 °C. The impregnated samples were activated, at 500 ºC, under continuous N_2 (99.999%, Air Liquide) flow (150 cm^3 STP/min) in a conventional tubular furnace. The activation temperature was reached at a heating rate of 10 °C/min and maintained for 2 h. The activated sample was cooled inside the furnace under the same N_2 flow and then washed with distilled water at 60 °C until neutral pH and negative phosphate analysis in the eluate [11]. The resulting activated carbon, denoted by ACP, was dried at 100 °C and grinded and sieved (100-300 μm). For the physical activation process, it was followed a procedure described previously by our group [12,13], by this manner the gasification conditions, i.e. gasification temperature and reaction time, as well as the particle sizes are set in order to

warrant chemical reaction control achieving a value of burn-off of around 55 %. An olive stone char was obtained by carbonization of the precursor under N_2 flow at 800 ºC. This char was heated under N_2 atmosphere to the gasification temperature (800 ºC), then, the gas feed was switched to CO_2 (99.998%, Air Liquide) with a flow rate of 150 cm^3 STP/min for 7 h. The resulting activated carbon was denoted by AC.

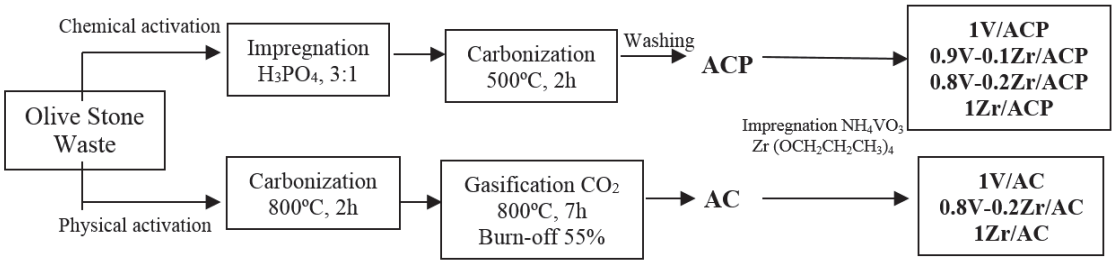

Scheme 1. Synthesis, procedure and nomenclature of the samples.

V-, Zr- and V+Zr-containing catalysts were prepared dissolving the required amount of precursor, NH_4VO_3 (99.99%, Sigma Aldrich) and/or $Zr(OCH_2CH_2CH_3)_4$ (70wt% in 1-propanol, Sigma Aldrich), in a 0.5 M oxalic acid (99%, Sigma Aldrich) solution. This solution was kept under stirring until all vanadium and zirconium dissolves, then, the corresponding support (ACP or AC) was added. This mixture was dried in a rotator evaporator at 80 ºC at a reduced pressure of 10-40 mmHg. The resulting solids were dried at 120 ºC for 24 h and then calcined at 250 ºC for 2h in air. These catalysts were prepared with a total V+Zr coverage of 1 atom per nm2 of activated carbon, and with different V/Zr molar ratio, which corresponds in weight percentage to 9.9 V% for 1V/ACP; 8.8 V% and 1.8 Zr% for 0.9V-0.1Zr/ACP; 7.8 V% and 3.5 Zr% for 0.9V-0.1Zr/ACP.

2.2. Characterization

Oxidation resistance of the different catalysts and the carbon support were obtained by non-isothermal thermogravimetric analyses, carried out in a CI electronics thermogravimetric system. The thermobalance automatically measures the weight of the sample and the temperature as a function of time. Experiments were carried out in air atmosphere, for a total flow rate of 150 cm^3 (STP)/min, employing sample mass of approximately 10 mg. The sample temperature was increased from room temperature up

to 900 ºC at a heating rate of 10 ºC/min. The porous structure of the activated carbons was characterized by N_2 adsorption-desorption at -196 ºC and by CO_2 adsorption at 0ºC, carried out in an ASAP 2020 model of Michromeritics Instruments Corporation. Samples were previously outgassed during 8 hours at 150 ºC. From the N_2 adsorption/desorption isotherm, the apparent surface area (A_{BET}) was determined applying the BET equation, the micropore volume (V_t) and the external surface area (A_t) were calculated using the t-method [14] and the mesopore volume (V_{mes}) was determined as the difference between the adsorbed volume at a relative pressure of 0.95 and the micropore volume (V_t) [15]. The narrow micropore surface area (A_{DR}) and volume (V_{DR}) were obtained by the Dubinin-Radushkevich method [16] applied to the CO_2 adsorption isotherm.

X-ray photoelectron spectroscopy (XPS) analyses of the samples were obtained using a 5700C model Physical Electronics apparatus, with MgKα radiation (1253.6 eV). For the analysis of the XPS peaks, the C1s peak position was set at 284.5 eV and used as reference to position the other peaks while the fitting of the XPS peaks was done by least squares using Gaussian-Lorentzian peak shapes. Fourier transform infrared (FTIR) spectra of the samples were acquired at room temperature in the 300 to 3900 cm^{-1} region using a Nicolet 205xB spectrophotometer, equipped with a Data Station, at a spectral resolution of 1 cm^{-1} and accumulation of 128 scans. The pellets were prepared with 2 mg of sample mixed with 100 mg of dry KBr and pressed into disks.

The surface acidity was studied by adsorption and desorption of pyridine (Py) and 2,6-dimetilpyridine (DMPy) carried out in a thermogravimetric system (CI Electronics) at 100 ºC. The inlet partial pressure of the organic bases was 0.02, and it was established saturating N_2 with the corresponding organic base in a saturator at controlled temperature. After saturation of the carbon, desorption is carried out at the adsorption temperature in Nitrogen flow.

2.3. Activity measurements

The catalytic experiments were carried out in a fixed bed quartz tubular reactor (i.d. 12 mm, length 400 mm), working at atmospheric pressure. Catalyst samples (0.1-0.4 mm particle size) were introduced in the reactor and diluted with 1-2 g of silicon carbide (0.5-0.75 mm particle size) in order to keep a constant volume in the catalyst

bed. The flow rate and the amount of catalyst were varied (from 25 to 100 cm^3 min^{-1} and from 0.25 to 1.0 g, respectively) in order to achieve different propylene conversion levels. The feed consisted of mixture of propene/oxygen/water/helium (1.6/6.8/15/76.5). Experiments were carried out in the 200-275 ºC temperature range. Reactants and reaction products were analyzed by on-line gas chromatography [17].

3. Results

Figure 1 shows the thermogravimetric analysis profiles in air for ACP (prepared by activation with phosphoric acid) and for AC (prepared by physical activation) activated carbon supports. As expected, the ACP carbon is resistant in air up to 500 ºC, lowering this temperature to 380 ºC when it is impregnated with the oxide active phase. Since the oxidation resistance of AC is much lower than that of ACP, it can be observed how the activated carbon AC loses weight at ca. 400 ºC, only ACP based catalysts will be tested under partial oxidation.

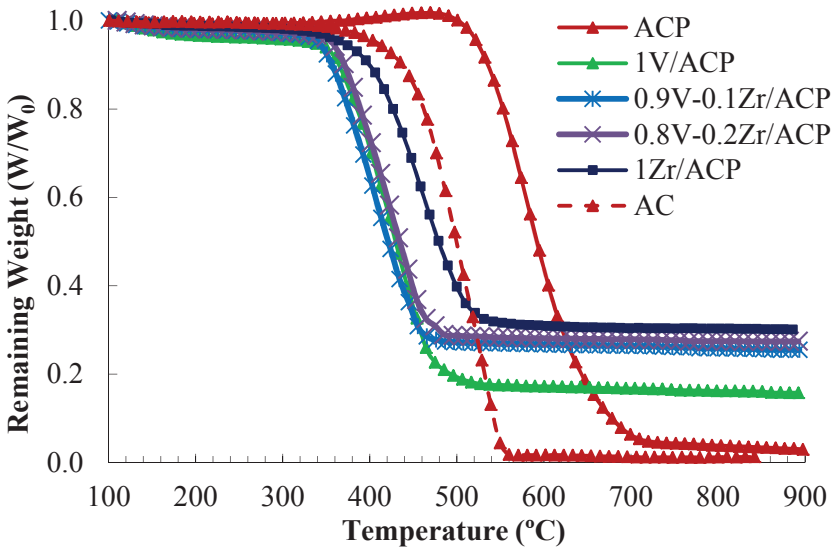

Figure 1. Non-isothermal oxidation resistances profiles (10 ºC/min).

In the catalysts containing vanadium and zirconium species, no diffraction peaks are detected in the wide angle XRD patterns (not shown), indicative that the active phases are well dispersed, since no V_2O_5 or ZrO_2 crystals are detected. Figure 2 shows N_2 adsorption-desorption isotherms for the activated carbon and for the vanadium and zirconium supported catalysts, whereas Table 1 summarizes the values of the structural

parameters that characterize the porous structure of the samples, as derived from N_2 adsorption-desorption and CO_2 adsorption isotherms. The activated carbon (ACP) presents high values of both BET surface area (1300 m^2/g) and mesoporous volume (0.930 cm^3/g), which confirm that phosphoric acid activation presents a significant contribution on mesoporosity. The activated carbon (AC), obtained by physical activation, presents a similar surface area (1355 m^2/g), but, in this case, the volume of mesoporous is lower (0.002 cm^3/g). The narrow-microporosity of the AC, as reflected by the CO_2 adsorption (Table 1), and the shape of the N_2 isotherms (Figure 2) is higher than those of ACP. The values of specific surface area, A_{BET}^{N2}, external surface area, At and mesoporous volume V_{mes}, obtained from the N_2 adsorption isotherms, decrease upon vanadium and/or zirconium impregnation, due to the partial blockage of the porous structure, although that, these values remain quite high for a catalytic application.

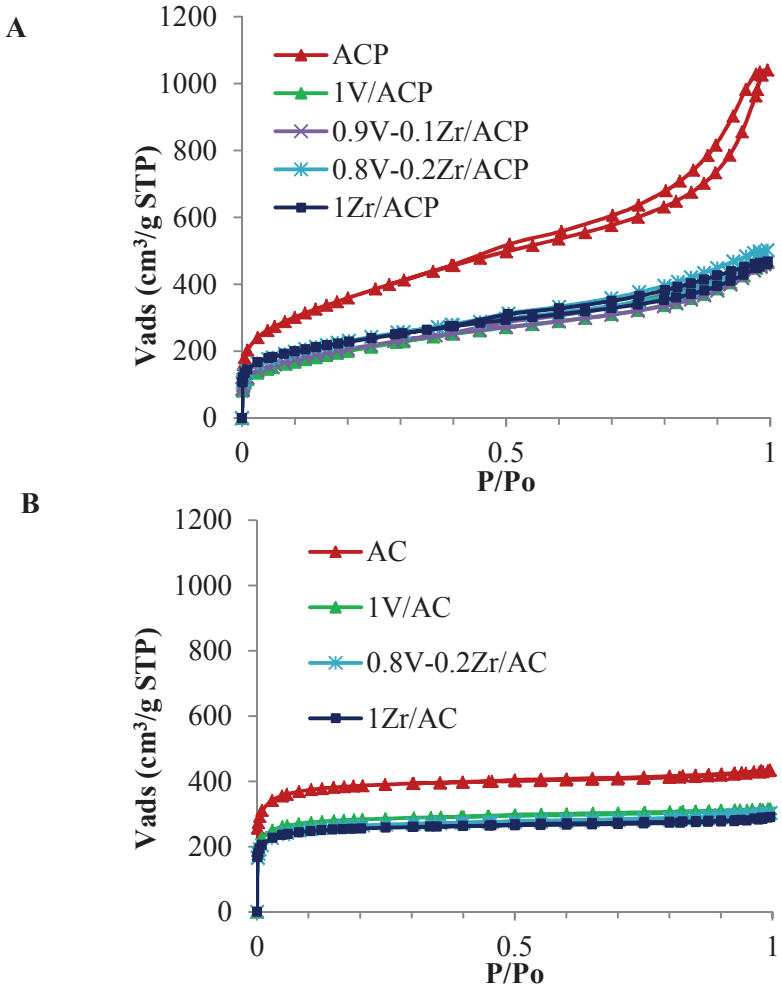

Figure 2. N_2 adsorption isotherms

Table 1. Structural parameters of carbon supports and V-Zr-O catalysts.

	N_2 isotherm				CO_2 isotherm	
	A_{BET} (m^2/g)	A_t (m^2/g)	V_t (cm^3/g)	V_{mes} (cm^3/g)	A_{DR} (m^2/g)	V_{DR} (cm^3/g)
ACP	1300	594	0.389	0.930	539	0.216
1Zr/ACP	818	268	0.282	0.378	440	0.176
1V/ACP	722	290	0.233	0.423	334	0.134
0.9V-0.1Zr/ACP	746	275	0.245	0.400	357	0.143
0.8V-0.2Zr/ACP	830	267	0.291	0.403	417	0.167
AC	1355	50	0.59	0.064	870	0.349
1Zr/AC	906	33	0.389	0.042	758	0.304
1V/AC	1000	40	0.43	0.048	826	0.331
0.8V-0.2Zr/AC	940	39	0.403	0.052	743	0.298

Figure 3 shows representative XPS spectra for V2p and Zr3d regions for 1V/ACP catalysts. The V2p region typically exhibits two components, the one at higher binding energy (517.1 eV) is assigned to V^{5+} species, whereas the component at lower binding energy (516.1 eV) is associated with V^{4+} species (18,19). The percentages of both contributions to V2p signal have been calculated by deconvolution and are shown in Table 2, that illustrates the V^{4+} and V^{5+} species percentage and also the V^{4+}/V^{5+} ratio. It can be observed that the amount of oxidized species (as V^{5+}) increases with zirconium content, although that, for the sample with the higher Zr content, there is still a considerable amount of V^{4+} species (15.3 %). By comparing these results obtained with the ACP supported catalysts with those achieved with AC (the activated carbon without phosphorous) support, it is clear that the amount of V^{4+} species is much higher in the case of ACP supported catalysts. Thus, it seems that phosphorous increases the amount of reduced vanadium species. Figure 3B shows the XPS spectra in the Zr3d region, with the characteristic doublet of Zr(IV) compounds, with bands near 183.3 and 185.7.

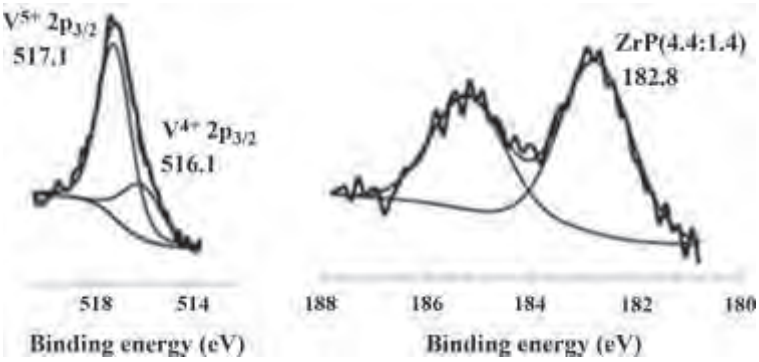

Figure 3. Representative XPS spectra for V2p and Zr3d regions (1V/ACP sample)

Table 2. Distribution of vanadium species obtained by deconvolution of V2p spectra of catalysts before and after catalytic test (T=225ºC).

	Before reaction			After reaction		
	$\%V^{4+}$	$\%V^{5+}$	V^{4+}/V^{5+}	$\%V^{4+}$	$\%V^{5+}$	V^{4+}/V^{5+}
ACP	-	-	-	-	-	-
1V/ACP	29.5	70.5	0.42	36.5	63.5	0.57
0.9V-0.1Zr/ACP	23.1	76.9	0.30	26.2	73.8	0.35
0.8V-0.2Zr/ACP	15.3	84.7	0.18	24.7	75.3	0.33
1Zr/ACP	-	-	-	-	-	-
AC	-	-	-	-	-	-
1V/AC	7.1	92.9	0.08	-	-	-
0.8V-0.2Zr/AC	4.7	95.2	0.05	-	-	-
1Zr/AC	-	-	-	-	-	-

Figure 4 shows the XPS spectra in the P2p region. Peaks in the range 134.0-134.6 eV are commonly assigned to phosphate species in which P atom is bonded to O atoms, whereas when P is bonded to one C atom this value shifts to lower values (around 133.6) [8,20,21]. The P2p value obtained for the carbon support (133.6 eV) indicates that the majority of phosphorus atoms are bonded to carbon atoms, as CPO_3 and C_2PO_2 groups, since the C-O-PO· and (CO·)-PO_3 groups appears at higher binding

energies. Upon vanadium addition, the BE peak for the P2p region remains essentially constant. In this case it should be considered that the BE for several VPO phases, such as $(VO)_2P_2O_7$, appears also near 133.7 (22), thus, the P signals corresponding to VPO species and to C-O-P would overlap.

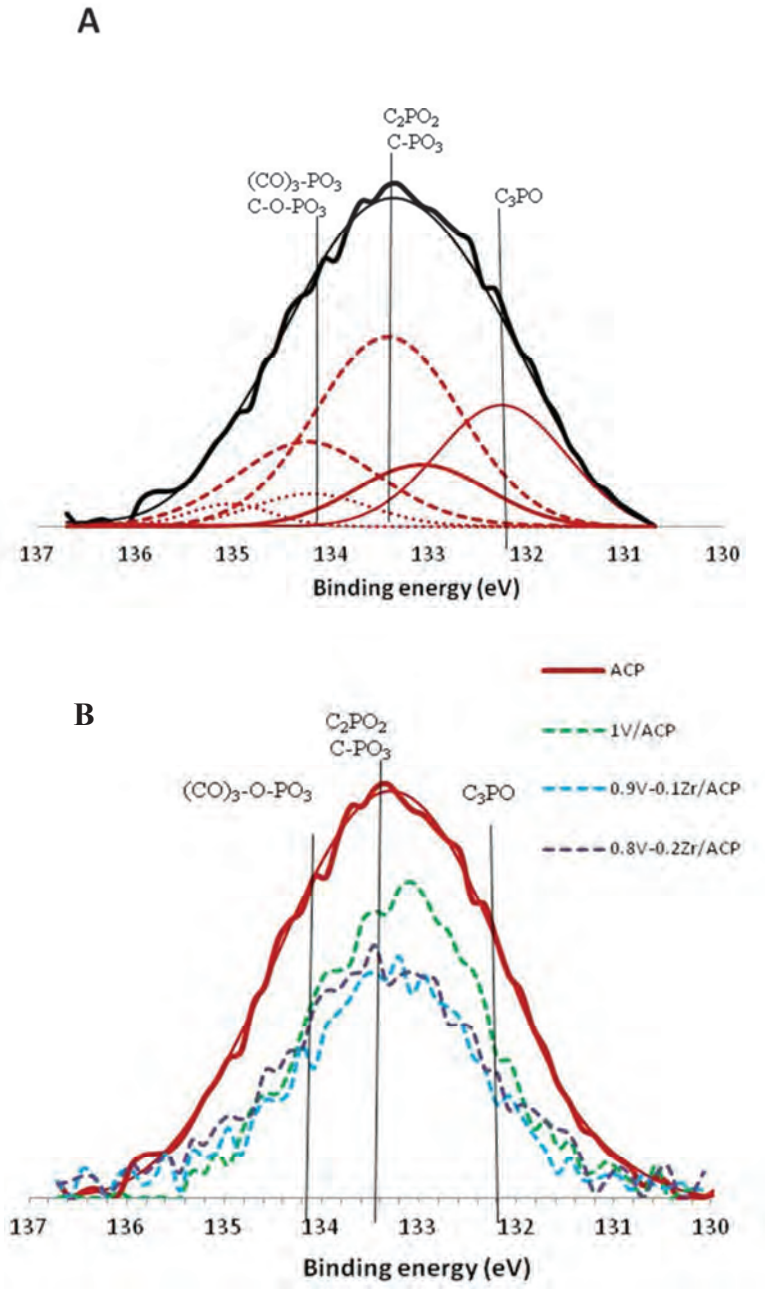

Figure 4. (A) Representative XPS spectra (P2p region) of ACP sample showing the deconvolution and (B) XPS spectra for ACP supported catalysts.

Figure 5 shows the FTIR spectra of the activated carbon ACP and ACP supported catalysts. These spectra are similar to that reported for phosphoric activated carbons [23,24]. The wide band near 3200-3600 cm^{-1} has been assigned to O-H stretching mode of hydroxyl groups on the surface of the carbon material and of adsorbed water. The band near 1580-1600 cm^{-1} is usually assigned to aromatic ring stretching vibrations, whereas the shoulder near 1720 cm^{-1} corresponds to C=O stretching vibrations of several functional groups (ketones, aldehydes, lactones or carboxyl). In addition, in the case of the samples with the highest vanadium oxide content, 1V/ACP and 0.9V-0.8Zr/ACP, some weak signals are detected near in the 980-1050 cm^{-1} range, that corresponds to V=O and V-O stretching vibrations dispersed oxide species [25].

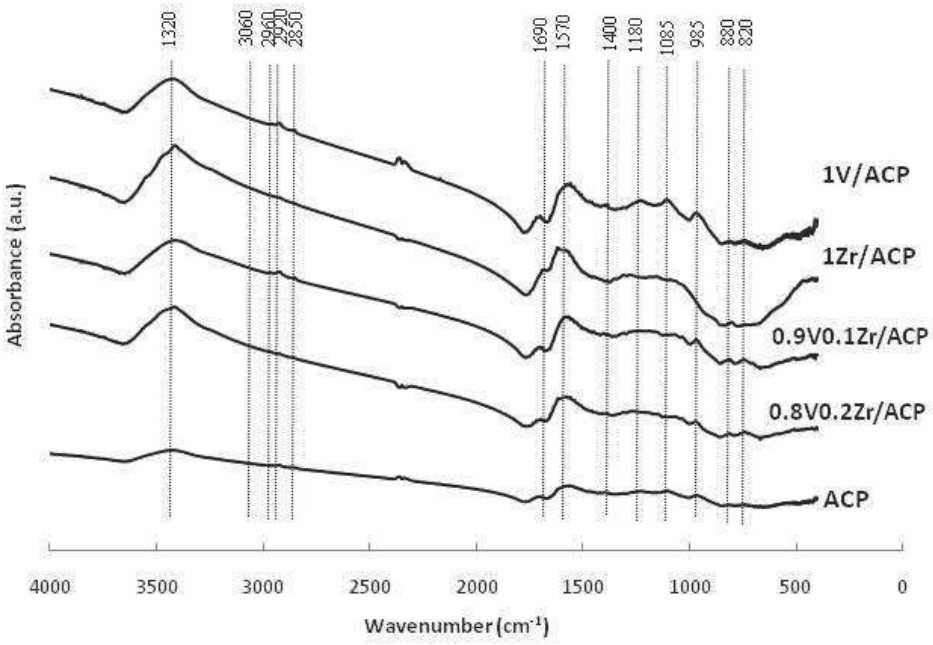

Figure 5. FTIR spectra of ACP supported catalysts.

In the reported spectra for phosphoric activated carbons [23,24] an intense band near 1180 cm-1, assigned to the stretching mode of P=O, O-C in P-O-C bonds and to P=OOH, is usually described, which appears more intense when high temperatures of activation (higher than 500ºC) are used. This is due to the formation of C-O-PO_3 and $(CO)_3$-PO_3 groups (species in which P is not directly bonded to C). In our case such

band is not detected, since ACP was prepared using a temperature of activation of 500ºC, indicating that the phosphorous in ACP is mainly bonded directly to carbon atoms, in line with the XPS results (Figure 4).

Pyridine and 2,6-dimethylpyridine molecules were used as probes in order to quantify the acid groups on the surface of catalyst, the results are shown in Table 3. It is well known that pyridine is a basic molecule able to interact with both Lewis and Brønsted acid sites, whereas 2,6-dimethylpyridine selectively adsorbs on Brønsted ones [26,27]. Thus, the total amount of adsorbed 2,6-dimethylpyridine gives an idea about the total number of Brønsted sites (column B in Table 3), whereas the difference between the amount of adsorbed pyridine and 2,6-dimethylpyridine gives an idea about the number of Lewis sites (column A-B in Table 3). As expected the ACP carbon presents a high amount of Brønsted acid sites on its surface, due to the presence of phosphate groups. Brønsted acid sites increase lightly with vanadium incorporation, while Lewis acid sites increases upon V and Zr oxides impregnation. This is due because transition metal oxides presents both Lewis and Brønsted acid sites. As expected, amount of both types of acid sites is high for 1Zr/ACP sample, since zirconium phosphates materials present strong acid sites [28].

Table 3. Total amount of adsorbed pyridine and 2,6-dimethylpyridine on the Zr-V-O catalysts.

	A, $mMol_{pyr}/g_{sample}$,	B, $mMol_{DMpyr}/g_{sample}$	A-B
ACP	0.882	0.882	0
1V/ACP	1.250	1.028	0.222
0.9V-0.1Zr/ACP	1.180	0.900	0.280
0.8V-0.2Zr/ACP	1.157	0.823	0.334
1Zr/ACP	2.580	1.331	1,249

The catalytic properties of these carbon materials have been studied for the partial oxidation of propylene. Table 4 shows the propylene conversion and the selectivity to main reaction products obtained at 225 ºC. Very low propylene conversion (1.1 %) is observed on the carbon support (ACP, which only posses Brønsted acid sites, Table 3), suggesting that it is not able to activate the propylene molecule. Similar

conclusion can be achieved from the catalytic results obtained over Zr-carbon supported (1Zr/ACP), which presents a propylene conversion of 2.6 %. However, both activity and selectivity drastically change in the case of V-containing catalysts. Thus, when VOx species are incorporated, the catalytic activity increases, being acetone the main oxygenate product, indicating a redox/acid mechanism.

In addition, the incorporation of Zr species to the VOx/ACP catalysts, as dopant, increases notably the propylene conversion: the conversion of propylene for 0.9V-0.1Zr/ACP and 0.8V-0.2Zr/ACP is twice the conversion obtained with the 1V/ACP catalyst (Table 4) at the same temperature.

A second aspect to be considered is related to the selectivity to partial oxidation products. The acetone selectivity vs propylene conversion profiles presented in Figure 6 and confirm that for all the propylene conversions studied, selectivity to acetone is higher for V-Zr-doped materials, suggesting that Zr is able to enhance redox activity of vanadium carbon-supported catalysts. In addition V-Zr-doped catalysts favor also the formation of acetic acid (Table 4), which is formed by a consecutive oxidation reaction from acetone [29]. However, Zr-free and V-free catalysts do not show any formation of acetic acid.

Table 4. Propylene conversion and selectivity to main products (225 ºC)

	Propylene conversion	Selectivity (%)				
		Acetone	Acrolein	Acetic acid	CO	CO_2
1V/ACP	6,9	43,7	1,5	0	13,8	40,9
0.9V0.1Zr/ACP	15,3	25,7	0,5	4,9	15,5	53,3
0.8V0.2Zr/ACP	13,4	23,2	0,6	4,1	17,7	54,3
1Zr/ACP	2,6	5,4	0,1	0,1	10,8	83,4
ACP	1,1	13,8	3,5	0	18,6	63,8

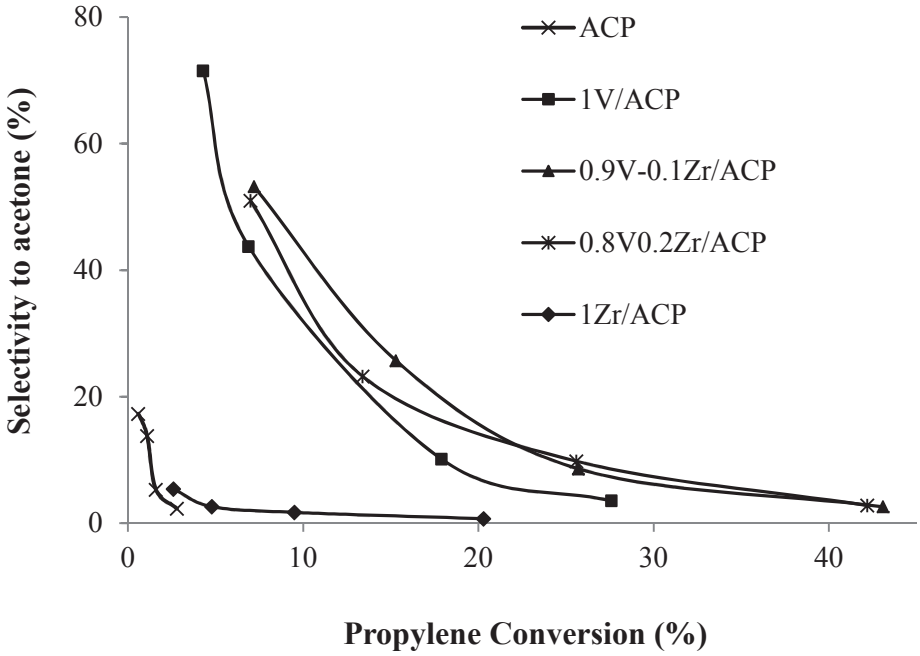

Figure 6. Conversion-selectivity profiles (200-275ºC), feed mixture: propene/oxygen/water/helium = 1,6/6,8/15/76,5.

In order to further study the stability of these carbon based catalysts under oxidation reaction conditions, the used samples were characterized. The amount of catalysts was weighted before and after the catalytic tests and remained constant, indicative that the ACP support was not gasified under reaction conditions, in line with the thermogravimetric experiments that showed how this materials are stable until ca. 380 ºC (Figure 1). Table 5 shows the structural parameters calculated from N_2 and CO_2 isotherms of the used samples. It can be observed how the morphologies of ACP support as well as 1Zr/ACP are quite stable under reaction conditions since only minor changes are observed for their parameters. On the contrary, the BET surface area value, as well as the mesoporous volume values of 1V/ACP sample, decreases considerably after reaction, indicative that structural changes, able to block the mesoporous of the carbon support, are occurring on the surface of catalysts. Since adsorption isotherms (Tables 1 and 5) as well as thermogravimetric experiments (Figure 1) shows that ACP is stable under reaction conditions, the changes observed in 1V/ACP must be related with vanadium species on the surface of catalysts. These data also indicates that Zr as dopant is able to stabilize, in part, the structure of these catalysts, since Zr containing samples

have high surface areas after reaction (0.9V-0.1Zr/ACP, 475 nm^2/g, and 0.9V-0.1Zr/ACP, 597 m^2/g), thus, the surface area decrease is lower as Zr content in the catalyst is higher. The XPS analyses of the used samples indicate that the atomic chemical composition of the materials remain stable after reaction (Table 6). Vanadium species are partially reduced under reaction conditions since the ratio V^{4+}/V^{5+} increases for all the catalysts after propylene oxidation (Table 2), this changes in the oxidation state of vanadium states could be related with the formation of VPO phases during reaction, since they are a high number of different VPO structures that have been described for both V^{4+} and V^{5+} species [30].

Table 5. Structural parameters after propylene oxidation reaction (225ºC)

	N_2 isotherm				CO_2 isotherm	
Sample	A_{BET} (m^2/g)	A_t (m^2/g)	V_t (cm^3/g)	V_{mes} (cm^3/g)	A_{DR} (m^2/g)	V_{DR} (cm^3/g)
ACP	1257	474	0.431	0.700	408	0.163
1Zr/ACP	710	238	0.242	0.339	397	0.159
1V/ACP	147	116	0.011	0.147	206	0.083
0.9V-0.1Zr/ACP	475	197	0.143	0.273	283	0.114
0.8V-0.2Zr/ACP	597	215	0.195	0.317	295	0.118

Table 6. Atomic surface concentrations (%) obtained by XPS for the catalysts before and after propylene oxidation reaction (225ºC)

	Fresh Catalysts						Used Catalysts					
	%C	%O	%N	%P	%V	%Zr	%C	%O	%N	%P	%V	%Zr
ACP	91.1	7.6	0	1.4	0	0	91.3	7.1	0.3	1.3	-	-
1V/ACP	80.7	15.1	1.7	1.1	1.5	-	77.7	18.7	1.4	0.8	1.4	-
0.9V-0.1Zr/ACP	82.2	14.5	1.4	0.7	1.1	0.1	80.6	16.2	1.4	0.7	0.9	0.1
0.8V-0.2Zr/ACP	81.8	14.7	1.3	0.9	0.9	0.5	80.7	16.0	1.4	0.6	0.9	0.4
1Zr/ACP	76.7	17.4	0.4	1.3	0.0	4.1	68.5	23.7	0.2	2.0	-	5.7

4. Discussion

With the methodology described in this paper it has been possible to prepare a mesoporous material (ACP) stable physical and chemically at relatively high temperatures and oxidant atmospheres. Thermogravimetric experiments (Figure 1) confirm that the presence of P in ACP material inhibits the oxidation of the material support (ACP is resistant in air up to 500 ºC), whereas in absence of P (i.e. AC sample), it begins to gasify around 400 ºC, limiting its use as catalyst or support in non-oxidant atmosphere conditions. These results are in agreement with those reported before [8]. Moreover, the addition of phosphorous also affects the morphology of the activated carbon, since the N^2 and CO^2 isotherms have shown that the activated carbon obtained by chemical activation with phosphoric acid presents a significant contribution of mesoporosity, whereas the activated carbon AC is essentially a microporous material. However, mesoporous materials are more attractive for most of catalytic applications, due to decreasing internal diffusional problems related with microporous supports [31], since after impregnation of the support with the corresponding active phases, usually them remain no accessible to reactants on the microporous. In addition, in the case of carbon supports, the use of microporous materials in catalysis usually induces the deactivation of catalysts due to the formation of coke [32]. Base probe molecules adsorption experiments have shown that this activated carbon (ACP) present a high number of Brønsted acid sites on its surface (Table 3). Thus, ACP is a mesoporous material, that possesses acid sites, and that is stable in a wide range of temperature under both oxidant and not oxidant conditions. Since they are many reactions catalyzed by acid sites, ACP is a suitable solid acid catalyst that founds a wide range of catalytic applications [33]; because it is well known that nowadays there is a necessity of replacing the pollutant and corrosive liquid acid catalysts (such as sulfuric acid) by more easily handling and recoverable catalysts, such as solids with strong acid sites.

In addition to its use as solid acid catalyst, ACP is suitable also as catalytic support. It has been shown how is possible to incorporate VOx active phases on the surface of ACP. The catalytic results during hydrocarbon partial oxidation have shown that 1V/ACP catalysts is selective to oxygenates, which demonstrated the presence of redox sites on the surface of the catalytic material due to the incorporation of the VOx active phases (Figure 6). The incorporation of zirconium to 1V/ACP catalysts induces a

higher stability of catalyst. Thus, composition (Table 6) and morphology (Table 5) of these materials remain more stable under reaction conditions when zirconium is incorporated as promoter, since Zr species seems to be able to improve physical properties of vanadium-supported catalysts. In addition, the Zr-doped samples also present a lower number of Brønsted and higher Lewis sites with respect the undoped catalyst 1V/ACP. Although Brönsted sites by themselves are not able to activate the propylene molecule, as can be observed in Figure 6, that shows negligible conversion for both ACP and 1Zr/ACP catalysts. However, a moderate number of Brönsted acid sites play a role in the partial oxidation mechanism, increasing hydrocarbon adsorption sites and improving the catalytic behavior of catalysts [33,34]. In addition, and for higher Zr/V molar ratio, it has been described the formation of tetrahedral $O=V(OZr)_3$ species that are active during oxidation reaction [35]. These species, in a minor extension, could also be present in the doped Zr catalysts (with a contribution for improving catalytic behavior as observed in Figure 6). Consequently, presence of Zr is able to increase selectivity to oxygenates in all the rage of conversions studied. Thus, Zr promoted V-carbon supported materials are more effective catalysts.

5. Conclusions

The proposed methodology has led to the preparation of a mesoporous non-expensive material (an activated carbon) from a biomass waste. The activation with phosphoric acid has led to an activated carbon material with high oxidation resistance for relatively high temperatures; whose morphology is essentially mesoporous and remains stable under catalytic tests. This material can be use in a wide range of industrial processes as an acid solid catalyst, being by this manner quite useful in any biorefinery.

In addition to its use as solid acid catalyst, the data presented in this paper have also demonstrated that it is possible to incorporate redox functionality by impregnation of this carbon with metal transition oxide active phases, obtaining a nanostructured vanadium oxide catalyst. Subsequently, the range of catalytic applications in which the biomass-derived mesoporous material can be used is increased. An additional advantage of the use of the carbon material as catalytic support is that once that the catalysts are

deactivated, the supported oxide active phases can be easily recovered by gasification of this carbon supports and the resulting gasification products can be used in the biorefinery as syn-gas.

Acknowledgements

This work was supported by the Spanish Ministry of Education and Science (CTQ-2009-14262 and CTQ-009-14495). M.J. V.-R. thanks the Spanish Ministry of Science and Innovation for her FPI predoctoral fellowship; and M.O. G.-P. is indebted to Junta de Andalucía (Incentivos Estancias de Excelencia 2/2009) for financial support during her stay at ITQ-CSIC. Thanks are extended to the organizers of the CatBior Conference and guest editors of this special issue, Profs. Manuel López-Granados and Pedro Maireles.

References

[1] E.L. Kunkes, D.A. Simonetti, R.M. West, J.C. Serrano-Ruíz, C.A. Gärtner, J.A. Dumesic, Science 322 (2008) 417

[2] M. Stöcker, Angew. Chem. Int. Ed. 47 (2008) 9200

[3] M.O. Guerrero-Pérez, J.L.G. Fierro, M.A. Bañares, Top. Catal. 41 (2006) 43

[4] F. Rodríguez-Reinoso, Carbon 36 (1998) 159

[5] J. Bedia, R. Ruiz-Rosas, J. Rodríguez-Mirasol, T. Cordero, AIChE 56 (2010) 1557

[6] J.M. Rosas, J. Bedia, J. Rodríguez-Mirasol, T. Cordero, Fuel 88 (2009) 88

[7] M.O. Guerrero-Pérez, J.M. Rosas, R. López-Medina, M.A. Bañares, J. Rodríguez-Mirasol, T. Cordero, Catal. Commun. 12 (2011) 989

[8] J.M. Rosas, R.Ruiz-Rosas, J. Rodríguez-Mirasol, T. Cordero. Carbon (2012), in presss, doi:10.1016/j.carbon.2011.11.030

[9] J. Haber, Catal. Today 142 (2009) 100-113

[10] J.M. López-Nieto, Top. Catal. 15 (2001) 189-194

[11] E. González-Serrano, T. Cordero, J. Rodríguez-Mirasol, L. Cotoruelo, J.J. Rodríguez, Water Res. 38 (2004) 3043-3050

[12] J. Rodríguez-Mirasol, T. Cordero, J.J. Rodríguez, Carbon 31 (1993) 53-61

[13] N. Tancredi, T. Cordero, J. Rodríguez-Mirasol, .J. Rodríguez, Fuel 75 (1996) 1505-1508

[14] S.J. Gregg, K.S.W. Sing, Adsorption, Surface Area and Porosity. Academic Press, 2nd Ed, London, (1982) 42-102

[15] F. Rodríguez-Reinoso, M. Molina-Sabio, M.T. González, Carbon 33 (1995) 15–23

[16] M.M. Dubinin, E.D. Zaverina, L.V. Radushkevich, J. Phys. Chem. (URSS) 21 (1947) 1351-1362

[17] P. Concepción, S. Hernández, J.M. López Nieto, Appl. Catal. A 391 (2011) 92

[18] R. López-Medina, J.L.G. Fierro, M.O. Guerrero-Pérez, M.A. Bañares, Applied Catalysis A: General 375(1), 55-62 (2010)

[19] R. López-Medina, H. Golinska, M. Ziolek, M.O. Guerrero-Pérez, M.A. Bañares, Catalysis Today 158 (1-2), 139-145 (2010)

[20] X. Wu, L.R. Radovic, Carbon 44 (2006) 141-151

[21] J. Bedia, J.M. Rosas, D.Vera, J. Rodríguez-Mirasol, T. Cordero, Catal. Today 158 (2010) 89-96

[22] Y. Surchorski, Appl. Surf. Sci. 253 (2007) 5904

[23] A.M. Puziy, O.I. Poddubnaya, A. Martínez-Alonso, F. Suárez-García, J.M.D. Tascón, Carbon **40** (2002) 1493

[24] A.M. Puziy, O.I. Poddubnaya, A. Martínez-Alonso, F. Suárez-García, J.M.D. Tascón, Carbon **43** (2005) 2857

[25] N. Magg, B. Immaraporn, J.B. Giorgi, T. Schroeder, M. Baumer, J. Dobler, Z. Wu, E: Kondratenko, M. Cherian, M. Baerns, P.C. Stair, J. Sauer, H.-J. Freund. J. Catal. 226 (2004) 88

[26] M.H. Healy, L.F. Wieserman, E.A. Arnett, K. Wefers, Langmuir 5 (1989) 114

[27] A. Travert, O.V. Manoilova, A.A. Tsyganenko, F. Maugé, J.C. Lavalley, J. Phys. Chem. B 106 (2002) 1350

[28] A. Sinhamahapatra, N. Sutradhar, B. Roy, A. Tarafdar, H.C. Bajaj, A.B. Panda, Apl. Catal. A. 385 (2010) 22

[29] T. Ono, Y. Kubokawa, J. Catal. 52 (1978) 412

[30] Z.-Y. Xue, G.L. Schrader, J. Phys. Chem. B 103 (1999) 9459

[31] K. Egeblad, C.H. Christensen, M. Kustova, C.H. Christensen, Chem. Mat. 20 (2008) 946

[32] V.R. Surisetty, A.K. Dalai, J. Kozinski, Appl. Catal. A 393 (2011) 50

[33] G. Busca, Chem. Rev. 107 (2007) 5366

[34] M.O. Guerrero-Pérez, M.A. Bañares, Catal. Today 142 (2009) 245

[35] W.C. Vining, J. Strunk, A.T. Bell, J. Catal. 281 (2011) 222

Chapter 7

Carbon materials as template for the preparation of mixed oxides with controlled morphology and porous structure

This chapter is based on the following publication:

Valero-Romero, M.J., Cabrera-Molina, A., Guerrero-Pérez, M.O., Rodríguez-Mirasol, J., Cordero, T. Catalysis Today, (2014) 233-241

Abstract VPO bulk catalysts with spherical morphology and high surface areas have been prepared by the use of a carbon material as template. The carbon material is an activated carbon prepared by the hydrothermal method, using cellulose as starting material. Thus, the synthesis method described is simple and low-cost. The morphology and porous structure of these materials have been characterized by SEM, TEM, N_2 and CO_2 adsorption isotherms. The chemical composition was analyzed by XPS, XRD and Raman spectroscopy, showing the presence of V_2O_5 and VPO phases on the surface of these spherical catalysts. Methanol oxidation reaction was used to characterize the active centers on the surface of these materials and showed that both acid and redox sites are present. These materials were also tested during the propane ODH reaction and the results demonstrated that they are able to activate the hydrocarbon selectively to propylene. The characterization of these materials after reaction demonstrated that the morphology and the chemical composition are quite stable under the reaction conditions studied, since both VPO and V_2O_5 phases are detected. It was also observed that the biggest spheres are not stable during reaction conditions.

Keywords: lignocelluloses, microspheres, template, biomass, activated carbon, carbon-supported catalysts.

1. Introduction and Objectives

Bulk oxide materials are widely used in many applications, such as catalysts in selective oxidation processes, electrocatalysts in fuel cells, gas sensors, and solid oxide electrolysers in the production of hydrogen. The properties of these materials depend basically on the interstitial cation and anion vacancies that play an important role in the conductivity and in the capability of the surface to adsorb/desorb certain molecules, which determine the properties of such materials. Such properties can be modulated by the incorporation of other cations, with different atomic ratio, into the crystal structure of the initial oxide structure. For example, vanadium oxide based-compounds are well known as oxidation catalysts [1]. This is due to the ability of vanadium atoms to possess multiple stable oxidation states, which results in the easy conversion between oxides of different stoichiometry by oxidation and reduction cycles during a catalytic reaction. These redox cycles may cause V_2O_5 amorphization, thus, for preparing active and selective catalyst vanadium oxide is usually deposited at the surface of a support or mixed with other component. All these factors make that some mixed oxide structures present good properties as catalysts (VPO, MoVTeO, $VSbO_4$, $CeZrO_x$, MoFeO ...) [2-7]. For instance, active and selective oxide catalysts are typically composed by more than one element since bimetallic catalytic systems can potentially achieve chemical transformations that are unprecedented on monometallic catalysts. The complexity of these powders (e.g., crystal structure and amorphous domains, variable oxidation states, variable coordination for each oxidation state, chemical nature of surface sites, participation of surface and bulk lattice oxygen atoms in oxidation reactions and presence of vacancies or defects), along with the difficulty in characterizing the surface of such materials, limit the development of their applications [8].

On the other hand, the importance of nanoparticles and their nanostructure on the performance of functional materials, such as catalysts, has stimulated wide efforts to develop methods for their synthesis and characterization, making this area of study an integral part of nanoscience. Due to the importance of nanoparticles and oxides, many synthesis methods for nanospheres of single oxides such as ZnO_2, SnO_2, TiO_2, In_2O_3, WO_x, CdO, CuO, NiO, TeO_2 or MoO_3, among others can be found in the literature [9-14]. Although there are a high number of papers dealing with the preparation of pure oxide nanomaterials, there are just a few works describing the synthesis of doped oxide

materials (mixed oxides) with controlled morphology [15]. This is in part because the methods for preparing nanostructures require the use of precursors that are expensive and sometimes not available for a mixture of several atoms due to the solubility. In addition, and in the case of doped mixed oxides, it is difficult to control the final composition of the surface of the final nanomaterials, which is directly related with their properties.

Thus, the aim of the present work is to develop a new strategy for the synthesis of a mixed bulk-oxide VPO material with spherical morphology that could be potentially apply for other mixed oxide systems. Vanadium and Phosphorous mixed phases (VPO) are well known as catalysts for hydrocarbon transformation since they are industrially used for the catalytic transformation of n-butane into maleic anhydride. The proposed methodology is simple and low cost and implies the use of a carbon material as a template or as support. Among the potential saccharides that can be employed to produce carbonaceous materials through hydrothermal carbonization, cellulose is the most promising material as it is by far the most abundant and inexpensive saccharide available. The synthesis of carbon spheres by the use of the hydrothermal method [16-18] has been reported. Thus, in the present work we investigate the potential of cellulose as precursor for the production of carbon microspheres containing phosphorous via hydrothermal carbonization. These materials will be used as support for the vanadium oxide active phases; by this way, spherical carbon-supported mixed oxide (VPO) catalysts will be prepared. These materials are calcined in order to eliminate the carbon material but keeping the shape in the oxide structure. By this way hollow mixed oxide spheres will be prepared. Thus, the present article describes the synthesis and characterization of these two types of materials: carbon-supported and bulk oxide spherical-shaped materials (scheme 1).

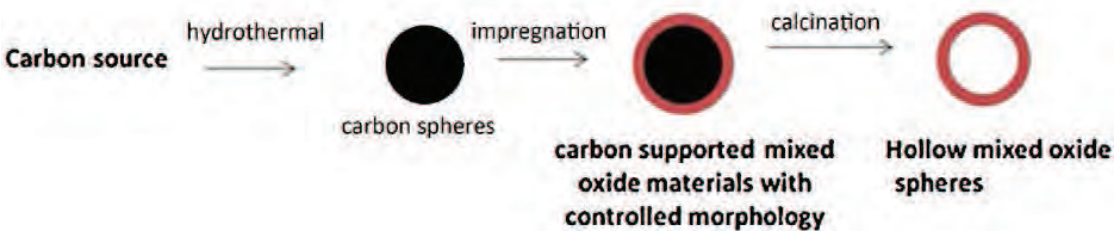

Scheme 1. Proposed procedure for the preparation of the mixed oxide spheres

Since VPO materials are well known as catalysts for hydrocarbon activation, they will be tested during the catalytic propane dehydrogenation into propylene. Nowadays ethylene and propylene are commercially produced by the steam cracking of naphthas. This is a quite endothermic process that requires high reaction temperatures (800-900ºC). Thus, this is a high energy consuming process and, in addition, many byproducts are obtained, being complicated also the separation and purification of propylene and ethylene. Such high temperatures also favor coke deposition on the active sites, which deactivated the catalyst [19]. Due to all these problems, there is a need to develop a new technology for ethylene and propylene production. One of the most promising technologies that are being developed nowadays is the exothermic oxidative dehydrogenation (ODH) of the corresponding alkane, ethane or propane, for the production of ethylene or propylene in one step. ODH processes are exothermic, and can be operated at lower temperatures (300-600ºC), requiring less energy input that the steam cracking of naphthas mentioned above. In addition, the presence of oxygen in the feed suppresses coke formation and prevents catalysts deactivation.

2. Experimental

2.1. Preparation of samples

The carbon supports were obtained by chemical activation of hydrothermally carbonized cellulose (Aldrich) according to the following procedure. This carbon precursor (cellulose 125 g/l) was impregnated with H_3PO_4 (85 wt.% in H_2O, Aldrich) at different mass impregnation ratios of 1, 2 and 3 (H_3PO_4/cellulose). The mixture was then placed in a teflon-lined autoclave, which was heated at 200 ºC and maintained at this temperature for 16 h. The ratio volume of solution/volume of autoclave is around 0.6. The hydrothermally impregnated samples were dried for 24 h at 80 ºC and activated under continuous N_2 flow (150 cm^3 STP/min), in a conventional tubular furnace at 500 ºC. The activation temperature was reached at a heating rate of 10 ºC/min and maintained for 2 h. The activated samples were cooled inside the furnace under N_2 flow and then washed with distilled water at 60 ºC until negative phosphate analysis in the eluate [20]. The resulting activated carbons were denoted by C1, C2 and C3.

These activated carbons were impregnated with a solution of NH_4VO_3 (99.99%, Sigma Aldrich). The concentration of solution contained the desired amount of vanadium ions to obtain a vanadium coverage of 4 vanadium atoms per nm^2 of carbon support, 4VC1, 4VC2 and 4VC3. This coverage has been found in other carbon to correspond to the dispersion limit loading of VOx species, understood as the maximum amount of vanadium oxide species that remain dispersed without the formation of V_2O_5 crystals [21]. This solution was prepared by mixing ammonium metavanadate with a 0.5 M solution of oxalic acid (99%, Sigma Aldrich) and was heated and stirred until all vanadium dissolves before impregnation the support. This mixture was dried in a rotator evaporator at 80 ºC at a reduced pressure of 10-40 mmHg. The resulting solids were dried at 120 ºC for 24 h and then calcined at 450 ºC for 40 min in air flow (150 cm^3 STP/min). These samples were denoted by 4V1, 4V2 and 4V3. Scheme 2 summarizes the preparation procedure and conditions for obtaining the supports and catalysts.

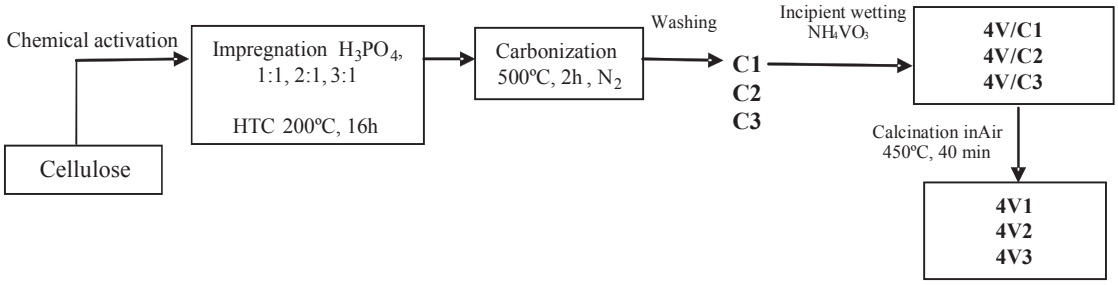

Scheme 2. Preparation procedure and notation of the supports and catalysts.

2.2. Characterization

Oxidation resistance of the different catalysts and the carbon supports were obtained by non-isothermal thermogravimetric analyses, carried out in a CI electronics thermogravimetric system. The thermobalance automatically measures the weight of the sample and the temperature as a function of time. Experiments were carried out in air atmosphere, for a total flow rate of 150 cm^3 (STP)/min, employing sample mass of approximately 10 mg. The sample temperature was increased from room temperature up to 900 ºC at a heating rate of 10 ºC/min.

The porous structure of the activated carbons was characterized by N_2 adsorption-desorption at -196 ºC and by CO_2 adsorption at 0ºC, carried out in an ASAP 2020 model of Micromeritics Instruments Corporation. Samples were previously outgassed during 8 hours at 150 ºC. From the N_2 adsorption/desorption isotherm, the apparent surface area (A_{BET}) was determined applying the BET equation, the micropore volume (V_t) and the external surface area (A_t) were calculated using the t-method [22] and the mesopore volume (V_{mes}) was determined as the difference between the adsorbed volume at a relative pressure of 0.95 and the micropore volume (V_t) [23]. The narrow micropore surface area (A_{DR}) and volume (V_{DR}) were obtained by the Dubinin-Radushkevich method [24] applied to the CO_2 adsorption isotherm.

X-ray photoelectron spectroscopy (XPS) analyses of the samples were obtained using a 5700C model Physical Electronics apparatus, with MgKα radiation (1253.6 eV). For the analysis of the XPS peaks, the C1s peak position was set at 284.5 eV and used as reference to position the other peaks while the fitting of the XPS peaks was done by least squares using Gaussian-Lorentzian peak shapes.

X-ray powder diffraction patterns of samples were acquired on a Philips X´Pert PROMPD diffractometer using CuKα radiation (λ = 1.5406 Å). The X-ray generator was set to 45 kv at 40 mA.

Raman spectra of the samples were acquired at 200 ºC in the 200 and 3900 cm^{-1} region using a Bruker Senterra micro-Raman spectrometer equipped with a cooled CCD detector and a hot stage (Linkam FTIR600). Laser excitation (Nd-YAG laser) used for micro-Raman analyses was of 785 nm with a laser power of 10 mW. The spectra acquisition consisted of an average of 10 spectra measured after 10 accumulations of 10s.

The surface texture and the structure of the samples were characterized by scanning electron microscopy (SEM) and by transmission electron microscopy (TEM) respectively. Scanning electron micrographs were obtained using a JEOL JSM-840 instrument, working at a high voltage of 20–25 kV and transmission electron micrographs were carried out in a CM200 apparatus (Philips), working at a high voltage of 200 KV.

2.3. Catalytic performance experiments

The methanol oxidation reaction was carried out in a fixed bed quartz tubular reactor (i.d. 4 mm, length 400 mm), working at atmospheric pressure. In a typical experiment 0.1 g of catalyst (0.1-0.3 mm particle size) were placed into the reactor and diluted in 0.2 g of silicon carbide. The flow rate was 80 ml/min and the feed consisted of a mixture of Methanol/oxygen/helium (4/8/88 mol %). Experiments were carried out at 250 ºC. Reactants and reaction products were analyzed by on line gas chromatography (490 micro-GC equipped with PPQ, 5A molsieve and Wax columns, Agilent).

The catalytic activity of the synthetized catalysts (4V1, 4V2 and 4V3) was studied during the oxidative dehydrogenation of propane in the gas phase at atmospheric pressure in a fixed bed microreactor (i.d. 4 mm, length 400 mm). The influence of different operation conditions, such as, space time (W/F = 0.048-0.12, $g \cdot s \cdot ml^{-1}$) and propane/oxygen ratio (C_3H_8/O_2 = 0.25, 0.5, 1 and 2) were analyzed. The flow rate and the amount of catalyst were varied (from 40 to 100 cm^3 min^{-1} and from 0.5 to 0.1 g, respectively) in order to achieve the desired conditions and different propylene conversion levels. In a typical run, the catalyst (0.1-0.3 mm particle size) was diluted in SiC in order to increase the bed length and avoid local heating. Experiments were carried out in the 500-600 ºC temperature range. Reactants and reaction products were analyzed by on-line gas chromatography (Agilent 490 micro-GC). As blank reaction, catalytic tests were also performed in absence of catalyst (only with SiC inside the reactor) and the propane conversion values were found negligible.

The conversion for both catalytic tests was defined as the ratio of the amount of methanol or propane converted to the amount of methanol or propane, respectively, supplied to the reactor. The selectivity (in mol%) was defined as the molar ratio of a specific product to all the products formed.

3. Results and Discussion

Figure 1A shows the thermogravimetric analysis profiles in air for the three activated carbons that have been prepared. As expected, and according to previous

results with similar carbon materials [25], all of them are resistant in air up to 500 ºC. This is due to the synthesis method by chemical activation with H_3PO_4 that has shown to increase the oxidation resistance of carbon materials due to the presence of different phosphorus functional surface groups, such as C–O–PO_3, C-PO_3 and C-P groups that act as a physical barrier blocking the active carbon sites [25-28]. After vanadium incorporation, the oxidation resistance is lower (Figure 1B) due to the vanadium oxide centers, active oxidation catalysts, which are able to catalyze the gasification of the activated carbon. Based on these results, and as indicated in the experimental section, the impregnated samples 4VC1, 4VC2 and 4VC3 were calcined in air at 450 ºC for 40 min. These conditions were selected in order to eliminate the major part of the activated carbon and keeping the spherical morphology in the oxide material. The elemental analysis show that after calcination the bulk oxide material present some carbon (about 10%) (Supporting information).

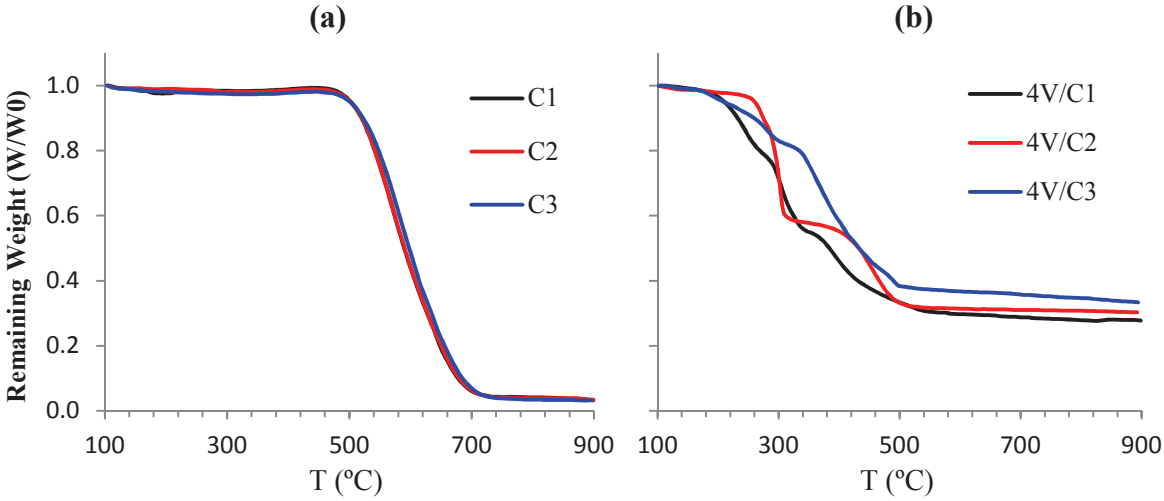

Figure 1. TGA patterns of carbon supports (a) and V supported catalysts (b). During the experiment, samples were heated under air flow with a heating rate of 10 ºC min^{-1}.

Figure 2 shows N_2 adsorption–desorption isotherms for the activated carbons (Figure 2a), for the vanadium-impregnated carbons (Figure 2b), and for the bulk oxides (Figure 2c), whereas Table 1 summarizes the values of the structural parameters that characterize the porous structure of the samples, as derived from N_2 adsorption–desorption and CO_2 adsorption isotherms. The activated carbons show a modified type I isotherm, corresponding to a well-developed microporous structure with a significant

contribution of mesoporosity, which depends on the impregnation ratio. The shape of the isotherms, with larger hysteresis loop at high relative pressures, reveals that an increase in the impregnation ratio from 1 to 2 gives rise to a widening of the porous structure of the resultant carbon [25,29].On the other hand, the amount of N_2 adsorbed at low relative pressures decreases for higher impregnation ratios, probably due to the widening of the micropores that may generate mesopores. C1 presents an H2 hysteresis loop, associated to pores with narrow necks and wide bodies (often referred to as 'ink bottle' pores), and H4 type hysteresis loops are observed for C2 and C3, often associated to slit-shaped pores. Similarly, the adsorption and desorption isotherms for the vanadium-impregnated carbons and for the bulk oxides is associated with narrow slit-like pores, and the type I isotherm character is indicative of microporosity. The apparent surface areas values obtained by the BET method (A_{BET}) and the mesopore volume values (V_{mes}) are very high for the activated carbons (Table 1). As expected, after vanadium incorporation the apparent (A_{BET}) and the external (A_t) surface area values decrease, due to the partial blockage of the porous structure, although, these values remain quite high for a supported oxide catalysts and suitable for catalytic application. C2 carbon presents the highest pore volume (V_t) and is the sample that presents the highest values of specific (A_{BET}) and the external (A_t) surface area after vanadium impregnation (4V/C2) and calcination (4V2). 4V2 bulk oxide sample presents a BET surface area higher than 100 m^2/g, which represents a high value for this kind of material. The shape of the isotherms (Figure 2c) and the BET surface area values obtained for the bulk oxide samples (Table 1) indicate that these materials present textural properties that make them quite suitable for catalytic application.

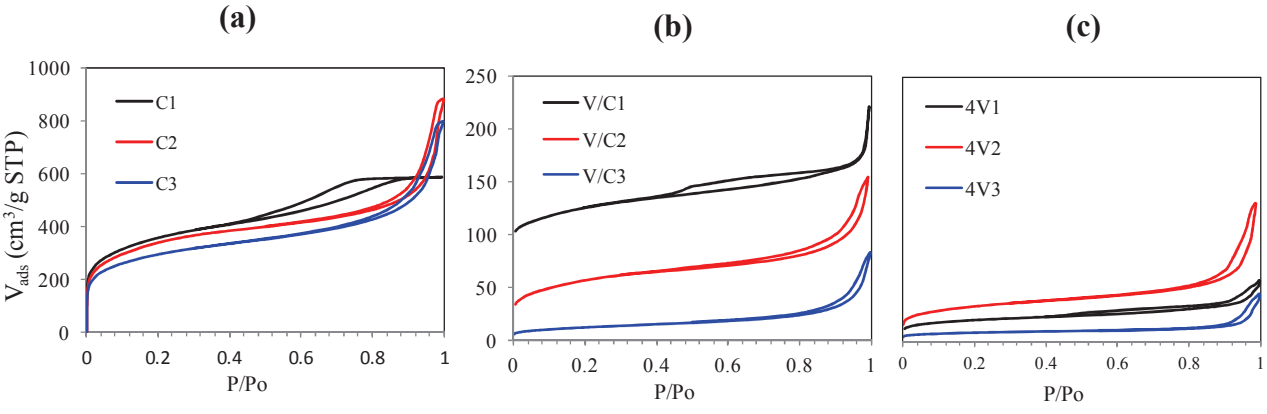

Figure 2. N_2 adsorption-desorption isotherms of activated carbon supports (a); V supported porous activated carbons (b) and V-O catalysts (c).

Table 1. Structural parameters of carbon supports, V supported catalysts and V-O catalysts.

	N_2 Isotherm				CO_2 Isotherm	
Sample	**A_{BET} (m^2/g)**	**A_t (m^2/g)**	**V_t(cm^3/g)**	**V_{mes}(cm^3/g)**	**A_{DR}(m^2/g)**	**V_{DR}(cm^3/g)**
C 1	1284	466	0.326	0.536	676	0.271
C 2	1223	265	0.444	0.464	619	0.248
C 3	1045	320	0.334	0.531	580	0.232
4V/C1	150	39	0.051	0.041	142	0.094
4V/C2	205	52	0.071	0.092	151	0.106
4V/C3	43	28	0.007	0.056	144	0.160
4V1	71	27	0.020	0.038	52	0.062
4V2	119	49	0.036	0.080	75	0.073
4V3	29	9	0.009	0.019	30	0.041

Figure 3 shows some representative XPS spectra in the P2p region. Peaks in the range 134.0–134.6 eV are commonly assigned to phosphate species in which P atom is bonded to O atoms, whereas when P is bonded to one C atom this value shifts to lower values (around 133.6 eV) [30]. This signal could overlap with that for VPO phases, such as $(VO)_2P_2O_7$, since its signal appears also near 133.7 eV [31,32]. Table 2 shows the Binding Energy values obtained for P2p region. The values obtained for activated carbons and for the vanadium impregnated samples indicate that the majority of phosphorus atoms are bonded to carbon atoms, as in CPO_3 and C_2PO_2 surface groups. After calcination, these values increase up to 133.6 eV, which may indicate the formation of VPO species.

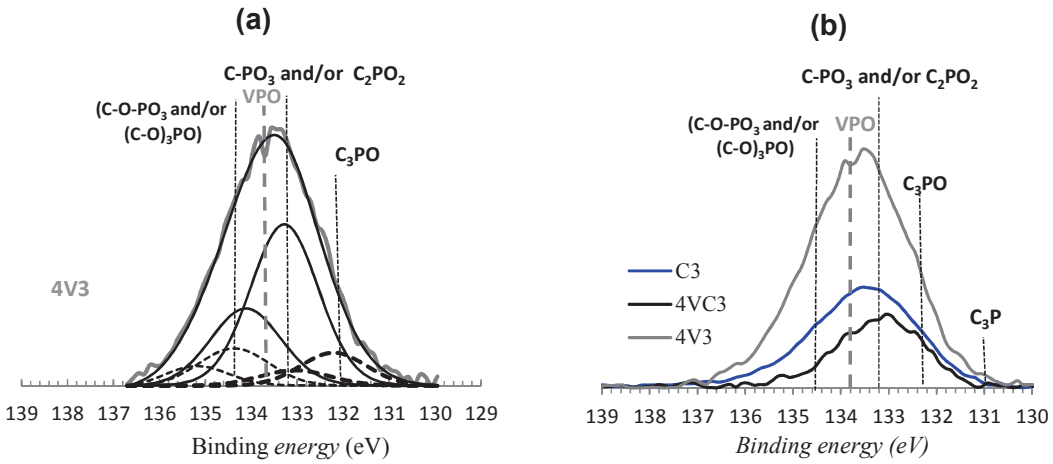

Figure 3. Representative XPS spectra for P2p region of 4V3 catalyst showing the deconvolution (a) and XPS spectra for samples C3, 4V/C3 and 4V3 (b).

Table 2. XPS results

Sample	P/V*	Be P2p (eV)	Be V^{4+} (eV)	Be V^{5+} (eV)	V^{4+}/V^{5+}
C1	n.a.	133.2	n.a.	n.a.	n.a.
C2	n.a.	133.5	n.a.	n.a.	n.a.
C3	n.a.	133.4	n.a.	n.a.	n.a.
4V/C1	0.31	133.0	516.1	517.3	0.44
4V/C2	0.75	133.1	516.3	417.7	0.37
4V/C3	0.34	133.1	516.1	517.2	0.40
4V1	0.29	133.6	516.1	516.4	0.37
4V2	0.41	133.5	516.1	517.3	0.43
4V3	0.32	133.5	516.1	517.3	0.42

**based on atomic surface concentrations calculated by XPS*

n.a:. not applicable,

Figure 4 shows a representative XPS spectrum of V2p region for 4V3. The V2p region typically exhibits two components, the one at higher binding energy (517.1 eV) is assigned to V^{5+} species, whereas the component at lower binding energy (516.1 eV) is associated with V^{4+} species [33,34]. The percentages of both contributions to V2p signal have been calculated by deconvolution and are shown in Table 2. These values indicate that the amount of oxidized and reduced vanadium species may vary, but in all the cases is higher the amount of V^{5+}.

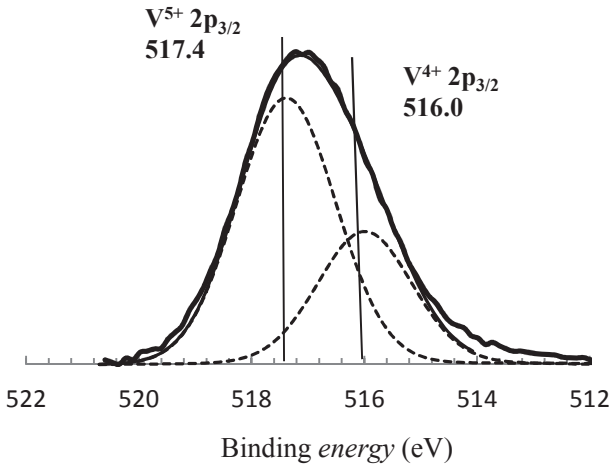

Figure 4. Representative XPS spectra for V2p region (4V3 sample).

XRD patterns of oxidized samples are show in Figure 5. There are two intense peaks that are visible in the three samples near 21.5 and 27.9 º. These peaks have been assigned to δ-$VOPO_4$ [35] and also to $(VO)_2P_2O_7$ [36], thus, they must belong to a VPO phase. This may be due to the nature of VPO phases, since many different structures have been described with different vanadium oxidation states and P/V molar ratio, and the inter-conversion between some of them, depending on the ambient conditions, is relatively easy [35]. The two most intense peaks of V_2O_5 phase (JCPDS file 41-1426) [37] are also visible in all the samples. Thus, according to XRD results, a mixture of vanadium oxide and VPO species is present in all the samples.

Figure 6 shows representative Raman spectra of an impregnated carbon (4V/2C) and of a bulk oxide material (4V2). Pure V_2O_5 exhibits Raman bands at 143, 283, 302, 405, 480, 526, 698, and 994 cm^{-1} [37], these bands are observed in both spectra, in line with XRD patterns (Figure 5), since the most intense peaks of V_2O_5 diffraction pattern

were detected. V_2O_5 oxide is a strong Raman scatter, although that, some of the Raman bands in Figure 6 are hardly detected (as those as 526 and 480 cm^{-1}); in addition, only the two most intense pattern peaks are visible in the XRD pattern (Figure 5). These results indicate that V_2O_5 oxide is present as small aggregates. In addition, two broad bands near 990 cm^{-1} and 930 cm^{-1} are also visible in the 4V2 sample. These Raman bands belong to the most intense Raman modes of $(VO)_2P_2O_7$ and $VOPO_4$ phases [38,39], in which vanadium is present as V^{4+} and V^{5+}, respectively. The coexistence of two oxidation states for vanadium ions is consistent with the XPS data (Figure 4 and Table 2). These results are in accordance with XRD patterns since VPO phases were also detected (Figure 5). Thus, Raman spectroscopy and XRD patterns show that both vanadium oxide and VPO species are present in the oxide samples.

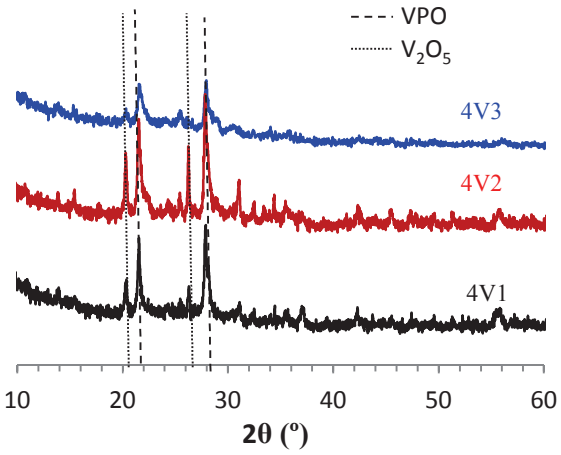

Figure 5. XRD Patterns of oxide samples.

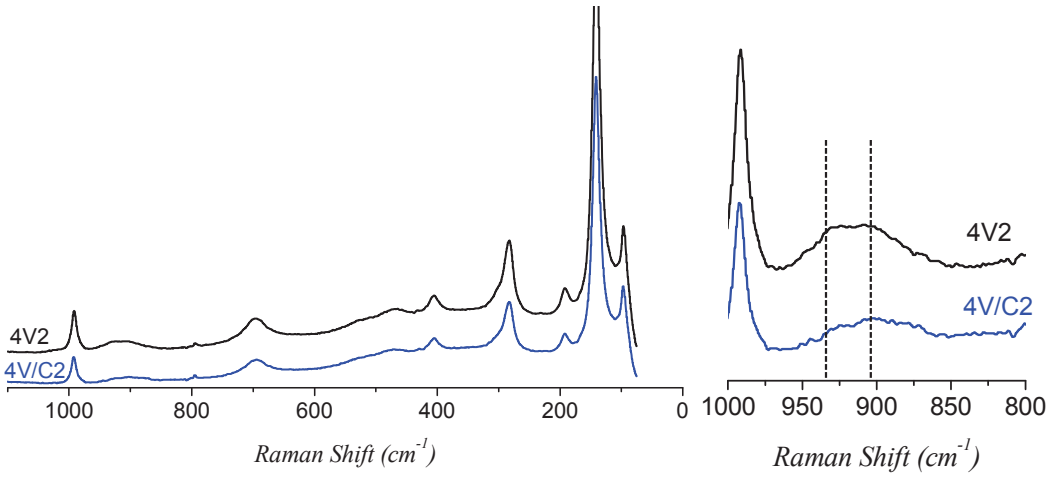

Figure 6. Raman spectra of 4V/C2 and 4V2 catalysts (air, 200 ºC).

SEM images for the cellulose obtained by hydrothermal treatment at 220 ºC for 16 h, included in Figure 7a and b, consist mainly of well dispersed and separated spherical particles with diameters that vary between 0.2 to 5 μm. These results are similar to previous studies published elsewhere [16]. Figure 8 shows SEM and TEM images for the activated carbon with an impregnation ratio of 2 (C2 carbon) (Figure 8a-c), for the corresponding vanadium-supported activated carbon (4VC2) (Figure 8d-f) and for the corresponding bulk oxide 4V2 (Figure 8g-i). Strong differences are found in the shape of the spherical particles due to the chemical activation with H_3PO_4 when compared with the carbon after the treatment without phosphoric acid (Figure 7). Such structures (Figure 8a-c) can be described as "interconnected" carbon spheres, which have an average diameter of 0.2-4 μm and usually tend to fuse with each other. TEM images for C2 and 4V2C samples, Figure 8c and 8f, respectively, clearly illustrate the coexistence of spheres of different sizes and their morphologies, which are in some cases interconnected by small particles within a matrix. SEM images in Figure 8g and 8h reveals that the bulk oxide material, 4V2, has replicated the external morphology of the activated carbon support. The TEM micrograph, Figure 8i, shows pores of around 90 nm in the surface of the bulk oxide material, which consists of the shell of the hollow spheres, probably generated from the removal of the carbon support.

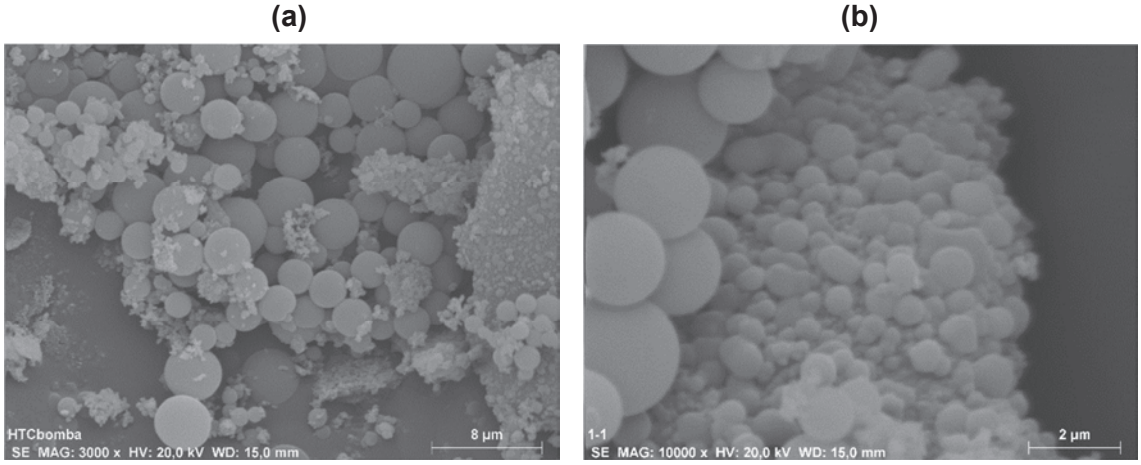

Figure 7. SEM images of hydrothermal carbonization of cellulose without activation with H_3PO_4. Scale bars correspond to 8 μm (a) and 2 μm (b).

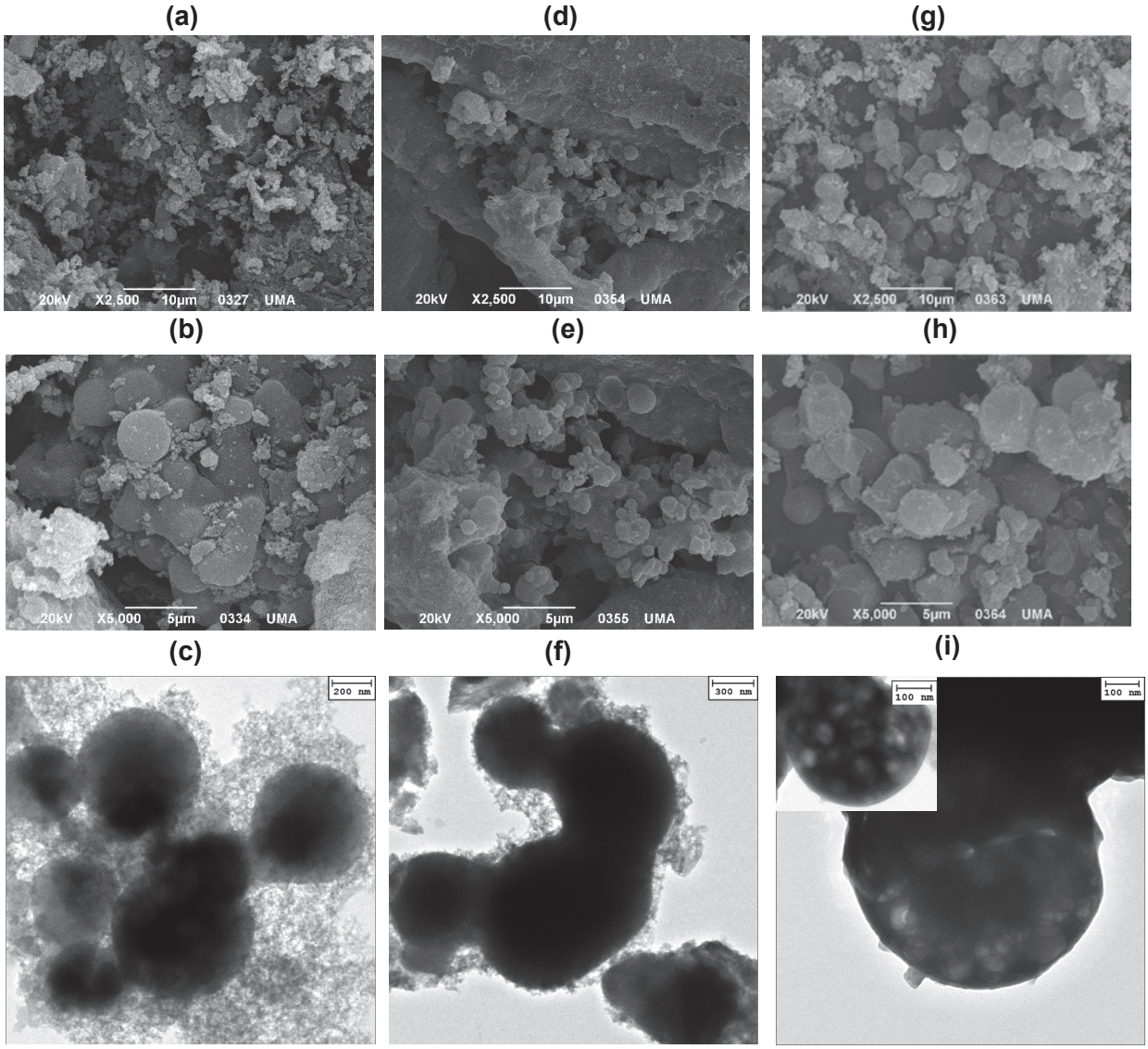

Figure 8. SEM and TEM images of C2 (a–c), 4V/C2 (d–f) and 4V2 (g–i). Scale bars correspond to 10 µm (a, d and g), 5 µm (b, e and h) and 200, 300 and 100 nm (c, f and i), respectively.

Figure 9 shows the evolution of propane conversion and the selectivity to main products as a function of reaction temperature for 4V2 catalyst. At 500 ºC, propylene is obtained with a high selectivity (80%) and a low propane conversion (5%). At 550 ºC, the conversion is higher but still lower than 10%, while the selectivity to propylene is lower and the selectivity to COx (mainly CO) increases. At 600ºC, the propane conversion is quite high and the yield to propylene, around 10%. This value is similar to those reported previously with several oxide catalytic systems, such as, Sb-V-O, V-Ga-O, V-Mg-O, V-Ga-O, V–Mo-O [40-43], among others. At this temperature (600 ºC) the

cracking reactions begin to be significant, in line with previous papers [41], obtaining ethylene and methane as products of this reaction, but yielding mainly propylene (Figure 9).

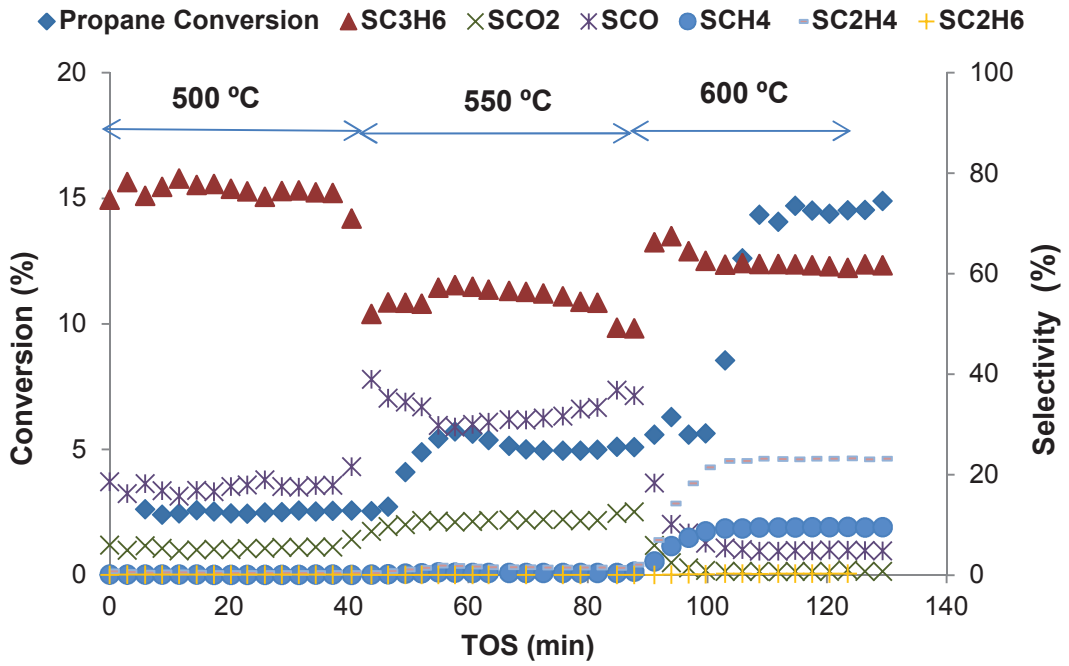

Figure 9. Propane conversion and selectivity to main products during the ODH reaction on 4V2 catalyst. Reaction conditions: 50 mg of catalyst (0.1-0.3mm particle size), total flow 40 ml/min, feed composition (%volume), $C_3H_8/O_2/N_2$ (45.7/11.4/42.9), W/F = 0.075 gcat·s·ml^{-1}.

Figure 10 shows the propane conversion and the selectivities for the bulk oxide catalysts. Catalysts 4V1 is the less active (4%) and selective for total oxidation products (CO and CO_2). The performance of samples 4V2 and 4V3, which contain a higher amount of phosphorus, is quite different, yielding a high selectivity to propylene at higher conversions. In fact, the XPS deconvolutions (Table 2) indicate that sample 4V1 presents more vanadium species as V^{5+} than the rest of samples, indicative of a higher amount of V_2O_5 oxide and oxidized VPO species, such as $VOPO_4$, since both are present and visible by XRD (Figure 5). XPS data (Table 2) indicate that 4V2 and 4V3 samples have a higher contribution of V^{4+} species, with a higher amount of phosphorus, being both selective to propylene. This indicates the presence of partial oxidation active phases on the surface of catalysts 4V2 and 4V3, such as vanadium pyrophosphate,

$(VO)_2P_2O_7$, identified by XRD and Raman spectroscopy in these samples (Figure 5 and Figure 6). Thus, the presence of a higher amount of phosphorous appears to be related with a higher amount of reduced V^{4+} species, which are found to be more selective to the partial oxidation reaction yielding propylene as the main product (Figure 10). These results are in line with previous studies since vanadium pyrophosphate is usually pointed out as the active phase of VPO catalysts during hydrocarbon partial oxidation reactions [39]. Also these results are according to previous studies with other catalytic vanadium based systems, such as V/TiO_2 or $VSbO_4$, that have shown that reduced vanadium species are required in order to have hydrocarbon partial oxidation selective catalysts [44,45].

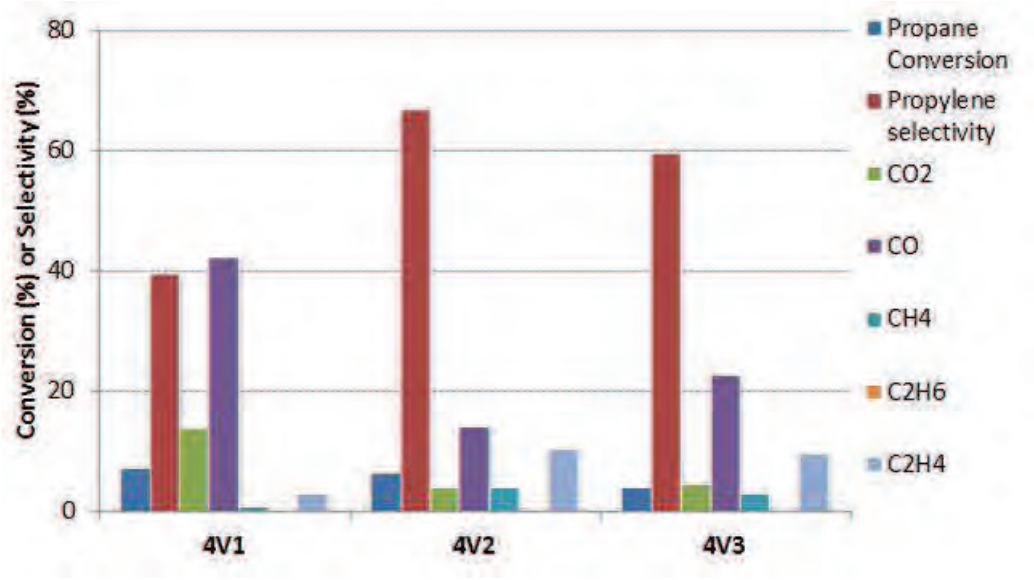

Figure 10. Propane conversion and selectivity to main products during the ODH reaction on bulk oxide catalysts. Reaction conditions: T = 575 ºC, 50 mg of catalyst (0.1-0.3mm particle size), total flow 40 ml/min, feed composition (%volume), $C_3H_8/O_2/N_2$ (45.7/11.4/42.9), W/F = 0.075 gcat·s·ml^{-1}.

The catalytic properties of these materials have been also characterized with the methanol oxidation reaction. Methanol is a well-established probe to determine the number of surface active sites present in metal oxide catalysts and the distribution of acid–basic and redox sites [46-50]. Methanol oxidation over metal oxides produces different reaction products depending on the surface active site: formaldehyde on

surface redox sites and dimethyl ether on surface acidic sites [51-54]. Combination of acid and redox or basic and redox sites will produce dimethoxymethane or methyl formiate, respectively [55-60]. Table 3 summarizes the methanol conversion and selectivity values to main reaction products obtained at 250 ºC after 1 hour of TOS for a carbon material and the corresponding vanadium containing catalysts (the carbon-supported and the bulk oxide). Very low methanol conversion (1.2 %) is detected with the C2 carbon. As expected, C2 is selective to dimethyl ether, indicative of acid sites on its surface. As described in the experimental section, this carbon material has been prepared thought a chemical activation of cellulose with H_3PO_4, which results in carbons with a high and predominantly Brönsted surface acidity because of the residual phosphorus groups that remain on the carbon surface [30]. The conversion is higher when vanadium sites are on the surface of catalysts (4V/C2 and 4V2), increasing also the selectivity CO and CO_2. The conversion is especially high in the case of the supported 4V/C2 catalyst, which may indicate that the spherical supported material performs better that the hollow oxide sphere. The selectivity to COx can be due to the oxidation of intermediate products, and also to the strong acid sites of the exposed carbon support, which are able to retain the reaction intermediates, then, the vanadium sites are able to oxidize them. The presence of dimethyl ether (DME), dimetoxymethane (DMM) and methyl formiate (MF) as reaction products for the vanadium containing catalysts (4V/C2 and 4V2), is indicative of redox and acid sites. The redox sites must be related with V_2O_5 and VPO species identified by XRD (Figure 5) and Raman spectroscopy (Figure 6).

Table 3. Catalytic activity in MeOH + O_2 reaction (stationary state-average values after 1 hour of TOS). Reaction Temperature: 250ºC

Catalyst	MeOH conversion (%)	Selectivity (%)				
		CH_3OCH_3	$HCOOCH_3$	$(CH_3O)_2CH_2$	CO	CO_2
C2	1.2	92.8	0.5	3.5	1.6	0.8
4V/C2	44.4	25.7	21.4	7.1	22.8	22.8
4V2	11.2	17.6	17.8	31.6	14.9	16.4

The used materials were characterized in order to study the stability of VPO phases and of the morphology of these catalytic materials during reaction. Raman spectra of used 4V2 catalyst in both reactions are shown in Figure 11. V_2O_5 (990 cm^{-1} band) and VPO phases (broad signals at 930 and 910 cm^{-1}) are present in the used sample, as well as in the fresh one (Figure 6). Thus, both phases are stable under reaction conditions, indicating that the chemical composition of the surface of catalysts is quite stable. SEM and TEM micrographs of the used 4V2 sample, after propane (Figure 12 a,b) and methanol oxidation (Figure 12 c,d) reveal some changes of the morphology with respect the fresh catalyst. SEM and TEM images of the used catalyst provides evidence of a population of spherical particles with diameters below 1 <μm, whereas the fresh catalyst was characterized with a large number of small particles coexisting with larger spheres whose sizes vary between 0.2-5 μm (Figure 8g-i). This evidences that the larger spherical hollow structures do not keep their spherical morphology after reaction. Although that, the smaller spheres keep the spherical morphology.

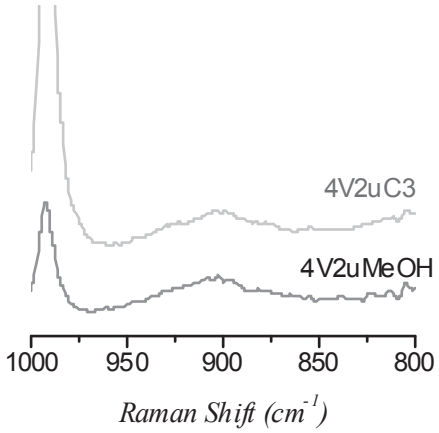

Figure 11. Raman spectra of used catalysts (200 ºC)

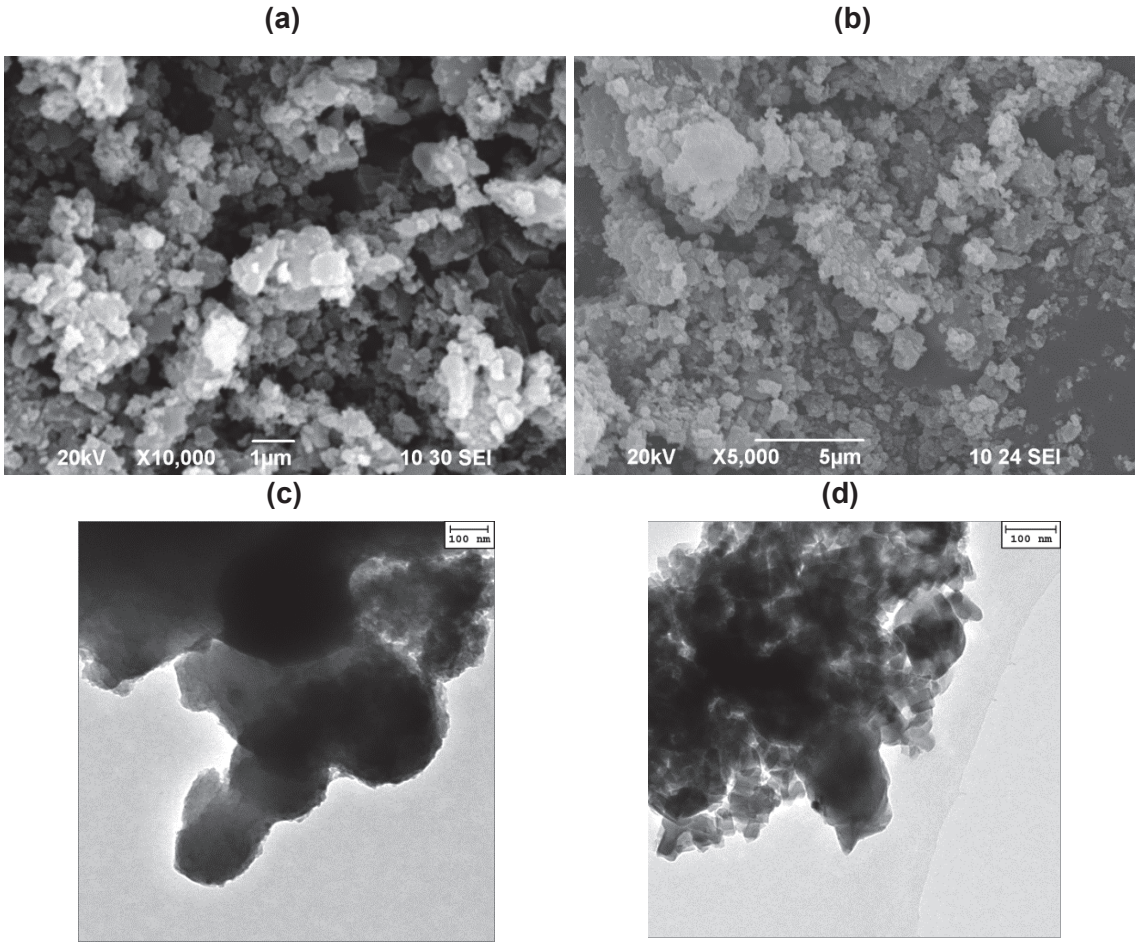

Figure 12. SEM and TEM images of 4V2 after reaction; methanol oxidation (a and b) and propane ODH (c and d). Scale bars correspond to 1 and 5 µm (a and c) and 100 nm (b and d).

4. Conclusions

It has been reported the successful preparation of VPO materials with spherical morphology. Two different spherical VPO catalysts have been described: a carbon-supported material and a bulk oxide, both with spherical morphology. These materials are promisingcatalysts since the vanadium-phosphate catalytically active phases have been identified by XRD and Raman spectroscopy. The catalytic properties of mixed oxides have been tested with two different reactions. Methanol oxidation showed that these materials have active acid and redox sites on their surface, whereas propane ODH demonstrated that they are able to activate the hydrocarbon (propane) in order to produce the partial oxidation product (propylene). The characterization of used samples

showed that the vanadium-phosphate mixed phases are stable under reaction conditions. It was also observed that the larger particles did not keep the spherical morphology under reaction conditions. This morphology, on the contrary, was keep by the smaller particles (below 1 μm).

Thus, a simple and low cost method for preparing VPO catalysts with spherical morphology and with a high surface area has been described. This technology could be applied to other oxide bulk materials. These materials are promising catalysts.

Acknowledgements

Spanish Ministry of Economics for project CTQ2012-36408 and Andalucía Regional Government for P09-FQM-5156 and P10-FQM-6778. M.J.V.-R. thanks Spanish Ministry for a FPI predoctoral fellowship.

Supporting information

Elemental composition of carbon supports, V supported catalysts and V-O catalysts.

Sample	C (%wt.)	H (%wt.)	N (%wt.)	O* (%wt.)
C1	80.0	1.9	0.1	18.0
C2	79.3	2.1	0.0	18.5
C3	78.4	3.5	0.1	18.0
4V/C1	32.7	3.1	5.2	--
4V/C2	31.1	2.5	4.5	--
4V/C3	40.4	3.0	4.7	--
4V1	13.5	0.2	1.1	--
4V2	11.8	1.1	1.3	--
4V3	9.8	0.4	1.4	--

**: obtained by difference (100% – C –O –H –S –ash)*

References

[1] J. Haber, Catal. Today 142 (2009) 100.

[2] F. Cavani, Catal. Today 157 (2010) 204.

[3] P. Botella, J.M. López Nieto, B. Solsona, A. Mifsud, F. Márquez, J. Catal. 98 (2002)445.

[4] G. Centi, Catal. Today 16 (1993) 5.

[5] E. Bordes, Catal. Today 1 (1987) 499.

[6] L.J. Burcham, I.E. Wachs, Catal. Today 49 (1999) 467.

[7] M.O. Guerrero-Pérez, J.L.G. Fierro, M.A. Vicente, M.A. Bañares, Chem. Mater. 19(2007) 6621.

[8] I.E. Wachs, K. Routray, ACS Catal. 2 (2012) 1235.

[9] S. Cheng, D. Yan, J.T. Chen, R.F. Zhuo, J.J. Feng, H.J. Li, H.T. Feng, P.X. Yan, J. Phys.Chem. C 113 (2009) 13630.

[10] X.-L. Li, T.-J- Lou, X.-M. Sun, Y.-D. Li, Inorg. Chem. 43 (2004) 5442.

[11] D. Zhang, L. Qi, J. Ma, H. Cheng, Adv. Mater. 14 (2002) 1499.

[12] Y. Chang, J.J. Teo, H.C. Zeng, Langmuir 21 (2005) 1074.

[13] N.S. Ramgir, D.J. Late, A.B. Bhise, M.A. More, I.S. Mulla, D.S. Joag, K. Vijayamo-hanan, J. Phys. Chem. B 110 (2006) 18236.

[14] M.M. Titirici, M. Antonietti, A. Thomas, Chem. Mater. 18 (2006) 3808.

[15] X. Liu, D. Wang, Y. Li, Nano Today 7 (2012) 448.

[16] M. Sevilla, A.B. Fuertes, Carbon 47 (2009) 2281–2289.

[17] X. Sun, Y. Li, Ang. Chem. Int. Ed. 43 (2004) 597.

[18] L. Xu, W. Zhang, Q. Yang, Y. Ding, W. Yu, Y. Qian, Carbon 43 (2005) 1090.

[19] S.M.K. Airaksinen, M.A. Bañares, A.O.I. Krause, J. Catal. 230 (2005) 507–513.

[20] E. González-Serrano, T. Cordero, J. Rodríguez-Mirasol, L. Cotoruelo, J.J.Rodríguez, Water Res. 38 (2004) 3043–3050.

[21] M.O. Guerrero-Pérez, J.M. Rosas, R. López-Medina, M-A. Bañares, J. Rodríguez-Mirasol, T. Cordero, J. Phys. C 116 (2012) 20396–20403.

[22] S.J. Gregg, K.S.W. Sing, Adsorption Surface Area and Porosity, 2nd ed., AcademicPress, London, 1982, pp. 42–102.

[23] F. Rodríguez-Reinoso, M. Molina-Sabio, M.T. González, Carbon 33 (1995)15–23.

[24] M.M. Dubinin, E.D. Zaverina, L.V. Radushkevich, J. Phys. Chem. (URSS) 21 (1947)1351–1362.

[25] J.M. Rosas, J. Bedia, J. Rodríguez-Mirasol, T. Cordero, Fuel 88 (2009) 19–26.

[26] X. Wu, L.R. Radovic, Carbon 44 (2006) 141–151.

[27] P.J. Hall, J.M. Calo, Energ Fuel 3 (1989) 370–376.

[28] S. Labruquère, R. Pailler, R. Naslain, B. Desbat, J. Eur. Ceram. Soc. 18 (1998)1953–1960.

[29] J.M. Rosas, J. Bedia, J. Rodríguez-Mirasol, T. Cordero, Ind. Eng. Chem. Res. 47(2008) 1288–1296.

[30] J. Bedia, J.M. Rosas, D. Vera, J. Rodríguez-Mirasol, T. Cordero, Catal. Today 158(2010) 89–96.

[31] Y. Surchorski, Appl. Surf. Sci. 253 (2007) 5904.

[32] M.O. Guerrero-Pérez, M.J. Valero-Romero, S. Hernández, J.M. López, J.Rodríguez-Mirasol, T. Cordero, Catal. Today 195 (2012) 155–161.

[33] R. López-Medina, J.L.G. Fierro, M.O. Guerrero-Pérez, M.A. Bañares, Appl. Catal.A: Gen. 375 (2010) 55–62.

[34] R. López-Medina, H. Golinska, M. Ziolek, M.O. Guerrero-Pérez, M.A. Bañares,Catal. Today 158 (2010) 139–145.

[35] B. Abdelouahab, et al., J. Catal. 134 (1992) 151–167.

[36] D. Farrusseng, A. Julbe, M. Lopez, C. Guizard, Catal. Today 56 (2000) 211–220.

[37] M.O. Guerrero-Pérez, J.L.G. Fierro, M.A. Vicente, M.A. Bañares, J. Catal. 206(2002) 339–348.

[38] Z.-Y. Xue, G.L. Schrader, J. Phys. Chem. B 103 (1999) 9459–9467.

[39] M.O. Guerrero-Pérez, J.M. Rosas, R. López-Medina, M.A. Bañares, J. Rodríguez-Mirasol, T. Cordero, Catal. Commun. 12 (2011) 989–992.

[40] S.A.D. Íppolito, M.A. Bañares, J.L. Garcia Fierro, C.L. Pick, Catal. Lett. 122 (2008)252–258.

[41] O.V. Buyevskaya, A. Brückner, E.V. Kondratenko, D. Wolf, M. Baerns, Catal. Today67 (2001) 369–378.

[42] F. Cavani, N. Ballarini, A. Cericola, Catal. Today 127 (2007) 113–131.

[43] A.A. Lemonidou , L. Nalbandian, I.A. Vasalos, Catal. Today 61 (2000) 333–341.

[44] A. Brüker, E. Kondratenki, Catal. Today 113 (2006) 16.

[45] M.O. Guerrero-Pérez, M.A. Bañares, Chem. Commun. (2002) 1292–1293.

[46] V.V. Guliants, H.H. Brongersma, A. Knoester, A.M. Gaffney, S. Han, Top. Catal. 38(2006) 41–50.

[47] J.M. Tatibouët, H. Lauron Pernot, J. Mol. Catal. A 171 (2001) 205–216.

[48] L.E. Briand, W.E. Farneth, I.E. Wachs, Catal. Today 96 (2004) 211.

[49] X. Wang, I.E. Wachs, Catal. Today 96 (2004) 211.

[50] M.O. Guerrero-Pérez, T. Kim, M.A. Bañares, I.E. Wachs, J. Phys. Chem. C 112(2008) 16858–16863.

[51] I.E. Wachs, J.M. Jehng, W. Ueda, J. Phys. Chem. B 109 (2005) 2275–2284.

[52] S.K. Korhonen, M.A. Bañares, J.L.G. Fierro, A.O.I. Krause, Catal. Today 126 (2007)235–247.

[53] I.E. Wachs, Y. Chen, J.M. Jehng, L.E. Briand, T. Tanaka, Catal. Today 78 (2003)13–24.

[54] H. Liu, E. Iglesia, J. Phys. Chem. B 109 (2005) 2155–2163.

[55] A.S. Elmi, T. Enrico, C. Cinzia, J.P. Gomez Martin, P. Forzatti, Ind. Eng. Chem. Res.28 (1989) 387.

[56] K.V.R. Chary, G. Kishan, C.P. Kumar, U.V. Sagar, J.W. Niemantsverdriet, Appl.Catal. A: Gen. 245 (2003) 303.

[57] M. Badlani, I.E. Wachs, Catal. Lett. 75 (2001) 137.

[58] J.M. Tatibouët, Appl. Catal. A 148 (1997) 213–252.

[59] S.A.R.K. Deshmukh, M. van Sint Annaland, J.A.M. Kuipers, Appl. Catal. A 289(2005) 240–255.

[60] Heqin Guo, Debao Li, Dong Jiang, Haicheng Xiao, Wenhuai Li, Sun. Yuhan, Catal.Today 158 (2010) 439–445.

General conclusions and future work

The chemical activation of lignocellulosic materials with phosphoric acid produces activated carbons with a relatively high concentration of phosphorus on the carbon surface, mostly in form of C-O-PO_3 and C-PO_3 groups. These phosphorus groups remain very stable at relatively high temperatures and provide the carbon a relatively high oxidation resistance and surface acid and redox sites, which open new possibilities for the use of carbon-based materials as catalysts and/or catalyst supports for reactions that take place under oxidizing conditions and at high temperatures. In this sense, it has been showed that the presence of oxygen in the reaction gas plays a key role on the catalytic decomposition of methanol and ethanol. Under oxidant conditions the P groups are continuously reoxidized and they ease an oxygen spillover on the catalyst surface, where the availability of labile oxygen inhibit catalyst deactivation and allow methanol and ethanol steady state conversions to be reached.When vanadium is incorporate to these carbon materials, a VPO (Vanadium and Phosphorous mixed oxides) catalyst is obtained. These VPO materials are commercially used as catalysts for the transformation of n-butane into maleic anhydride and we have shown that they can be used for alkane partial oxidation reactions. These activated carbons can be also prepared with controlled morphology, by this manner VPO supported catalysts with spherical morphology and high surface areas have been described. By calcinations of those carbon supported materials, it is possible to obtain bulk oxide VPO materials with high surface areas.

But there is still more work to finish and to do.

- ✓ Taking into account the importance of deactivation in the economic viability of a process, we have been studying recently the deactivation of ethanol over phosphoric acid activated carbons. Thus, the kinetic modelling of ethanol and methanol decomposition by considering catalyst deactivation, as well as, some others aspects concerning process conditions of great significance in the kinetic modeling have to be studied, as the inhibiting effect of water.

- ✓ It has been shown the feasibility of phosphoric acid activated carbons with high oxidation resistance as supports for vanadium species. Thus, these catalytic supports may be also used for different metal oxides catalysts for reactions that take place at relatively high temperatures under oxidizing conditions.
- ✓ It has been described a simple and low cost method for preparing VPO catalysts with spherical morphology and high surface areas. This technology could be applied to other oxide bulk materials. In fact, we have been preparing Sb-V-O catalysts with hollow spherical morphology and high surface area. These materials are promising catalysts for the amoxidation of propane to acrilonitrile. Although these bulk oxide catalysts are still to be tested.
- ✓ In addition, we are currently developing new strategies for the preparation of VPO mixed oxides with controlled porosity by using activated carbons with different surface areas and pore volumes. Moreover, different morphologies, not only mixed oxides supported catalysts with spherical morphology, but also fibers are being studied.
- ✓ Hollow mixed oxide spheres have been tested as catalysts in the present thesis. However, these types of materials have been demonstrated to be attractive for drug delivery, adsorption, gas sensors, lithium ion batteries due to the unique hollow structure that may boost mass transport by offering short diffusion distances, and many others. Therefore, others possible applications are very interesting to be investigatedd.

Resumen

Los materiales de carbón han atraído mucha atención en las últimas décadas debido a sus múltiples aplicaciones en distintos campos de investigación, tales como la catálisis, adsorción en fase líquida y gas y en el almacenamiento de energía. Además, su preparación a partir de residuos biomásicos supone un beneficio no sólo económico, sino también medioambiental, que puede resultar clave en el contexto energético e industrial actual. Sin embargo, el uso de materiales de carbono en catálisis no está muy extendido debido a que este tipo de materiales se gasifican a CO_2 (o CO) en presencia de una atmosfera oxidante y a temperaturas relativamente bajas. Sin embargo, en trabajos anteriores el grupo de investigación ha mostrado que es posible preparar carbones activos con un contenido relativamente elevado de fosforo sobre la superficie de estos materiales mediante activación química de residuos lignocelulósicos con ácido fosfórico. A pesar del proceso de lavado, una cantidad significativa de fósforo, permanece unida de forma estable a la superficie de los carbones obtenidos proporcionando una elevada concentración de grupos superficiales ácidos y una alta resistencia a la oxidación, lo que les confiere una particular química superficial. Este hecho, unido al notable desarrollo de la estructura porosa, con una contribución significativa de la microporosidad ancha y de la mesoporosidad, hace que estos carbones activos sean adecuados para ser empleados no solo como catalizadores, sino también como soportes catalíticos en ciertas aplicaciones. Así, en esta tesis además de abordar el papel del fosforo en la resistencia a la oxidación de este tipo de carbones, se van a estudiar dos tipos de reacciones en fase gas: (i) la descomposición de etanol y metanol sobre este tipo de carbones activos ácidos y (ii) la oxidación selectiva de hidrocarburos ligeros sobre catalizadores de vanadio soportados en los carbones activos obtenidos. Además se propone un método sencillo y de bajo coste para la preparación de óxidos mixtos de vanadio y fosforo (VPO) con un área superficial elevada. Se persigue, por tanto, la valorización de estos residuos biomásicos mediante su transformación en productos de alto valor añadido para su utilización en procesos de interés tecnológico.

La memoria de la tesis se ha estructurado en siete capítulos. El primer capítulo, de introducción y el presente resumen están escritos en español. El resto de la tesis está escrita en inglés.

En el capítulo de introducción se estudian aspectos generales sobre el carbón activo, centrándose fundamentalmente en seis aspectos: i) el proceso de activación con ácido fosfórico, ii) el papel que actualmente juega el carbón activo en los procesos de catálisis heterogénea, iii) el problema de la baja resistencia a la oxidación de los carbones y el dopado con compuestos de fósforo, iv) se analizan las reacciones catalíticas de descomposición de alcoholes, centrándose en la descomposición de bioetanol y biometanol, iv) la importancia de las reacciones de oxidación química selectiva en lograr un futuro energético sostenible, v) los catalizadores mixtos de vanadio y fosforo (VPO) y por último, vi) la utilización de los carbones como moldes de sacrificio para la preparación de óxidos con morfología controlada mediante la técnica de nanomoldeo.

En los Capítulos 2 y 3 se estudian aspectos generales sobre los carbones activos preparados mediante activación química con ácido fosfórico, centrándose fundamentalmente en la evolución de la química superficial de estos materiales en atmósfera oxidante y en atmósfera inerte a elevadas temperaturas. Además, se ha abordado el papel del fósforo en la mejora de la resistencia a la oxidación de los carbones activos.

En los dos capítulos posteriores (Capítulos 4 y 5) se analizan las reacciones catalíticas de descomposición de metanol y etanol sobre un carbón activo obtenido mediante activación química con ácido fosfórico de hueso de aceituna. Se ha estudiado la influencia de la presencia de vapor de agua y de oxígeno sobre estas reacciones, prestando una especial atención a la desactivación del catalizador, principal problema de los sistemas catalíticos usados en este tipo de reacciones. La descomposición del etanol generó, además de los productos de deshidratación, una pequeña cantidad de producto de deshidrogenación. Además, se han llevado a cabo estudios cinéticos para conocer los mecanismos de reacción y obtener los parámetros cinéticos necesarios para el cálculo y dimensionamiento de futuros reactores catalíticos.

Para finalizar, en los Capítulos 6 y 7 se han estudiado la preparación de catalizadores de óxidos de vanadio soportados sobre carbones activos preparados mediante activación química de hueso de aceituna con ácido fosfórico. Los catalizadores obtenidos se caracterizaron mediante diversas técnicas experimentales y se

usaron para la reacción de oxidación parcial de propileno y la reacción de deshidrogenación oxidativa de propano.

Estos capítulos están organizados de forma que comienzan con un resumen del estudio realizado y un apartado de introducción sobre el tema en cuestión. Posteriormente, se incluye el procedimiento experimental y se exponen y discuten los resultados. Cada capítulo finaliza con las conclusiones más relevantes en cada caso.

Por último, la memoria finaliza con las conclusiones generales del trabajo realizado y se plantean trabajos futuros o ya comenzados y que no se han incluido en la presente memoria, pero que son el resultado de los trabajos realizados durante la tesis doctoral.

En el presente resumen, se describe la metodología experimental general aplicable a toda la tesis y los resultados más relevantes de cada capítulo.

1. Metodología experimental

Como acabamos de mencionar, éste apartado desarrolla una metodología experimental general aplicable a toda la tesis. En concreto, se analiza los procesos de preparación de los carbones, su caracterización y la instalación empleada en los ensayos catalíticos.

1.1. Preparación de los catalizadores

Los carbones activos (con o sin fósforo) se prepararon mediante activación química con ácido fosfórico o mediante activación física. Para la preparación de los carbones activos se utilizaron como precursores hueso de aceituna y celulosa

En el proceso de activación física el hueso de aceituna se carboniza a 800 ºC obteniéndose de esta forma un material carbonoso altamente ordenado. Posteriormente se realiza una gasificación parcial con CO_2 (99.998%, Air Liquide) de los carbonizados a la misma temperatura hasta alcanzar un burn-off entre 50-60 %, obteniéndose así carbones activados por activación física.

Durante el proceso de activación química, la primera etapa consiste en la impregnación del agente activante, H_3PO_4 (Sigma-Aldrich, disolución al 85%), con la materia prima carbonosa, en las proporciones adecuadas para satisfacer la relación de impregnación. La impregnación del hueso de aceituna se realiza mezclando el precursor con el H_3PO_4 en un vaso de precipitado, y homogeneizándolo durante una hora a temperatura ambiente. En el caso de la impregnación de la celulosa, el impregnado se sometió a un proceso posterior de carbonización hidrotermal en un autoclave a 200 ºC durante 16 horas. La activación se lleva a cabo en un horno con una corriente de N_2 de 150 cm^3 STP/min. Se eleva la temperatura a una velocidad de calentamiento de 10 ºC/min, manteniendo el caudal de N_2, hasta alcanzar la temperatura de activación deseada. La temperatura de activación se mantiene durante dos horas.

Tras el proceso de activación es necesario extraer el agente activante que se encuentra ocluyendo los poros y de esta forma liberar la estructura porosa del carbón. El lavado se realiza con agua destilada a 60 ºC en un sistema de filtración a vacío, empleando un embudo Büchner, hasta que se obtiene un agua de lavado con pH constante.

Una vez filtradas las muestras, el sólido resultante, se seca en estufa durante 24 horas a 80 ºC, obteniéndose el carbón seco que posteriormente se tamiza a un tamaño de partícula entre 100 y 300 μm.

Los carbones obtenidos se emplearán directamente como catalizadores o bien como soportes para depositar sobre ellos una fase activa, que el caso concreto de este estudio serán Vanadio y Zirconio.

En el caso de utilizarlos como soportes catalíticos, el carbón activo preparado se impregnó con una disolución 0.5M de ácido oxálico (99%, Sigma Aldrich) con distintas proporciones de NH_4VO_3 (99.99%, Sigma Aldrich) y/o $Zr(OCH_2CH_2CH_2)_4$ (70wt% in 1-propanol, Sigma Aldrich). El exceso de agua se retiró en un sistema rotavapor a 80 ºC y a una presión de 0.07-0.08 MPa. Una vez finalizado este proceso, se deja secar la muestra durante 24 horas a 120 ºC en la estufa de vacío para de esta forma eliminar el agua y el ácido oxálico. En la siguiente etapa se procede a la calcinación de las muestras para conseguir la fijación de la fase activa a la superficie del catalizador. Para esto se introduce la muestra en el interior del horno y se calienta hasta 250 ºC a una velocidad

de calentamiento de 10 ºC/min en un flujo de 150 cm^3 STP/min de aire, manteniendo la muestra a esta temperatura durante dos horas.

Se han preparado catalizadores con diferentes proporciones de V, con y sin Zr. En el caso de obtener catalizadores másicos de óxidos con morfología y porosidad controladas, los catalizadores fueron sometidos a un proceso de calcinación en atmosfera de aire con la finalidad de eliminar el soporte carbonoso utilizado como molde, mediante gasificación.

1.2. Caracterización de los catalizadores

Concluida la etapa de preparación de los catalizadores se procede a la caracterización de los mismos. Se caracterizó la estructura porosa y la morfología y química superficial. Para el estudio de la estructura porosa, se obtuvieron las isotermas de adsorción-desorción de N_2 y de adsorción de CO_2, mientras que para el estudio de la química superficial se realizaron análisis de XPS, XRD, FTIR, RAMAN y DTP. La acidez superficial se determinó mediante ensayos de adsorción-desorción-DTP de diferentes moléculas sonda, como amoniaco, piridina y 2,6-dimetilpiridina. En algunos casos se analizó la morfología superficial mediante las técnicas de microscopia SEM y TEM.

1.2.1. Análisis elemental y cenizas

El análisis elemental proporciona el contenido total de carbono, hidrógeno, nitrógeno, azufre y oxígeno (por diferencia del total de muestra seca, descontadas las cenizas), de una muestra. Los análisis elementales se realizaron en un equipo LECO® CHNS-932, en el cual se introduce la muestra seca, previamente pesada y empaquetada en un contenedor de estaño/aluminio, a una temperatura de aproximadamente 1000 ºC en atmósfera de oxígeno puro se produce la combustión y las cantidades de CO_2, SO_2 y H_2O se cuantifican mediante sensores de infrarrojos y el N_2 mediante un catarómetro.

Para el cálculo de las cenizas se empleó un horno tipo mufla, para ello un crisol con aproximadamente 1 g de muestra se introduce en la mufla, aumentando la temperatura hasta 650 ºC, manteniéndose a esta temperatura hasta pesada constante, tal y como establece la norma ASTM 2866-83.1

1.2.2. Estructura porosa

La superficie específica, el volumen de poro y la distribución de tamaño de poro, son propiedades de gran importancia en relación con la capacidad de adsorción de los carbones activos y con la actividad de los catalizadores.

La estructura porosa de las muestras se caracterizó mediante adsorción-desorción de N_2 a -196 ºC y adsorción de CO_2 a 0 ºC en un equipo ASAP 2020 de Micromeritics®. Las muestras fueron previamente degasificadas durante al menos 8 horas a una temperatura de 150 ºC.

A partir de las isotermas de adsorción-desorción de N_2, se ha calculado el área aparente (A_{BET}) mediante la aplicación de la ecuación BET, el volumen de microporo (V_t) y el área externa (A_t) se determinaron empleando el método t y el volumen de mesoporo (V_{mes}) se calculó como la diferencia entre el volumen de nitrógeno adsorbido a la presión relativa de 0.95 y el volumen de microporo (V_t). Por otro lado, el área de microporo estrecho (A_{DR}) y el volumen de microporo estrecho (V_{DR}) se obtuvieron mediante la aplicación del método de Dubinin-Raduskevich aplicado a las isotermas de adsorción de CO_2.

1.2.3. Química superficial

1.2.3.1. Espectroscopia fotoelectrónica de rayos-X (XPS).

Los análisis de XPS se llevaron a cabo usando un espectrofotómetro modelo 5700C de la casa Physical Electronics® con radiación MgKα de 1253.6 eV. Para el análisis de los espectros de alta resolución del XPS, la posición del pico del C1s fue establecida en 284.4 eV y usada como referencia para posicionar los demás picos del espectro. Los espectros de alta resolución se deconvolucionaron usando curvas Gaussiana-Lorentziana.

Una vez obtenido el espectro de baja resolución e identificados los elementos que corresponden a cada uno de los picos, se obtienen los espectros de alta resolución o picos de cada elemento, gracias a los cuales pueden visualizarse con claridad los estados de oxidación de los distintos elementos de la muestra, así como el tipo de enlace que forma con otros elementos presentes en la superficie.

1.2.3.2. Espectroscopia infrarroja

Los espectros FTIR se realizaron en un espectrómetro infrarrojo modelo Nicolet 205xB, realizando 256 barridos en el rango de número de onda de 3900-300 cm^{-1} y a una resolución de 1 cm^{-1}. Las muestras se mezclaron en una proporción de alrededor de 1:50 con KBr para obtener la pastilla.

1.2.3.3. Espectroscopia vibracional raman

El equipo utilizado es un Microraman Senterra de la marca Bruker que consta de tres líneas de láser Neodimio-YAG de 532, 633 y 785 nm de longitud de onda. El equipo también consta de un detector DCC (Charge Couple Device) enfriado termoeléctricamente.

Se ha realizado medidas de espectroscopia Raman de las muestras soportadas con vanadio. Los análisis se han realizado a temperatura ambiente y tras aumentar la temperatura a 100 y 200 ºC. Se obtuvo el espectro Raman en varios puntos para, así, tomar una media representativa de la muestra. Las condiciones de medida son: laser de 532 nm, potencia de 2 mW y tiempo de integración de 10 s.

1.2.3.4. Difracción de rayos-X (XRD)

Los datos de difracción de rayos-X se adquirieron usando un difractómetro Philips X´Pert PRO MPD. El sistema óptico de este equipo consta de un monocromador primario del tipo Johansson con un cristal de Ge (111), que proporciona una radiación estrictamente monocromática CuKα (λ = 1.5406 Å). Las rendijas de divergencia y antidivergencia se fijaron a ½º y se utilizaron rendijas Soller (haz incidente y difractado) de 0.04 rad. El sistema de detección consiste en un X´Celerator RTMS (Real Time Multiple Strip) constituido por 128 detectores de Si colocados en línea, con la longitud activa al máximo.

Las medidas se realizaron desde 2θ = 5º a 80º durante 37 min, con un tamaño de paso de 0.017º. La radiación incidente fue de 45 kV y 40 mA. Las medidas se realizaron en un portamuestras giratorio de zero-background.

1.2.3.5. Desorción térmica programada (DTP).

Los experimentos de DTP se realizaron empleando un reactor de cuarzo tubular situado en el interior de un horno eléctrico. Las muestras (aproximadamente 0.1 g) se introdujeron en el interior del reactor y se calentaron desde temperatura ambiente hasta 900 ºC a una velocidad de calentamiento de 10 ºC/min en un flujo de helio (200 cm^3 STP/min). Las cantidades de CO y CO_2 desorbidas se monitorizaron con analizadores de gases mediante infrarrojos no dispersivos (NDIR, Siemens® ULTRAMAT 22) y las cantidades desorbidas de otros gases con un espectrómetro de masas de Pfeiffer Vacuum® modelo ThermoStar MSC-200.

1.2.3.6. Acidez superficial.

El conocimiento de la acidez del catalizador es fundamental para establecer su ámbito de aplicación más adecuado. No solo es importante conocer la cantidad de sitios ácidos y la fuerza relativa de los mismos, sino también establecer si son sitios ácidos de Brönsted, aquellos capaces de ceder protones, o sitios ácidos de Lewis, capaces de aceptar un par de electrones.

La técnica de DTP es una de las técnicas más flexibles y ampliamente utilizadas para la caracterización de los sitios ácidos de catalizadores sólidos. En esta técnica la muestra se satura con una molécula sonda a una temperatura adecuada, posteriormente se realiza una desorción a la temperatura de adsorción para eliminar las moléculas débilmente adsorbidas o fisisorbidas. Finalmente se realiza una DTP para eliminar las moléculas más fuertemente adsorbidas o quimisorbidas. Las cantidades globales desorbidas, en la DTP, permiten cuantificar la acidez de la muestra, mientras que las temperaturas a las cuales se produce la desorción establecen la fuerza de los sitios ácidos, ya que las moléculas adsorbidas sobre sitios ácidos débiles desorben a menores temperaturas que si están adsorbidas sobre sitios ácidos fuertes.

Entre las moléculas sonda más empleadas se encuentra el amoniaco. El amoniaco es una molécula muy pequeña, lo que hace que, en ocasiones, pueda sobreestimar la cantidad de sitios ácidos disponibles para la reacción catalítica. Su pequeño tamaño le permite penetrar en el interior de los poros más pequeños, mientras que las moléculas más grandes habitualmente empleadas en catálisis solo tienen acceso a los microporos más anchos y mesoporos. La acidez total y la distribución de la fuerza

de acidez de los carbones y/o catalizadores se han determinado mediante desorción térmica programada de amoniaco. La DTP-NH_3 se ha realizado con 80 mg de muestra que se saturan con 20 % vol. de NH_3 a 100 ºC. Después de la saturación, el NH_3 débilmente adsorbido se desorbe en un flujo de helio (100 cm^3 STP/min) a la temperatura de adsorción, hasta que no se detecta NH_3 en los gases de salida. La DTP se realiza aumentando la temperatura hasta 500 ºC a una velocidad de calentamiento de 10 ºC/min. El NH_3 desorbido se mide mediante un espectrómetro de masas (Pfeiffer Vacuum® modelo ThermoStar MSC-200).

Además, se han utilizado otras moléculas de mayor tamaño como pueden ser la piridina (Py) y la 2,6-dimetilpiridina (DMPy). La piridina se adsorbe sobre los dos tipos de centros ácidos, Brönsted y Lewis, mientras que la 2,6-dimetilpiridina se adsorbe únicamente sobre los centros ácidos de Brönsted, por lo que el empleo de estas dos moléculas permite no solo cuantificar la cantidad de sitios ácidos, sino también la proporción de sitios ácidos Brönsted-Lewis, lo cual es de suma importancia para establecer las posibles aplicaciones del catalizador. Para diferenciar entre sitios ácidos del tipo Brönsted o Lewis se realizaron ensayos de adsorción-desorción de piridina y 2,6-dimetilpiridina en un sistema termogravimétrico (CI Electronics).

1.2.4. Morfología superficial y estructura.

La morfología superficial se examinó mediante microscopia electrónica de barrido, SEM ("Scanning Electron Microscopy"). El microscopio electrónico empleado es un modelo JSM 840 de la casa comercial JEOL® trabajando a un elevado voltaje de entre 20 y 25 kV.

Para analizar la estructura de algunas de las muestra se utilizó microscopía de transmisión electrónica, TEM ("Transmission Electron Microscopy"). El TEM empleado es el modelo CM200 de la casa comercial Philips®.

Ahora se describen las instalaciones utilizadas para los procesos de carbonización, activación, gasificación, descomposición de alcoholes y oxidación de alcanos/alquenos.

1.3. Instalaciones utilizadas

1.3.1. Carbonización/activación química/Gasificación

Para la realización de los experimentos de carbonización se ha empleado una instalación como la que se muestra en la Figura 1 y consta de los siguientes elementos:

- Botella de gases (N_2 y/o CO_2)
- Medidor de flujo másico. Es un elemento transductor de señal (caudal-señal eléctrica). Se ubica a la salida de la botella de nitrógeno. El medidor usado es de la marca BROOKS, modelo 5850 TR.
- Controlador de flujo másico. Este dispositivo junto con los medidores de flujo másico permite fijar el caudal de gas usado en los experimentos. El controlador usado es de la marca GOOSEN, modelo 5878.
- Horno. El horno utilizado es de tipo tubular horizontal. Permite obtener temperaturas de hasta 1000 ºC a las que se llega con un calentamiento de 10 ºC/min. El horno utilizado es de la casa CARBOLITE FURNACES, modelo CFT 12/75, de 75 mm. de diámetro y 750 mm, de longitud de zona calefactada.

En la carbonización y activación química las muestras se introducen en el horno y se deja pasar una corriente de 150 cm^3 (STP)/min de nitrógeno (N50) durante 30 minutos para purgar el horno y mantener una atmósfera inerte durante la carbonización y así evitar que se queme la muestra. La velocidad de calentamiento es de 10 ºC/min desde temperatura ambiente hasta la temperatura deseada. La temperatura final se mantiene durante 2 horas y después se deja enfriar manteniendo la corriente de 150 cm^3 (STP)/min de nitrógeno, con objeto de preservar la muestra de la oxidación.

Para llevar a cabo el proceso de gasificación se utiliza la misma instalación que aparece en la Figura 1 con la salvedad, de que hay que añadir una botella de dióxido de carbono, que es el agente activante utilizado en este caso. El proceso es similar al de la carbonización, con la salvedad de que cuando se alcance la temperatura de gasificación deseada se cambia el flujo de nitrógeno por el de CO_2 manteniéndose el reactor a temperatura constante durante el periodo de activación preestablecido, para, una vez concluido éste, dejar enfriar hasta temperatura ambiente en un flujo de N_2, evitando así que continue el quemado de la muestra.

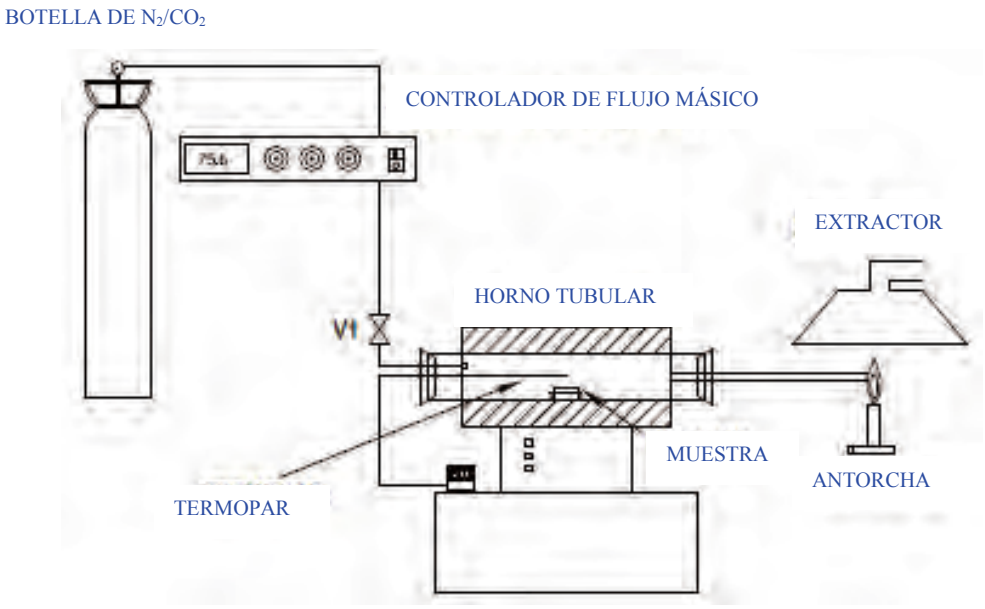

Figura 1. Instalación para la carbonización, activación y gasificación.

1.3.2. Reacción de descomposición de alcoholes/oxidación selectiva

Para la realización de los experimentos de descomposición de metanol se ha empleado una instalación como la que se esquematiza en la Figura 2 y que consta de los siguientes elementos:

- Botellas de gases.
- Medidores de flujo másico. Elementos transductores de señal (caudal-señal eléctrica). Se ubican a la salida de las botellas de gases. El medidor usado es de la marca Brooks, modelo 5850 TR.
- Controlador de flujo másico. Este dispositivo junto con los medidores de flujo másico permite fijar el caudal de gas usado en los experimentos. El controlador usado es de la marca Goosen, modelo 5878.
- Reactor, tubo de cuarzo de 4 mm de diámetro interior y una longitud de unos 40 cm, en el interior del cual de deposita el catalizador y en el que se realiza la reacción.
- Cable térmico, mediante el cual se calefactan las conducciones de entrada y salida del reactor para evitar que se produzca condensación de reactivos o productos en las paredes de estas conducciones.

- Horno, para elevar la temperatura en el interior de reactor.
- Termopar, para poder medir y controlar la temperatura en el interior del reactor.
- Controlador del horno, compara la temperatura del termopar con la temperatura programada y actúa en consecuencia.
- Jeringas de inyección (Cole-Parmer® 74900-00,-05 Syringe Pump), para introducir el Metanol/Etanol/Agua en el sistema.
- Rotámetro, situado a la salida del reactor, para comprobar y controlar la pérdida de carga en el reactor.
- Analizadores de gases, para poder seguir la evolución de los reactivos y de los productos de reacción. Se emplearon un espectrómetro de masas y un cromatógrafo de gases. El espectrómetro de masas es de la casa Pfeiffer Vacuum® modelo OmniStar. El cromatógrafo de gases es de la marca Agilent modelo 490 micro-GC, y está equipado con las columnas PPQ, 5A molsieve y Wax. El método de análisis online diseñado permite la toma de datos cada 3 minutos.

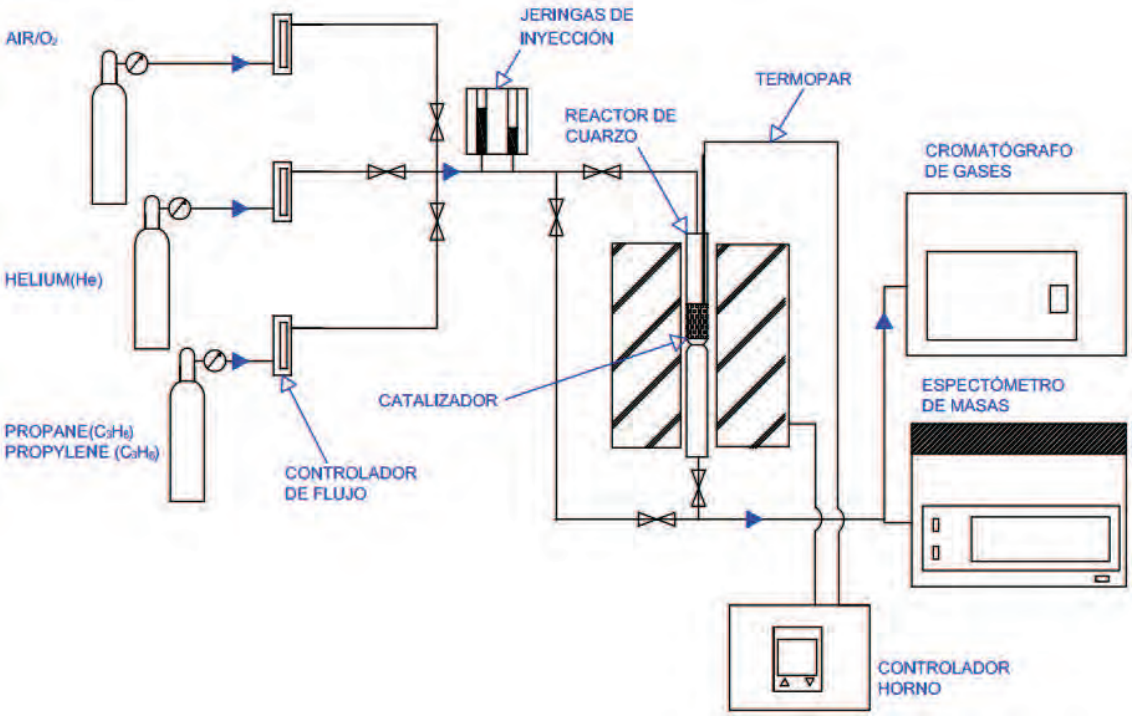

Figura 2. Esquema de la instalación utilizada para la descomposición de alcoholes y oxidación selectiva de propano y propileno.

2. Resultados

En este apartado se exponen los resultados más relevantes derivados de cada capítulo.

En trabajos anteriores se ha observado que los carbones activados preparados mediante activación química de residuos lignocelulósicos con ácido fosfórico presentan, además de una elevada superficie específica, una química superficial muy particular debido a la presencia de grupos funcionales superficiales de fósforo, en forma de C-O-PO_3, C-P-.O_3 y C_3P, que muestran una alta estabilidad química y térmica. Estos grupos confieren a los carbones elevada resistencia a la oxidación y gran acidez superficial, convirtiéndolos en materiales muy interesantes para aplicaciones catalíticas.

En el Capítulo 2 se ha realizado un estudio sobre el papel de los grupos superficiales de fósforo en las reacciones de oxidación y reducción de la superficie de este tipo de carbones activos. Para ello el carbón activo se ha expuesto a una atmósfera oxidante (aire) y a distintas temperaturas de reacción (20-350 ºC) durante 2 h. Antes y/o después de las oxidaciones se realizaron ensayos de DTP de CO y CO_2, de adsorción/desorción de NH_3 y análisis de XPS. Los resultados de DTP y XPS mostraron que los grupos superficiales de fósforo reaccionan preferentemente con el oxígeno, antes de la gasificación del carbón, a través de la oxidación de enlaces de tipo C-P a C-O-P. Éste tipo de grupos, C-O-PO_3, presentan una elevada estabilidad térmica ya que descomponen a CO (y CO_2) a elevadas temperaturas (T > 700 ºC) dando lugar a grupos superficiales de fósforo más reducidos (probablemente C-P-O_3). Hemos observado que los grupos de fósforo de tipo C-P-O_3 se re-oxidan en contacto con aire, incluso a temperatura ambiente, formando nuevamente enlaces de tipo C-O-P. Por lo tanto, la presencia de estos grupos superficiales de fósforo les confiere a los carbones funcionalidad de tipo redox, de elevada estabilidad térmica y química, la cual es responsable del elevado contenido en oxígeno y de la elevada resistencia a la oxidación de este tipo de carbones porosos.

En el Capítulo 3 se ha analizado la estabilidad térmica de los grupos de fósforo presentes en dos carbones preparados mediante activación química con ácido fosfórico a distintas temperatura de activación, 500 y 800 ºC. Se ha observado que la temperatura de activación influye en la estabilidad térmica de los grupos de fósforo de tipo C-O-P

presentes en la superficie del carbón y que descomponen a CO (y CO_2) a temperaturas superiores a 700 ºC. Aquellos grupos en los que el fósforo está unido al carbón mediante un oxígeno (puede incluir estructuras de polifosfatos) y poseen uno o dos grupos –OH, tales como C-O-PO_3, están presentes, principalmente, en carbones preparados a bajas temperaturas (500 ºC). Éstos carbones, además, mostraron una elevada cantidad de H_2 desorbido durante los experimentos de desorción térmica programada (DTP), lo que sugiere la presencia mayoritaria de éstos grupos.

Cuanto los carbones son tratados a temperaturas superiores a la de descomposición de los grupos C-O-PO_3, aumenta la concentración de grupos de fósforo más reducidos, tales como C_3-PO. Como se vió en el Capítulo 1, estos grupos se reoxidan fácilmente cuando los carbones se ponen en contacto con aire, generando así grupos C_2-PO(OC), C-PO$(OC)_2$ y C-O-PO$(OC)_2$. Éstos grupos se caracterizan porque el fósforo está unido al carbón a través de más de un enlace de oxígeno, y además descomponen a CO (y CO_2) a temperaturas superiores (860 ºC). Se ha observado que estos grupos de fosforo están presentes, mayoritariamente, en los carbones activos tratados térmicamente a 900 ºC y/o activados a elevadas temperaturas (800 ºC).

Se ha estudiado la eficacia de un carbón obtenido por activación química de hueso de aceituna con H_3PO_4 (relación de impregnación 2:1 y temperatura activación de 800 ºC) en las reacciones de descomposición (deshidratación y/o deshidrogenación) de metanol y etanol en fase gas, en un reactor continuo de lecho fijo de laboratorio. La formación de dimetil éter (DME), olefinas ligeras y formaldehído durante la reacción térmica programada de metanol (TPRS-MeOH) sobre el catalizador preparado y el análisis de adsorción de piridina, 2,6-dimetilpiridina y NH_3 confirmaron la presencia de sitios activos ácidos y centros redox en el carbón estudiado. Se ha analizado la conversión en estado estacionario en función de la temperatura, la presión parcial de los distintos alcoholes, la velocidad especial y la presencia (distintas presiones parciales) de otros compuestos como vapor de agua y oxígeno. Así mismo, se ha examinado el estado transitorio hasta alcanzar el estado estacionario y la posible desactivación de los catalizadores.

Los resultados mostrados en el Capítulo 4 indican que el carbón ácido preparado es activo para la conversión catalítica de metanol, obteniéndose una selectividad superior al 80 % hacia dimetil éter, a 350 ºC, y una conversión de metanol del 60 % en

las condiciones de operación analizadas. Por otro lado, los resultados obtenidos al utilizar distintas atmosferas de reacción (aire o helio) indican que el oxígeno juega un papel muy importante en la actividad de este tipo de catalizadores. En ausencia de oxígeno, se observa una progresiva desactivación debido a la deposición de coque en los centros ácidos de tipo Brönsted de mayor fortaleza y a la reducción de los grupos de fósforo del tipo C-O-PO_3 (a C-PO_3), los cuales mostraron tener acidez de tipo Lewis de menor fortaleza. Sin embargo, cuando la reacción se lleva a cabo en presencia de oxígeno no se observa desactivación del catalizador. A partir de los resultados de actividad y de la caracterización de los carbones usados en reacción tanto en atmósfera de aire como de helio, indican que la actividad del catalizador en presencia de oxígeno está relacionado con la presencia de los grupos superficiales de fósforo muy estables térmicamente. Estos complejos pueden producir la disociación de oxígeno molecular, creando un posible spillover de oxígeno sobre la superficie del carbón, donde la disponibilidad de un oxígeno lábil podría detener la formación de especies carbonosas que ocasiona la pérdida de actividad del catalizador en atmósfera inerte e incluso regenerar los centros de fósforo, de C-P-O_3 a C-O-P_3, como se describió en el Capítulo 1.

En el caso de la descomposición catalítica de etanol sobre el catalizador ácido preparado (Capítulo 5), genera principalmente productos de deshidratación, mayoritariamente etileno (selectividad >91% a 325 ºC), aunque a conversiones bajas se puede obtener una alta selectividad a dietil éter y a acetaldehido como producto de deshidrogenación. En este caso, en ausencia de oxígeno el catalizador sufre una progresiva desactivación, más o menos rápida en función de la condiciones de análisis. Al emplear aire como gas de reacción se produce un aumento significativo de la actividad y no se aprecia desactivación del catalizador.

Se han analizado las cinéticas de los resultados experimentales obtenidos en la descomposición de los alcoholes y se han planteado modelos mecanísticos basados, inicialmente, en los ya propuestos en la bibliografía y se han formulado nuevos modelos, se ha estudiado la validez de éstos en base a la bondad de los ajustes y, finalmente, se obtuvieron las constantes cinéticas y termodinámicas para cada uno de los procesos ensayados. Para la descomposición de metanol se ha supuesto un modelo cinético que considera que la reacción superficial se produce entre una molécula de metanol adsorbida y otra molécula de metanol en fase gas, SN_2, obteniéndose una

energía de activación próxima a los 85 kJ/mol. En el caso del etanol, los resultados experimentales se han ajustado a un modelo cinético que incluye una reacción de eliminación tipo E2, en un único paso, para la formulación de etileno y acetaldehio, y una reacción de sustitución tipo SN_2 para la formación de dietil éter. La energía de activación de la formación del etileno, producto mayoritario, es de alrededor de 165 kJ/mol.

Los óxidos mixtos son materiales que se utilizan en muchas aplicaciones, tales como catalizadores en reacciones de oxidación parcial, sensores de gases, electrocatalizadores para pilas de combustible, etc. Los óxidos de vanadio y fósforo (VPO) se enmarcan en este grupo de materiales, y son interesantes puesto que son catalizadores capaces de activar hidrocarburos saturados, por ejemplo, se usan industrialmente en la transformación de n-butano en anhídrido maleico.

En el Capítulo 6 se ha preparado un carbón activado de hueso de aceituna con ácido fosfórico y se ha usado como soporte de especies de óxido de vanadio y zirconio. De esta manera se ha identificado la presencia de fases VPO soportado en el carbón activo y se ha estudiado su uso en la reacción de oxidación parcial de propileno. La incorporación de vanadio y zirconio al soporte de carbón activo disminuye la temperatura de oxidación de éste, pero, en cualquier caso, los catalizadores son estables en las condiciones de operación estudiadas. Se ha comprobado que variando el recubrimiento podría modularse el estado de oxidación de las fases activas de vanadio, y, por tanto, su actividad. El catalizador obtenido es activo y selectivo en la oxidación parcial de propileno a productos oxigenados. Además, se ha observado como la incorporación de zirconio como dopante en este sistema mejora la actividad redox de estos catalizadores.

Por último, en el Capítulo 7 se ha descrito un material de carbón usando celulosa como material de partida mediante tratamiento hidrotermal con ácido fosfórico y posterior carbonización. Los análisis SEM de este carbón mostraron que está formado por esferas de hasta 2 μm de diámetro. Este material carbonoso fue impregnado con precursor de vanadio, obteniéndose así un material VPO soportado sobre carbón con morfología esférica. Además, se obtuvieron catalizadores másicos de VPO con morfología esférica y estructuras huecas tras una etapa de calcinación a 450 ºC. Una de las principales características de estos sistemas catalíticos es la elevada área superficial,

tanto de los óxidos soportados como másicos lo que los hace muy interesantes para aplicaciones catalíticas. A partir de los análisis de Raman y de XRD se identificó principalmente la presencia de la fase pirofosfato de vanadilo ($(VO)_2P_2O_7$) y el óxido V_2O_5. La presencia de la fase de pirofosfato de vanadio hace que estos materiales sean prometedores catalizadores, puesto que dicha fase ha sido descrita como la fase activa en catalizadores comerciales VPO para distintas reacciones de oxidación parcial de hidrocarburos. Además, la presencia del óxido V_2O_5, en el cual el vanadio se encuentra como V^{5+}, es posiblemente beneficiosa para la actividad catalítica; puesto que la actividad de estos catalizadores redox está relacionada con la presencia de fases en las cuales el vanadio se encuentre con estados de oxidación IV y V. Los datos de actividad fueron interesantes, especialmente en este caso de la reacción de deshidrogenación oxidativa de propano, que resultaron muy próximos a los valores más altos reportados para esta reacción, lo cual hace a estos catalizadores prometedores para su uso en reacciones de oxidación parcial de hidrocarburos, a la vez que abre una nueva posibilidad a los carbones activos para ser usados como soportes catalíticos en presencia de oxígeno a elevadas temperaturas.

Agradecimientos

Cuantas ganas tenía que llegase este momento, el momento de escribir los agradecimientos. Esto tiene muchos significados, el principal de todos es que he "terminado" la tesis doctoral y el trabajo realizado en los últimos cinco años. Un trabajo que no hubiera sido posible sin la colaboración y apoyo de muchas personas que me han acompañado en este tiempo. Escribo "terminado" entre comillas porque los que os dedicáis a ésta profesión sabéis que un trabajo de investigación nunca tiene un final. Al contrario, unos resultados te llevan a otros y todavía quedan muchas cosas por descubrir. Pero hasta aquí, he escrito un punto y seguido.

Personas a las que agradecer,

En primer lugar, a los directores de este trabajo de tesis doctoral, los Profesores José Rodríguez Mirasol y Tomás Cordero, por la confianza depositada en mí desde el primer día, su accesibilidad, disposición y consejo durante estos años.

A la Profesora Olga Guerrero, por haberme enseñado e introducido en el mundo de los óxidos mixtos. Gracias por tus consejos y colaboración.

To my supervisors at the Catalysis Engineering group, Prof. Freek Kapteijn and Prof. Jorge Gascon. You gave me a warm home during the two research stays I did in your group. Thank you for giving me the opportunity to continue learning and working with you.

A los doctores predecesores del grupo, Jorge Bedia, Nani Rosas y Ramiro Ruíz, con los que comencé esta aventura. ¡Pusisteis el listón muy alto!, espero haber aprendido y mantenido ese listón tan alto como lo dejasteis. Nani, regresaste en el mejor momento. Gracias por tus buenos consejos. Ramiro, siempre disponible.

Al doctor Raúl Berenguer, por los buenos momentos de discusión en el laboratorio.

A mis compañeros de tesis, comencé con Aurora, seguí con Fran y con Elisa y los últimos meses los terminé con Juanjo, José y Paul. Desde aquí os doy las gracias por los buenos momentos de laboratorio, por la ayuda prestada cuando la necesité y en definitiva por permitirme aprender con ustedes. Fran, te debo al menos 10 cafés.

A los proyectandos que han pasado por nuestro laboratorio durante el periodo de realización de esta tesis y cuyos trabajos he codirigido, Elisa, Antonio, Dani, Marta, Mar, Javi y mis amigos los portugueses Luis Ferro, Luis Beato, Pedro, Filipa y Marilucia. De todos ellos he aprendido algo y por este motivo una parte de esta tesis es suya.

A los técnicos del Servicio Central de Apoyo a la Investigación (SCAI) de la Universidad de Málaga, María Dolores (sólidos porosos), Valle (XPS), Laura (XRD) , Augusto (análisis elemental), Cristina (Raman). A Goyo (SEM) y Adolfo (TEM) por sacarme una sonrisa. Gracias a todos por la realización de los diferentes análisis y por vuestra disposición y amabilidad infinitas.

A mi familia, por su cariño, confianza y apoyo en todos los sentidos. Gracias a mis padres, Miguel y Josefina, por sus enseñanzas de perseverancia y dedicación que me han ayudado a afrontar la determinación de los problemas sin importar el tamaño. Habéis sido mi ejemplo a seguir.

A mi marido y mejor amigo, Juan Jesús, por su apoyo incondicional y su cariño durante estos años.

En el campo de los agradecimientos institucionales quiero agradecer al Ministerio de Economía y Competitividad la concesión de una beca de Formación de Personal de Investigación (BES-2010-032213), y la concesión de dos ayudas para la realización de dos estancias predoctorales en el departamento de Ingeniería Química de la Universidad de Delft.

Además quiero expresar mi gratitud a la Universidad de Málaga donde me he formado y en cuyas instalaciones he realizado la tesis doctoral. En especial, al Departamento de Ingeniería Química por haberme permitido realizar mis primeras tareas docentes.

M.J.V.R

Málaga, Enero 2015

Curriculum

Journals

This work is a compendium of the following publications:

M. J. Valero-Romero, J. Rodríguez-Mirasol, T. Cordero. "*Role of surface phosphorus complexes on the oxidation of porous carbons"*. Submitted.

M. J. Valero-Romero, E.M. Calvo-Muñoz, R. Ruiz-Rosas, J. Rodríguez-Mirasol, T. Cordero. "*Insights into the catalytic performance of a carbon-based acid catalyst in methanol dehydration: Reaction scheme and kinetic modeling"*. Submitted.

[1] M.O. Guerrero-Pérez**, M.J. Valero-Romero**, S. Hernández, J.M. López Nieto, J. Rodríguez-Mirasol, T. Cordero. "*Lignocellulosic-derived mesoporous materials: An answer to manufacturing non-expensive catalysts useful for the biorefinery processes"*. Catalysis Today, 2012 (195) 155-161.

[2] **M.J. Valero-Romero**, A. Cabrera-Molina, M.O. Guerrero-Pérez, J. Rodríguez-Mirasol, T. Cordero. "*Carbon materials as template for the preparation of mixed oxides with controlled morphology and porous structure"*. Catalysis Today. 2014 (227) 233-241.

Other publications by the author:

[3] Sartipi, S., Parashar, K., **Valero-Romero, M.J.**, Santos, V.P., Van Der Linden, B., Makkee, M., Kapteijn, F., Gascon, J. "*Hierarchical H-ZSM-5-supported cobalt for the direct synthesis of gasoline-range hydrocarbons from syngas: Advantages, limitations, and mechanistic insight"*. Journal of catalysis. 2013 (305) 179-190.

[4] **M.J. Valero-Romero**, E.M. Márquez-Franco, J. Bedia, J. Rodríguez-Mirasol, T. Cordero. "*Hierarchical porous carbons by liquid phase impregnation of zeolite*

templates with lignin solution". Microporous and Mesoporous Materials. 2014 (196) 68-78.

[5] R. Ruiz-Rosas, **M. J. Valero-Romero**, D. Salinas-Torres, J. Rodríguez-Mirasol, T. Cordero, E. Morallón and D. Cazorla-Amorós. "*Electrochemical Performance of Hierarchical Porous Carbon Materials Obtained from the Infiltration of Lignin into Zeolite Templates"*. ChemSusChem. 2014 (7) 1458-1567.

[6] M. Calzado, **M.J. Valero-Romero**, P. Garriga, A. Chica, M.O. Guerrero-Pérez, J. Rodríguez-Mirasol, T. Cordero. "*Lignocellulosic waste-derived basic solids and their catalytic applications for the transformation of biomass waste"*. Catalysis Today. 2014, Doi: 10.1016/j.cattod.2014.06.038.

[7] Juana María Rosas, Raúl Berenguer, **María José Valero-Romero**, José Rodríguez-Mirasol, Tomás Cordero. "*Preparation of different carbon materials by thermochemical conversion of Lignin".* Frontiers in Materials, section Carbon-Based Materials. 2014. ISSN: 2296-8016. Article type: Review Article.

This work has also generated the following congress and workshop contributions:

Oral presentations

[1] **M.J. Valero-Romero**, E.M. Calvo-Muñoz, R. Ruiz-Rosas, J. Rodríguez-Mirasol, T. Cordero. "*Methanol dehydration on carbon-based acid catalysts and their chemical surface"*. The Annual World Conference on Carbon. Krakow, Poland, Junio 2012.

[2] **M.J. Valero-Romero**, M.O. Guerrero-Pérez, J. Rodríguez-Mirasol, T. Cordero. "*Carbon materials as template for the preparation of mixed oxides with controlled morphology"*. 5Th Czech-Italian-Spanish Conference on Molecular Sieves and Catalysis (CIS-5). ISBN-10: 84-616-4731-9, ISBN-13: 978-84-616-4731-9. Segovia, España, Junio 2013.

[3] **M.J. Valero-Romero**, J. Rodríguez-Mirasol, T. Cordero. "*Acid activated carbons with a versatile chemical surface"*. XXXIV Reunión Bienal de la Real Sociedad Española de Química. ISBN: 978-84-695-8511-5. Santander, Septiembre 2013.

[4] **M.J. Valero-Romero**, E.M. Calvo-Muñoz, R. Ruiz-Rosas, J. Rodríguez-Mirasol, T. Cordero. "*Methanol dehydration on carbon-based acid catalysts"*. XXXIV

Reunión Bienal de la Real Sociedad Española de Química. ISBN: 978-84-695-8511-5. Santander, Septiembre 2013.

[5] **M.J. Valero-Romero**, J. Rodríguez-Mirasol, T. Cordero. "*Generación de grupos superficiales oxigenados en carbones activados con H_3PO_4*". XII Reunión Grupo Español del Carbón. (ISBN) 978-84-695-8694-5. Madrid, Octubre 2013.

[6] A. Cabrera-Molina, **M.J. Valero-Romero**, M.O. Guerrero-Pérez, J. Rodríguez-Mirasol, T. Cordero. "*Materiales carbonosos como molde para la preparación de óxidos mixtos con morfología controlada"*. XII Reunión Grupo Español del Carbón. (ISBN) 978-84-695-8694-5. Madrid, Octubre 2013.

[7] **M.J. Valero-Romero**, J. Rodríguez-Mirasol, T. Cordero. Oxidation of activated carbons containing surface phosphorus functionalities. VIII International Congress of ANQUE. (ISBN) 978-84-697-0726-5. Madrid, Julio 2014.

[8] M. O. Guerrero-Pérez, **M.J. Valero-Romero**, J. Rodríguez-Mirasol, T. Cordero. Applications in Catalysis of Activated Carbons prepared by Chemical Activation with Phosphoric Acid. VIII International Congress of ANQUE. Contribución oral. (ISBN) 978-84-697-0726-5. Madrid, Julio 2014.

[9] **María José Valero-Romero**, José Rodríguez-Mirasol, Tomás Cordero. Role of surface phosphorus complexes on the oxidation of porous carbons. Contribución oral. The World Conference on Carbon. Korea, Julio 2014.

Poster presentations

[1] **M.J. Valero-Romero**, S. Hernández, J.M. López Nieto, M.O. Guerrero-Pérez, J. Rodríguez-Mirasol, T. Cordero. "*New Zr-V-O carbon-supported catalysts for oxidation reactions*: *Surface active sites and thermal stability*". International Conference on Functional Materials: Catalysis, Electrochemistry and Surfactants. COST Action D36 Final Workshop.Fuengirola, España, Mayo 2011.

[2] **M.J. Valero-Romero**, E. Calvo-Muñoz J. Bedia, J. Rodríguez-Mirasol, T. Cordero. *"Kinetic Study of Methanol Dehydration on Carbon Acid Catalysts"*. First International Congress on Catalysis for Biorefineries (CatBior). Torremolinos-Málaga, 2011.

[3] **M.J. Valero-Romero**, E.M. Calvo-Muñoz, R. Ruiz-Rosas, J. Rodríguez-Mirasol, T. Cordero. "*Methanol decomposition on acid carbon based catalysts prepared*

from lignocellulosic residues". Anque. Internacional Congress of Chemical Engineering. Sevilla, España, Junio 2012.

[4] **M.J. Valero-Romero**, E.M. Calvo-Muñoz, R. Ruiz-Rosas, J. Bedia, J. Rodríguez-Mirasol, T. Cordero. "*Conversión catalítica de metanol sobre catalizadores de carbono ácidos"*. XII Reunión Grupo Español del Carbón. Publicación: (ISBN) 978-84-695-8694-5. Madrid, Octubre 2013.

[5] **M. J. Valero-Romero**, E. M. Calvo-Muñoz, M. Rodrigues-Gomes, M. Serrano-Pérez de Gracia, J. Rodríguez-Mirasol, T. Cordero. "*Role of oxygen in the dehydration of methanol and ethanol on carbon-based acid catalysts"*. VIII International Congress of ANQUE. Award best poster. (ISBN) 978-84-697-0726-5. Madrid, Julio 2014.

[6] M. O. Guerrero-Pérez, **M.J. Valero-Romero**, J. Rodríguez-Mirasol, T. Cordero. "*Vanadium based catalysts with controlled morphology and porous structure obtained by a simple and low cost method"*. 8th International Symposium on Group Five Elements. Publicación: (ISBN) 978-84-697-0726-5. Málaga, Julio 2014.

Predoctoral research stays

[1] Department of Chemical Engineering, Catalysis Engineering Section. Faculty of Applied Sciences. Delft Universisity of Technology.
Supervisor: Professor Freek Kapteijn
Period: From 9th of January to 29th of June, 2012
Topic: *Bifunctional catalysts for the direct production of liquid fuels from syngas*

[2] Department of Chemical Engineering, Catalysis Engineering Section. Faculty of Applied Sciences. Delft Universisity of Technology.
Supervisor: Professor Freek Kapteijn
Period: From 22nd of April to 28th of August, 2014
Topic: *Carbon/H-ZSM-5 composites as supports for bi-functional Fischer-Tropsch synthesis catalysts*